Microstructure and texture evolution during thermo-mechanical processing of two phase titanium alloy Ti-6Al-4V

Thesis

The Open University

Faculty of Mathematics, Computing and Technology

Department of Design, Development, Environment and Materials

Microstructure and Texture Evolution during Thermo-Mechanical Processing Of Two Phase Titanium Alloy Ti-6Al-4V

By

Bama Perumal

M.Sc. (Phys), M.E. (Mat.Sci.)

07 February 2012

A Thesis submitted to The Open University (UK) for the degree of Doctor of Philosophy

Date of Submission: 7 February 2012
Date of Award: 3 April 2012

The Open University

EX12 (February 2011)

RESEARCH SCHOOL

Library Authorisation Form

Please read and complete this form in conjunction with the EX11 Examination Guidelines for Students. You should return this form to the Research School, The Open University, Walton Hall, Milton Keynes, MK7 6AA with the three bound copies of the thesis and any non-text component, if applicable to be deposited with the University Library. Please note that only theses which comply fully with the binding and presentation criteria as set out in the research degree regulations and the EX11 Examination Guidelines for Students will be accepted for deposition in the University Library. All candidates should complete parts one and three of the form. Part two only applies to PhD candidates.

Part One: Candidates Details

Name: Bama Perumal PI: Y9091115

Degree: PhD

Thesis title: Microstructure and Texture Evolution during Thermo-Mechanical Processing of Two Phase Titanium Alloy Ti-6Al-4V

Part Two: British Library Authorisation [PhD candidates only]

If you want like a copy of your PhD thesis to be available on loan to the British Library Thesis Service as and when it is requested, please tick Section A of this form.

The University has agreed that your participation in the British Library Thesis Service should be voluntary. Please tick either (a) or (b) to indicate your intentions.

(a) ☑ I am willing for The Open University to loan the British Library a copy of my thesis.

(b) ☐ I do not wish The Open University to loan the British Library a copy of my thesis.

Part Three: Open University Library Authorisation [All Candidates]

I confirm that I am willing for my thesis to be made available to readers by The Open University Library, and that it may be photocopied, subject to the discretion of the Librarian.

Signed: Bama Perumal. Date: 27/04/2012

An electronic version of this form can be downloaded from:
http://www.open.ac.uk/research/research-degrees/directly-registered-students/examinations.php

Abstract

Understanding the relationship between high-temperature deformation and microstructure evolution during hot forging of aero-engine alloys is important in ensuring optimum material properties in the final component. Of particular interest, with respect to two-phase titanium alloys is the break-up, below the beta-transus temperature, of an initial transformed alpha-lamellar microstructure during thermo-mechanical processing; this plays a key role in the development of the equiaxed alpha microstructure desired for the final product. Significant research effort has been put into understanding the mechanism for dynamic globularization, formation of kinking and shear banding within the alpha lamellae that can lead to break-up, but no complete quantitative analysis of the evolution of microstructural parameters and crystallographic texture with deformation currently exists. Therefore, reliable quantitative microstructural data associated with this process is important for both informing and validating models describing high-temperature metal-forming.

To investigate the influence of hot working parameters, strain, strain rate and temperature, on microstructure evolution in Ti-6Al-4V a series of hot isothermal axis-symmetric compression tests have been carried out at temperatures both low and high in the alpha + beta stability field (880°C and 950°C, respectively), using strain rates (0.01, 0.1 and 1/s) relevant to industrial press forging. The experimental results showed that the morphology of the secondary α phase transforms gradually from lamellar to equiaxed under the influence of the deformation parameters and that the α lath thickness appears to have little influence on flow behaviour. It was also found that, at lower strains, the alpha laths appeared to be undeformed or only partially distorted. As strain progressed the laths were further broken up by distortion, bending and kinking. The mean aspect ratio of the alpha laths was found to exhibit a gradual reduction with increased strain. The lath area, length and perimeter showed a tendency to decrease with increasing strain.

Furthermore, orientation image mapping (by EBSD) and texture analysis (by neutron diffraction) of the alpha phase were used to study the textural evolution during the hot deformation of the specimens and the mechanism involved on development and evolution of crystallographic texture during the α→β→α phase transformation. The strengthening of the β-phase texture is observed on heating the sample during α→β phase transformation, where it was observed that Burgers relationship was followed but no evidence of preferential transformation was detected. In contrast a definite deviation from the Burgers relationship was observed during hot-compression. During β→α phase transformation upon cooling, however, the Burgers relationship was followed, which is evidence for a texture memory effect due to the growth of the primary alpha phase present at high temperatures.

This thesis is dedicated to my late supervisor, Dr. Martin A. Rist, my dad Perumal and my dear daughter Neha.

Acknowledgements

My special thanks to my helpful supervisors, late Dr Martin. A. Rist, Dr Salih Gungor and Professor Jeffery. W. Brooks for their supervision support and continuous guidance during this PhD. The co-operation is much indeed appreciated.

I am extremely grateful and thankful to late Dr Martin. A. Rist for his continuous encouragements and motivation during my PhD.

Sincere thanks to Prof. Brooks, for his expert advice on hot forging and support during my PhD. Further, I would like to appreciate him for spending his valuable time for correcting my chapters.

I am grateful to Professor Mike Fitzpatrick for this incredible opportunity to work at Materials Engineering Department and his extraordinary support during stressful times of writing thesis.

I gratefully thank Professor Dave Rugg for his constructive, effective comments on this thesis and furthermore, using his precious times to read texture chapter and gave his critical comments about it.

I am thankful Richard Moat who always kindly grants me his time even for answering some of my unintelligent questions about Neutron diffraction. Furthermore, I have also benefited by advice and guidance from him especially for texture measurements.

My special thanks to Prof. John Bouchard for his support and help during my PhD.

I am grateful to Shirley Northover for her support and help during EBSD measurements.

Many thanks go to Mr Stan Hiller for his continuous support and help on mechanical testing machine, Mr Gordon Imach for his training on scanning electron microscopy, EBSD and also spending his valuable time to work out good pattern during EBSD measurements, Mr Peter Ledgard for providing specific geometry specimens with EDM machining and Mr Ian Norman for technical advice.

My special thanks to Paul Courtnage for his encouragements and help during my PhD. I also would like to thank Angie Swain, Claire Emburey and Olivia Acquah for their help and support during my studies.

My very special thanks to Susan, her husband David and her sons Michael, Joe for their nice friendship, and support.

I am very grateful to Yuki, who frequently visited my room and encouraged me during stressful time.

I would like to thank Genoveva for her nice friendship and help during my PhD.

My special thanks to Prof. Narayanasamy (NIIT Trichy, India) for his continuous support and encouragements during my studies.

I am thankful to my friends, Ammu, Maheswari, Nithya, Swarna and Shantha, (AmBaMaNiSwSh) for their incredible love, continuous encouragements and they all played an important role in shaping my personality.

My special thanks to Senthil and Bhagavathi for their love and motivation.

My deepest gratitude goes to my family members for their love and support throughout my life; this dissertation is simply impossible without them. I would like to thank my husband Narendran and my daughter Neha for their unconditional love and moral support. They provided the inspiration for me to complete this dissertation.

I am indebted to my father, Perumal, who stimulated and supported my desire to become a researcher. As a typical father in Indian family, he worked hard to support the family of five children and spare no effort to provide the best possible environment for me to grow up and attend school. He had never complained in spite of all the hardships in his life.

I would like to thank my mother Parameswari, who sacrificed her whole life by doing best for me and her belief in my abilities.

I would like to express my special thanks to my dear brother, Bhaskaran who constantly provide emotional support and encouraged me to do research in United Kingdom. I am grateful to my sisters, Bhavani, Bharathi and Priya for their constant support and special prayers during my PhD.

I am grateful to my sister-in law, kamala and brother-in-laws, Santh Gyaneshwar Mari, Raghulan who always encouraged me for pursuing higher study. My hearty love and kisses to Riteesh and Ikshitha

Thanks to God for this wonderful journey. You have given me the power to believe in myself and pursue my dreams.

Preface

This thesis is submitted for the degree of Doctor of Philosophy of The Open University, Milton Keynes, United Kingdom. The work described in this dissertation was carried out in the Department of Materials Engineering of the Faculty of Technology, between March 2008 and February 2012, under the supervision of internal supervisors, late Dr. Martin A. Rist, Dr. Salih Gungor and external supervisor Professor Jeffery. W. Brooks. This was a collaborative project between The Open University, Milton Keynes and QinetiQ plc. Farnborough to study the microstructure and texture evolution of two phase titanium alloys with an initial lamellar microstructure. To best of my knowledge, it is an original work of the author except where reference is made to the work of others. None of this work has been submitted or is in the process of submission in whole or part for a degree at this or any other university. Some of the results of this work have been published in conference proceedings and will be published in journals in the near future are listed below:

Paper published in conference proceedings:

- Morphological and textural evolution of the alpha phase during hot deformation of two-phase Ti-6Al-4V, Bama Perumal, Martin A. Rist and Jeffery W. Brooks **Presented paper at The 12th world conference on Titanium (Ti-2011) on 19-24 June 2011, Beijing, China.**
- Characterisation of Microstructure evolution in alpha-beta Titanium alloys for process modelling, Bama Perumal, Martin A. Rist and Jeffery W. Brooks poster presented at **Optimising Performance through Integrated Modelling conference (OPTIMOM)** on 26, 27,28th September 2010 at Queens College, Cambridge, organized by IOM3.
- Microstructure evolution during hot forging of Ti-6Al-4V, Bama Perumal, Martin Rist, Salih Gungor, Jeffery Brooks and Hector Basoalto poster presented at **European Titanium Conference**, on 23-24 June 2009 at Belfry Golf Club and Conference Centre, Birmingham, which was jointly organised by Titanium Information Group (TIG) in association with the Special Metals Forum and NAMTEC

Papers to be published in journals (under development):

- Investigation on Microstructure and Texture evolution during Thermo-Mechanical processing of two phase titanium alloy-Ti-6Al-4V for Materials Science & Engineering A (Under preparation).

- A study of the $\alpha \rightarrow \beta \rightarrow \alpha$ phase transformation mechanism and texture evolution of a Ti-6Al-4V using neutron diffraction for Acta Materialia (Under preparation).

Table of Contents

Chapter 1

Introduction

Since 1950s, the usage of titanium alloys in many areas, such as in aerospace industry and medical applications, has increased considerably due to their remarkable properties such as high strength and toughness, good fatigue behaviour, excellent corrosion resistance, low weight and biocompatibility. The Ti-6Al-4V alloy - the material used in the present study - is one of the most extensively used titanium alloys. It exhibits mechanical properties that fit aerospace applications and also provide significant economic benefit in these applications. The balance of mechanical properties of Ti-6Al-4V, such as fatigue properties with intermediate fracture toughness are depends on the chemical composition, microstructure, deformation and heat treatment history [1].

This project was aimed to study the microstructure evolution of two phase titanium alloys with an equiaxed microstructure using thermo-mechanical processing (TMP). The main objective of the work was to delineate the necessary details of the mechanism by which globularization occurs during TMP of two-phase ($\alpha+\beta$) titanium alloys with a lamellar preform microstructures. Because of the technical importance, the mechanism of the globularization process has been the subject of many studies over the years but there have been a limited number of studies on deformation texture of Ti-6Al-4V during hot compression tests, simulating the forming process of components made from these alloys. Better understanding of the kinetics of globularization will help to develop new processing routes by which the manufacturers can produce reliable components with improved mechanical properties.

The design of such processes relies greatly on quantitative description of constitutive behaviour and the change in microstructure, which is the basis of plastic-flow behaviour. Depending on the specific TMP practice, the three principal microstructures commonly formed in Ti-6Al-4V [2] are fully lamellar alpha, fully equiaxed alpha and bi-modal (duplex). Generally, two-phase ($\alpha+\beta$) titanium alloys can exhibit a variety of microstructures, for example the development of lamellar α colonies during cooling from high-temperature, single-phase β field. This microstructure has moderate strength and fatigue crack resistance, but low ductility [3]. In contrast, a microstructure comprising globular α in a matrix of β or transformed β possesses a better balance of strength and ductility and it's more desirable microstructure for many service applications [3].

The microstructural parameters such as the aspect ratio and morphology of different phases, texture and grain size have great influence on the performance of titanium alloys. In order to control microstructure in plastic working, it is very important to reveal the mechanism and regulation of microstructure evolution. A general procedure to investigate the microstructure evolution in hot working depends on stress-strain curves as well as processing maps. Hot working processes in the ($\alpha+\beta$) field such as forging, extrusion, rolling, etc. at temperatures below the beta transus at which $\beta \rightarrow \alpha$ comprise the main approaches to breakdown of the fully lamellar microstructure, and thus to obtain an equiaxed-alpha microstructure called globularization or spheroidization process.

Basically, there are two mechanisms that may contribute to the globularization (or spheroidisation, as it is known in the titanium industry) of lamellar microstructures in the titanium alloys during thermomechanical processing (TMP) [4-6]. The first mechanism is termination migration (a spheroidization-like process driven by the reduction of ($\alpha+\beta$)

interface energy during long annealing times [7]) has been used to analyse the diffusional coarsening and globularization of lamellar platelets during hot working [6]. The second mechanism contributing to globularization during TMP consists of a fragmentation of lamellae via the boundary splitting (driven by residual dislocation substructure during short annealing times, [8]) associated with the instability of 90° dihedral angles between interphase α/β boundaries and interphase α/α boundaries [9] (discussed in chapter 5).

The TMP of conventional titanium alloys have a number of similarities to the TMP of steels. Typically, both steel and titanium alloys are melted, cast into ingots or continuous bloom/billet, and undergo a series of primary and secondary hot working steps to make semi-finished or finished products. The main goal of many hot working operations for both titanium alloys and steels is to develop a fine, uniform microstructure, suitable for subsequent processing of final heat treatment. Although the degree of microstructure control during TMP of conventional titanium alloys is high, the nature of the hexagonal crystal structure and the dependence of flow stress on temperature of these materials make them noticeably more difficult to hot work than ferrous alloys. The HCP crystal structure is close-packed, like FCC, but has fewer available slip systems. As a result of this lack of independent slip systems, most HCP metals exhibit extensive deformation twinning as a method of strain accommodation. Thermal activation has the effect of both lowering the yield stress and decreasing the effect of strain hardening within HCP metals [10]. The thermomechanical behaviour of HCP metals fall between FCC and BCC metals. Thus, HCP metals tend to work harden due to an increase in the amount of dislocation interactions with increasing strain and reach a steady-state flow stress due to dislocation recovery processes.

Hot axisymmetric compression tests are useful in obtaining flow data in terms of true stress – true strain curves. The hot workability of various alloys can be determined using

compression test with small cylindrical specimens [11]. However, the flow data obtained from compression tests are prone to adiabatic heating and frictional effects from deformation which need to be corrected by appropriate methods (explained in section 4.3). In addition to the flow data, microstructural details in terms of volume fraction, aspect ratio, globularization mechanism during hot working can be revealed. In this work, in order to understand the influence of deformation parameters such as temperature, strain, strain rate and cooling rate on the microstructure and texture evolution on Ti-6Al-4V, the small cylindrical samples have been used successfully with various deformation tests.

The major contribution of this work is, in the first place is, to the identification of deformation and globularization mechanisms and in the second place, to the understanding of the evolution of texture by studying the orientation distribution or rotation of one of the phases (α-laths) in the Ti-6Al-4V during deformation. Therefore, the present work, was intended to study the dynamic globularization kinetics of Ti-6Al-4V alloy with initial lamellar microstructure using isothermal hot compression tests at both near-transus and sub-transus temperatures (880°C & 950°C) and at a range of strain rates (0.01, 0.1 and 1.0/s). The influences of temperature and strain rate on the deformation behaviour have been studied, with the aim of determining the extension of the texture evolution for this alloy. The mechanical behaviour of Ti–6Al-4V depends on the microstructure and texture developed during TMP [4]. Studying the microtexture and bulk texture is necessary in understanding the texture evolution of Ti-6Al-4V during hot working.

During plastic working of titanium alloys, due to the inherent anisotropy of the hexagonal crystal structure of the α phase which has a strong influence on the properties, such as strength, fatigue life, corrosion resistance [12-14]. In the work of Zeng et al., [15] the texture evolution of CP (commercially pure) titanium after compression tests at elevated temperature was found that the basal planes of grains both (fine and coarser) in the

deformed samples tended to rotate from the initial orientations, perpendicular to the compression axis, to an inclination of 45°. According to the work by Luetjering [2] there is a strong link between microstructural and texture evolution during material processing.

For the above consideration, the work in this project concentrated on the following four areas:

- to study the deformation behaviour of Ti-6Al-4V by conducting a series of isothermal hot compression tests at fixed nominal strain - rates and temperatures relevant to industrial hydraulic press-forging;
- to study the microstructure and texture evolution during high temperature deformation of Ti-6Al-4V with various initial microstructure;
- to understand the initial spheroidisation process and the deformation texture, using EBSD and neutron diffraction;
- to quantify the microstructure present in two-phase titanium Ti-6Al-4V.

1.1 Structure of thesis

This thesis is organized into seven separate chapters.

Chapter 1 sets out the main objective and intention of the work. It also introduces the alloys and methods used in the study.

Chapter 2 presents a literature review on many aspects of titanium alloys relevant to the present work. The chapter starts with a brief development history of the titanium alloys and then information on their classifications and information about typical applications are presented. Typical production process and corresponding microstructure evolution are discussed next. Particular attention is paid to the Ti-6Al-4V alloy, its application and the evolution of microstructure and texture. The observation of different phases change during TMP and finally, the description of the different mechanisms of deformation and

globularization are given in this chapter.

Chapter 3 covers a description of the material and the details of the tests performed in this work to investigate the deformation behaviour of the Ti-6Al-4V alloy including hot axisymmetric compression testing. The experimental and analytical techniques and tools employed in the project are described in this section. These include microstructure analysis using optical and electron microscopy, the quantitative metallography analysis using MTEX-MATLAB toolbox and microtexture measurements using electron backscattered diffraction (EBSD) and finally the bulk texture measurements using GEM instrument at ISIS, Oxford.

Chapter 4 covers the experimental flow stress behaviour of two-phase Ti-6Al-4V and the methodologies used for flow stress correction to take account of the machine compliance test, adiabatic heating and internal friction. The effects of initial microstructure on the flow behaviour of Ti-6Al-4V and temperature and strain-rate were also established. The influence of change in α-morphology on flow softening during thermomechanical processing was also discussed.

Chapter 5 provides a detailed microstructure evolution of deformed Ti-6Al-4V material with various initial microstructures at both subtransus temperature and microstructural measurements under different processing conditions such as strain, strain rate and temperature.

Chapter 6 discusses the bulk texture measurements of Ti-6Al-4V and evolution of texture during high temperature deformation.

Chapter 7 gives the conclusions drawn from the investigation carried out in this dissertation and suggestions for further work.

Chapter 2

Background and Literature Review

In 1791 Reverend William Gregor, an amateur mineralogist, discovered a new material in the magnetic sand of the local river in the Menachan valley in Cornwall, England and named it menachite (the ore he found is now known as ilmenite). The element was rediscovered several years later in 1795, by German chemist Martin Heinrich Klaproth in rutile ore. Klaproth named the metal oxide "titanium" after the Titans, the giants of Greek mythology, who symbolized power and strength[16].

2.1. Physical properties of titanium alloys

There are 112 chemical elements in the periodic system; about 85% are metals or metalloids. These metals are classified as ferrous or non-ferrous, light or heavy metals. Titanium is classified as a nonferrous metal with an atomic number of 22 and atomic weight of 47.90. As compared to aluminum, titanium has higher melting point which makes it an ideal choice for structural applications at temperature above 200°C. Table 2.1 list the properties of titanium alloy compared to iron (Fe), aluminum (Al) and nickel (Ni) [17].

Table 2.1 Properties of titanium as compared to some other common metals [17].

Properties	Ti	Fe	Ni	Al
Melting Temperature (°C)	1670	1538	1455	660
Allotropic Transformation (°C)	β→α	γ→α	-	-
Crystal Structure	bcc→ hex	fcc→bcc	fcc	fcc
Room temperature E (GPa)	115	215	200	72
Yield Stress Level (MPa)	1000	1000	1000	500
Density (g/cm^2)	4.5	7.9	8.9	2.7
Comparative Corrosion resistance	Very High	Low	Medium	High
Comparative Reactivity with Oxygen	Very High	Low	Low	High
Comparative price of Metal	Very High	Low	High	Medium

The most important property of titanium is a superior corrosion resistance because of its high affinity with oxygen. When titanium is exposed to air, it forms a thin adherent oxidized surface layer which exhibits excellent corrosion resistance in both hostile and aggressive environments. Alloying elements also influence the corrosion properties of titanium because they are responsible for the composition of the protective oxide film [18].

2.2. Application of titanium alloys

The Titanium Metals Company of America (TMCA) produced the first commercial titanium product around 1950 [19, 20]. Over the last 50 years, the production of titanium and its alloys has grown at an annual average rate of about 8%, largely because of the technically superior and cost-effective nature of these materials for many structural applications. More specifically, a wide variety of aerospace applications are now commercially viable due to the high strength to weight ratio, excellent corrosion resistance, biocompatibility and good toughness of titanium alloys. In recent years, titanium and its alloys have been widely used in the automobile, chemical and food industries and for applications in shipbuilding medicine and civil engineering. Although titanium usage is strongly limited by its higher cost when compared to that of competing materials this is balanced with higher weight efficiency when compared to steel and aluminium alloys, which is most important in the aircraft industry.

2.2.1 Aerospace applications

The outstanding mechanical properties of titanium and its alloys have led to a wide range of successful applications in various aerospace and space industries. In particular, high

specific strength, heat resistance, fatigue resistance, crack resistance and corrosion resistance make titanium an ideal choice for many aerospace applications.

The main drivers for titanium's use in aerospace applications are[20]:

- weight reduction (substitute for steels)
- application temperature (substitute for Al alloys)
- corrosion resistance (substitute for Al alloys and low-alloyed steels)
- galvanic compatibility with polymer matrix composites(substitute for Al alloys)
- space limitation (substitute for Al alloys and steels).

The main area of application for aerospace titanium alloys are in the gas turbine engine, which accounts for nearly half of annual titanium production. In the beginning of 1950s, the first jet engines introduced by Pratt & Whitney in the USA and Rolls-Royce in England contained titanium alloys. In particular, compressor blades were the first engine components to be made from titanium. In recent years, besides nickel-based superalloys, titanium alloys are the standard engine material because of their weight advantage over steels.

The maximum working temperature limit for Ti-6Al-4V is about 315°C, making it suitable for use in low-pressure compressor applications. On the other hand, the elevated temperature properties of near-α alloy mean that they can be used for high-pressure compressor applications. For example, IMI 834 (Ti-5.8Al-4Sn-3.5Zr-0.7Nb-0.5Mo-0.35Si) was developed for use in elevated temperature applications up to 600 °C.

It has been found that a 15% volume fraction of primary alpha in the bio-modal microstructure provides the optimum material for jet engine applications. Furthermore, to

increase the high temperature strength and minimize the risk of titanium fire, titanium aluminides (TiAl) have also been developed for jet engine components. More generally, titanium alloys with strength up to 1200MPa are used in a wide variety of airframe applications. Nowadays, titanium makes up to 10% of the weight of a commercial airplane. In the Boeing 777 airplane, for example, TIMETAL 21S is used for the plug and parts of the nozzle assembly, and Ti-10V-2Fe-3Al (Ti 10-2-3, a beta forging alloy) is used in the landing gear. Indeed, the structure of GE-90 aero-engine contains many components manufactured using titanium alloys. Figure 2.1 shows titanium usage for the components within a GE-90 aero-engine [17].

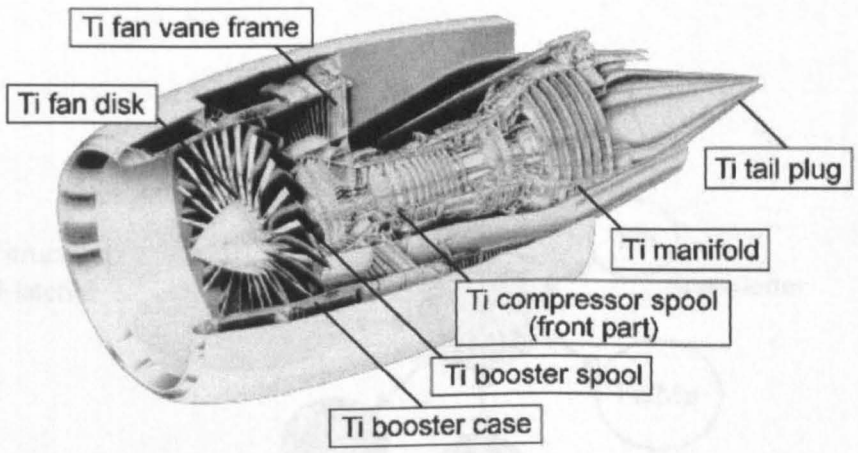

Figure 2.1: The components of a GE-90 aero-engine made by titanium [17].

The alloy Ti-6Al-2Zr-2Zn-2Mo-2Cr-0.25Si has moderate temperature strength and is used in the airframes of the US F-22, making up part of the wing box. The forged Ti-6Al-4V alloys are used as rotor heads for the BK117 and Euro copter BO 105 helicopters. However, high strength β-alloys are also used for the rotor mast and rotor head for US RAH-66 Comanche helicopter. For example, Ti-3Al-2.5V was developed for low temperature applications because of its good toughness and maximum ductility down to

cryogenic temperature. These properties make Ti-3Al-2.5V a useful material for high-pressure piping in the hydrogen pumping systems of the US space shuttle.

2.2.2 Application of Ti-6Al-4V

Ti-6Al-4V is a well known alloy for its good machinability and excellent mechanical properties. Because of its outstanding performance for a variety of weight reduction applications in aerospace, automotive and marine equipment, make it a most widely used alloy in the titanium alloys. The range of applications and relevant alloying elements of Ti-6Al-4V is shown in Figure 2.2.

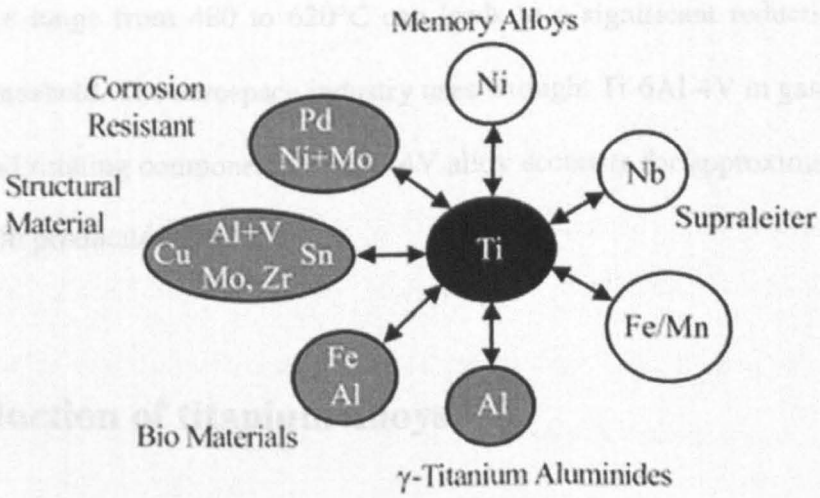

Figure 2.2: Application for titanium with relevant alloying elements [21].

In recent years, the use of titanium has expanded in other fields like nuclear power plants, food processing plants and oil refinery heat exchangers. The Ti-6Al-4V is specifically designed to resist stress corrosion in aqueous salt solutions as well as for high fracture toughness. The reduction of oxygen content (< 0.13%) in Ti-6Al-4V (grade 23) alloy

confers fracture toughness and improved ductility, with medium strength, has been widely used in critical airframe structures and offshore applications.

Due to its price constrains, Ti-6Al-4V has limited usage in the automotive industries. Applications include racing cars and rotating parts such as valves, valve springs, connecting rods and rocker arms. Ti-6Al-4V has significant usage in marine applications such as deep submergence applications, hydrofoils, and water-jet inducers for hydrofoil propulsion and seawater ball valves for nuclear submarines.

Ti-6Al-4V has a good fatigue and fracture properties and is used in all product forms including bar, casting, forging, extrusion, plates and fasteners. The solution treated and aged (STA) Ti-6Al-4V alloy provides the maximum strength and hardenability, are used as fasteners on commercial aircraft [22]. It is also found that a slow cooling rate from the temperatures range from 480 to 620°C can leads to a significant reduction in the stress corrosion threshold. The aerospace industry uses wrought Ti-6Al-4V in gas turbine engines for static and rotating components.Ti-6Al-4V alloy accounts for approximately 45% of the total titanium production [23].

2.3 Production of titanium alloys

Since 1940 the principal method of industrial-scale Ti production has been the Kroll process having replaced the Hunter process for almost all commercial production [24]. A more recently developed process which may eventually replace the Kroll process is known as the FFC Cambridge process [25]. Basically, the processing of titanium metal occurs in four major steps including extraction, purification, production of the sponge and alloy creation [26].Titanium cannot be produced by reduction of its dioxide because of its high affinity with oxygen at high temperatures.

2.4 Structure and properties of titanium alloys

2.4.1 Crystal structure of Titanium alloys

In general there are many different types of crystal structure but most metals crystallize in one of the three following simple structures: face-centred cubic (fcc), body centred cubic (bcc) and hexagonal closed-packed (hcp). Titanium is an allotropic element; like many other metals, such as Ca, Co, Ce, Fe and Sn, Ti can crystallize in more than one crystalline state. The complete transformation from one crystal structure to another is called allotropic transformation and the transformation temperature is called the transus temperature of the metal or alloy.

The microstructures of titanium are almost completely dependent on the size, shape and distribution of two primary crystallographic phases: the hcp alpha (α) phase and the bcc beta (β) phase. Pure Ti, as well as the most titanium alloys exists in the hexagonal closed packed α-phase structure at room temperature. At high temperature, the structure of Ti transforms to the body-centred cubic β-phase. The β-transus temperature for pure titanium is 880°±2°C. The β transus temperature is a critical point which separates the single phase β field from the dual phase (α+β) field, specific temperature of which is dependent on alloy chemistry [27]. Most commercial heat treatment routes are carried out with reference to some point above or below the β transus temperature [17].

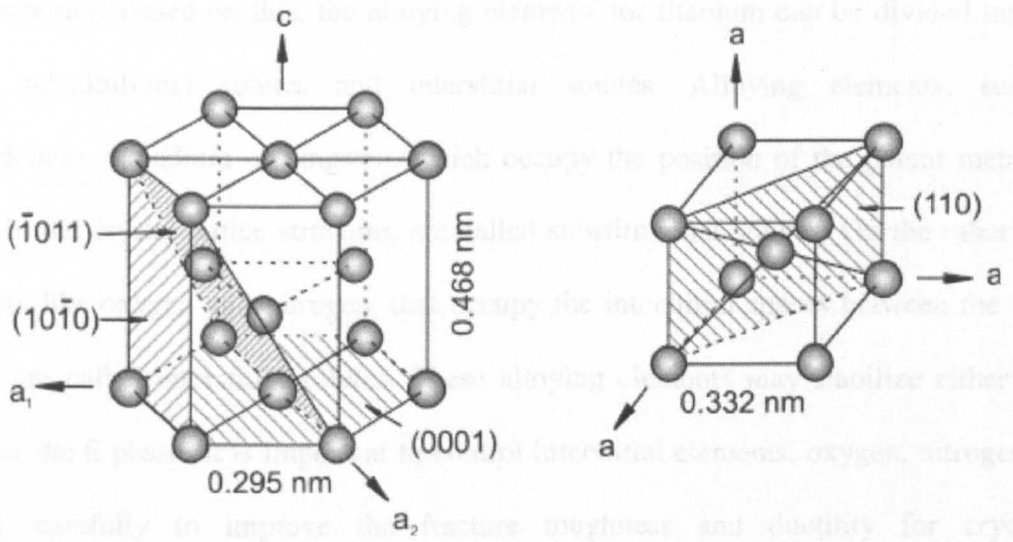

Figure 2.3: Unit cell of hcp α phase and bcc β phase for pure Ti [17].

The hexagonal unit cell of the α-phase and the body centred cubic unit cell of the β-phase are illustrated in Figure. 2.3 showing the c/a ratio for pure α-titanium is 1.586 which is smaller than the ideal ratio of 1.633 for the hexagonal close-packed crystal structure. The occurrence of the two different crystal structures and their respective transformation temperatures are the key parameters in the production of various microstructures, which in turn is the basis for the large variety of properties displayed by titanium alloys.

2.4.2 Effect of alloying elements

Titanium has a relatively low density, 4.5 g/cm^3 – just over half that of steel, and also has low strength when pure, although alloying increases it considerably. The additions of small amounts of alloying elements to titanium which either produce little change in the transformation temperature, or cause it to increase, are known as a stabilizer; they are simple metals (SM) or interstitial elements.

The exact temperature for transformation from one phase to another is influenced by the metal's purity. Based on this, the alloying elements for titanium can be divided into two types: substitutional solutes and interstitial solutes. Alloying elements, such as molybdenum, vanadium or tungsten, which occupy the position of the parent metal (Ti) atoms in the crystal lattice structure, are called substitutional solutes. On the other hand, elements like oxygen and nitrogen, that occupy the interstitial spaces between the parent atoms, are called interstitial solutes. These alloying elements may stabilize either the α phase or the β phase. It is important to control interstitial elements, oxygen, nitrogen, and carbon, carefully to improve the fracture toughness and ductility for cryogenic applications. The structural differences between interstitial and substitutional formation within the parent metal is shown in Figure 2.4 [28].

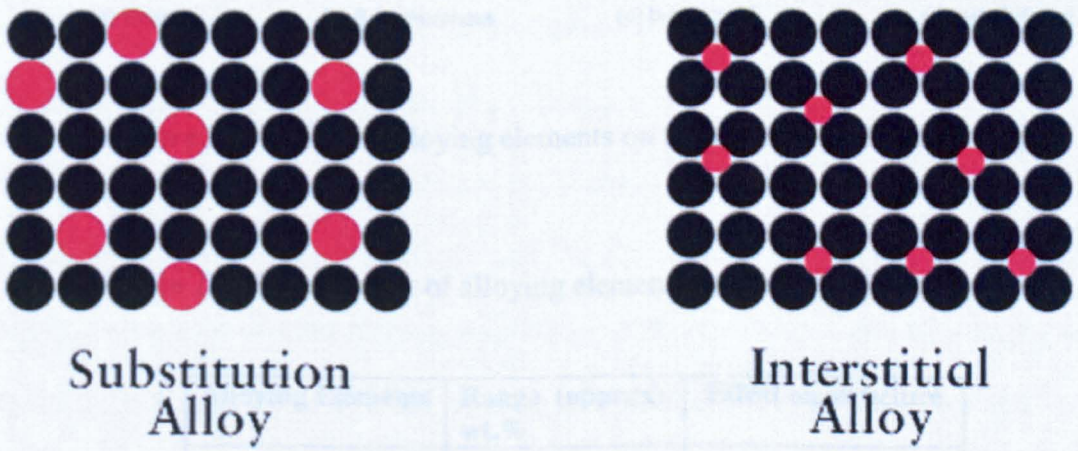

Figure 2.4: (a) substitutional and (b) Interstitial elements [28].

2.4.3 Phases and stabilizing elements

Titanium alloying elements are classified as neutral, α-stabilizers or β-stabilizers depending on their influence on the β-transus temperature. The α-stabilizing elements

increase the α-phase field to higher temperature, while β-stabilizing elements decrease the β-phase field to lower temperature. Neutral elements have little influence on the transformation temperature. There are other elements added to titanium, which are neither alpha nor beta stabilizers; Zirconium is such an element, being used to contribute solid solution strengthening [27].The influences of alloying elements on titanium phase diagrams are shown in Figure 2.5 [27]. The major alloying elements and their influence on the titanium alloy structure are shown in Table 2.2.

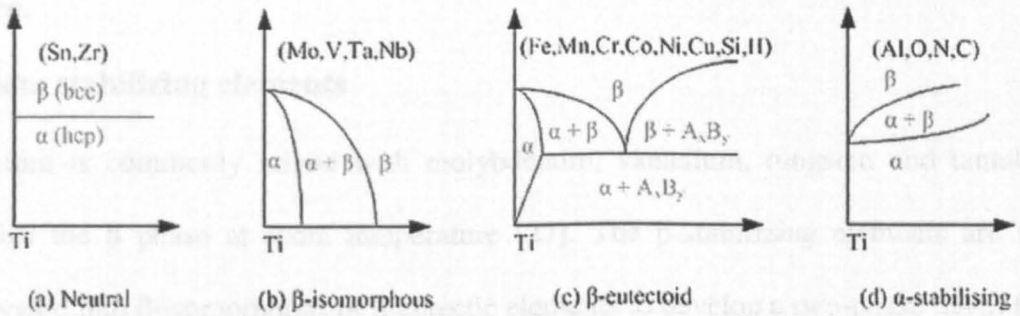

Figure 2.5: Effect of alloying elements on titanium phase diagram [27].

Table 2.2 The influence of alloying elements on titanium structures [26].

Alloying Elements	Range (approx) wt.%	Effect on structure
Aluminum	2 - 7	α stabilizer
Tin	2 - 6	α stabilizer
Vanadium	2 - 20	β stabilizer
Molybdenum	2 - 20	β stabilizer
Chromium	2 - 12	β stabilizer
Copper	2 - 6	β stabilizer
Zirconium	2 - 8	α and β strengtheners
silicon	0.2 - 1	improve creep resistance

(a) Alpha stabilizing elements

The most important α-stabilizing element of titanium is aluminium. Because it is an only common metal which could exhibit a significant solid solubility level in α phase in two phase microstructure. The interstitial elements oxygen, nitrogen and carbon also stabilize the α-phase by raising the β transus temperature with increasing solute content. In particular, oxygen is frequently used as an alloying element in the application of titanium alloys to achieve the desired strength level. Boron, gallium and rare earth elements are rarely used as α-stabilizers because of their lower solubility level than that of aluminium or oxygen.

(b) Beta stabilizing elements

Titanium is commonly mixed with molybdenum, vanadium, tungsten and tantalum to stabilize the β phase at room temperature [27]. The β-stabilizing elements are further subdivided into β-isomorphous or β-eutectic elements to develop a two-phase (α+β) field.

Type-1: Isomorphous β stabilizing elements

The β-isomorphous elements stabilize the β-phase and continuously lower the β-transus temperature. Elements such as V, Mo and Ta, are the commonly preferred β-isomorphous stabilizers because of their higher solubility in titanium. The addition of small amounts of Fe, Mn, Cr, Ni, Cu, Si and H can be used as β-isomorphous stabilizers which can lead to the formation of intermetallic compounds. Considerable amounts of Fe and Mn are often preferred alloying with titanium in order to enhance the hardenability and heat treatment response.

Type-2: Eutectoid β-stabilizing elements

Like the β-isomorphous stabilizers, the β-eutectoid stabilizers also decrease the β-transus temperature but exhibit low solubility in α-titanium. Chromium, iron, and silicon are the most important eutectoid β-stabilizing elements and nickel, copper, manganese, and

bismuth are also used as a β-eutectoid stabilizing elements.

(c) Neutral stabilizing elements

Sn and Zr are examples of neutral elements which contribute to the strengthening of the α-phase but have very little influence on (α + β) phase field.

2.5 Classification of titanium alloys

According to their contribution of the phase composition, titanium alloys are classified into three main groups; α phase alloys, β phase alloys and α + β phase alloys, with further subdivision into near-α and meta-stable β alloys. The alloy classes can be superimposed on a three dimensional phase diagram which consists of two-phase diagrams with α- and β-stabilising elements, as shown schematically shown in Figure 2.6, and discussed in the subsequent sections.

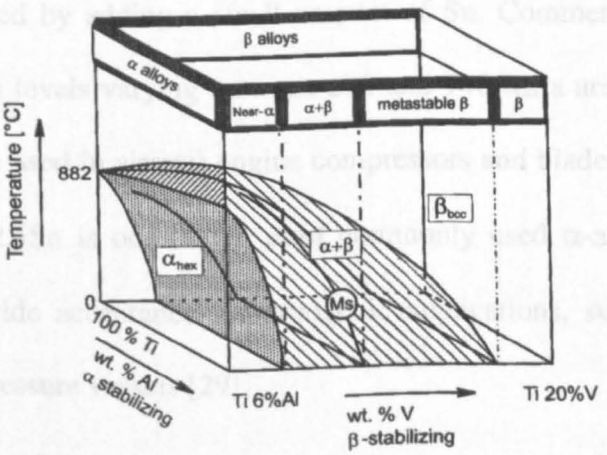

Figure 2.6: Schematic three-dimensional phase diagram for titanium alloys [20].

2.5.1 α–alloys

Alpha alloys are so-called because they consist almost entirely of α-phase; however they also contain a small fraction of β. They contain aluminium as the major alloying element,

stabilizing the α-phase. Due to their single phase state, these alloys cannot be heat treated to modify their mechanical properties by manipulating the microstructure [27, 29]. As compared to α + β and β alloys, the properties of alpha alloys are completely dependent on composition. Combined with moderate strength, these alloys also have high temperature fracture toughness and creep resistance. Due to their hcp crystal structure they possess a high rate of work hardening which limits their formability. However, they have good ductility at very low temperature and their tensile strength is also consequently low. They can be strengthened by grain size strengthening, texture strengthening, precipitation hardening and solid solution strengthening by interstitial and substitutional elements [17, 30]. To avoid embrittlement effects, the α-stabilizers are limited to 9% in titanium.

These alloys are mostly used in applications where corrosion resistance and weldability are desired properties. The addition of small amounts of interstitial elements, oxygen and nitrogen, can increase the hardness and tensile strength of alpha alloys. Ductility of alpha alloys can be improved by adding a small amount of Sn. Commercially pure grades of titanium with strength levels varying between 290 and 740 MPa are also produced using alpha alloys. They are used in aircraft engine compressors and blades, and for sheet-metal applications. Ti-5Al-2.5Sn is one of the most commonly used α-alloys in the annealed condition, and has wide acceptance for cryogenic applications, such as a material for hydrogen tanks and pressure vessels [29].

2.5.2 Commercially pure titanium

Commercial titanium (CP) or unalloyed titanium is available in several ASTM grades according to the amount of interstitial α-stabilizers, including carbon, hydrogen, iron, nitrogen and oxygen. CP titanium alloys differ by the amount of oxygen and iron that is present within each alloy. Alloys with higher interstitial content have higher strength,

hardness and transformation temperature than that of high-purity titanium. The properties of commercially pure titanium are largely determined by the oxygen content. Among the CP-Ti grades, Grade 1 has the lowest level of strength with good cold formability, mostly widely used for steel reactors cladding. In contrast to Grade 1, Grade 3 has a very high strength and is exclusively used for pressure vessel applications. The tensile and yield strength of CP-Ti increases as grade number increases. CP titanium is usually forged, hot rolled, and heat treated in the α-phase field. Examples of CP titanium alloys are shown in

Table 2.3 Examples of CP titanium alloys [26, 31, 32].

Grades of CP-Ti	Alloy specification
CP Ti grade 1	Ti-0.5Fe-0.4O-0.18N-0.08C-0.015H
CP Ti grade 2	Ti-0.25Fe-0.2O-0.25N-0.08C-0.015H
CP Ti grade 3	Ti-0.03Fe-0.2O-0.35N-0.08C-0.015H
CP Ti grade 4	Ti-0.2Fe-0.15O-0.40C-0.015H

On account of their low density these alloys are widely used for non-structural applications such as lavatory areas, floor support structures, ducting for anti-icing and environmental control systems (where ducts needs to operate at about 230 °C, too high for aluminium alloys).

2.5.3 Near α alloys

Near-α alloys contain up to 2% β stabilizing elements, which broaden the α + β

temperature range for the possibility of hot working to be carried in the α + β field as well as in the β field. Although some β is retained to provide supplemental microstructure and property control, these alloys act more like α alloys than α + β alloys. Near α-alloys have similar mechanical properties to α-alloys in untreated condition, but are heat-treatable, due to the small amount of β-phase present, to give them higher strength. They provide a balance between the creep resistance of the simple α alloys and the high strength properties of the α + β alloys.

Near alpha alloys have mainly been developed to meet aerospace requirements in the application of airframe structures and high temperature blades in turbine engines. The formation of martensitic structure α' (produced by rapid quenching from the β phase field) enhances the strength and creep resistance of the near α -alloys. As a result, they have a higher tensile strength at room temperature than the α-alloys, and have superior creep resistance properties at elevated temperature, above 400 °C, when compared to all titanium alloys used in aero engine applications. Most of the near α -alloys are normally used in the duplex annealed (as discussed in the section 2.6.1.2) condition to retain the primary α-phase. Examples of α and near α-alloys are listed in Table 2.4.

Table 2.4 Examples of α and near α-alloy.

Alloy types	**Examples**
Alpha Alloys	Commercially Pure – ASTM grades 1,2,3 and 4 Ti/Pd Alloys – ASTM grades 7 and 11 Ti-3Al-2.5V Ti-5Al-2.5Sn
Near-Alpha Alloys	Ti-8%Al-1%Mo-1%V Ti-6%Al-5%Zr-0.5%Mo-0.2%Si-IMI 685 Ti-6%Al—2%Sn-4%Zr-2%Mo-0.08%Si Ti-5.5%Al-3.5%Sn-3%Zr-1%Nb-0.3%Mo-0.3%Si – IMI 829 Ti-5.8%Al-4%Sn-3.5%Zr-0.7%Nb-0.5%Mo-0.3%Si – IMI 834 Ti-6%Al-3%Sn-4%Zr-0.5%Mo-0.5%Si – Ti 110

2.5.4 (α + β) alloys

The (α + β) alloys contain metallurgically balanced amounts of both α and β-stabilizing elements. The α-stabilizing element stabilizes and strengthens the α-phase, and typically 4-6% of β stabilizing elements allow 10-50% of beta phase to be retained after quenching from the β and (α + β) phase fields [27]. Generally, (α + β) alloys have medium to high strength, good creep resistance (up to 400°C) and good high cycle fatigue and fracture toughness properties. These alloys are heat treatable and weldable. The addition of small amounts of palladium (0.05%), nickel (0.5%) and ruthenium (0.1%) significantly increase the corrosion resistance of α + β alloys in acid and sour environments. The tensile strength of α + β alloys varies from 620 to 1250 MPa, by subsequent tempering or ageing treatments this value can exceed 1400MPa at room temperature.

Ti-6Al-4V (IMI318), the most commonly used alpha-beta titanium alloy, was initially developed in the early 1950s at the Illinois Institute of Technology in the United States to provide improved forgeability and tensile strength over other titanium alloys. It is commercially available in two major grades: a low oxygen (ELI) grade and a high oxygen (commercial) grade. In particular, the high oxygen grade has been widely used in gas turbine engine parts, chemical reactors and bioengineering applications. Usually, these materials are produced by an ingot metallurgy route with a series of mechanical processing steps which have the specific microstructural goals. Ti-6Al-4V accounts for over 80% of the total alloy sales in Europe and United States [33, 34].

The mechanical properties of Ti-6Al-4V strongly depend on the microstructure and texture evolution of the alloy during thermomechanical processing (TMP). Depending on the cooling rate, there are three principle microstructures commonly formed during TMP of this material [2], namely: fully lamellar alpha, fully equiaxed alpha, and bi-modal (duplex).

The microstructure of two-phase titanium alloys depends primarily on the chemical composition, processing history and thermal treatment procedures [1, 35, 36]. Various working parameters such as, strain, strain rate and cooling rate have a strong influence on the microstructure, e.g., the phase volume fraction of α and β, the α-colony size and width of the α-lamellae. In particular, the aspect ratio of the α lamella phase is an important factor that influences the creep properties of the Ti–6Al–4V alloy [35, 37, 38]. Other examples of α + β alloys includes: Ti-3Al-2.5V- a medium strength alloy used for hydraulic tubing, Ti-6Al-2Sn-4Zr-6Mo used as creep and oxidation resistance engine alloy and Ti-4Al-4Mo-4Mn-0.5Si, a high strength alloy used in airframe application.

2.5.5 β-alloys

The β-alloys are metastable alloys and they have a tendency to transform to the equilibrium alpha-plus-beta structure [26]. The addition of 10-30% of β-stabilising elements such as vanadium, niobium, and molybdenum to titanium allows the retention of a completely stable 100% β-phase at room temperature. This decreases the β transus temperature of the alloy and thus promotes the development of the bcc β-phase. The β alloys are classified as stable beta, metastable beta, and beta-rich α/β alloys. These alloys have better forgeability than α-alloys over a range of temperature, and also have good cold working capabilities due to their bcc cubic structure [23]. As compared to (α+β) titanium alloys, the β-alloys possess superior fatigue resistance and moderate fracture toughness. In particular, due to their excellent combinations of properties, they are used in sheet, heavy sections, fasteners and spring applications.

Beta alloys are easily heat treatable to achieve a variety of strength levels which can exceed 1380 MPa. The hardenability level of β-alloys depends on the concentration of β-stabilizing elements. The most common thermo-mechanical processing of beta alloys

involves solution treatment or hot working operations (450°C to 650°C) followed by aging or heat treatment. This develops formation of finely dispersed α particles in the retained beta. The β-alloys are not the right choice for cryogenic applications because of their susceptibility to fracture below the ductile-brittle transition temperature [39].Ti-13V-11Cr-3Al (Ti-13-11-3) was the first commercial β-alloy to be used extensively; it comprised about 95% of the structural weight of the SR-71 "Blackbird" reconnaissance airplane [40]. Due to its outstanding high temperature properties, it has been used for wings, body skins, frames ribs, rivets and nose landing gears in airplanes [22]. The high strength (1240 to 1450 MPa) Ti-3Al-8V-6Cr-4Mo-4Zr (Beta-C) is a metastable titanium alloy developed in the 1960s. Like other β-alloys, they are used for various titanium spring applications, such as in landing gear springs, centring springs for the yoke, hydraulic return springs, and flight control springs [41]. A typical pseudobinary phase diagram for titanium with a beta stabilizer is shown in Figure 2.7.

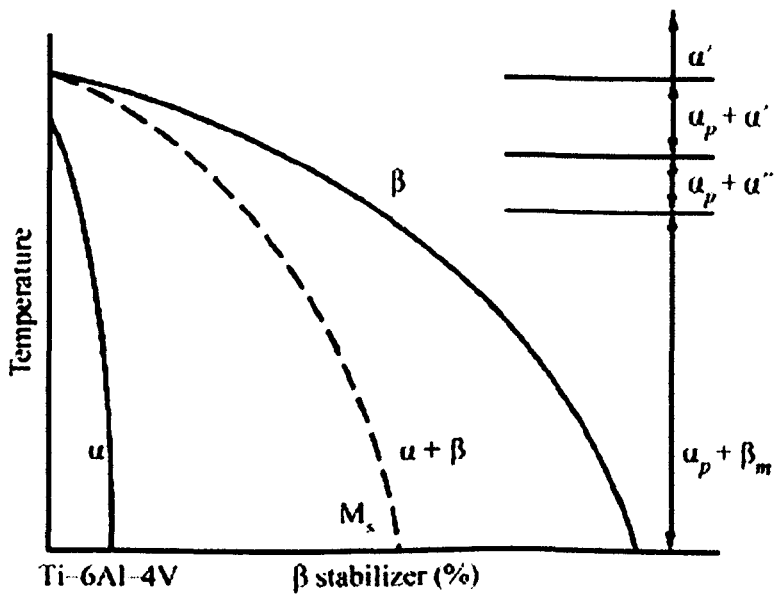

Figure 2.7: Pseudobinary phase diagram of titanium and a beta stabilizer [42, 43].

These alloys can also be found in other applications, e.g., aerospace, power plant, sporting goods, automotive, orthopaedic implants and other service applications due to their high strength along with good corrosion resistance. The finer beta grain structure of β-alloys enhances ductility at lower solution temperatures.

2.5.6 Near β-alloys

To reduce the martensitic start temperature (M_s) down to room temperature, a minimum limit of (10-15%) of β-stabilizing elements are added to titanium, thus creating near-β or meta-stable β alloys [44]. This means that there are adequate β stabilizers to avoid cooling through the M_s line (in Figure 2.11), thus avoiding martensitic formation. This allows retention of small amount of β-phase by avoiding the martensitic (α′) structure formed during rapid quenching. The retained β-phase is called meta-stable because it can still precipitate α-phase during heat treatment below the beta transus temperature [45]. If the alloy is hot worked, the β-phase can still be transformed into martensitic (α′) structure by rapid quenching. However, previous studies have observed that, above room temperature, there is possibility for deformation-induced martensite to form [46, 47].

The most widely used Near-β alloy is Ti-10V-2Fe-3Al (Ti-10-2-3). It has good forgeability properties and is used at three strength levels: 965, 1105 and 1190 MPa [48]. Its use for the production of landing gear on the Boeing 777 resulted in a weight saving of about 270kg per airplane. Ti-10V-2Fe-3Al also provides excellent fatigue properties, similar to those of mill-annealed Ti-6Al-4V. In particular; the fatigue strength of Ti-10V-2Fe-3Al is beneficial in the helicopter industry and for use in rotor systems.

In general, the near-β alloys have been used extensively in aerospace, power plant, sporting good, automotive, orthopedic implant, and down hole service applications. Typical Beta and Near-β alloys include: Ti-13V-11Cr-3Al, Ti-8Mo-8V-2Fe-3Al, Ti-15V-3Cr-3Al-3Sn (Ti-15-3), Ti-3Al-8V-6Cr-4Mo-4Zr (Beta C) and Ti-11.5Mo-6Zr-4.5Sn (Beta III).

2.6 Microstructure of titanium alloys

The microstructure of titanium alloys play an important role in determining their mechanical properties such as strength, ductility, fracture toughness and creep resistance. Microstructure development depends primarily on alloy composition, heat treatment, and thermo-mechanical processing (TMP)[49]. Microstructures may be classified into three main groups: undeformed (initial), deformed, and recrystallized. It is widely accepted that the shape of the α-phase particles plays a key role in the development of microstructures [50]. Typically, the initial undeformed α-phase tends to form rectangular plates (or laths), the deformed α-phase consists of recrystallized α structure consists of curved plates which reflect different degrees of spheroidisation [50]

Furthermore, there are two main microstructures resulting from the extreme composition of alpha and beta phases, i.e., acicular/lamellar and globular/equi-axed microstructures [51]. Previous studies [17] have shown that the transformation of the β phase to the α phase can occur by diffusion controlled nucleation and growth, or by a martensitic process, depending on the cooling rate and the composition of the alloy. Generally, the alpha phase in titanium alloys may appear in four different forms:

- as 'primary' or untransformed alpha
- as 'secondary' alpha or transformed β
- as a martensitic α' (hcp) phase
- as a martensitic α" (orthorhombic) phase

2.6.1 Primary α or untransformed alpha

Primary α is an untransformed alpha phase which is remained untransformed when the alloy was heated in the α+β phase field or β phase field during medium to slow cooling. The volume fraction of α decreases as the β transus temperature is approached, when heat-treated at a temperature in the (α+β) field. Sufficient soaking time at a temperature in the (α+β) phase field influences the diffusion-controlled α↔β transformation to approach an equilibrium volume fraction of phases. The various morphologies of the primary α have a strong influence on the mechanical properties of the titanium alloys. For example, fine microstructure increases the strength and ductility of alloys. On the other side, a coarse microstructure is more resistant to creep and fatigue crack growth.

2.6.2 Secondary α or transformed beta

This describes the type of continuous alpha structures that arise during annealing below the transus or cooling through the subtransus region. The beta to martensite transition is responsible for an acicular (plate-like) structure by nucleation and growth in quenched martensite or metastable beta regions. It has various appearances and may be acicular or lamellar, plate like, or widmanstätten structure. Among this acicular or lamellar alpha is

the most common transformation product formed through the transus[52]. Slow cooling from the β phase field results in a fully lamellar microstructure. The formation of alternative plates of α and β during transformation from β phase filed known as lamellar microstructure [17]. During the transformation process, the α-phase starts to nucleate at grain boundaries and grows as lamellae into the parent beta grain. The lamellar structure becomes finer if there is an increase in the cooling rate (as shown in Figure 2.8) [2].

The lamellar microstructure has very good creep resistance and high fracture toughness. The small amount of retained beta at room temperature depends on the concentration of beta stabilizing elements. This alpha/beta lamellar structure is also called a Widmanstätten structure (as shown in Figure 2.9 a). With increasing cooling rate the size of the α colonies as well as the thickness of the individual α plates become smaller. During nucleation, to minimize the overall elastic strains, there is growth of new α plate on the broad face of an existing α plate nearly perpendicular to that plate. This selective nucleation and growth mechanism in combination with the smaller number of α plate within the colonies called basket weave structure or widmanstätten structure.

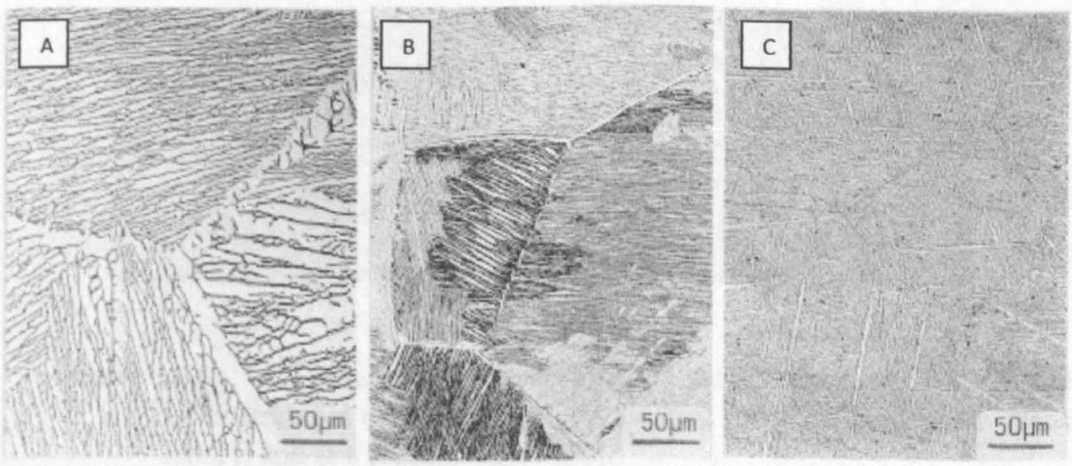

Figure 2.8: Lamellar structures with different cooling rates. A: 1 °C/min, B: 100 °C/ min, C: 8000 °C/min[2]

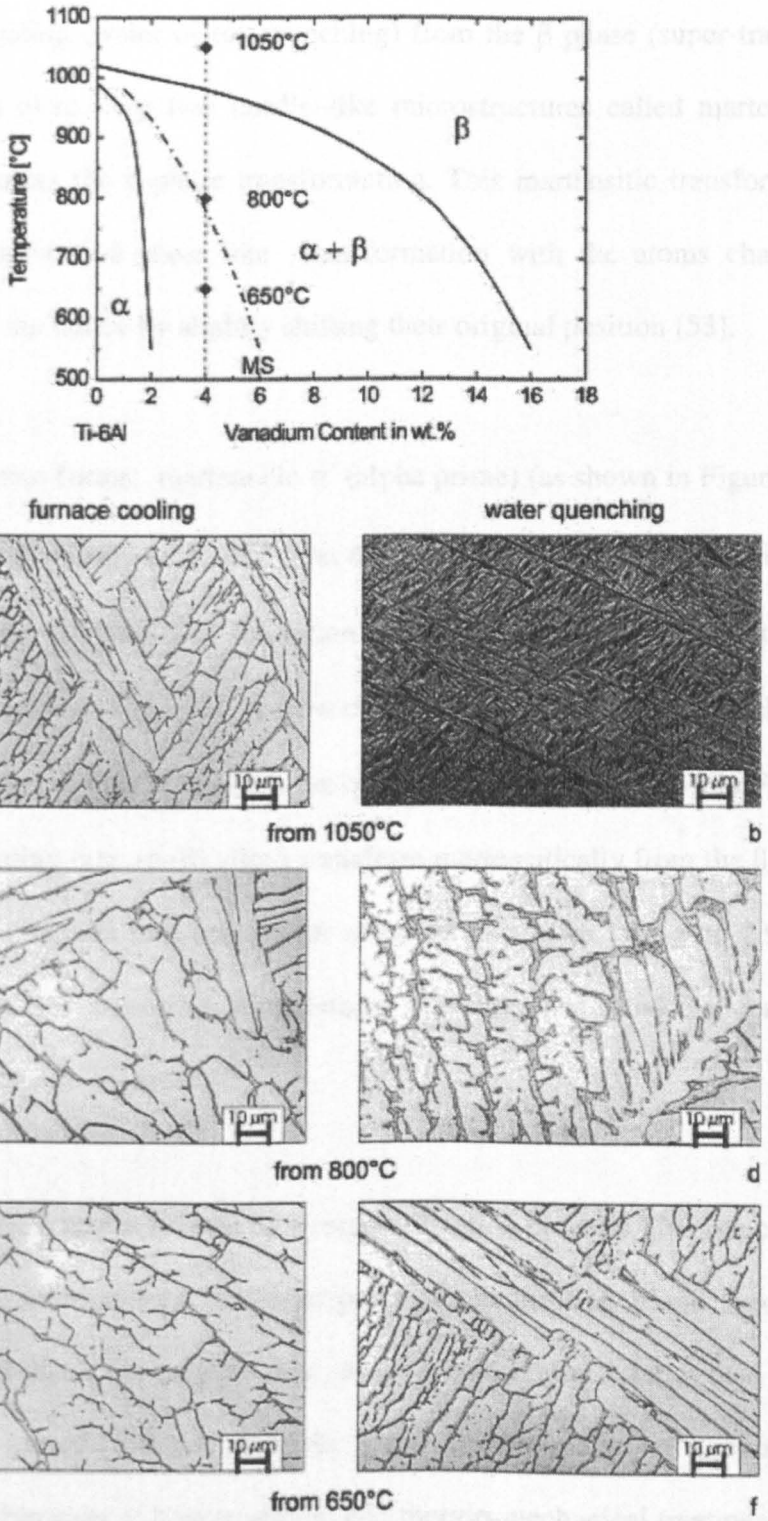

Figure 2.9: A schematic pseudo-binary phase diagram of Ti-6Al-4V; microstructure obtained after slow cooling (50°C/hr) and water quenching from β and α + β phase fields [20].

During high rate cooling (water or oil quenching) from the β phase (super-transus) field, the beta transforms in to very fine needle–like microstructures called martensite. Such rapid cooling eliminates the α-phase transformation. This martensitic transformation is a diffusionless, displacive and shear like transformation with the atoms changing their relative positions in the lattice by slightly shifting their original position [53].

Usually, it can take two forms: martensitic α′ (alpha prime) (as shown in Figure 2.9.b) has a (hcp) structure and orthorhombic α″(alpha double prime). Increasing the β stabilizing elements increases the likelihood of formation of α″ rather than α′. Both forms possess very high strength and low toughness. A slow cooling from the (α+β) phase field results in small amounts of retained beta in between the coarser α lamellae as shown in Figures 2.9.c and e. With high cooling rate, (α+β) alloys transform martensitically from the β phase field to room temperature, results in a martensitic structure as shown in Figure 2.9.d. At low temperature, there is not enough β to transform into martensite and the corresponding microstructure is shown in Figure 2.9.f.

The equiaxed microstructure is created by a recrystallization process. This is a combination of hot working and solution heat treatment processes in the α+β phase field. Here the morphology of the α-phase appears globular, as shown in Figure 2.10. It also has a good ductility and very good fatigue strength, leads preferentially to the superplastic deformation. A combination of heat treatment and thermo-mechanical treatment below the beta-transus temperature results in a bi-modal microstructure.

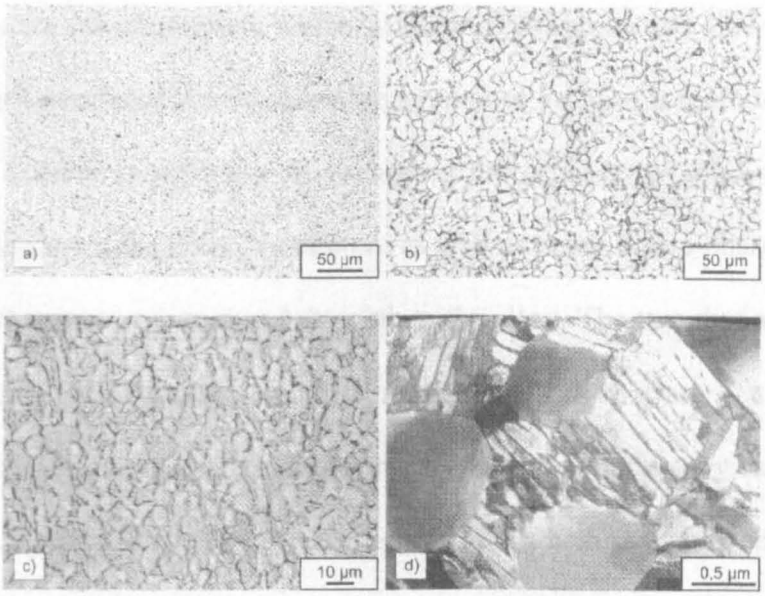

Figure 2.10: Globular microstructures of Ti-6Al-4V: a). fine; b). coarser; c). and d). bimodal microstructures (optical and transmission electron micrograph) [20].

2.7 Ti-6Al-4V

Among titanium alloys, the two-phase Ti-6Al-4V alloy is the most widely-used alloy due to its excellent mechanical properties as well as good corrosion resistance. Ti-6Al-4V was first introduced in 1954 and is considered to be the "workhorse of the industry". This alpha-rich two-phase titanium alloy was originally developed as a construction alloy for the aircraft industry and has also found significant application in the biomedical industry. As well as its high strength-weight ratio, this alloy possesses good fracture toughness, good formability, stiffness, and high temperature properties, which make it an attractive choice for aerospace and military applications.

2.7.1 Phases and microstructure

Ti-6Al-4V alloy has 6% aluminium, which stabilizes the α-phase and 4% vanadium, which stabilizes the β phase; contains a considerable amount of β-phase at room temperature. The 6% aluminium content is sufficient to strengthen the α-phase by solid solution without causing embitterment in the alloy. Vanadium, as well as being a beta-phase stabilizer, also helps to refine the microstructure and strengthen the alloy. The two distinct phases of Ti-6Al-4V can easily be identified by their relative optical contrast – a result of their respective average atomic mass. The alpha phase, which is stabilized by elements with low atomic number, appears darker relative to beta phase, which is stabilized by the heavier elements. The β–transus temperature of Ti-6Al-4V is 995± 5 °C. Figure 2.11 shows the development of microstructures in Ti-6Al-4V after solution treatment.

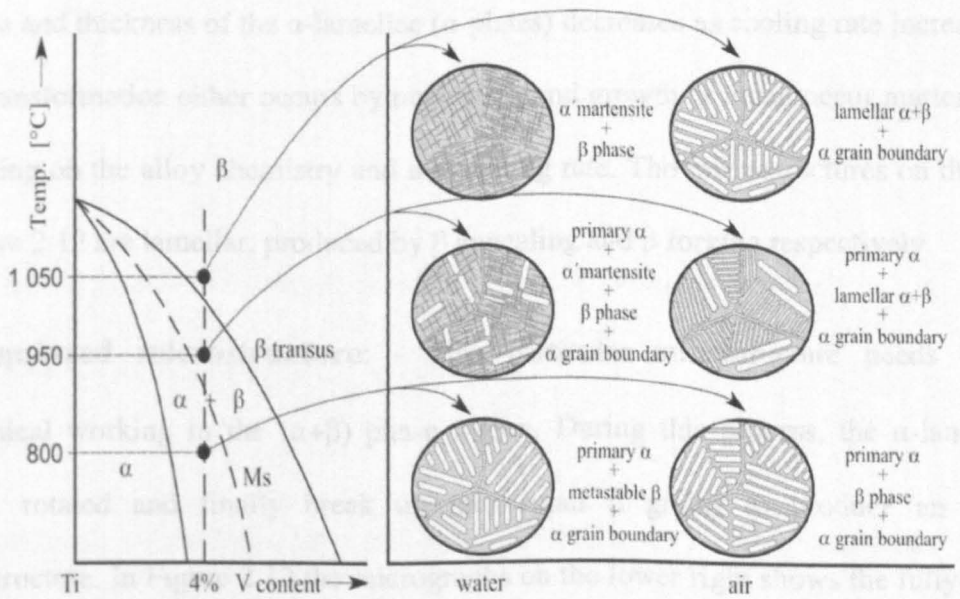

Figure.2.11: Development of microstructures after solution treatment of Ti-6Al-4V [31].

Beside the alpha and beta phases, depending on the thermo-mechanical processing and the cooling rate, Ti-6Al-4V also exhibits other phase's α', α'' and α_2 as described below.

- **α' (hexagonal close packed martensite)** - formed when the alloy is quenched from a near-transus temperature (e.g. 900°C). It has an either acicular or fine lamellar microstructure and crystallographically similar to the α-phase.
- **α'' (Orthorhombic martensite)** –obtained by quenching the alloy in the temperature range of 750 -900 °C. It is softer than α' martensite.
- **α_2 (Ti3Al precipitation)** – This occurs when the oxygen content is less than 0.2wt% after heat treatment in the temperature range 500-600 °C.

(a) Lamellar microstructure: - can be obtained in the final step of thermo-mechanical treatment i.e., by annealing above the beta transus - also called "β annealed" structure. The most important parameter which influences the characteristic features of the lamellar microstructure is the cooling rate from the beta phase field. Slow cooling produces coarser plates of α-phase and fast cooling produces needle like α' martensite. The size of the α/β colonies and thickness of the α-lamellae (α-plates) decreases as cooling rate increases. This $\alpha \rightarrow \beta$ transformation either occurs by nucleation and growth or it can occur martensitically, depending on the alloy chemistry and the cooling rate. The microstructures on the top left in Figure 2.12 are lamellar, produced by β annealing and β forging respectively.

(b) Equiaxed microstructure: - This particular microstructure needs extensive mechanical working in the (α+β) phase region. During this process, the α-lamellae are kinked, rotated and finally break up into small α grains to produce an equiaxed microstructure. In Figure 2.12 the micrographs on the lower right shows the fully equiaxed microstructure of two-phase titanium alloy.

(c) Bi-modal microstructure: - This is obtained by cooling below the β transus temperature i.e., in the (α+β) region and consists of a combination of equiaxed primary α grains dispersed within a β transformed matrix. The bi-modal microstructures are shown in the upper right of the Figure 2.12.

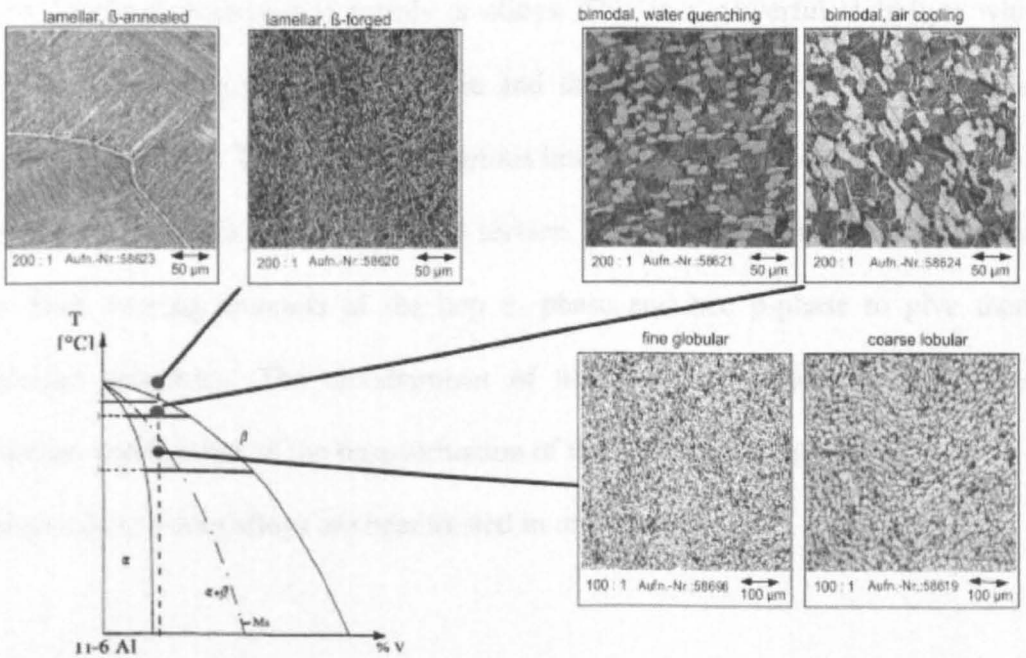

Figure 2.12: Typical microstructures of the alloy Ti-6Al-4V[54].

2.8 Thermo-mechanical processing of titanium alloys

2.8.1 Introduction to heating processes

Heat treatment is a fundamental metallurgical process and has a series of processing steps consisting of heating and cooling of metals in solid state in order to produce desired properties. However, the responses to heat treatment vary depending on the composition of the metals and alloys used for the process. The heating processes can make metal stronger,

harder and also enhance ductility. The most of the heat-treatment processes are similar to each other, but differ in the temperature to which the metal is heated up and rate at which it is cooled. Thus, the heat treating processes are influenced by the working temperature, soaking time, rate of cooling and quenching medium used.

The thermo-mechanical processing (TMP) is a combination of working (deformation) and thermal (heating) treatment in metals or alloys. This is a powerful technique which can control or manipulate the microstructure and the mechanical properties during cooling from beta phase field. The purpose of various hot working operations is to develop a fine, uniform microstructure suitable for final service. Most of the commercially used titanium alloys have varying amounts of the hcp α- phase and bcc β-phase to give them their remarkable properties. The development of titanium microstructures depends on the mechanism and kinetics of the transformation of the β-phase during cooling.

Titanium and titanium alloys are heat treated in order to [55]:

- relieve residual stresses developed during fabrication process called stress relieving.
- increases strength for the special application purpose by solution treating and aging.
- produce an optimum combination of ductility, machining, dimensional and structural stability by annealing process.
- enhance the special properties such as fracture toughness, fatigue strength, and high temperature creep strength by solution treatment process.

2.8.2 Annealing

To achieve a stress-free, equilibrium structure, the titanium and titanium alloys are annealed at temperature range 600°C to 900°C with various time duration depending on the

size, shape and amount of cold work performed on the material. In the processes of achieving desired mechanical properties, various types of bulk annealing treatments are introduced such as, single, duplex, beta and recrystallization annealing [56].

This process enhances the material properties such as toughness, dimensional stability, low temperature ductility and improved machinability. During this process, the development in desired properties is generally produced at the expense of some other property [57]. Thus; annealing cycle should be carefully selected according to their final service. Typically, the alloys such as a near-alpha and the alpha-beta alloys may need more than one annealing treatment in order to improve their final properties. The common annealing treatments are:

- Mill annealing
- Duplex annealing
- Recrystallization annealing
- Beta annealing

Mill annealing

Mill annealing is a general heat treatment given to all mill products, particularly Ti-6Al-4V alloy, which is commonly used in the mill annealed condition. Heating the product to a temperature between 710 ℃ and 790℃, holding for one to four hours and followed by air cooling is a typical mill annealing process for Ti-6Al-4V.

Duplex annealing

Duplex annealing is applied to Ti alloys to improve their creep resistance and/or fracture

toughness. This is achieved by annealing the material twice, which alters the shapes, sizes and distributions of phases to a required level. For example, in the duplex anneal of the Corona-5 (Ti-4.5A1-5Mo-1.5Cr) alloy [58], the first annealing is very close to the beta transus (at 900°C one hour +air cooling) to globularize the deformed α as well to minimize its volume fraction and followed by low-temperature anneal (close to 788°C + 30 minutes and air cooling) to precipitate new acicular α between the globular α particles [59]. The subsequent annealing after first annealing treatment further stabilizes the two-phase microstructure and affords high strength, good ductility and toughness.

Recrystallization annealing

The deformed titanium and titanium alloys are heated close to α+β range, soaked for two to three hours and slow cooled in order to improve their properties such as, fracture toughness and resistance to stress-corrosion cracking at an annealed strength level. This type of treatment tends to enrich a low volume fraction of residual beta phase or produce an equilibrium microstructure composed of equiaxed alpha and residual beta- phase. The purpose of recrystallization annealing is to regenerate the crystals by re-forming the microstructure, without causing phase transformations. This removes the results of any heavy plastic deformation during fabrication, such as in the case of highly shaped cold formed tools.

Beta annealing

Beta annealing is also used to improve fracture toughness of the material. It is accomplished by heating the material to a temperature slightly above the β transus in order to avoid excess grain growth during annealing process. Beta annealing is followed by slow

cooling. Heating above beta transus temperature results in complete beta microstructure which transforms to an acicular alpha structure upon cooling. These, transformed beta microstructures have excellent toughness which is a desirable properties for service applications. For example, the alloy Ti-6Al-4V (rolled strip) is beta-annealed to prevent excessive grain growth.

2.8.3 Solution treating and aging

This heat treatment is used to achieve varying degree of strength levels in the α + β alloys by developing a metastable β-phase in α + β phase field or β-phase field. The metastable β-phase, which existed in α + β phase field, is retained at ambient temperature by rapid cooling from the elevated temperature. Here, the soaking time increases with increasing the thickness of material because this relates to the temperature uniformity (within the section) and solid solubility equilibrium conditions.

A rapid cooling from the solution treated temperature promotes the maximum heat treatment response, for example strengthening or hardening in α + β alloys. This also helps to avoid the formation of grain boundary alpha which in turn improves the ductility of the material and also prevent decomposition of the β-phase during cooling. Thus, the rate of cooling from the solution treating temperature has a strong effect on strength of the alloy. In general, titanium and titanium alloys are solution treated either above or below the beta transus temperature in the alpha-beta region. However, the solution treating temperature depends on the alloy composition and specific property requirements after aging. Eventually, the change in temperature alters the amounts of β-phase as well as change the aging response of the alloy (see figure 2.13).

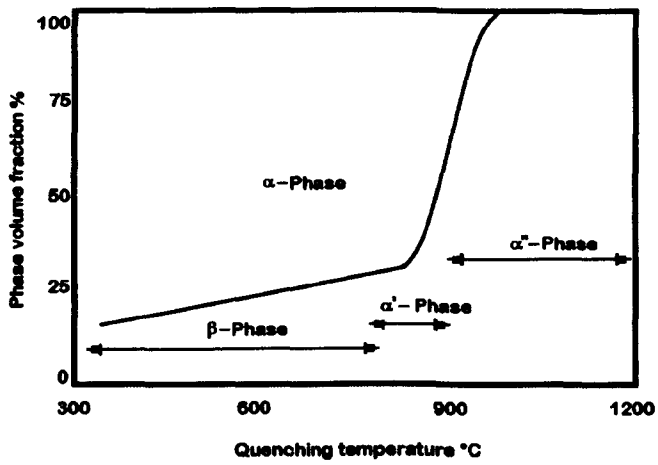

Figure 2.13: Volume fraction of β- phase constituent after quenching [60].

To obtain high strength with adequate ductility, α + β alloy solution treated at temperature 20°C to 80°C below the β- transus temperature. On the other hand, the β- alloys are heat treated above the β- transus temperature to obtain rapid grain growth in the single phase. β-annealing or β-solution treating may be used to improve fracture toughness or stress corrosion resistance. Usually, the combination of properties such as ductility, creep, fracture toughness and stress-rupture properties are achieved by heat-treating α + β alloys below β- transus temperature. If the α + β alloys are heat treated slightly above the β-transus temperature provides enhanced creep resistance with decreased ductility and fatigue strength. The typical time/temperature combinations for general industrial solution treatments for two-phase Ti-6Al-4V alloy are given in table 2.5 [55].

Table 2.5 Typical solution and aging treatments for Ti6Al4V [55]

Solution temperature [°C]	**Solution time [h]**	**Cooling rate**	**Aging temperature [°C]**	**Aging time [h]**
955-970	1	Water	480-595	4-8
950-970	1	Water	705-760	2-4

Normally, the aging treatments are recommended to achieve high strength in titanium alloys. This is considered a final step in the heat treating process and cause the transformation of high temperature metastable β-phase to α′ phase during aging. Finally, leaves a residual enriched beta phase and alpha precipitate upon aging. However, during aging there is a possibility for several reactions to take place simultaneously, to promote wide range of strength levels in material. For example, there is formation of intermetallic components upon aging.

2.9 Introduction to forming processes

The term metal-forming refers to a group of manufacturing processes by which a metal billet or blank is plastically deformed between tools or dies to obtain the desired final shape. It is one of the oldest and principal fabrication processes as compared to other fabrication processes such as casting and powder metallurgy. Until the 13^{th} century, most of the metal forming process was done by hand using tilt hammer to fabricate hot forged bars and plates. The design and control of metal forming processes are very complex and depend on many factors, including the mechanical properties of the work piece at the process temperature, plastic flow, and the friction at the tool-material interface, the heat generation and transfer during plastic flow and temperature. Several forming operations may be necessary to transform the initial simple geometry into a complex geometry without degrading materials properties. Metal forming processes can be classified into two groups [61] ; they are 1. Bulk metal forming processes (Table 2.6), 2. Sheet metal-forming processes (Table 2.7).

Table 2.6 Various types of bulk metal forming processes [61]

Forging	Rolling	Extrusion	Drawing
1. Open-die forging 2.Closed-die forging 3.Coining 4.Forward & Backward Extrusion Forging 5.Radial forging or Cogging 6.P/M forging 7.Upsetting	1. Sheet rolling 2. Shape rolling 3. Tube rolling 4. Ring rolling 5. Cross rolling 6. Surface rolling 7. Shear forming	1. Non lubricated hot extrusion 2. Lubricated extrusion 3. Hydrostatic extrusion	1. Die drawing 2. Drawing with rolls 3. Ironing 4. Tube sinking

Table 2.7 Sheet metal forming processes [61]

Forming process	Examples
Bending	Break bending and roll bending
Surface contouring of sheet	Stretch forming, creep forming, bulging
Linear contouring	Linear stretch forming, roll forming
Deep recessing and flanging	Spinning, deep drawing, rubber pad forming.
Shallow recessing	Dimpling, drop hammer forming, electromagnetic forming, explosive forming, joggling.

Titanium alloys can be relatively difficult to form because of their high deformation resistance (sensitive to strain rate), low ductility, large anisotropy, and strong microstructural sensitivity to processing. These properties confine the size, precision and quality of titanium products and increase the production cost and cycle [62]. The other

characteristics that may cause nonuniformities in sheet forming include notch sensitivity, low shrink capabilities and embrittlement by interstitial contamination. At room temperature the unalloyed titanium behaves like cold-rolled stainless steel, but at 650°C the formability of most of the titanium alloys is comparable to the annealed stainless steel at room temperature. Therefore, hot forming promotes the forming characteristics of titanium by increasing the ductility, decreasing the yield strength at the same temperature and also diminishes the spring back and spring back non-uniformity characteristics of titanium with increasing forming temperature.

2.9.1 Forging of titanium alloys

Forging plays a vital role in the manufacture of wrought metal products such as nuts, bolts, crank shafts, and turbine discs for power generation turbines and air-craft engines. Therefore, the forging process in titanium alloys creates both cost-effective forging shapes as well as in combination with thermal treatment to develop unique or tailored microstructures to achieve the desired final mechanical properties through TMP routes [63].

Forging is used to fabricate large cross sections and near net shape parts of titanium alloy components in order to control the microstructure by thermomechanical processing. A number of forging shapes together with variety of forging processes such as radial, precision, rotary, metal powder, and isothermal forging and finally superplastic forming, have recently been introduced and used for the application of sophisticated process design tools. The pressure requirement during forging primarily depends on the chemical compositions of the alloy, forging strain rate, lubrication conditions, die temperature and the type of forging being manufactured. In general, forging in titanium alloys is performed

either above or below β-transus temperature to break up the initial cast structure into a fine-grained equiaxed α/β microstructure. In many cases, additions of two or more forging methods are performed to obtain desired final microstructure [64].

There are two main metallurgical approaches to the forging of titanium alloys [63]: (a) the conventional α-β forging or forging the alloy below the beta transus; (b) the β forging is performed above the beta transus temperature (in figure 2.14) [65].

a. Conventional α-β forging

- forging can be usually performed at a temperature about 30°C to 100°C below the β transus.
- α-β forging is performed for α, α-β, and metastable β alloys at temperature where both α and β phase are present and also used to develop optimal strength/ductility combinations and optimal high/low-cycle fatigue properties.
- during deformation, the heating time and temperature must be carefully controlled to avoid overheating of the microstructure as well as cracking problems at high strain rate.
- the desired microstructural developments can be produced by controlling the amount of deformation and strain rate resulting from recrystallization process.
- with this technique, it is easy to achieve the resultant as- forged microstructure, that is deformed or equiaxed primary α in a transformed β matrix. Usually, air cooling is preferred after α/β forging to maintain the final desired microstructure.

b. β forging

- this forging technique applies to α, α-β, and metastable β alloys in which most

of the forging work is done at temperature above the beta transus of the alloy.

- to avoid excessive grain growth and hydrogen pick-up during forging, the soaking time prior to forging must be carefully controlled and maintained.
- this technique usually results in a microstructure consisting of Widmanstätten or acicular primary α morphology in a transformed β matrix.
- this process can enhance the properties such as fracture toughness, fatigue crack propagation resistance and creep resistance of the α-β alloys.

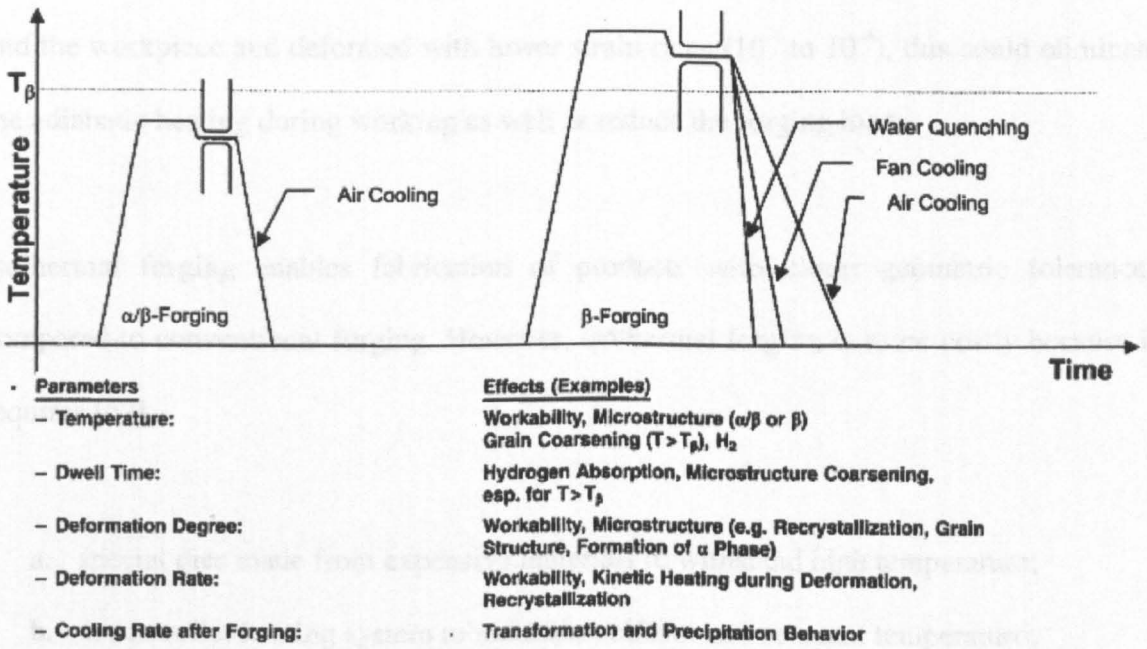

Figure 2.14: Influence of forging parameters on titanium alloys forging [65].

2.10 Isothermal forging of titanium alloys and advantages

During conventional forging, the dies are pre-heated to a temperature of about 315 to 425°C before being forged in order to reduce the die chilling effect. A die chilling can affect the forging characteristic as well as the quality of the forged products. If there is a

decrease in working temperature due to die chilling, this would alter the flow behaviour and enhance the flow stress of titanium alloys, which may cause cracks or defects in the final forged parts. During isothermal forging (IF), the dies are at nearly the same temperature as the work piece in order to avoid die chilling effect. Therefore, the workpiece can be formed at constant temperature with low strain rate. IF process is capable of producing a wide range of microstructures, by a combination of mechanical working and controlled heat treatment conditions, that would not be possible from heat treatment alone [66]. If the isothermal forging is performed at a constant temperature between dies and the workpiece and deformed with lower strain rates (10^{-1} to 10^{-4}), this could eliminate the adiabatic heating during working as well as reduce the forging loads.

Isothermal forging enables fabrication of products with closer geometric tolerances compared to conventional forging. However, isothermal forging is more costly because it requires [67];

a. special dies made from expensive materials to withstand high temperature;
b. a controller heating system to maintain uniform and constant temperature;
c. high temperature lubricant acting as thermal insulators;
d. high temperature coating or inert atmosphere conditions to protect from oxidation.

2.10.1 Workability of metals

Workability of a metal is an important design consideration in a forging process and it is defined as a type of complex property describing the relative ease with which a metal can be shaped through plastic deformation. The evaluation of the workability of a metal involves the measurement of the metals resistance to deformation and determination of maximum possible plastic deformation without fracture taking place [68].

The workability of materials is usually described by its flow stress and flow stress functions such as strain, strain rate and temperature as well as failure of materials and the metallurgical transformations involved. In order to assess the workability of a material, several laboratory simulation tests include compression, tension, torsion and bending have been developed and used successfully [68]. As compared to other tests, the compression or hot upset test has been used to investigate the workability of metals because of its capability of achieving maximum amounts of plastic deformation without any geometrical instability, such as necking, which is a major problem in tension tests. To optimise forging processes, several mechanical test methods and modelling techniques have been developed [69] and utilized for designing a better forging process in order to achieve the best quality finish in terms of grain size, grain flow characterization and uniform microstructure of materials.

2.10.2 Deformation mechanism and restoration process

Hot working of metal and alloys at temperatures above $0.5T_m$ (melting temperature) have several advantages than cold working. Firstly, since the flow stress is lower at high temperatures, less pressure is required to attain required deformation compared to cold working. Secondly, metals are usually capable of achieving larger strains at high temperatures without fracturing. Furthermore, high temperature deformation assists in the homogenization of the cast metal structure [70] and increase the ductility of metals. In general, an increase in strain rate intensifies the flow stress, whereas an increase in temperature decreases the flow stress.

It is an established fact that, for a metal, the external force is accommodated by the relative displacement of atomic planes and this phenomenon is well known as 'slip'. Slip in crystals occurs mainly by movement of dislocations. Other mechanisms can be active at elevated temperatures, such as vacancy migration by the diffusion of atoms and cross slip whereby dislocations jump from their slip planes to another plane.

Dislocations are a type of defect found in all metals. To some extent all real crystalline solids contain imperfections, i.e., the distortion of regular pattern of the crystal lattice. In the case of the pure metals, there are two types of defects on the atomic scale, namely point defects and line defects. The point defects are characterised by the local removal/introduction of single atoms whereas line defects are the imperfect region extends in one dimension, such as dislocations. Plastic deformation of annealed metallic materials increases the number of lattice defects by several orders of magnitude. In particular, the densities of dislocations increase with deformation. The increase in dislocation density makes the flow stress to increase, because the generation and movement of new dislocations become more difficult as they interact and cause tangles. This phenomenon is called strain hardening.

If the metal is subjected to large plastic deformation, most of the plastic work is almost instantaneously converted into heat and the remaining energy (~1%) is stored in the material as defects, such as dislocations [71]. Therefore, small amount of the work expended during deformation is not transformed into heat, but retained in the elastic distortion fields surrounding each individual crystal defect.

If a plastically deformed metal is heated above certain temperature, the density of lattice defects is lowered to the pre-deformed state by two irreversible processes called recovery and recrystallization, which were driven by the stored energy. Recovery process involves

the annihilation and restructuring of dislocation clusters into energetically more favourable configurations [72]. Recovery is followed by recrystallization, which involves nucleation and growth of new grains.

If the deformation takes place at high temperatures, there is a possibility for the occurrence of these restoration processes to occur during the deformation, i.e. while the stored energy continues to be introduced. The processes are therefore called dynamic recovery and dynamic recrystallization, as opposed to the static annealing processes. The static and dynamic processes have many features in common, but they have different deformation and softening mechanism. The dynamic restoration processes have great industrial significance, but it does not well characterize in titanium alloys due to their experimental difficulties and theoretical modelling problems. It is usually occurs during metalworking processes such as hot rolling, extrusion, and forging.

2.10.3 Dynamic recovery and Recrystallization

Dynamic recovery and recrystallization play a significant role in lowering the flow stress and thus reducing the forces during the mechanical shaping processes such as rolling, forging, and extrusion when the work pieces are large.

(a) Dynamic recovery

During the hot deformation, dynamic recovery (DRV) occurs in metals and alloys that have high stacking fault energy (SFE). Dynamic recovery (DRV) process gradually decreases the number of dislocations as well as promotes the rearrangements of remaining

atoms into orderly arrays. Like diffusion process, the rate of recovery depends on temperature and so recovery appears to involve diffusion.

Heating a cold-worked metal to temperature below recrystallization results in minor dislocation rearrangements and the elimination of excess vacancies that were generated during the working process referred as a recovery processes which tend to change physical properties of metal. This dislocation rearrangement helps to relieve elastic stresses or strains without softening the metal.

The reduction in stress during dynamic recovery improves ductility and also reduces the stress concentrations at any notch or defects in metals. Moreover, the dynamically recovered structure is quite stable and considerably stronger than the recrystallized structure. The stable structure can be retained if the hot-worked metal is quenched quickly to room temperature. For example, extruded and unrecrystallized, aluminium-magnesium alloy have enhanced strength for architectural purposes.

(b) Dynamic recrystallization

Dynamic recrystallization involving dislocation elimination by grain boundary (GB) migration in the formation of new grains occurs after a critical strain rate. This phenomenon was initially discovered by Claude Rossard and P. Blain in France and by D.Hardwick, C. Micheal Sellars and Tegart in 1966 [73]. Dynamic recrystallization nucleates from grain boundaries which usually form from the dense tangles of dislocations due to the unlimited cross-glide and climb and in-sufficient annihilation. According to Sakai and Jonas [74], dynamic recrystallization occurs in materials with moderate to low stacking fault energy when they are subjected to high temperature deformation.

During deformation, metals become stronger due to work hardening. Cold metal working processes causes grains to elongate in the flow direction and to become thinner in other directions but the grain volume remains unaltered which results in increased dislocation density. As a result of increased dislocation density and increased grain boundary area, a metal is higher in energy which leads to a structural change in the metal. This can be softened through an elevated temperature heat treatment which can produce strain-free grains (i.e. grains with low dislocation density), consisting of equiaxed grains with much lower dislocation density, termed as recrystallization process [75]. This called can be used to restore metal ductility and enhance further cold deformation.

When recrystallization occurs after deformation, it is known as static recrystallization (SRX). In some cases dynamic recrystallization (DRX) may initiate through nucleation, but may not proceed to completion during deformation. In such cases, the recrystallization is completed after deformation by the growth of dynamically nucleated grains, known as Metadynamic or post dynamic recrystallization (MDRX) [76].

MDRX is sensitive to the strain rate applied during the deformation, but is relatively insensitive to the total strain and temperature of the deformation. On the other hand, SRX is sensitive to the total strain imposed on the material during deformation as well as the temperature, but insensitive to the strain rate. For example, during rolling and extrusion, the recovery and recrystallization can be revealed by change in the grains scale as portrayed in figure 2.15.

In cold-rolling (Figure 2.15(a)) the grains are flattened, hardened and internally

distorted by the applied strain and persist until the metal is annealed. In hot-rolling (Figure 2.15(b)), the crystals remain soft due to dynamic recovery and the grains are similarly flattened, but are not distorted to the same extent as compared to cold-rolling. Here, there is no sign of recrystallization, but there would be static recrystallization after deformation because the metal remains hot.

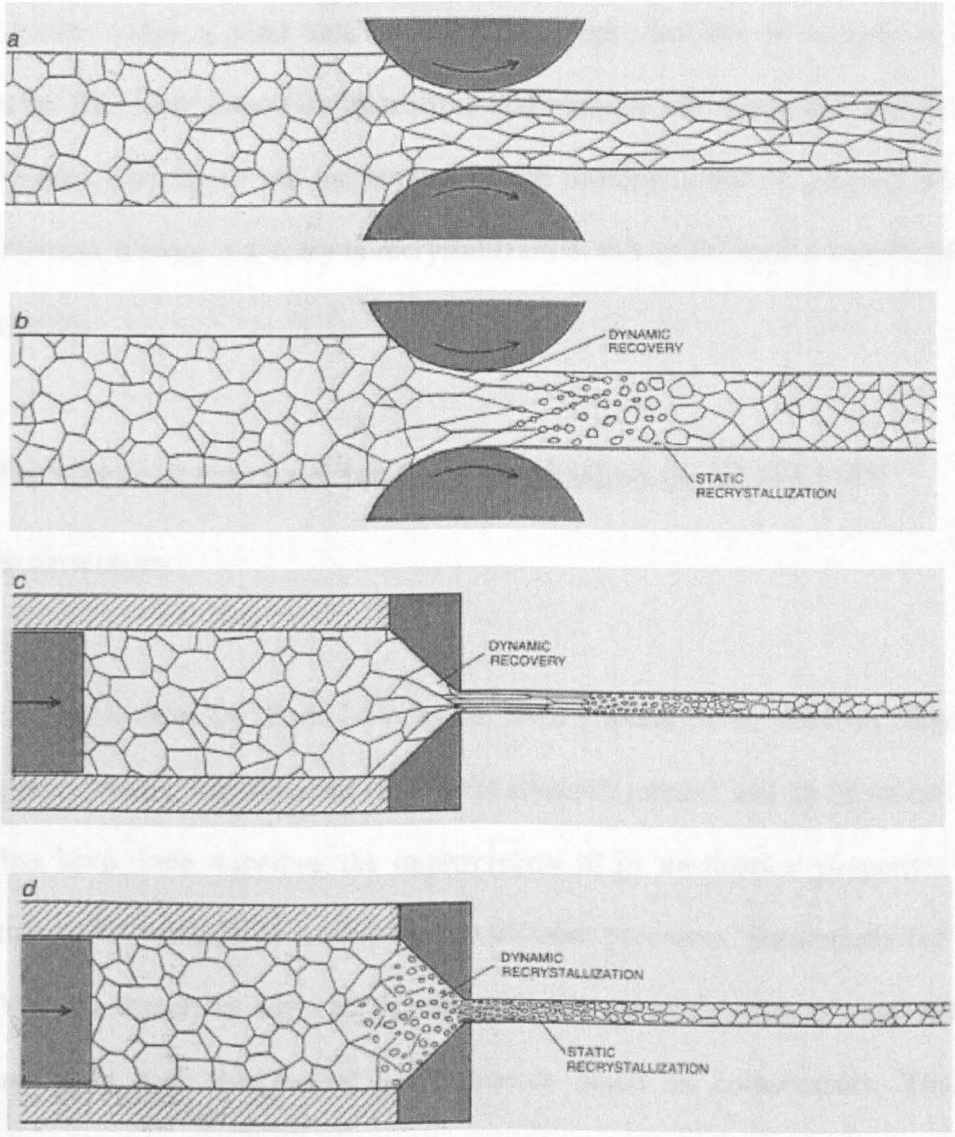

Figure 2.15: Schematic diagram describing recovery and recrystallization during metal forming process: (a) cold-rolling; (b) hot-rolling; (c). cold-extrusion; (d) hot-extrusion (adapted from [77]).

In hot extrusion at a high strain the metals that undergo dynamic recovery do not recrystallize until after deformation (Figure 2.15(c)), whereas metals in which recovery is limited recrystallize dynamically during deformation and again statically after deformation (Figure 2.15d).

In general, the actual grain size of most metals is from 10 to 1,000 microns. Dynamic recrystallization plays a vital role in imparting high ductility to metals at elevated temperatures. The most important microstructural variable like grain size depends on the recrystallization, and hence, on the control of the forming schedule. During normal hot working process, if there is a delay in recrystallization, this could lead to coarser grains and poor properties.

2.11 Microstructure and texture evolution in Ti-6Al-4V

(a). Microstructure

As discussed in section 2.5, Ti-6Al-4V, as the most popular ($\alpha+\beta$) titanium alloy used in the aerospace industry, has attracted significant research interest and an enormous amount of work has been done regarding the improvement of its mechanical properties through heat treatment, hot working or a combination of these processes. Particularly for forging, Ti-6Al-4V is an important material for the near net shape forming of medium weight components with high mechanical performances (such as compressor). Thus, great attention is given in the scientific literature to the study of the behaviour of this alloy under deformation. Most of the research centred on improving the microstructure and texture in order to attain appropriate mechanical properties.

The main objective of the present work is to establish advanced characterization techniques to quantify the effect of TMP parameters on the evolution of microstructure and texture in two phase (α+β) Ti-6Al-4V. However, no quantitative analysis of the evolution of microstructure parameters with deformation texture in Ti-6Al-4V has been reported in literature before. The breakdown of the colony-alpha microstructure during (α+β) thermomechanical processing plays a pivotal role in obtaining a uniform, fine equiaxed-alpha microstructure in forging bar and billet, plate and other alpha/beta titanium mill products. Most of the research in this area has focused on the workhorse alloy of the aerospace titanium industry, Ti-6Al-4V. A number of investigators have examined the kinetics of the globularization of (α+β) titanium alloys during subtransus hot working [1, 5, 78]. Most of these efforts have focussed on modes of loading such as uniaxial compression, tension during deformation. The possible mechanisms by which lamellar microstructures coarsen or transform to a globular morphology have been studied by various investigators [79-84]. As a result, a number of mechanistic models have been proposed to describe the process which includes, boundary splitting and lamellar termination migration [85-90].

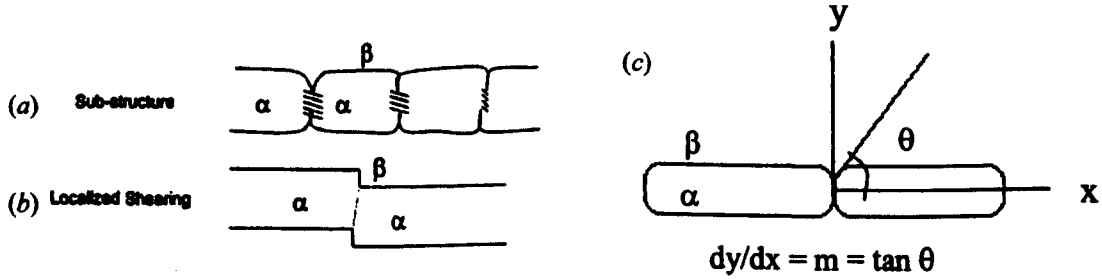

Figure 2.16: Illustration of the splitting of alpha/alpha boundaries created by (*a*) recovery and (b) shearing of the alpha phase and (c) schematic illustration of the grooving/boundary splitting process showing the definition of the slope m [7].

Boundary splitting mechanism has been explained by Stefansson and Semiatin [112]. This mechanism requires an internal boundary through the thickness of one of the lamellar phases as shown in Figure 2.16. The boundary may be a pre-existing grain boundary or a subgrain boundary/deformation band introduced during cold or hot working (Figures 2.16 (a) and (b)). Such a boundary creates an unstable (90°) dihedral angle. To lessen surface tension, the dihedral angle is reduced and stabilized by the diffusion of inter lamellar phase into the boundaries (Figure 2.16 (c)). Eventually, the diffusion of the second phase into the boundary (thermal grooving) results in a pinch off and two new terminations due to the elimination of the inter lamellar boundary [86]. Later, the mechanism by which the colony-alpha phase is converted into a globular morphology during deformation and post deformation annealing of alpha-beta titanium alloys such as Ti-64 has been studied by Margolin and Cohen [91], Weiss and co-workers[5, 92-94] , and Peters et al. [95].

The work of Weiss et al., [96]on Ti-6Al-4V provided insight into the mechanism of globularization and showed that the main driving force for dynamic globularization was the formation of intense shear bands within the alpha lamellae. They also identified two ways by which the lamellae globularize; both involve boundary splitting due to creation of boundaries across the alpha lamellae as shown in figure 2.16. They observed that the alpha-alpha boundaries derive from the formation of a recovered substructure or by intense localized shear across the alpha lamellae as a result of deformation. If the strain is large enough, shear bands may lead to fracture and complete segmentation of an alpha lamella. In the absence of fracture, the alpha/alpha interfaces formed by shear bands or internal high-angle boundaries can give rise to surface-tension driven penetration of the alpha plates by beta phase, as postulated by Margolin and Cohen [113]. They stated that the rate of penetration by the beta phase depends on diffusion kinetics and the ratio of the interfacial energies of alpha/alpha boundaries and the alpha/beta interface.

Finally, Stefansson and Semiatin [7] investigated static globularization behaviour following hot working. At longer times, globularization was controlled by mass transport from the ends to the centre of residual alpha platelets, thereby resulting in alpha particles whose diameter was substantially greater than the initial alpha platelet thickness.

The kinetics and mechanism that control the globularization of the platelet, or widmanstätten, alpha morphology have been investigated by number of researchers [46, 91, 96-98]. Margolin and Cohen [91], also proposed a model for the globularization of both lamellar plates within the prior-beta grains as well as grain-boundary alpha. The mechanism of globularization of widmanstätten alpha during hot working is depicted in Figure 2.17 (a-d). The creation of new terminations due to boundary splitting, as described above in Figure 2.16, leads to termination migration, which consists of the transfer of mass from the curved surfaces of the lamellar terminations to the flat surfaces of the lamellae as shown in Figure 2.17 (a-d). The driving force is provided by curvature differences between the lamellar terminations and the flat lamellar interfaces [85, 87].

Lutjering [2] has shown that among the all microstructural characteristics, the alpha colony size has the most significant influence on the mechanical properties. It has been shown that parameters such as the cooling rate from the β-phase field, the initial β grain size and the presence of interstitial impurities (oxygen and carbon), can affect the geometrical arrangement within the microstructure of the Ti-6Al-4V alloy.

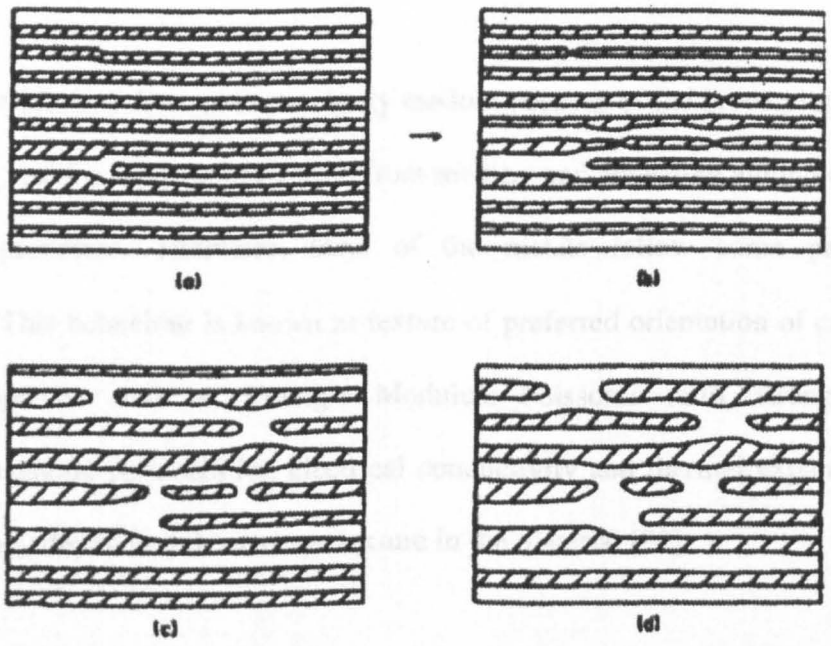

Figure 2.17: Progression of lamellar termination migration stages during hot working. The sequence (a ,b, c & d) indicates the increase in strain during the process [81].

Several investigations have also elucidated the effect of strain level and the mode of deformation on globularization behaviour during hot deformation. For example, Semiatin et al., [1] showed that after an upset reduction of approximately 65 percent at $T=T_{\beta}$-90°C and strain rate $2x10^{-3}$ s^{-1}, Ti-6242 contained an appreciable fraction of essentially undeformed Widmanstätten colonies. A similar work was done by Malcor et al., [78] on forging of Ti-64 at T_{β}-30°C and strain rate of $1.4s^{-1}$. In this study, only partial globularization was observed.

(b) Texture

Grain orientations in polycrystals are rarely random because of the processing history such as hot rolling, cold rolling, solidification from melting and annealing among other thermo-mechanical processes. Therefore, most of the metals follow some pattern in the orientations. This behaviour is known as texture of preferred orientation of crystals. Many material properties such as Young's Modulus, Poisson's ratio, strength, ductility, toughness, magnetic permeability, electrical conductivity and thermal expansion (in non-cubic materials) depend on the average texture in the material [99].

In general, a practical way to denote an orientation is via the Miller indices. It is a system of notation which denotes the orientation of the faces of a crystal and the planes and directions of atoms within that crystal. The orientation of a crystal plane is most commonly defined by the intersection of crystal plan on main crystallographic axes of the solid. A set of numbers which represents the intercept and used to uniquely identify the plane is known as Miller indices (hkl). In HCP metals the Miller-indices are denoted by the (h,k,i,l). Orientation distribution function (ODF), describes the frequency of occurrence of particular orientations in a three-dimensional (Euler) orientation space. This space is defined by three angles (Euler angle), which constitute a set of three consecutive rotations that bring the crystallographic axes (e.g. a1- or c-axis) of each crystallite into coincidence with the specimen axes. The orientation g is normally identified using three Euler angles ($g = \{\varphi_1, \varphi, \varphi 2\}$. The Euler angles then describe the transition from the sample's reference frame into the crystallographic reference frame of each individual grain of the polycrystals. The three reference axes are labeled as **X, Y & Z**; also commonly known as ND, RD, and TD. The three crystal axes are labeled as **X', Y' & Z'**; also commonly known as [100],

[010] & [001] in cubic crystals. The texture in rolled sheet hexagonal metals, are commonly represented by $\{h\ k\ i\ l\}$ $\langle u\ v\ t\ w\rangle$, which means that the $\{h\ k\ i\ l\}$ planes of these grains lie parallel to the sheet plane, whereas their $\langle u\ v\ t\ w\rangle$ direction point parallel to the rolling direction [100]. Examples of typical rolling textures in the form of pole figures, as a function of c/a ratio is shown in Figure 2.18 and other typical textures in hexagonal materials are shown in Figure 2.19.

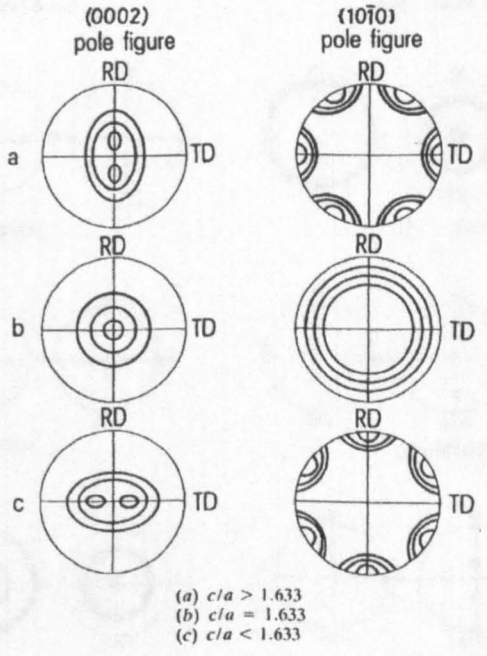

Figure 2.18: (a).Schematic sheet textures in hcp materials as a function of c/a ratios. a. c/a > 1.633, b. c/a = 1.633, c. c/a < 1.633

The crystallographic textures developed during the hot working of alpha/beta titanium alloys have been well documented because of its large effect on a variety of mechanical

properties, [101-103]. For example, during rolling and extrusion these textures are a strong function of the deformation mode, deformation temperature, and per cent reduction. For hexagonal, phase component, textures are often represented by (0002) pole figures that depict the spatial distribution of the normal (poles) to the basal planes on stereographic projections.

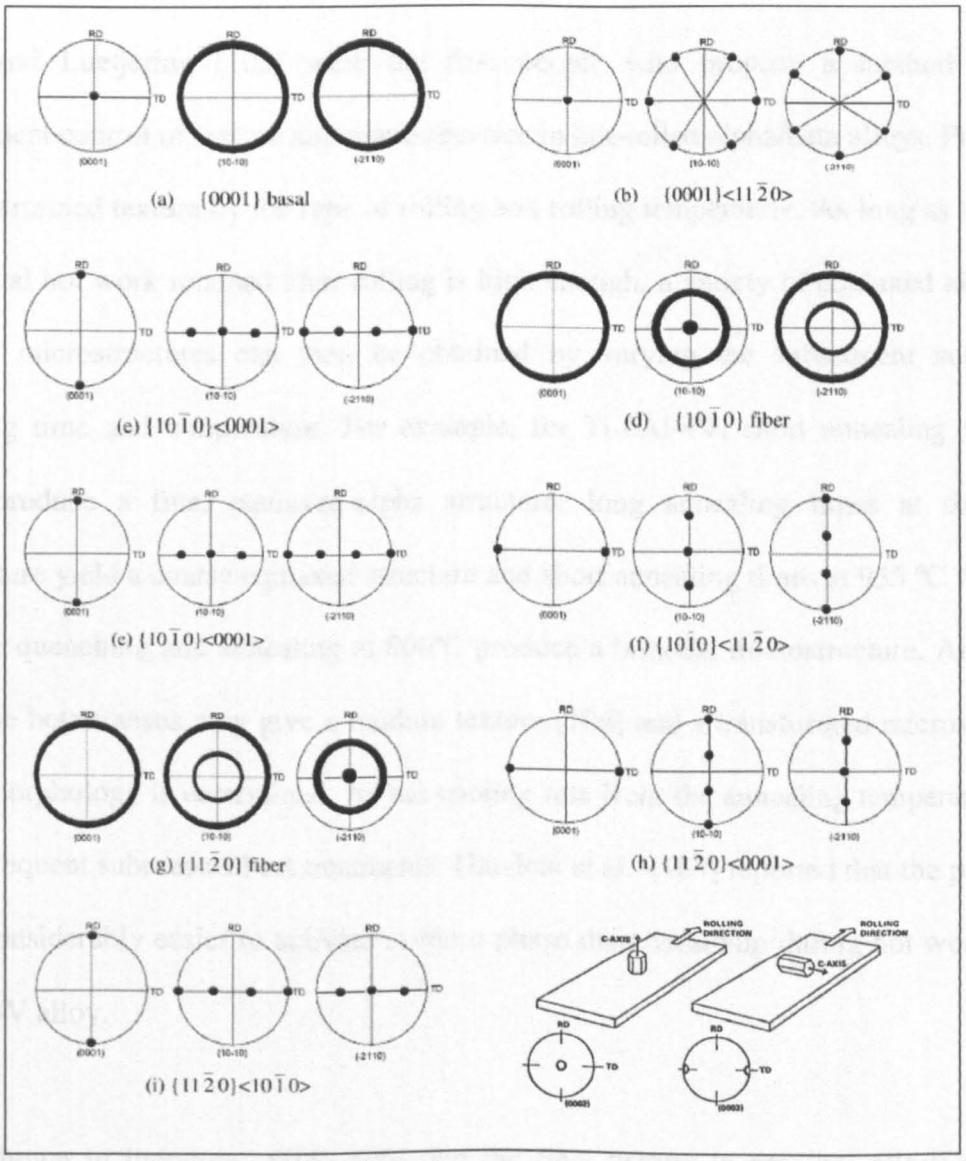

Figure 2.19: Ideal pole figures of hcp materials-Mg (c/a = 1.624)[104]

Sometimes due to the uncertainty of the crystallite orientation with respect to rotations about the basal pole, a second pole figure of (10-10) is measured. Williams and Stark [105] have summarized the textures developed during unidirectional hot rolling of Ti-64, show that the hot working temperature relative to the beta transus temperature has a strong influence on the deformation textures that are developed.

Peters and Luetjering [103] were the first people who propose a method for the independent control of texture and microstructure in hot-rolled alpha/beta alloys. Primarily, they determined texture by the type of rolling and rolling temperature. As long as the level of residual hot work retained after rolling is high enough, a variety of equiaxed alpha and bimodal microstructures can then be obtained by varying the subsequent subtransus annealing time and temperature. For example, for Ti-6Al-4V, short annealing times at 800°C produce a fine, equiaxed-alpha structure; long annealing times at the same temperature yield a coarse equiaxed structure and short annealing times at 955 °C followed by water quenching and annealing at 800°C produce a bimodal microstructure. Annealing above the beta transus may give a random texture [106] and a transformed microstructure whose morphology is determined by the cooling rate from the annealing temperature and any subsequent subtransus heat treatments. Glavicic et al., [107] reported that the prismatic slip is considerably easier to activate in the α phase than basal slip during hot working of Ti-6Al-4V alloy.

It was shown in literature [108, 109] that the final texture in titanium alloys strongly depends on processing (deformation and heat treatment) parameters, but only a few of them [110, 111] have been concerned with attempts to clarify the influence of phase

transformation on final texture. In Ti-6Al-4V alloy it was found [111] that the $\beta \rightarrow \alpha$ phase transformation could proceed with or without the variant selection depending on the heat treatment employed.

Due to the low volume fraction of the β phase (<10%) [112, 113], the deformation behaviour is dominated by the hexagonal close-packed hcp alpha phase which has a structure with limited number of slip systems [114]. Although slip in the body-centred cubic β phase has an effect on the deformation of Ti-64, the majority of the plastic strain is accommodated by the hcp phase (α) and texture evolution is not noticeably affected by slip in the β phase [115].

Chapter 3

Materials and Experimental Methods

This chapter describes the details of the hot isothermal compression tests carried out on the material and the metallurgical characterization of the material studied in this project. In order to evaluate the workability of a material at high temperatures, the hot isothermal compression testing method is frequently used because it has been proven to be more suitable method than conventional tensile testing[116]. As part of present work, isothermal hot compression upset tests were performed on cylindrical specimens at temperatures and strain rates similar to those used in industrial forging operations. Isothermal processing has an advantage over normal processing in that the temperature gradient between the dies and the specimen is much lower than the normal processing [117] which eliminates the chilling effect of the dies on the specimen.

This chapter briefly describes all the techniques used in the present work. The microstructural evolution of the material with various heat treatment procedures and thermo-mechanical treatment (i.e. hot isothermal compression testing) was studied using Light Optical Microscopy (LOM) and Scanning Electron Microscopy (SEM).

3.1 Microscopy and Diffraction Techniques

3.1.1 Quantitative metallography and Image analysis

Quantitative metallography is a general term which includes several techniques for characterisation of three dimensional microstructures from two dimensional sections. Several methods have been developed and published by ASTM to measure various microstructural features, but these are often insufficient to characterize the complexity of microstructure observed in titanium alloys. One of the image analysis software employed was 'Image J', a public domain, java-based image processing program developed at the National Institute of Health (USA) [118] . This software was specifically developed for use in image analysis of biological tissues, but has many tools that are applicable in the analysis of metallurgical microstructures.

In the present work optical micrographs were analysed using the quantitative image analysis software ImageJ [119] and Image Tool [120]. Here, ImageJ software was used to quantify the volume fraction of primary α-phase, whilst Image Tool was used to determine area, length, width, perimeter, orientation and aspect ratio of the primary α-phase.

3.1.2 Texture measurements

The texture of a polycrystalline material is a representation of the orientations of its crystallites with respect to a macroscopic sample coordinate system [121]. By measuring texture, important information about the degree of anisotropy of the material can be

obtained. Most commonly, the techniques used for texture analysis rely on diffraction and Bragg's law. X-rays, neutrons or electrons are diffracted by lattice planes. The main techniques for texture measurement with respect to the type of radiation used to examine can be classified as Macrotexture (i.e. average orientation data from many grains) and Microtexture (i.e. single orientation). X-rays and EBSD are the most popular methods for macrotexture and microtexture analysis respectively. Pole figures and ODF (orientation distribution functions) can be used to represent the aspect of macrotexture and microtexture measurements.

A set up reference is used to specify an orientation, each of which is known as a coordinate system. For example, for a rolled product, the direction associated with the rolling direction (RD), the direction normal to the rolling direction (ND) and the transverse direction (TD) are chosen according to direction associated with the external shape of the specimen. The relationship between the specimen coordinate system and the crystal coordinate system is shown in Figure 3.1.

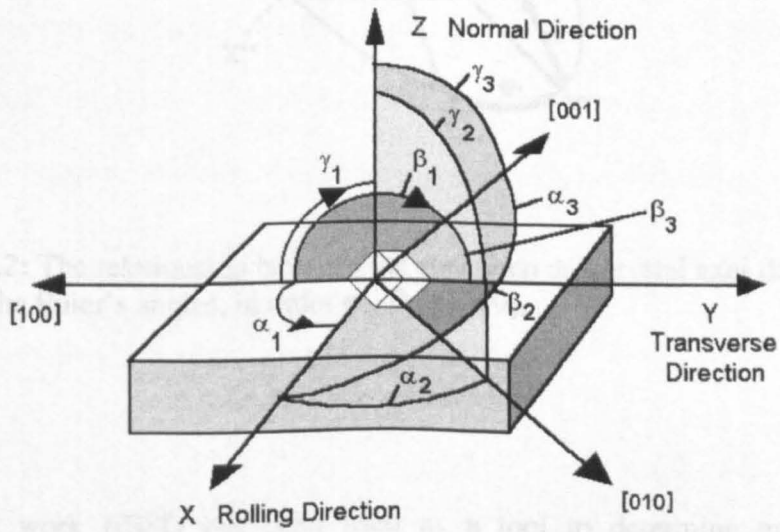

Figure 3.1: The schematic representation of relationship between coordinate system XYZ (for a rolled product) and the crystal coordinate system [100], [010], [001] [99].

The orientation distribution in textured materials can be evaluated by the crystallite orientation distribution function analysis (ODF) [122]. This ODF describes the frequency of occurrence of particular orientations in a three-dimensional Euler's space. This space is defined by three Euler angles (φ_1, Φ, φ_2) which are related to the macroscopic axis of the sample (as shown in Figure 3.2). For hexagonal specimen symmetry, these axes φ_1, Φ, and φ_2 with each of the Euler angles ranging from 0 to 90°.

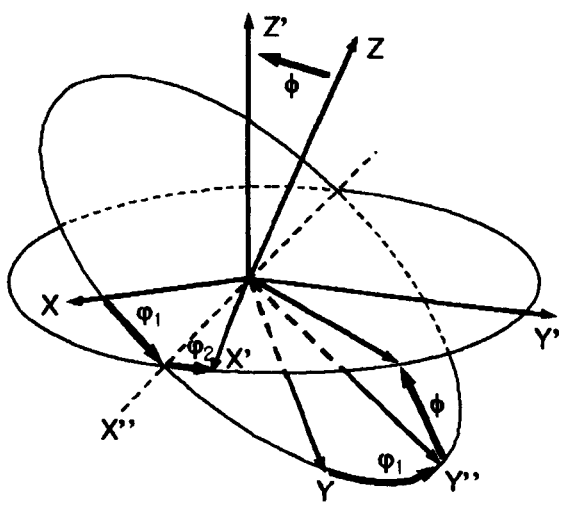

Figure 3.2: The relationship between the specimen and crystal axes directions through the Euler's angles, in order φ_1, Φ, φ_2 [99].

In the present work EBSD has been used as a tool to determine grain orientation distribution and neutron diffraction has been used for bulk texture measurements during

hot compression testing. Some of the computation was carried using the versatile features of the free and open-source MATLAB (Math Works, Natick, MA, USA) software toolbox MTEX [123, 124] providing a unifying approach to texture analysis with individual ('EBSD') [123]or integral ('pole figure') orientation measurements. MTEX is a MATLAB Toolbox designed to visualize crystallographic geometries, diffraction data, recover orientation density function (ODFs) and also used to calculate texture characteristics like pole figures, inverse pole figures and ODFs. In particular, this method can be used to determine the arbitrary crystal and diffraction geometries, superposed pole figures and the unknown normalization coefficients of the pole figures along with ODF measurements [125].

3.1.3 Electron backscatter diffraction method (EBSD)

The electron backscatter diffraction (EBSD) technique is used for determining the crystallographic information of individual crystals in a polycrystalline material [126] using the field emission gun scanning electron microscope (FEGSEM). The use of EBSD technique has become widely popular due to its significant advances in pattern acquisitions and data processing routines, which are time consuming. Nowadays, EBSD is relatively fast and highly sensitive method, with which local electron diffraction analysis can be performed over large area. In recent years the development of the EBSD technique is reviewed by Randle and Engler [99] and Adam [127].

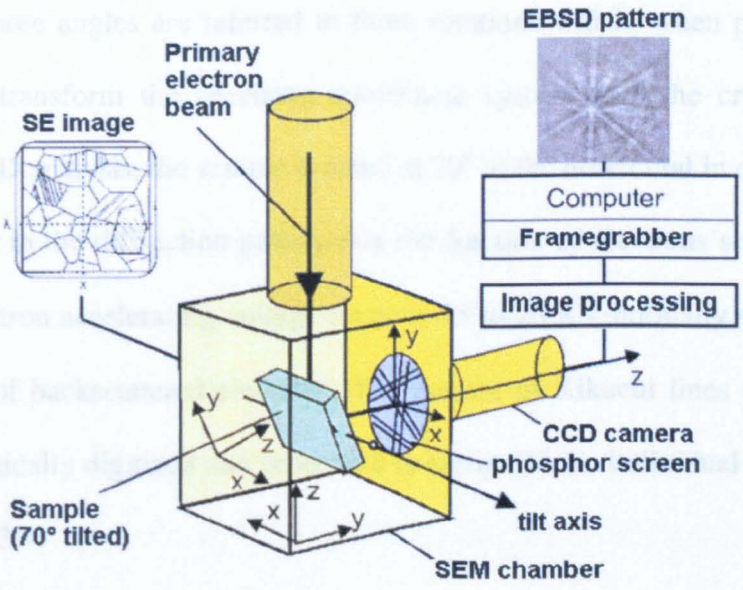

Figure 3.3: The setup for EBSD analysis [128].

The microstructural parameters, which are not obtainable from conventional methods of grain characterisation, are now routinely available from EBSD analysis. The EBSD acquisition hardware generally comprises a sensitive CCD camera, and an image processing system for pattern averaging and background subtraction. Using the EBSD acquisition software, it is easy to control the data acquisition and store the respective data.

In EBSD, the orientation of a crystal at a particular location is deduced from a diffraction pattern which is produced by the back-scattered electrons. During the process, a stationary electron beam hits a tilted crystalline sample (shown in Figure 3.3) and the diffracted electrons can produce a pattern on a fluorescent screen. The pattern reveals the characteristic of the crystal lattice structure and orientation of the sample region from which it was generated. The characteristic pattern is called a 'Kikuchi' pattern, as shown in Figure 3.4.

The resultant orientation is typically expressed in the form of a set of Euler angles, Φ_1, Φ, and Φ_2. These three angles are referred to three rotations which, when performed in the right sequence, transform the specimen coordinate system onto the crystal coordinate system. For EBSD analysis, the sample is tilted at 70° to the horizontal in order to optimise both the contrast in the diffraction pattern and the fraction of electrons scattered from the sample. The electron accelerating voltage range is 15 to 20 KV normally used, to generate a large number of backscattered electrons. The pattern of Kikuchi lines on the phosphor screen is electronically digitized and processed to recognize the individual Kikuchi lines as shown in Figure 3.4.

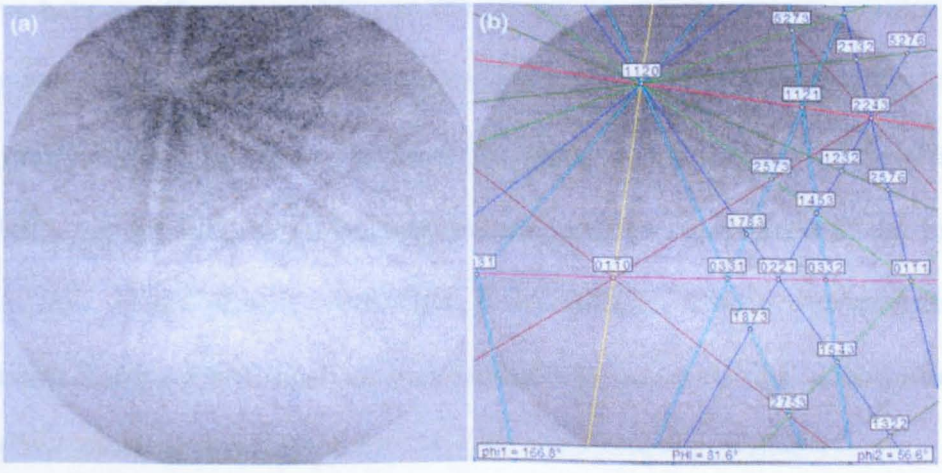

Figure 3.4: A characteristic Kikuchi pattern of Ti-6Al-4V[129].

If the tilt angle is less than 70° than the contrast in the diffraction pattern decreases. The scanned beam in a grid across a polycrystalline sample and the measured crystal orientation at each point and the resulting map will reveal the information about grain morphology, orientation and boundaries. Using EBSD data it is possible to evaluate the

texture of the high-temperature phase from the measured orientation of the low-temperature phase in cases where the phase transformation obeys a specific orientation relationship [130].

A quantitative representation of the sample microstructure can be established with EBSD. Diffraction patterns recorded on a phosphorous screen are then used to determine the texture of the material at the scanned points. After data processing, one can get pole figures and inverse pole figures. The stereographic projections of the scanned surface present the texture distribution over the analysed surface. Using these measurements, it is also possible to determine the average grain size and grain size distribution, and get information about grain boundaries. The EBSD measurements are useful to determination of the local relationships between microstructure and crystal orientation. For example, direct correlation between the orientations of the grains in which some particular event is occurring, such as oxidation, recrystallization, grain boundary crystallography etc., can be obtained. Furthermore, EBSD is also used for phase identification or crystal structure. Using EBSD, the quantitative microstructural analysis can be obtained in the form of an orientation map. In the present work, HKL CHANNEL5 software was used for texture measurements and the EBSD analysis was carried out on as-received, solution-treated and deformed Ti-6Al-4V specimens.

3.1.4 Neutron diffraction method using GEM

The neutron diffraction technique is a powerful tool to obtain the quantitative texture analysis of materials. Neutron texture analysis are useful in the determination of bulk and local textures of compact samples, the determination of coarse grained materials, and the determination of minority second phases [121]. Neutron diffraction texture analysis

fundamentally relies on Bragg's law and operated in the conventional constant-wavelength mode with steady-state reactors and, using time-of-flight techniques, with pulsed neutron source. This law stipulates that neutron waves reflect on lattice planes if the condition $2d_{hkl} \sin\theta = \lambda$ is satisfied.

According to Bragg's law, d-spacing patterns, which with a continuous source are collected by applying the conventional angle-dispersive method (variation of the instrumental parameter θ) at a constant wavelength λ, are here recorded by using the wavelength- or (energy)dispersive method (variation of the instrumental parameter λ) at fixed scattering angle(s). In a polycrystalline material a detector at a particular orientation relative to the incident neutron beam only records signals from the lattice planes that satisfy the reflection condition. In textured sample the overall signal intensity changes if the sample is rotated relative to the detector and, if several detectors are available, each detector records different intensities and differently oriented crystals. From these intensity variations for different lattice planes (hkl) the orientation distribution can be obtained.

Quantitative texture measurements utilizing X-rays or electrons require careful sample preparation to minimize surface effects and corrections for absorption but using neutrons for such measurements all of the above issues are easily avoided. Due to the high penetrating capability of neutrons, bulk texture can be easily investigated. Since the 1960's neutron diffraction has been employed regularly to determine crystallographic textures. Using TOF neutron diffraction complete spectra with many diffraction peaks, rather than individual peaks, are recorded. A detector at a fixed scattering angle θ are used to records a whole d-spectrum for each sample orientation. The relative intensity differences between hkl's for different detectors of a bank are indicative of texture.

The principle of texture analysis by X-rays or neutron diffraction for all materials is independent of their crystal structure. The texture analysis of multi-phase materials and/or structures with low crystal symmetry have problem like diffraction peak separation which have to be considered [131]. The peak separation is occurred by three major issues, firstly, peak-rich diffraction spectra in both multi-phase and low symmetry materials, secondly the volume fraction of the various phases in multi-phase materials and finally anisotropic of the reflected X-rays in multi-phase materials. In peak-rich diffraction spectra due to the overlapping of various diffraction peaks the separation of the contributions of the corresponding reflections/ phases are directed affected. In particular during pole figure analysis, the peak broadening at high sample tilting can lead to a substantial overlapping of diffraction peaks, which makes texture analysis in complex crystal structures. In contrast to the partial coincidence of reflection peaks, diffraction peaks can also completely overlap and the Bragg's angles are identical too. There are also more severe cases where all diffraction peaks of a given phase are systematically overlapped by another phase which is usually related by a phase transformation. For example, primary α –phase and the martensitic α''-phase in two-phase titanium alloys[115].

Dahms and Bunge [132] developed an analytical technique which achieves peak separation by an iterative procedure of ODF- calculation and recalculation of the corresponding pole figures until proper peak separation is obtained. Later, a similar method has been developed by Kallend et al [133] to separate overlapping peaks based on the direct WIMV-method which assigns weights to discrete points in orientation-space based on measured data in an iterative process. It is a more efficient method to use the whole diffraction spectrum and extract texture information similar to Rietveld technique [134] by which crystallographers usually extract structural information from a powder pattern. A method

proposed by Wenk et al [135] relies on an iterative combination of crystallographic Rietveld profile analysis and quantitative ODF-calculation (RITA, Rietveld texture analysis). According to Rietveld method, the analysis of a diffraction pattern can be pursued by two different approaches: i.e., a full-pattern profile-fitting procedure stating with random texture and structure models of all phases of the material.

Besides the problem of overlapping peaks, it is difficult to determine pole figures for minor phases (small volume fractions) in multi-phase materials. Because, the diffraction peaks of the minor components are much smaller than those of the major components resulting in poor signal-to-background ratio. This is because of the reflected intensity is proportional to the volume fraction of the respective phase. Using, X-ray diffraction there is some limits for texture analysis in order to estimate the minor phase whereas due to the higher penetration depth of neutrons a much larger volume contributes to the reflected intensities in neutron diffraction.

In deformed materials the various phases are highly aligned along the deformation direction. During X-ray texture measurements [131], the difference in the absorption of X-rays in the different phases can cause errors in estimating the texture. Depending on the sample setting-i.e. Bragg angle θ and pole figure angles of two different phases –the intensity reflected in a given phase has to pass through different lengths of the other phases and, hence, is differently attenuated by absorption coefficients in the pole figures obtained. For neutron diffraction, absorption is much lower and –independent of the sample setting – the neutrons are scattered from the total sampled volume so the neutron absorption is not affected by a possible alignment of the various phases [136, 137].

Thus, neutron diffraction method is an efficient method to estimate texture information directly from the Rietveld method, which is capable of determining crystal structures based on the whole diffraction spectrum. The software packages are available to implement texture analysis in the Rietveld method: MAUD (Material Analysis using Diffraction) using both direct and spherical harmonic method [138] and GSAS (General Structure Analysis System) [139] only using the harmonic method. In the present study, the bulk texture measurements of heat treated and deformed Ti-6Al-4V samples were carried out at the GEM facility of the ISIS neutron spallation source at the Rutherford Appleton Laboratory, UK. GEM (General Materials power diffractometer) is a high-count-rate materials neutron diffractometer (shown in Figure 3.5) constructed at ISIS pulsed neutron source in December 2003 [140].

It was designed to study the structure of both crystalline and amorphous (including liquid) samples [141]. The GEM detector array has 7270 individual detector elements in 86 modules with 6 detector banks (banks 1 and 6 covering forward backscattering angles). For texture analysis 164 separate detector groups were generated, with each group covering approximately 10° x 10°. The GEM vacuum vessel is made of 25mm grade 304 stainless steel and is designed to attain pressures as low as 1×10^{-6} mbar. The size of a typical data file for one run on GEM is nearly 37 megabytes. The GEM detectors cover a scattering angle range from 1.1° to 169.3°.

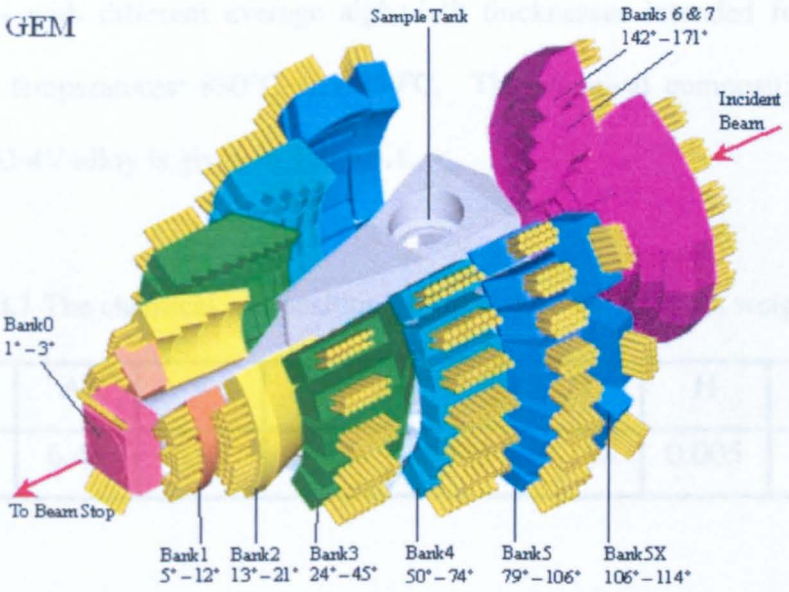

Figure 3.5: A schematic layout of the GEM detector array with detector bank.

3.2 Materials

A round bar of 40mm diameter with lengths of about 90mm of two-phase α+ β titanium alloy Ti-6Al-4V produced by TIMET UK Ltd (Birmingham, UK) was supplied by QinetiQ Ltd (Farnborough, UK). This material was produced by using a standard grade double vacuum arc remelting of TIMETAL Ti-6Al-4V ingot. Using an open die forging press the ingot was β hot-forged to reduce its size down to an intermediate rectangular section. This forging operation was performed in a number of steps and followed by re-heats. The rectangular section was further cut into multiple pieces and β hot-rolled down to an intermediate square section, which was then α + β hot-rolled to reduce its size down to the

final product [142]. The Ti-6Al-4V material investigated here was received in the mill-annealed condition and subsequently heat-treated to produce a range of uniform microstructures with different average alpha-lath thicknesses intended for compression testing at two temperatures: 880°C and 950°C. The chemical composition of the thus obtained Ti-6Al-4V alloy is given in Table 3.1.

Table 3.1 The chemical composition of the Ti-6Al-4V alloy (in weight percent).

Ti	Al	V	Fe	C	O	H	N
89.29	6.48	3.99	0.22	0.023	0.158	0.005	0.002

3.3 Experimental methods

3.3.1 Specimen geometry

In order to conduct the hot compression tests, cylindrical specimens measuring 10mm in diameter and 15mm in height were machined from the supplied material by using Electrical Discharge Machine (EDM) in the Department of Materials Engineering, at The Open University. The specimen geometry for hot isothermal compression test is shown in Figure 3.6. The orientation of the specimens were chosen such that the long axis of the cylindrical specimens corresponds to the long axis of the forged bar. That is, the compression applied during the test was perpendicular the forging direction of the bar manufacturing. The aspect ratio of the specimen, which is defined as the ratio of the original height to the original diameter, was chosen as 1.5 in this study. This is the recommended and widely used geometry for in hot compression testing [143]. In general,

to minimise the effects of friction and die chilling, a long thin test-piece is usually preferred, so that most of the specimen volume is unaffected by the dead-metal zones at the platens. However, buckling can occur if the test-piece aspect ratio is larger than 2 [144].

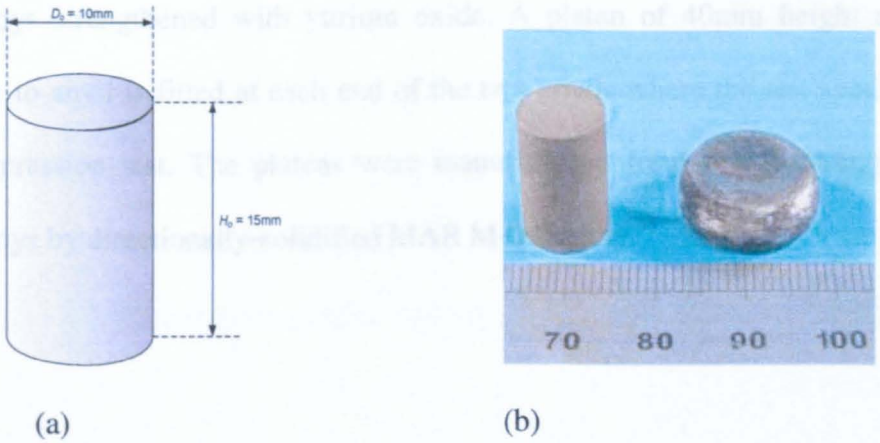

(a) (b)

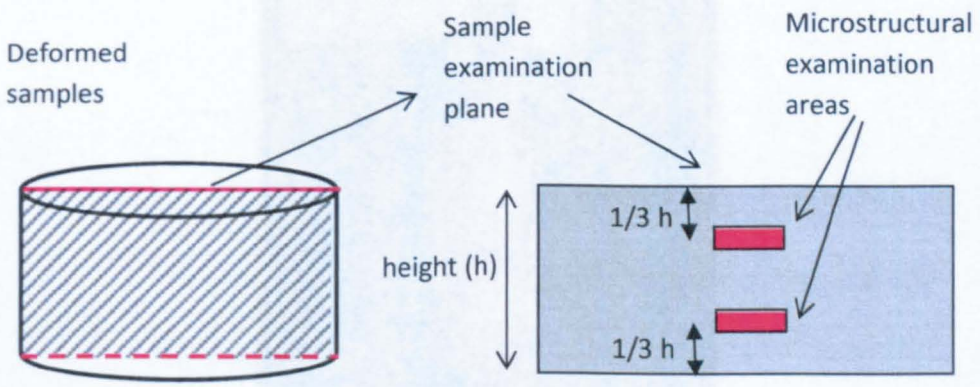

(c)

Figure 3.6: (a) Geometry of the specimens used in the hot isostatic compression testing; (b) A photograph showing undeformed and deformed specimens, and (c) a schematic showing the locations of microstructural examination areas on deformed samples..

3.3.2 Hot compression testing

A series of hot compression 'upset' tests were carried out by using a computer-controlled servo-hydraulic MTS 100kN machine coupled with an Instron Severn Furnaces Ltd

Radiant Furnace model RHS1856A as shown in Figure 3.7. With a 100kN capacity load cell, the testing machine includes two 50mm-diameter rod-like anvils; the upper anvil is attached to the load cell and the bottom anvil is connected to the actuator. These anvils were manufactured via powder metallurgy route from dispersion-strengthened Ni-Cr superalloys strengthened with yttrium oxide. A platen of 40mm height and of similar diameter to anvil is fitted at each end of the two anvils where the test specimen is placed for compression test. The platens were manufactured from a high strength nickel-base superalloys by directionally-solidified MAR M-247 alloy.

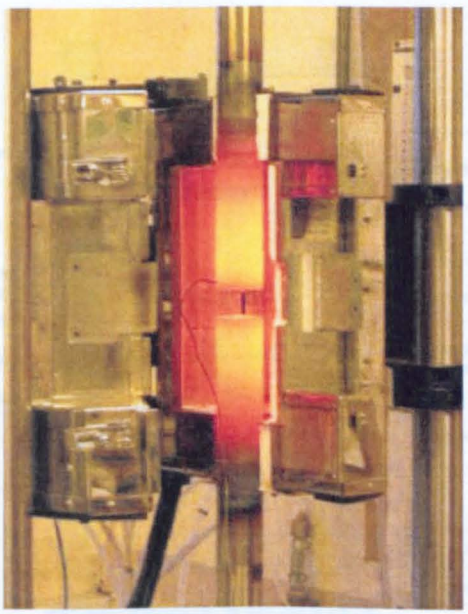

Figure 3.7: The MTS testing system coupled with radiant furnace-Hot compression testing machine.

The radiant furnace, which contained twelve infrared tungsten halogen lamps (240V/1000W each) surrounding both the platens and the specimen, is capable of

achieving a maximum temperature of 1100°C. The furnace was designed in such way that, it can be cooled by water as well as air during operation [145]. The schematic diagram of the hot deformation testing machine is shown in Figure 3.8. The mechanical test system is controlled by Multi-Purpose Testing (MPT) software [146], produced by the MTS Corporation, to perform the hot compression tests under various test conditions. A linear variable differential transformer (LVDT) was attached to the platens to measure specimen displacement during the tests. The main output from the testing was the load measured by the 100 kN load cell and the corresponding displacement measured by the LVDT.

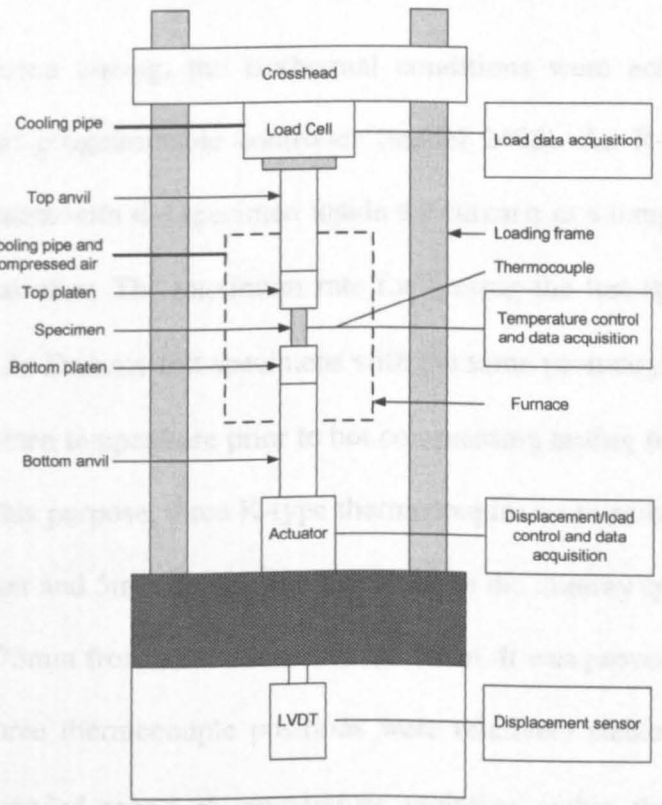

Figure 3.8: Schematic diagram of hot compression-testing machine.

The load – displacement data was then converted into true stress–true strain data using standard equations. Before hot compression testing, it is a standard practise to coat the specimens with a lubricant for surface protection and to reduce friction between platens and specimen[116]. In this work, the specimens were evenly coated with a glass lubricant, Acheson Delta glaze FB-412, for protection against high temperature oxidation. Furthermore, on the top of the glass lubricant, a hexagonal-boron nitride lubricant was applied to minimise the specimen-platen interfacial friction. The boron nitride lubricant was utilised to reduce the specimen barrelling and also helps in separating the dies from the specimen after the test. The lower and upper surfaces of the platens were also coated with the same lubricant.

During hot-compression testing, the isothermal conditions were achieved by using a Eurotherm 8-segment programmable controller (model 2408). An R-type thermocouple was put in direct contact with the specimen inside the furnace as a temperature sensor and plugged into the controller. The maximum rate for heating the test specimen to the test temperature was 1°C/s. Dummy test specimens with the same geometry were used in order to calibrate the specimen temperature prior to hot compressing testing for each temperature measurements. For this purpose, three K-type thermocouples were embedded within small holes, 0.5mm diameter and 5mm depth were machined in the dummy specimen at the mid-height and also at 3.75mm from each end of the specimen. It was proven that the test-piece temperature at all three thermocouple positions were relatively stable within a range of ± 2°C. The recommended range of temperature variation within the test-piece in hot compression testing is ± 4°C [143]. During testing, the two K-type thermocouples were inserted into the upper and lower platens and an R-type thermocouple was attached to the middle of the specimen to monitor its surface temperature. Prior to compression test, a

small compressive load of 150N was applied under load control mode in order to grip the specimen between the platens and also to ensure proper thermal contact between them. During heating, the thermal expansion in the specimen was automatically compensated in the load control mode, which allowed the thermal expansion of the specimen by adjusting the displacement to keep the load constant.

After the test specimens were heated at a rate of 1°C/s to the test temperature, they were allowed to soak for 30 minutes to get a homogenous distribution of temperature throughout the specimen. The specimen was then deformed under constant true strain rate control to a nominal true strain of 1, in a direction that is perpendicular to the forging axis of the original bar. The deformed specimens were then water-quenched as quickly as possible, with a typical time delay of between 3-12 seconds, in order to preserve the as-deformed microstructure. A set of specimens were also heated to the deformation temperature, without subjecting to deformation, given an identical soak, and water quenched in order to determine the undeformed microstructure. Later, these undeformed microstructures were used as reference in order to investigate the microstructure evolution of deformed specimens at different strain rates.

3.3.3 Determination of flow stress by hot compression tests

The data obtained from the compression testing are the load F from the load cell and displacement ΔH (mm) from the LVDT. The true stress is defined as the load F divided by the instantaneous cross-sectional area of the cylinder with diameter D_i. For a homogeneous upsetting test, a uniaxial cylinder with initial height H_0 is deformed to an instantaneous height of H_i resulting in the expansion of the initial diameter D_0 following the law of

volume conservation:

$$D_o^2 H_o = D_i^2 H_i \qquad \text{(Eq.3.1.1)}$$

Assuming frictionless conditions, the uni-axial compressive stress (flow-stress), σ, associated with external applied deformation force F is calculated by:

$$\sigma = \frac{F}{A_i} = \frac{4F}{\pi D_i^2} = \frac{4F}{\pi D_o^2 H_o} \qquad \text{(Eq. 3.1.2)}$$

The true strain in a compression test can be calculated as a function of the instantaneous height H_i of the cylinder by:

$$\varepsilon = \ln\left(\frac{H_i}{H_o}\right) = \ln\left(\frac{H_o - \Delta H}{H_o}\right) = \ln\left(1 - \frac{\Delta H}{H_o}\right) \qquad \text{(Eq. 3.1.3)}$$

The true strain rate $\dot{\varepsilon}$ during compression testing can be expressed in terms of the instantaneous crosshead velocity V_i and the instantaneous height H_i given by:

$$\dot{\varepsilon} = \frac{d\varepsilon}{dt} = \frac{d(\ln H_i / H_o)}{dt} = \frac{1}{H_i}\frac{dH_i}{dt} = \frac{V_i}{H_i} \qquad \text{(Eq. 3.1.4)}$$

As H_i decreases, in order to maintain the constant true strain rate during the test, a servo-hydraulic machine can be employed to reduce the velocity of the moving ram continuously based on the above equation.

3.3.4 Determination of interfacial friction at the interface

During metal forming processes, changing the shape of the workpiece is caused by forcing it to flow through a die system, which requires immediate contact between the die (tool) and the workpiece. Generally, the workpiece and the die move relative to each other under pressure or deforming force which is normal to the die/workpiece interface. This generates tangential frictional forces at the interface of the die /workpiece to resist this relative movement. Therefore, the frictional conditions at the interface of the die and workpiece

greatly influence the metal flow as well as affecting the total deformation load, final properties of the specimen, and cause energy losses or premature die wear [147]. Using an appropriate lubricant, the interfacial friction can be controlled for a specific application. In order to assess the performance of the lubricant and to predict forming pressure or load, it is important to quantify the interfacial friction in terms of a coefficient or a factor [148, 149]. The frictional shear stress τ is calculated by:

$$\tau = \mu\sigma_n \quad \text{or} \quad \tau = f\sigma = \frac{m_f}{\sqrt{3}}\sigma \qquad \text{(Eq. 3.1.5)}$$

Therefore, the value of m_f lies between 0 (frictionless condition) and 1 (sticking condition). From equation 3.1.5, it can be seen that, the frictional shear stress τ, is proportional to the normal stress σ_n (which is the same σ in equation 3.1.2) acting at the interface and also on the friction coefficient μ. The shear stress is also dependent on the flow stress of the material σ, and the friction factor f, of the shear factor m_f.

Thus, in terms of the distribution of strain within a specimen, it is imperative that the degree of friction is known. The friction conditions can be estimated by applying a ring test. The ring-compression test is an experimental test used for the determination of frictional conditions in bulk metal forming. It is a standard method of measuring the friction factor f, developed by Kunogi [150] and Male and Cockcroft [151], which provides quantitative evaluation of friction and gained wide acceptance around the world. It is a simple method where a flat ring shaped specimen is deformed to a known axial reduction. The change in the inner diameter of a short ring specimen when it is compressed between two flat, parallel platens provides information about the coefficient of friction at the workpiece-die interface. During deformation, if the friction is low (good lubrication) the

internal diameter increases; whereas if the friction is high (poor lubrication) the internal diameter decreases. To obtain the friction factor, the internal diameter of the deformed ring must be compared with the values predicted by using various friction factors, f or friction coefficients, μ. The measurements are presented in the form of calibration curves in which the geometry change of a series of rings deformed at various friction coefficients. As shown in Figure 3.4, μ is plotted against the percentage reduction in height of the ring for a range of friction values. As recommended in the literature, each of the ring geometry has its own specific set of curves. Thus, once the percentage of reduction in internal diameter and height are known, one can easily determine the coefficient of friction using the appropriate chart regardless of the ring material and test conditions. Figure 3.9 shows sets of curves that change according to ring geometry of each specimen. The most commonly ring test are performed by deforming ring specimens with the ratio of outside diameter (OD): inside diameter (ID): height (H) of 6:3:2 [152].

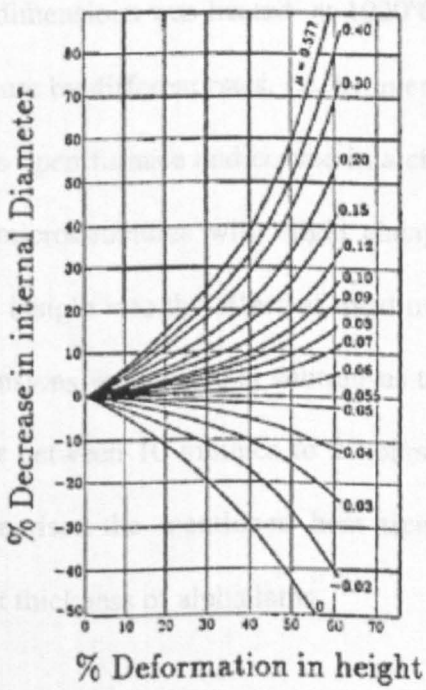

Figure 3.9: Friction calibration curves from ring compression test in terms of μ [152].

The advantages of the ring-compression test are that it does not require any force measurement and also involves large-scale deformation of the workpiece material, as is the case in actual practice. This test can also be used to rate different metalworking fluids.

3.4 Test plan

A preliminary experimental investigation was planned to develop an understanding of the effect of heat treatment on two-phase microstructure and, in particular, on the final thickness of alpha laths – a key microstructural parameter. For this purpose, the microstructural characteristics of the alloy have been studied in temperature ranges covering both $\alpha + \beta$ and β phase fields. To investigate the effect of initial microstructure in the as received material, two samples with dimensions of 4.5mm x 10mm were heated to 950 °C and soaked for 30 minutes, and followed by water and air cooling. Then, a set of five specimens of the same dimensions was heated at 1020°C and soaked for 30 minutes and cooled to room temperature by different rates, i.e. by quenching in water, cooled in air, cooled by a fan, cooled in an open furnace and cooled in a closed furnace. The above sets of experiments resulted in microstructures with slight changes in Widmanstätten α lath thickness. To obtain further insight into the effect of heat treatment a further set of eight specimens of the same dimensions was heated at subtransus temperatures (950 °C and 900 °C) temperatures, soaked for between 10 minutes to 2 hours and then followed by water quenching. Table 3.2 summarises the mentioned heat treatment procedures that were carried out to obtain different thickness of alpha laths

In order to investigate the effect of deformation (strain) on microstructure and texture of Ti-6Al-4V, a series of compression tests were carried out at both subtransus (880°C) and

near-transus (950°C) temperature at strain rates of 0.01, 0.1, and 1.0. Additional tests were carried out at a strain rate of 0.1, which were interrupted at various strain levels of 0.1, 0.2, 0.4, 0.7 and 1.0 to study the evolution of microstructure. For this study, the as-received material with equiaxed initial microstructure, as shown in Figure 3.10, was heat treated by holding at sub-transus temperature of 950°C for 10 minutes, then heating to a super-transus

temperature of 1030°C for 2 minutes and finally water quenched. The heat treated specimens, characterised by acicular microstructure, as shown in Figure 3.11 were subjected to hot compression testing at both sub-transus and near-transus temperature in order to investigate the effect of initial microstructure on the flow stress behaviour. The Figure 3.12 shows the various hot working tests that were carried out to investigate the globularization mechanisms in Ti-6Al-4V.

Table 3.2 Preliminary test program on Ti-6Al-4V

Heat Treatment –I

Alloy	Temp° C	Time	Cooling
Ti-6Al-4V	1020°C	30mins	Water Cooled
	1020°C	30mins	Air Cooled
	1020°C	30mins	Fan Cooled
	1020°C	30mins	Furnace Cooled
	1020°C	30mins	Open Furnace Cooled

Heat Treatment -II

Heat Treatment	Temp ° C	Holding Time	Cooling Medium
950 ° C / 10 Min + 1030 ° C/ 2 Min	950 ° C	2 hours	Water quenched
	950 ° C	30 Min	,,
,,	950 ° C	10 Min	,,
,,	900 ° C	2 hours	,,
,,	900° C	30 Min	,,
,,	900° C	10 Min	,,

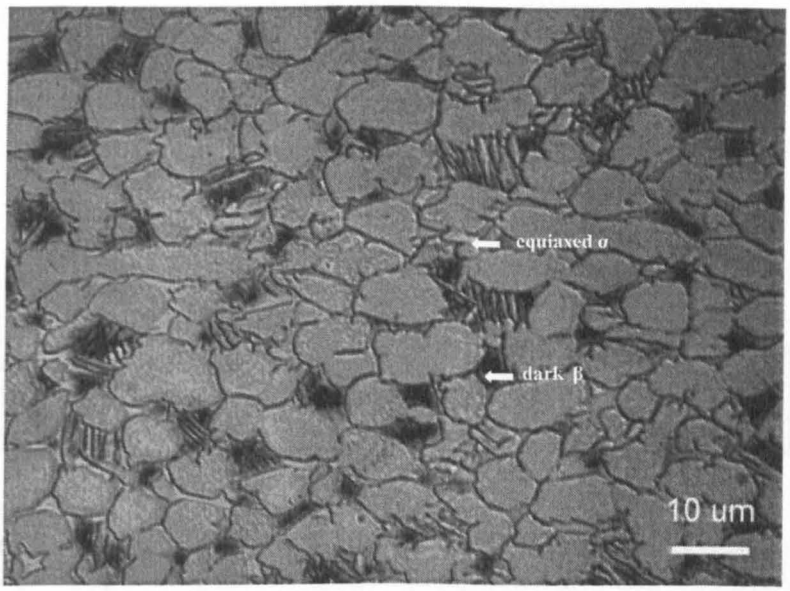

Figure 3.10: Light micrographs of as-received Ti-6Al-4V used for this study.

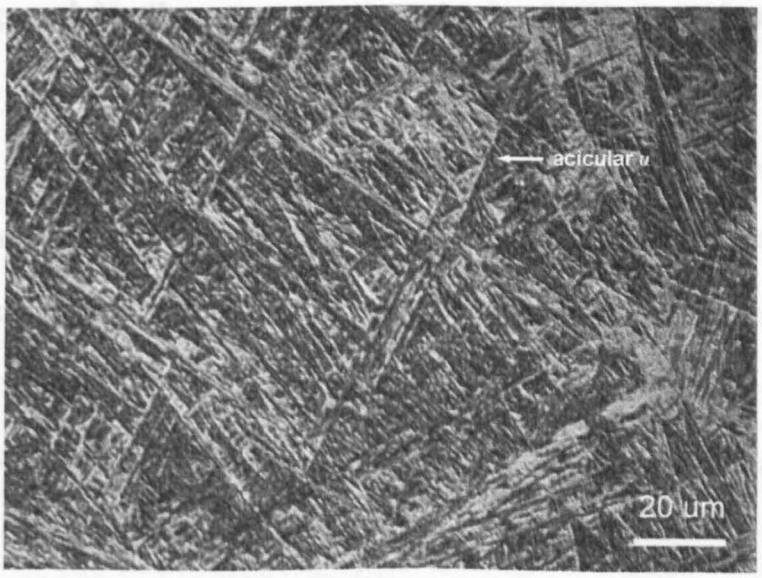

Figure 3.11: Light micrographs of pre-test Ti-6Al-4V used for this study.

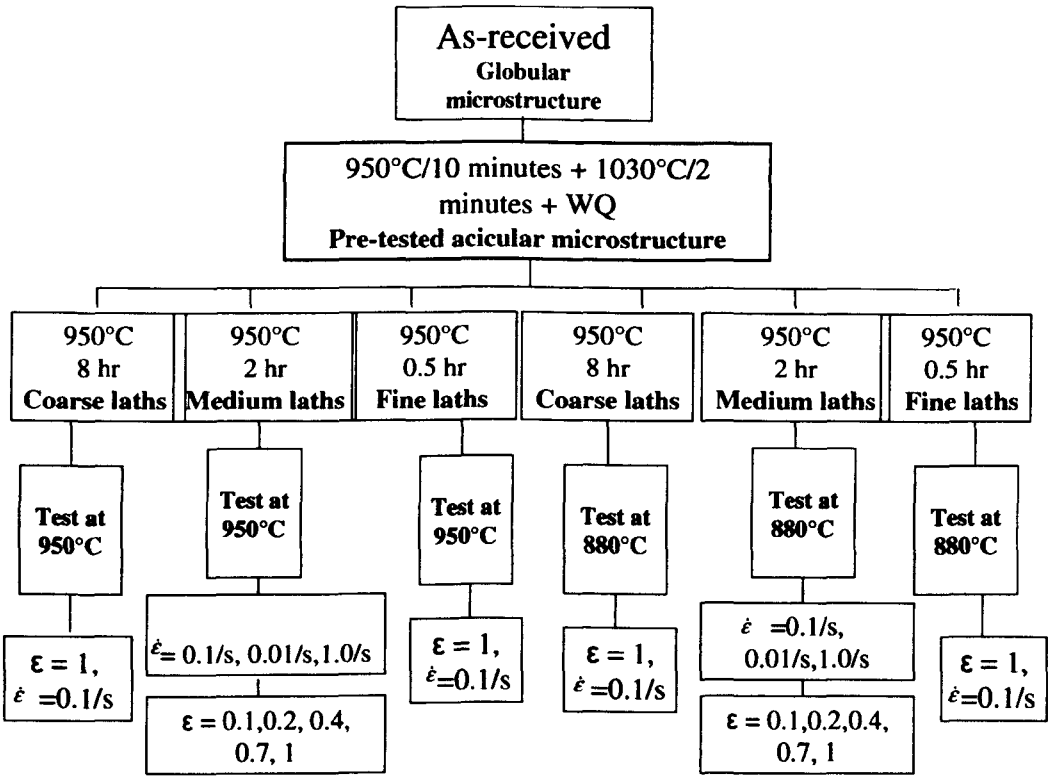

Figure 3.12: Hot compression test plan for the microstructural examination.

The specimens that had been subjected to hot compression testing at both sub-transus (880°C) and near-transus (950°C) with strain rate of 0.01/s, 0.1/s, and 1.0/s at $\varepsilon = 1$ and were water quenched immediately, in order to capture the evolved microstructure at the compression temperature. The microstructures of the specimens that were subjected to the same heating cycle without deforming were also investigated for comparison purposes. The resulting microstructures will be discussed in detail in chapter 5.

3.5 Metallographic procedure for Microstructural Analysis

This section describes the procedures involved in metallographic sample preparation used in the present work. This includes cutting, mounting, mechanical grinding, polishing, and

etching. A proper metallographic preparation of metallic materials is vital for obtaining good quality micrographs on LOM (light optical microscope) and SEM (Scanning electron microscope). Especially, good surface finish is very important for EBSD (Electron backscattered diffraction) to analyse texture of titanium alloys, which are known to be more difficult to prepare for metallographic examination than steels.

3.5.1 Sample preparation

As described in section 3.3.1, EDM was used to machine cylindrical specimens of 10mm diameter x 15 mm height from the forged bar of Ti-6Al-4V. After hot compression testing (deformed specimens) or heat treatment (undeformed specimens), the specimens were sectioned through the centre parallel to the longitudinal axis of the cylinder (i.e. compression axis of the deformed specimens) by EDM for metallographic investigation. The sectioned specimens were mounted under pressure using conductive Bakelite powder at ~300°C to facilitate their handling during metallographic preparation.

After mounting the specimens, the subsequent grinding was done with silicon carbide (SiC) papers with grit sizes varying from 220 to 2500. Silicon carbides (SiC) paper is the traditional method for fine grinding. After, plane grinding steps, specimens were thoroughly washed with water, and then followed by polishing steps on a hard surface, using MD-Nap clothes produced by Struers [153]. Diamond paste suspensions of 6μm, 3μm, and 1μm were used in order as abrasive material during polishing.

Finally, a chemical-mechanical polishing with a mixture of colloidal silica (OP-S) and 30% hydrogen peroxide (H_2O_2) was carried out. During the chemical-mechanical polishing, the reaction product of the H_2O_2 with titanium is continuously removed from the sample surface with the silica suspension and leaves the polished surface free from

mechanical deformation. Then, the polished samples were immersed for about 10 seconds in an etchant that is consisted of 0.5ml HF, 5ml lactic acid and 94.5cc distilled water[142]. On the other hand, for EBSD analysis a further polishing with ¼ μm-diamond paste suspensions and solution containing colloidal silica suspension was used for better results. During polishing care was taken using the colloidal silica as it forms a thin solid glass layer on the specimen surface. To prevent this, the samples were washed with distilled water every 3-5 minutes and a fresh solution was applied on the cloth, which was repeated for every 30 minutes of polishing cycle.

3.5.2 Optical microscopy (OM) and Electron microscopy

In the present work, an inverted type light microscope (Reichert Jung - model MeF3) was used to capture micrographs of undeformed and deformed specimens. The magnification range of this microscope is 50× to 1800×. A camera, supplied by 'Q-imaging', micropublisher 3.3RTV, was coupled with the microscope and incorporated for image acquisition. In this study, an SEM type SUPRA^{TM} 55VP with the improved GEMINI ® FESEM column, has been used to capture micrographs as well as EDSB maps. For EBSD analysis, the sample is tilted at 70°, the accelerating voltage 20 KV with working distance 15mm and 1μm step size were used.

GEM texture measurements

In the present work, the texture measurements were carried out for heat-treated Ti-(α→β→α) and deformed Ti-6Al-4V samples at room temperatures, sub-transus (850°C), and near-transus (980 °C) temperatures. The hot deformation test programme was carried out on GEM as shown in Table 3.3 & Table 3.4. Initially, the as-received equiaxed α has

been pre-tested at 950 °C/ 10 mins and 1030 °C / 2 mins(above beta transus) and water quenching to produce acicular α microstructure. These bet-annealed Ti-6Al-4V samples have been heat treated at 850°C and 980°C and these samples were measured at room temperature (RT).

Table 3.3 GEM –temperature cycle test programme

Sample No	Prior heat treatment	GEM Run. No	Temp	Comments
0	As-received	50277	RT	
1	Beta-annealed +WQ +30mins@980°C+WQ	50292	RT	
2	Beta-annealed +WQ +30mins@850°C+WQ	50293	RT	
3	Beta-anneal +WQ	50294 50295 50296 50414	RT 780 850 RT	T cycle-4hrs; sample removed before 2nd RT measurement
4	Beta-anneal +WQ	50297 50299 50300 50301 50302 50303 50304 50305 50306 50413	RT 890 920 950 980 950 920 890 280-180 RT	T cycle-4hrs; sample removed before 2nd RT measurement
Empty furnace		50307 50308	RT	

Then, to study the high temperature beta-phase texture the beta-annealed + water quenched Ti-6Al-4V samples were measured at 850°C & 980°C temperature cycles. Further, to study the deformation texture characteristic of Ti-6Al-4V, a complete $\alpha \rightarrow \beta \rightarrow \alpha$ phase transformation was carried out for samples hot forged at 850°C & 980°C with a strain rate of 0.1/s and $\varepsilon = 1$ below transus temperatures were calculated.

Table 3.4 GEM- Hot deformation test programme

Sample No	Temp & Strain rate	GEM Run. No	Temperature
0	980°C, 0.1/s, ε =1	50644	RT
1	980°C, 0.1/s, ε =1	50641 50642	RT RT
2	850 °C,0.1/s, ε =1	50643	RT
3	850 °C,0.1/s, ε =1	50645 50646 50647 50648	RT 780°C 850°C 300°C
4	980°C, 0.1/s, ε =1	50649 50650 50651 50652	RT -55°C 980°C RT-300°C RT-120°C

3.5.3 MAUD - Data analysis

The texture of Ti-6Al-4V samples in this study has been measured in situ by time-of-flight (TOF) neutron diffraction [154]. The analysis of neutron TOF data is performed with a full-pattern approach, of the availability of neutron intensities over a large d-spacing range. A Rietveld method is used to determine the crystal structure from a continuous whole diffraction spectrum of a Ti-6Al-4V sample. This method relies on the premise that a diffraction spectrum is given by the incident beam characteristics, line-broadening/instrumental parameters (such as peak shape, background function, Lorentz-polarization corrections etc.), and structural parameters (cell parameters, atomic positions, temperature factors etc.). From the measured spectrum these parameters can be refined using a non-linear least squares method. packages are currently employed to analyse HIPPO (high pressure preferred orientation) texture data MAUD [138] and GSAS [155]. Both minimize the differences between measured and calculated data-points following a

least squares scheme. A major difference between the two packages is that GSAS has all derivatives coded in the software while MAUD evaluates the derivatives numerically. GSAS therefore is somewhat faster than MAUD during the refinement while MAUD has the advantage of being able to include non-analytical models into the analysis. An important example of such a discrete model for texture analysis is the WIMV (E-WIMV) [156] method, which assigns weights to discrete points in orientation-space based on measured data in an iterative process. MAUD is used from two-dimensional X-ray diffraction images e.g., (Lonardelli et al., 2005). MAUD is written in JAVA and works with any operating system for which a java implementation is easily available (WINDOWS, MAC OS X, LINUX, and UNIX). For this work, we have used WINDOW XP. Because of the complexity of the program and large data arrays, MAUD usually requires large memory; however, 1 giga byte is sufficient for most cases.

Therefore, comparison of texture results can be obtained using MAUD with the spherical harmonics [132] and the WIMV approaches. In the beginning of the MAUD analysis, a procedure was performed to find the lattice and profile parameters, as well as a correction for small sample misalignment, which affects only peak positions. After this, these parameters were kept fixed and parameters affecting the peak intensities were refined; these parameters include isotropic displacement factors, absorption, extinction and the grain orientation distribution described by the spherical harmonics function [157]. Finally, data are refined taking into account by first refining instrument parameters and background, then crystallographic and microstructural parameters, and finally all other parameters such as the texture and volume fractions of the phases.

Chapter 4

Flow stress behaviour of Ti-6Al-4V during hot compression testing

This chapter covers the hot compression test results related to the isothermal flow stress behaviour of (β-heat-treated) two-phase Ti-6Al-4V samples with three different microstructures ('coarser', 'medium' and 'fine') in order to establish the effect of starting microstructure and hot working conditions on flow behaviour and globularization kinetics. The effect of processing parameters such as working temperature, strain and imposed strain rate on flow response and microstructure evolution is established. The corrected flow stress for machine compliance, friction and deformation heating are presented.

During this investigation hot compression tests were carried out at two different temperatures, 880°C and 950° C, with three different strain rates, 0.01, 0.1 and $1.0s^{-1}$, (as shown in Figure 3.7). The effect of test temperature and strain rate on the flow behaviour of these three distinct starting microstructures are discussed and the flow curves for all temperatures and strain rates are presented in the form of true stress – true strain plots. Finally, the constitutive relationships which correlate the effect of strain rate and temperature on the flow stress are discussed.

4.1 Hot compression and plastic deformation

In the aerospace industry, conventional hot working processes, like forging and extrusion used extensively to produce structural and engine parts. During metal forming processes, the determination of forces and forming energy are the most important aspect of mechanical design [158], which requires knowledge of the flow stress of the alloys. The determination of the flow behaviour of materials during hot working is a complex process because the flow stress during the hot deformation is influenced by many factors such as the prior–beta grain size, strain rate, and working temperature (deformation temperature).

However, understanding their effects on plastic flow behaviour has become necessary to analyse their mechanical properties. Both the hardening and softening mechanisms are significantly affected by the temperature and strain rate [159].

The deformation rate is important for manufacturing production rate and also has a dominant role in controlling the evolution of the microstructure. Therefore, experiments to find the flow stress of an alloy at different loading conditions, for example various strain rates and temperatures, are necessary to quantify the constitutive behaviour of workpiece materials and also to analyse plastic flow at high temperatures [160]. Although, various studies on the deformation behaviour of two-phase alloys have been reported, [161]a complete understanding of these materials does not exist. Semiatin et al. [162] analysed plastic-flow behaviour during hot working of the two-phase Ti-6Al-4V alloy. The microstructure evolution during hot forging of Ti-6Al-4V with a lamellar colony microstructure has been probed [162] to understand the flow stress behaviour of Ti-6Al-4V. In particular, the flow softening response observed in the true stress-strain curves

determined from isothermal hot compression tests has been studied to understand the nature of the deformation associated mechanism. In Ti-6Al-4V alloy, the flow softening behaviour during compression is known to occur due to deformation heating and microstructural evolution [163] . So far, considerable work has been done on the constitutive behaviour transformed β structures in commercial Ti-6Al-4V during hot-working [5, 98]and the mechanism of globularization of the lamellar structure. Further, Semiatin et al. [163] attempted to relate the kinetics of globularization to the plastic strain in the specimen; Seshacharyulu et al. [164, 165] established a correlation between the size of the globules with temperature and strain rate through the Zener-Hollomon (Z) parameter. Optimization of deformation processing as well as innovation in the design will lead to large savings and improved service life of components.

Generally, the hot working properties of alloys are determined using axisymmetric compression tests at elevated temperatures ($T > 0.5\ T_m$), where T_m is the absolute melting point of the material [11], and also provide information on the optimum processing routes for materials during industrial forging and rolling. However, the response of the material to each hot deformation step depends on the starting microstructures. In order to design a manufacturing process for controlled workability as well as microstructural evolution, it is necessary to understand the constitutive behaviour of the material with different starting microstructures. More experimentation and investigation are still necessary for better understanding of the responses between temperature, strain and strain rate during the plasticity processing of titanium alloys.

4.1.1 Validity of the hot compression tests

The flow stress calculated from during hot compression tests is subject to errors, due to friction between specimen/ platen interface, adiabatic heating at high strain rate and the effect of machine compliance [11]. Moreover, the macroscopic deformation mode in the test piece is also important to ensure validity of the test [116]. The various deformation modes for cylindrical specimens subjected to uniaxial compression with different *h/d* (height to diameter) ratio are shown in Figure 4.1. Generally, cylindrical specimens with *h/d* ratio < 5 are safe from buckling, however *h*/5 > 5 leads to elastic and plastic buckling as shown in Figure 4.1 (a). Previous studies [116] show that, for ductile materials, *h/d* values less than 2.5 lead to shear distortion (as shown in Figure 4.1 (b)). Hence, to achieve accurate measurements, *h/d* ratios above 2 are normally avoided to prevent non-uniform deformation during compression testing.

In addition to *h/d* ratio, friction between the specimen/platen interfaces constrains the outward flow of the material under the axial load, which results in barrelling of specimens. Basically, barrelling is an indication of non-uniform deformation, due to non-homogeneous distribution of stress and strain within the specimen[11].

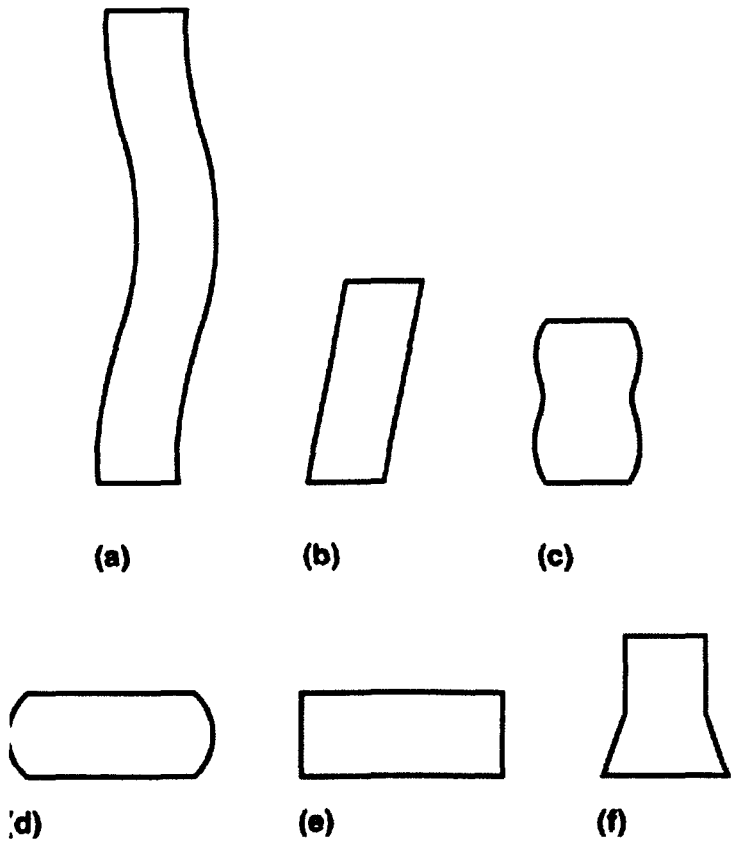

Figure 4.1: Macroscopic modes of deformation during hot compression tests (a). Elastic and plastic buckling, (b). Shear distortion, (c). Double barrelling, (d). Single barrelling, (e). Homogenous deformation and (f). Irregular deformation [116].

If *h/d* is greater than 2, double barrelling may result as shown in Figure 4.1 (c) whereas, in the case of $h/d < 2$, single barrelling may occur as shown in Figure 4.1 (d). Figure 4.1 (e) shows the ideal condition, where friction is minimal without barrelling and deformation is homogeneous. On the other hand, figure 4.1 (f) shows irregular deformation due to work softening of the material caused by localized expansion or temperature non-uniformity. Thus, *h/d* ratio value between 1-2 can be used as an ideal value for compression testing[143]. As discussed in chapter 3, cylindrical specimens of 10mm diameter (*d*) and 15mm in height (*h*) were used in this study for hot compression testing, hence the *h/d* ratio in the present case is 1.5.

The geometry of the test piece should be measured after deformation to ensure that the deformation is uniform across the test piece and excessive barrelling has not occurred during deformation. For example, if barrelling is greater than a specified amount the flow stress data will be significantly in error. The shape measurements are defined as the Barrelling Coefficient (B), Ovality coefficient (O) and Height Coefficient (H)[143] .

Barrelling Coefficient (B):

This is defined as

$$B = h_f d_f^2 / h_0 d_0^2 \qquad \text{Eq.4.1}$$

Here, h_0 and d_0 are initial height and diameter of the test piece measured before deformation, h_f and d_f are final height and diameter measured at mid-length of the test piece after deformation. B is the ratio of the final volume of the test piece (final height and diameter measured at the mid-length of the test piece) divided by the initial volume. Variations from unity are caused by the friction at the specimen/platen interface and B increases with increasing amounts of barrelling. In this study, the barrelling coefficient has been measured for all compression tests. The calculated values from selected compression tests are summarized in Table 4.1, where the minimum and maximum d_f from all the tests and the standard deviation for the height measurements are given.

Height Coefficient (H)

This is a ratio of the standard deviation of four height measurements to the average height of the deformed test piece. This is defined as

$$H = Sh_f / h_f \qquad \text{Eq. 4.2}$$

Here, Sh_f is standard deviation of final height measurements and h_f is the average height of the deformed test piece. If the calculated value of H is equal to or greater than 0.04 then the test is invalid[143].

Ovality Coefficient (O):

This is defined as the ratio of the maximum to the minimum diameters of the deformed test piece. The texture and microstructure can affect the ovality. In particular, it can be severe for hexagonal close packed metals and alloys. This is measured by using the following formula:

$$O = d_{f\,max} / d_{f\,min} \qquad \text{Eq. 4.3}$$

The measured ovality values are given in Table 4.1. It can be seen that the values are very close to the ideal value of 1.

Table 4.1 Measured shape coefficients values of Ti-6Al-4V for selected test conditions.

Tests	950°C–0.01/s		950°C–1/s		880°C–0.01/s		880°C–1/s	
	h_f	d_f	h_f	d_f	h_f	d_f	h_f	d_f
Max	5.95	17.33	5.94	17.44	5.91	17.32	6.05	17.14
Min	5.82	16.51	5.88	16.55	5.80	16.24	5.99	15.83
	5.78	16.83	5.93	16.91	5.86	16.62	5.96	16.70
	5.68	16.92	5.88	16.41	5.96	16.07	5.97	16.45
Mean	**5.81**	**16.89**	**5.91**	**16.83**	**5.88**	**16.52**	**5.99**	**16.53**
S/hf	**0.112**		**0.032**		**0.068**		**0.040**	
B	**1.193**		**1.207**		**1.184**		**1.187**	
H	**0.019**		**0.005**		**0.012**		**0.007**	
O	**1.050**		**1.054**		**1.066**		**1.083**	

In this present work all the hot compression tests were carried out to achieve a nominal strain of 1. Equation 5.4 shows the conventional true strain formula [166], where the negative sign indicates compression.

$$\varepsilon = - \ln (h/h_0) \qquad \text{Eq. 4.4}$$

In theory, a 15mm height cylindrical specimen should deform to a height of 5.519mm after applying a nominal true strain of 1. In the present work, the measured final height (h_f) of the specimen at the lower strain rate of 0.01/s was 5.81 (minimum) as compared to the h_f at the higher strain rate of 1/s was 5.99. The difference in h_f occurs because some of the applied strain is taken up by the loading system, known as the compliance effect, as discussed in section 4.3.1.

4.2 Initial Microstructure

In this present study, the hot deformation behaviour of Ti-6Al-4V with a transformed β (Widmanstätten) preform microstructure was characterized over a range of temperatures and strain rates. The equiaxed as-received microstructure of the preform is shown in Figure 4.2 (a) and the average grain size of the equiaxed α was 15.4 μm.

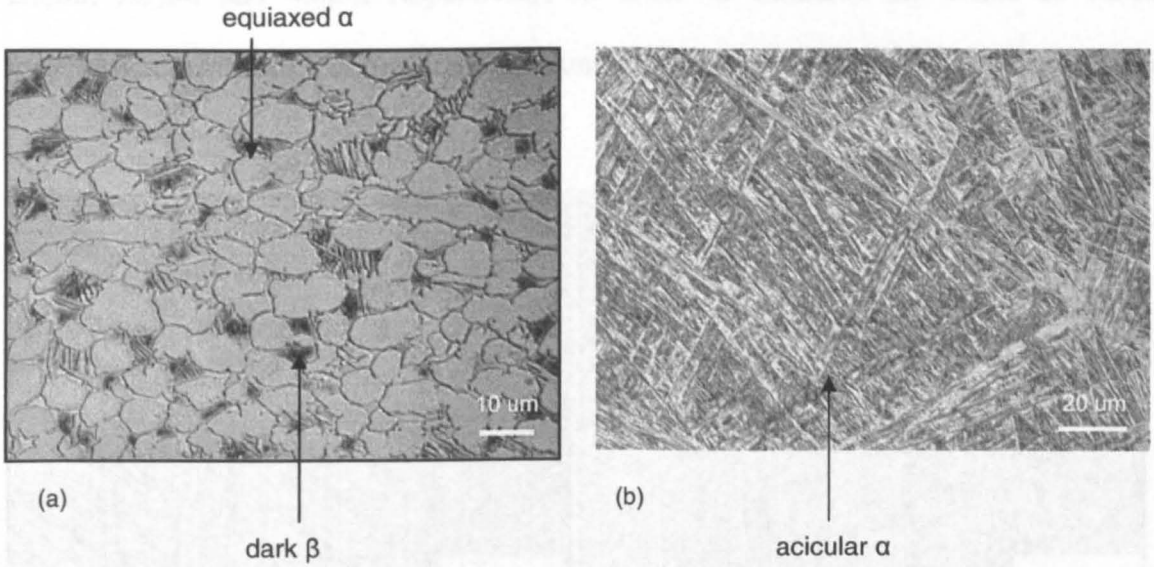

Figure 4.2: Light micrographs showing (a) the as received microstructure, and (b) the same material after heat treatment of 950°C/10min + 1050°C/2min followed by water quenching.

The as-received alloy was then annealed at 950 °C for 10 minutes followed by soaking at 1030 °C for 2 minutes before it was water quenched. This resulting microstructure consists of colonies of acicular (needle-like) α phase (Figure 4.2.b) with approximately 0.25µm-thick laths within coarse prior-beta grains of 300-400µm.

To investigate the effect of starting microstructure on hot deformation characteristics of the titanium alloy studied, the initial acicular microstructure was then altered by further heat treatment. The heat treatment procedures for the materials used in hot compression tests at 880°C and 950°C were slightly different.

Material to be used in hot compression testing at 950°C was soaked for ½hr, 2hr or 8hr at 950°C to produce 'fine', 'medium' and 'coarse' alpha platelets with average thicknesses of 2.3μm, 2.9μm and 4.0μm respectively, in order to establish the effect of starting microstructure and hot working conditions on flow behaviour and globularization kinetics.

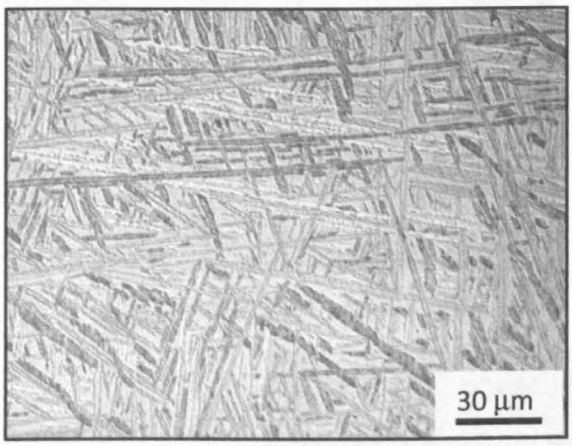

(a). Fine laths (1/2 hrs) (2.3 ± 0.7 μm)

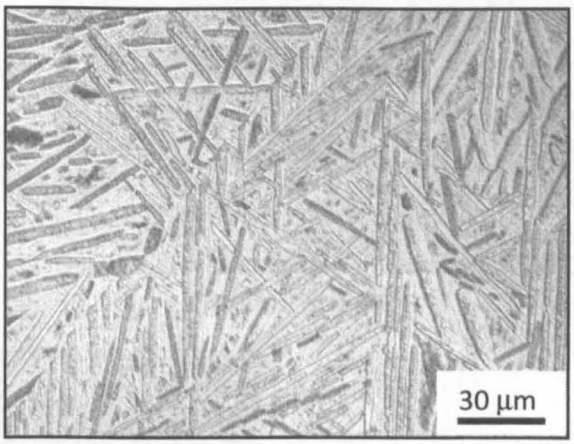

(b). Medium laths (2 hrs) (2.9 ± 0.8 μm)

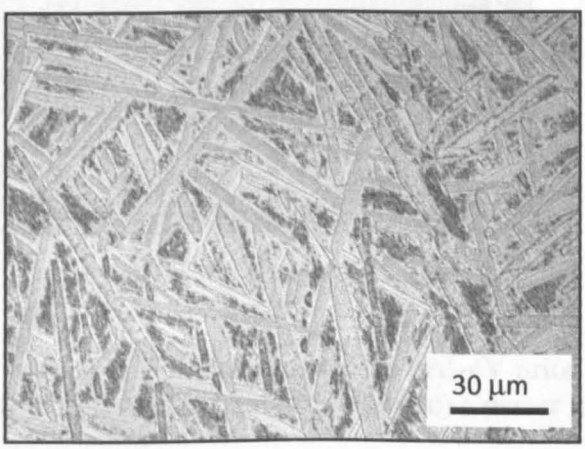

(c). Coarser laths (8hrs), (4.0 ± 1.2 μm)

Figure 4.3(a): Optical micrographs of heat treated Ti-6Al-4V prior to deformation processed by: (a) Fine (0.5hrs), (b) Medium (2hrs) and (c) Coarser laths (8hrs) due to water cooling at 950 °C.

The optical micrographs of pre-test microstructures of Ti-6Al-4V tested at 950°C are given in Figure 4.3 (a). Material to be used in testing at 880°C was heat-treated in the same way except that the final ½hr of each soak was carried out at the test temperature of 880°C.

This procedure produced slightly larger laths with average thicknesses of 2.8μm, 3.7μm and 4.6μm respectively. The optical micrographs of pre-test microstructure of Ti-6Al-4V tested at 880°C are shown in Figure 4.3 (b).

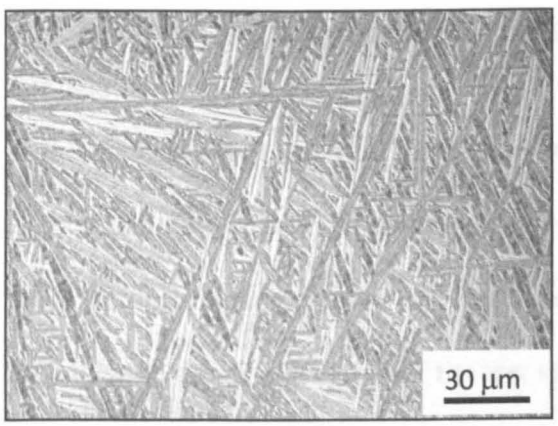

(a). Fine laths (1/2 hrs), (2.8 ± 0.6 μm)

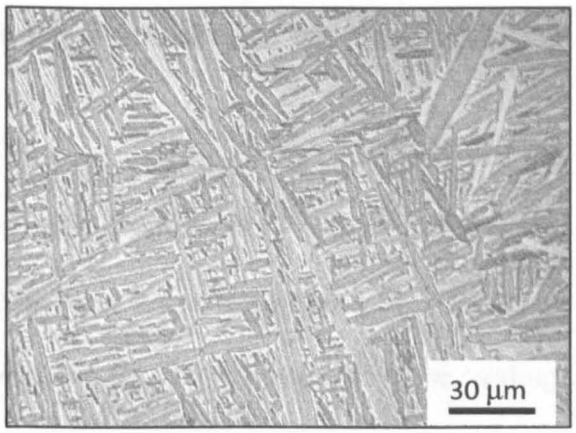

(b.) Medium laths (2 hrs), (3.7 ± 1.0 μm)

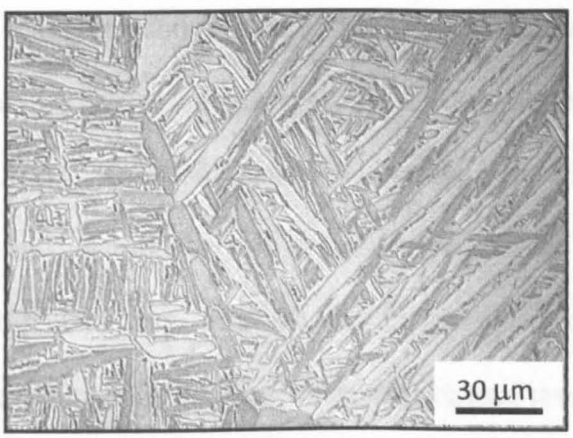

(c). Coarser laths (8 hrs), (4.6 ± 1.9 μm)

Figure 4.3(b): Optical micrographs of heat treated Ti-6Al-4V prior to prior to deformation processed by: (a) Fine (0.5hrs), (b) Medium (2hrs) and (c) Coarser laths (8hrs) due to water cooling at 880 °C.

The compression tests were carried out under constant axial (true) strain-rate conditions at two temperatures: 880°C and 950°C using servo-hydraulic apparatus, at rates relevant to industrial press forging ($0.01s^{-1}$, $0.1\ s^{-1}$ and $1.0\ s^{-1}$) to a final constant strain of (ε=1) and samples were immediately removed from the furnace and water quenched to preserve the as-deformed microstructure. Further, the interrupted tests were carried out at various nominal strain levels (0.1, 0.2, 0.4, 0.7 and 1.0) for both 880 °C and 950 °C at strain rate of 0.1/s.

4.3 Flow stress corrections on Ti-6Al-4V

4.3.1 Effect of machine compliance on flow stress measurements

In this present work, the flow curves generated by compression testing were corrected for friction and deformation heating using the approach highlighted by Brooks and Dickenson [167] (as described in chapter 3). Here, the displacement measured by the LVDT does not only include the displacement of the test specimen, but also the deformation of the loading system (i.e. the elastic component of the entire system of servo-actuator, platens and load cell). To compensate for the above effect the load-displacement curves produced were measured by subtracting the deformation of the loading system from the displacement measured by the LVDT. The compliance calibration was conducted by applying the maximum load obtained during the test at the temperature of interest with the top and bottom platens in direct contact. Initially, the platens were coated with lubricant and brought together to make them in contact. Then, the nominal test temperature was achieved and maintained for 30 minutes for the same soaking time as in the tests. The load was increased at a rate of 500 N /s, across the faces of the platens until the maximum load achieved during testing at each particular temperature was reached.

At different test temperatures, the deformation of the loading frame system was estimated, in order to correct the flow stress curves obtained from the hot compression. The compliance of the test machine/platen setup for various test temperatures was measured by plotting the displacement and the load readings, to give a direct measure of the machine compliance as a function of load. As an example, the displacement vs. load data obtained for a temperature of 880°C is given in Figure 4.4.

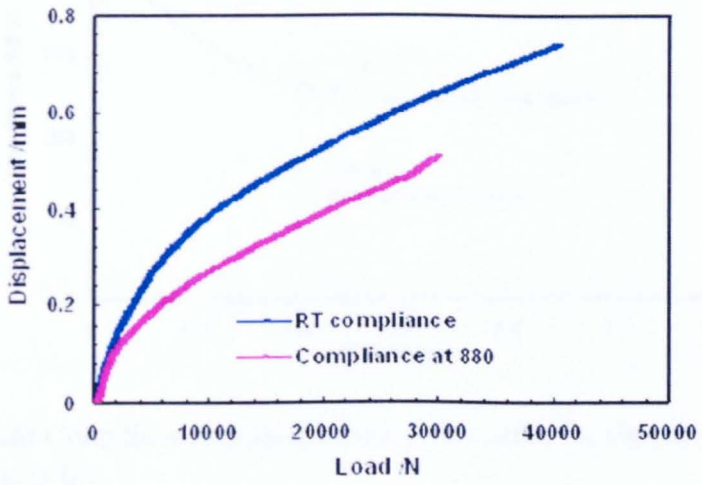

Figure 4.4: Displacement vs load curve for the loading frames at 880°C

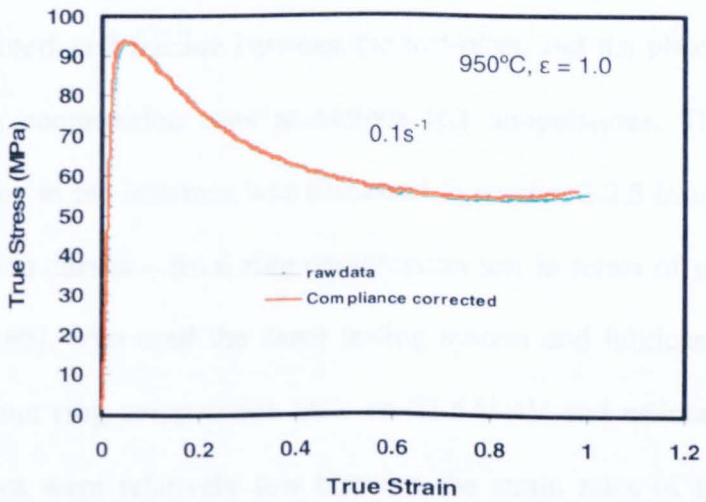

Figure 4.5: Compliance corrected flow stress curve for the acicular Ti-6Al-4V at 950°C and 0.1/s.

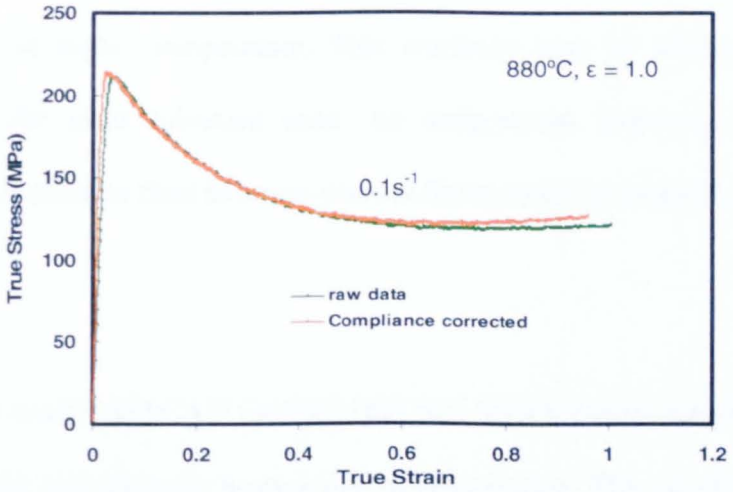

Figure 4.6: Compliance corrected flow stress curve for the acicular Ti-6Al-4V at 880°C and 0.1/s.

The effect of the compliance correction on the flow curves for both test temperatures (950°C & 880°C) are shown in Figure 4.5 & 4.6. It can be seen that the effect on the data is small.

4.3.2 Effect of friction and adiabatic heating on flow stress measurements

Generally, the interfacial friction between the test-piece and the platens is established by conducting ring compression tests at various test temperatures. The determination of interfacial friction at the interface was discussed in section 3.2.5 in detail and the typical friction calibration curves – from ring compression test in terms of μ is shown in Figure 3.4. Mulyadi [168], who used the same testing system and lubricants as in the present study, carried out ring compression tests on Ti-6Al-4V and estimated that the friction coefficient values were relatively low between the strain rates of 0.03/s to 0.1/s. This confirmed that the lubricant system used can minimise the friction effectively and also concluded that, with increasing working temperature, the interfacial friction between the dies and work-pieces increases slightly, as indicated by higher values of both μ and m_f

(shear factor) at higher temperature. This tendency may be attributed to the inherent properties of the glass lubricant used. As temperature increases, the glass viscosity decreases and it starts to flow as a non-viscous fluid, which in turn reduces its effectiveness as lubricant.

In this present work, MathCAD routine [169] was used for correcting flow stresses for the effect of friction and adiabatic heating due to deformation. This correction is based on the slab analysis[170]. Here, the adiabatic heating correction calculates the energy under the flow stress curves subtracts the conduction heat losses from the ends and converts the remainder to a temperature rise. Then, the temperature correction to the flow stress then assumes linear temperature sensitivity and the value are obtained from the flow stress data.

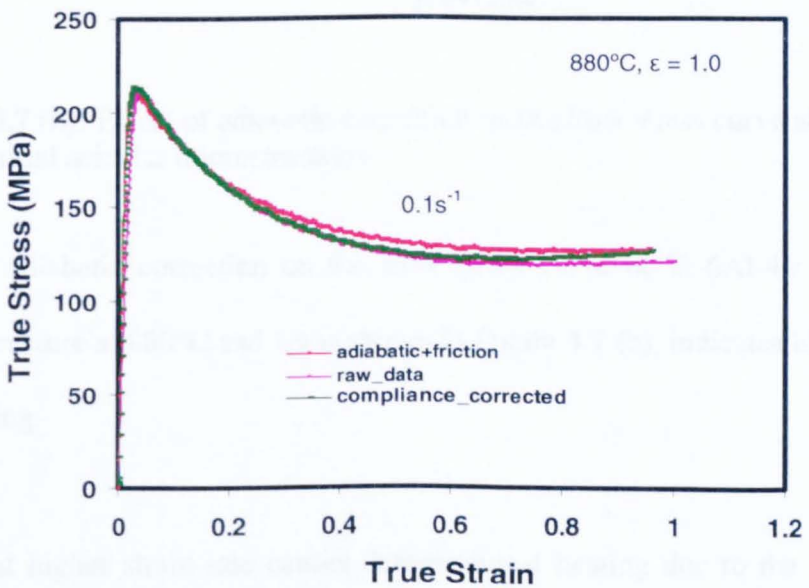

Figure 4.7 (a): Effect of adiabatic, friction and compliance correction on the flow stress curve at 880°C and 0.1/s for initial acicular microstructure.

The effects of the friction change on the flow stress curves of Ti-6Al-4V with an acicular initial microstructure at 880°C and 950°C were corrected together with adiabatic heating. The effect of both adiabatic-friction and compliance-correction on the flow stress curve of Ti-6Al-4V with acicular initial microstructure at 880°C and 0.1/s is shown in Figure 4.7(a).

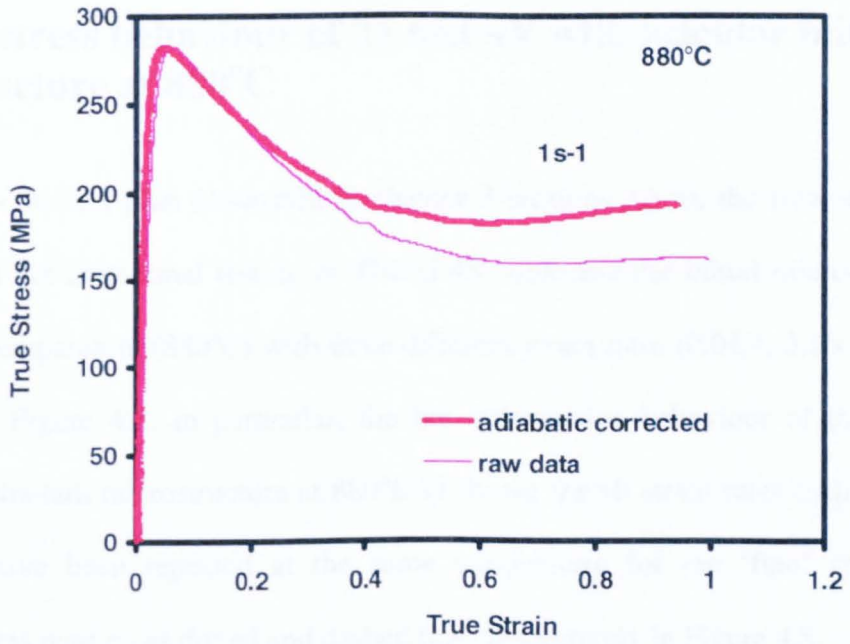

Figure 4.7 (b): Effect of adiabatic correction on the flow stress curve at 880°C and 1/s for initial acicular microstructure.

The effect of adiabatic correction on the flow stress curve of Ti-6Al-4V with acicular initial microstructure at 880°C and 1/s is shown in Figure 4.7 (b), indicates higher effect of adiabatic heating.

Deformation at higher strain rate causes deformational heating due to the conversion of applied strain energy into heat. In metal working, most of the work done is released as heat and the rest will be stored within the material as defects such as dislocations [71]. Therefore, a rapid deformation rate can disrupt the isothermal condition by raising the

work-piece temperature, leading to a reduction in flow stress. Flow stress curves presented in the following sections have been corrected for the effects of adiabatic heating, friction and machine compliance. The friction-corrected flow stress shows only a slight difference when compared to the compliance-corrected flow stress, due to the low interfacial friction coefficient. In general the effect of these corrections is relatively small.

4.4 Flow stress behaviour of Ti-6Al-4V with acicular initial microstructure at 880°C

According to the test plan (discussed in chapter 3 sections 3.3.3), the flow stress curves derived from hot isothermal testing of Ti-6Al-4V with acicular initial microstructures at sub-transus temperature (880°C) with three different strain rates (0.01/s, 0.1/s and 1/s) are presented in Figure 4.8. In particular, the hot deformation behaviour of the 'medium' thickness alpha-lath microstructure at 880°C is shown for all strain rates (solid lines); the 0.1/s tests have been repeated at the same temperature for the 'fine' and 'coarser' microstructures marked as dotted and dashed lines respectively in Figure 4.8.

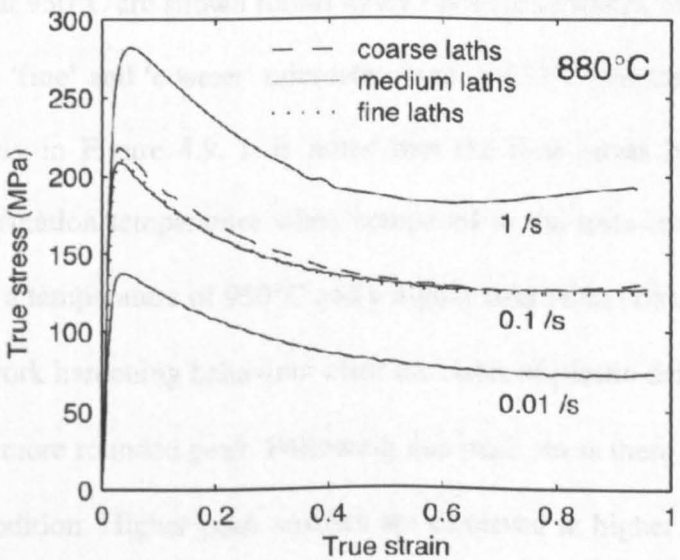

Figure 4.8: Flow curves of Ti-6Al-4V with acicular initial microstructure at 880°C (sub-transus temperature) with strain rates of 0.01/s, 0.1/s and 1/s.

These curves clearly indicate that the flow stress curves are strongly dependent on applied strain rate. All the flow curves show the characteristic features of strong initial strain hardening, a broad peak at low strains, followed by moderate to extensive flow softening beyond the peak stress until a steady state stress is reached. This type of behaviour is well documented in the literature on the hot deformation of Ti-6Al-4V with an acicular structure [171, 172]. In this present study, to establish the effect of starting microstructure and hot working conditions on flow behaviour and globularization kinetics a series of hot compression tests have been carried out. It is noted here, the influence of three different ('coarser', 'medium' and 'fine') microstructures showed a little effect on the flow softening with constant strain and strain rate.

4.5 Flow stress behaviour of Ti-6Al-4V with acicular Initial microstructure at 950°C

Flow curves from compression tests at 0.1/s of the 'medium' thickness alpha-lath microstructure at 950°C are shown for all strain rates (solid lines); the 0.1/s tests have been repeated for the 'fine' and 'coarser' microstructures at 950°C, marked as dotted and dashed lines respectively in Figure 4.9. It is noted that the flow stress has decreased with the increasing deformation temperature when compared to the tests carried out at 880C. It is apparent that at a temperature of 950°C and a higher strain rate (1/s), the flow stress curves exhibit initial work hardening behaviour after the onset of plastic deformation at a strain of ~0.02 to give a more rounded peak. Following this peak stress there is a gradual decay to a steady-state condition. Higher peak stresses are observed at higher strain rates and lower temperatures.

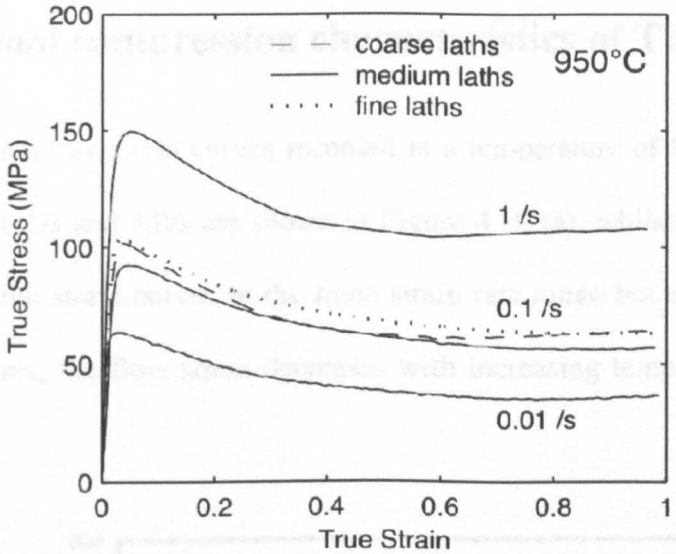

Figure 4.9: Flow curves of Ti-6Al-4V with acicular initial microstructure at 950°C (near-transus temperature) with strain rates of 0.01/s, 0.1/s and 1/s.

The flow softening effect is most pronounced at 950°C, whereas at higher strain rates, the flow stress curves only exhibit flow softening without significant work hardening behaviour. The insensitivity of flow behaviour to initial microstructure is surprising given that alpha lath thickness has been successfully used as an indicator for the progress of dynamic spheroidisation of the alpha phase during hot forging of Ti-6Al-4V [173]. The above systematic investigation of the hot deformation behaviour of Ti-6Al-4V at 880°C and 950°C, using a range of initial lamellar microstructures, has proved that there is little influence of alpha lath thickness on overall flow behaviour for the range considered. Therefore, the significant flow softening, observed for all deformation conditions is believed to be associated with spheroidisation of the lamellar structure and also progressive realignment of alpha laths with their long axes perpendicular to the uniaxial compressive loading axis which appear to coincide with the attainment of the steady-state flow stress.

4.6 Isothermal compression characteristics of Ti-6Al-4V

Typical true stress-true strain curves recorded at a temperature of 880°C and at the strain rates of 0.01/s, 0.1/s and 1.0/s are shown in Figure 4.10 (a), whilst Figure 4.10 (b) shows the true stress-true strain curves in the same strain rate range but at 950 °C. As observed from these figures, the flow stress decreases with increasing temperature and decreasing strain rate.

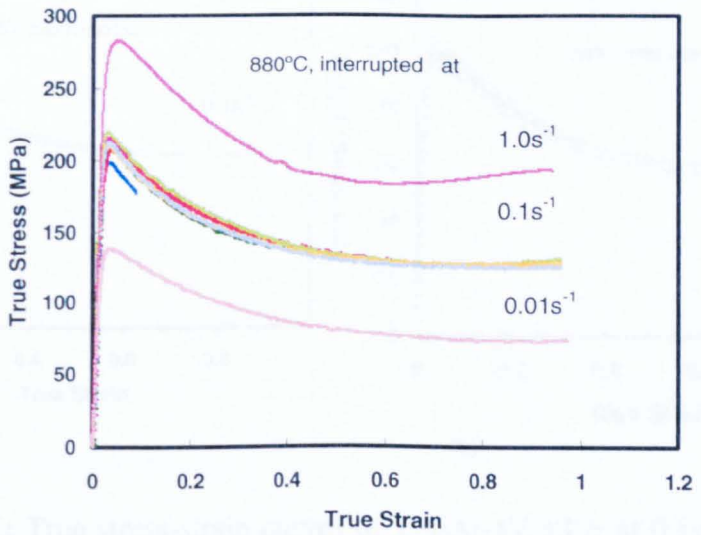

(a)

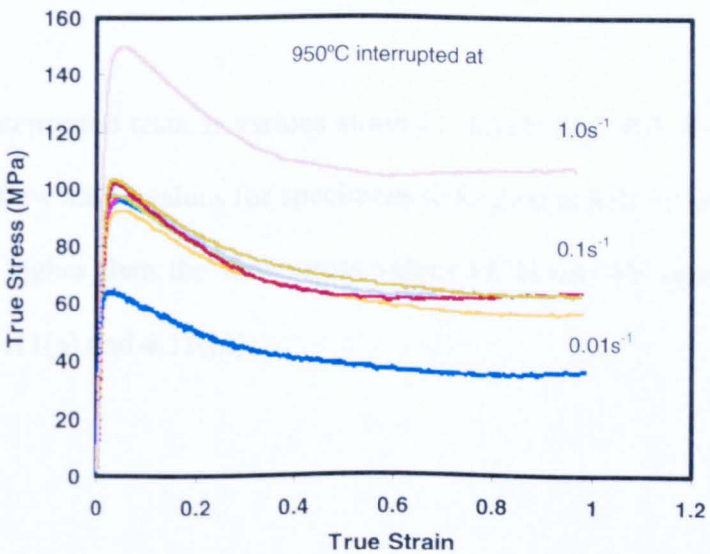

(b)

Figure 4.10: True stress-strain curves of Ti-6Al-4V alloy at: (a) 880°C; and (b) 950°C; for all the strain rates tested.

At the sub-transus temperature of 880°C, the flow stress is found to be about 218MPa for specimen deformed at a strain rate of $1.0s^{-1}$ (Figure 4.10(a)), while at 950°C (near-transus), under the same strain rate level, it decreases to 149 MPa (Figure 4.10(b)). This shows that the rate of work hardening at sub-transus temperatures in the initial stages of deformation is greater than at 950 °C, and is slightly dependent on the strain rate.

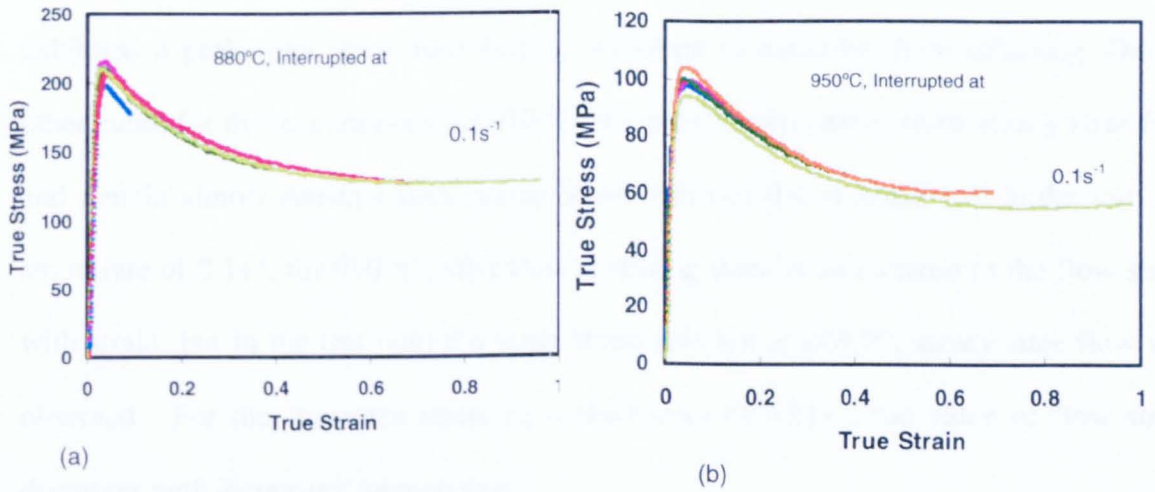

Figure 4.11: True stress-strain curves of Ti-6Al-4V alloy at $0.1s^{-1}$and strain of 0.2, 0.4, 0.7, and 1.0: for the temperatures: (a) 880°C; and (b) 950 °C

Similarly, the interrupted tests at various strain of levels (0.2, 0.4, 0.7, and 1.0) at strain rates $0.1s^{-1}$, the flow stress values for specimens deformed at 880 °C are 210 MPa and 138 MPa which are higher than the flow stress values of Ti-6Al-4V specimens deformed at 950°C (Figure 4.11(a) and 4.11(b)).

4.7 Stress-strain characteristics of Ti-6Al-4V alloy

The measured stress-strain (flow) curves resulting from uniaxial compression tests for Ti-6Al-4V at temperatures of 880°C, 950 °C at the strain rates of 0.01, 0.1 and $1s^{-1}$ are presented in Figures 4.10 (a) & (b). It has been observed that the influence of the test temperature is more pronounced than the strain rate. That is, the flow stress obtained at 880°C is greater, when compared with the flow stress obtained at 950 °C. The test at 880°C with a strain rate of $1s^{-1}$ in Figure 4.10 (a), exhibits a slight drop in flow stress indicating thermal softening behaviour, when the true strain is greater than 0.4. All of the curves exhibited a peak flow stress followed by moderate to extensive flow softening. On the other hand, for the test temperature 950 °C, the stress strain curves show steady state flow and remain almost constant from a true strain value of 0.4 to about 1.0. In the test at a strain rate of $0.1s^{-1}$, for 950 °C, after flow softening there is an increase in the flow stress with strain, but in the test with the same strain rate but at 880 °C, steady-state flow was observed. For the specimen tested at a strain rate of $0.01s^{-1}$, the value of flow stress decreases with increasing temperature.

Overall, the stress vs strain behaviour of Ti-6Al-4V deformed at subtransus temperatures with strain rates of 0.01, 0.1 and 1.0/s shows the influence of working temperature and strain rate imposed during testing. Previous reports suggest that the obtained flow softening may be attributed to the globularization of lamellar structures, deformation heating and micro cracking or flow instability due to flow localization [174, 175]. Furthermore, other reasons for flow softening in the $\alpha + \beta$ field is due to the break up and globularization of some lamellar α at lower strain rate ($\leq 1s^{-1}$). Moreover, limited dynamic recrystallization levels have been reported for Ti-6Al-4V [176, 177]. In the present study, it is noted that, the flow softening behaviour of Ti-6Al-4V is associated with break up and globularization of α –lamellar during hot-compression (discussed in chapter 5).

4.8 Strain-rate effect

The variation of flow stress with strain rate can be seen clearly in Figure 4.12, where the flow stress at a true strain of 1.0 is plotted as a function of the logarithm of the strain rate for 880 °C and 950 °C. The resultant curves in Figure 4.12 show a significant linear increase of flow stress observed within the strain rate range from $0.01s^{-1}$ to $1\ s^{-1}$. These results are well in agreement with the deformation behaviour of titanium alloys and other metals [178, 179].

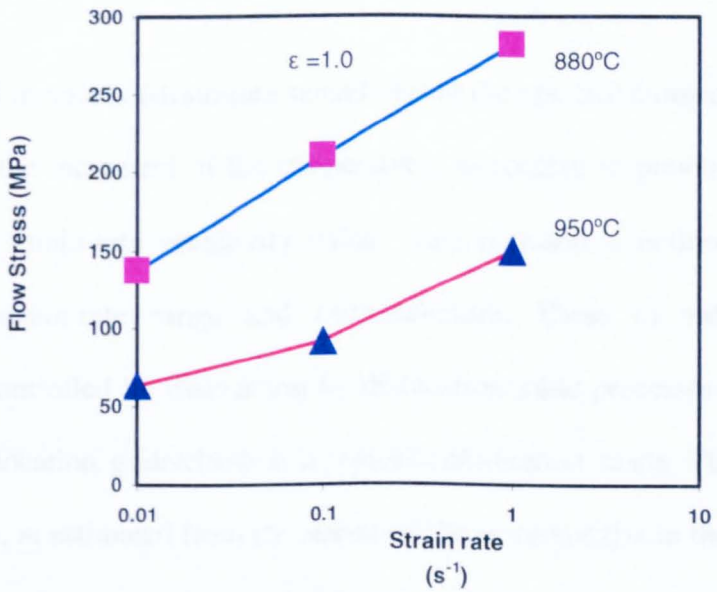

Figure 4.12: Effect of strain rate on the peak flow stress at a plastic strain of 1.0 for test temperatures 880°C and 950°C.

Strain rate sensitivity (m) quantifies the effect of strain rate on the flow stress of a material. It gives a measure of the stress (σ) increase required to generate a certain increase in plastic strain-rate at a given level of plastic strain ($\dot{\varepsilon}$) and a given temperature.

$$m = log\ (\sigma_2 / \sigma_1) / log\ (\dot{\varepsilon}_2 / \dot{\varepsilon}_1) \qquad \text{(Eq. 4.5)}$$

Where the values of σ_1 and σ_2 correspond to the same strain value, and the strain rates $\dot{\varepsilon}_1$ and $\dot{\varepsilon}_2$, respectively. Similar behaviour has been observed for Ti-6Al-4V where σ increases with increasing the imposed strain rates. The m value is determined by the tests as shown in Table 4.2.

Table 4.2 Strain- rate sensitivity (m) and different subtransus temperatures.

Temperature	Peak stress	Steady state
880°C	0.15	0.20
950°C	0.20	0.22

The calculated m-values (strain-rate sensitivity) at the two test temperatures reveal a slight increase with the increment of the temperature. According to previous studies [46, 163], the values of strain-rate sensitivity value (m) revealed a noticeable dependence on temperature, strain-rate range and microstructure. These m values are typical of deformation controlled by dislocation by dislocation glide processes. When m is smaller than 0.30, dislocation glide/climb is a typical deformation mode. The variation of strain rate sensitivity, *m* estimated from the slopes of above curves lies in the range 0.15-0.20 for temperature regimes of 880°C and 950°C.

4.9 Temperature effect

Figure 4.13 illustrates the effect of test temperature on the flow behaviour of Ti-6Al-4V specimens deformed to a strain of 1.0 at three different strain rates. Plotting the flow stress directly as a function of test temperature can reveal the temperature effect on deformation

of Ti-6Al-4V. In the present work, it is observed that the flow stress decreases rapidly with increasing temperature for all strain rate levels.

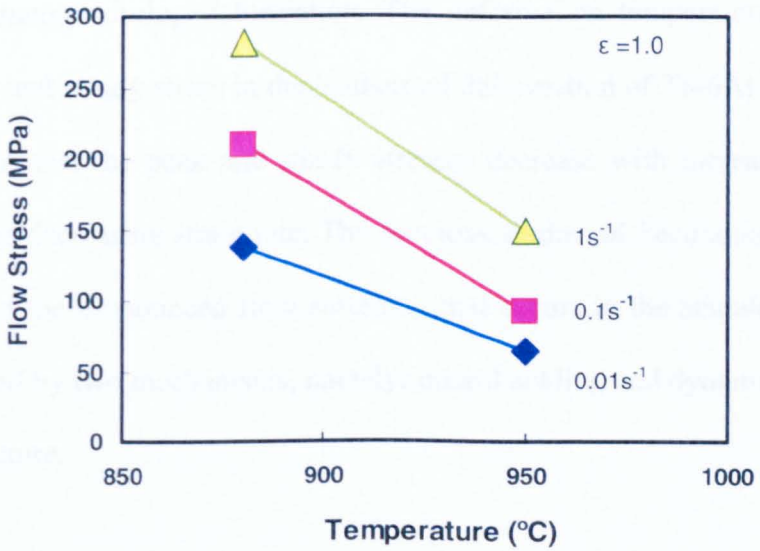

Figure 4.13: Effect of the temperature on the peak flow stress as a function of strain rate.

4.10 Flow softening behaviour of Ti-6Al-4V

It is important to understand and predict flow softening in titanium alloys, to control final microstructure and properties in forged components. Flow softening is a common phenomenon observed during the hot forging of titanium alloys, particularly at subtransus temperatures [180]. It is well understood that flow softening occurs due to adiabatic heating effects or changes in microstructural morphology, substructure or texture [181]. The adiabatic heating effect is responsible for the majority of the flow softening at relatively low temperatures and high strain rates (e.g. $>10^{-1}$ s^{-1}) and the microstructural changes, such as evolution in substructure, phase morphology (such as dynamic

globularization of the alpha phase) and texture at relatively low strain rates ($<10^{-1}$ s^{-1}) are wholly responsible for flow softening.

In the present investigation, a flow-softening phenomenon is observed for all testing conditions and the flow stress curves presented in Figures 4.9 and 4.10 were corrected for adiabatic heating. The flow softening must, therefore, be related to morphological changes in the microstructure during deformation. The deformation temperature and strain rate affect the peak and steady stress in the isothermal deformation of Ti–6Al-4V alloy greatly. It was observed that the peak and steady stresses decrease with increasing deformation temperature and decreasing strain rate. The previous studies of Seetharaman and Semiatin [182] show that the pronounced flow softening that occurs in the acicular morphology is mainly governed by two mechanisms, namely: microbuckling and dynamic globularization of the lath structure.

With increasing strain, the α lath structure has undergone significant distortion, by bending, kinking or buckling which in turn orient the laths into preferred directions: most noticeable in those laths which lie almost parallel to the metal flow resulting in a net reduction of the flow stress. The second possible mechanism responsible for flow softening is related to the size and volume fraction of the dynamically globularized α structure.

Shell and Semiatin [171] found that dynamic globularization occurred in Ti-6Al-4V at strains in excess of those at which flow softening initiated, concluding that the buckling of alpha plates prior to dynamic globularization was responsible for flow softening and changes in dislocation substructure and texture during the deformation led to minimal flow softening. Since at low strain the volume fraction of globularized α is small, flow softening is mainly controlled by micro buckling. With increasing strain, the globularized fraction is

increased which in turn dominates the flow softening. Chapter 5 will discuss the microstructure evolution of β-heat treated acicular Ti-6Al-4V in detail. Another mechanism that might be responsible for flow softening is a change of crystallographic texture [181]. Texture influences may be due to the result of the specific slip systems activated in the α and β-phases and also due to the interface sliding between them. In the undeformed material, the (0001) plane and one <1120> direction of the α phase were nearly parallel to one of the (110) planes and one of the <111> direction in the plane of the β phase, respectively [145].

During the deformation processes in the (α+β) phase field, crystallographic textures in the hexagonal α phase and in the bcc β phase can develop. At 'low' deformation temperatures a high volume fraction of α phase is present during deformation which develops an alpha deformation texture, a so- called basal/transverse (B/T) type of texture. In this present work, in order to evaluate the extent of flow softening during the deformation, the softening of flow stress ($\Delta\sigma = \sigma_{Peak\ stress} - \sigma_{applied\ stress}$) was determined using the approach highlighted (for softening of the flow stress) by Weiju Jia et al. [183]. Figure 4.14 shows the variation of flow softening against temperature at different strain rates and strain values. The values of the stress corresponding to the applied strain (0.2, 0.4, 0.7, and 1.0) are considered as the steady-state stress.

Figure 4.14 clearly shows that the strain rate has a significant effect on the extent of softening; the flow softening increases with increasing strain rate from 0.01 to $1s^{-1}$. This behaviour is similar to the flow softening behaviour observed by Weiju Jia et al on Ti-60 alloy [184].

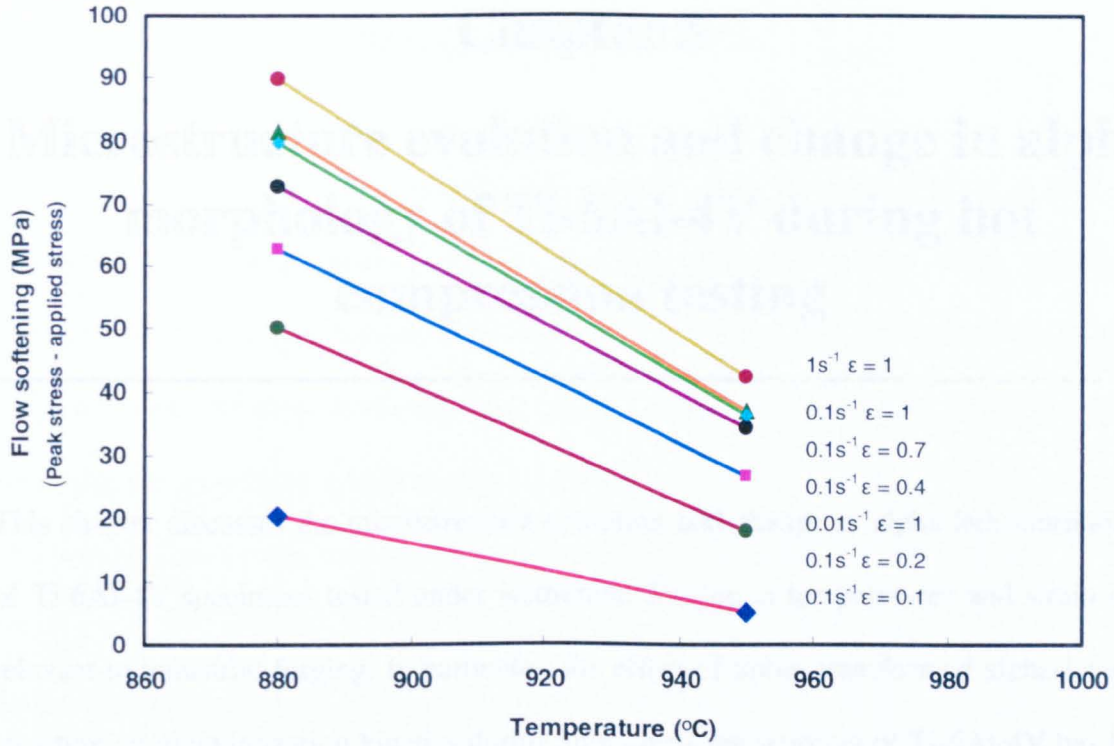

Figure 4.14: Flow softening behaviour of Ti-6Al-4V with increasing temperature for various strain rates and strains.

4.11 Conclusion

- Flow stress curves of Ti-6Al-4V with acicular initial microstructure exhibited a strong dependence on working temperatures and applied strain rates. For all experimental conditions, the flow stress increases as strain rate increases. On the other hand, as temperature increases, flow stress decreases.

- Significant flow softening was observed for all deformation conditions. The post-peak softening is proportionately more significant at higher strain rates, and at the lower test temperature of 880°C.

Chapter 5

Microstructure evolution and change in alpha morphology of Ti-6Al-4V during hot compression testing

This chapter discusses the microstructure evolution and change in alpha lath morphology of Ti-6Al-4V specimens tested under isothermal forging at temperatures and strain rates relevant to industrial forging. In particular, the effect of initial transformed alpha-lamellar structure on globularization kinetics during subtransus hot working of Ti-6Al-4V has been studied. The microstructure evolution of Ti-6Al-4V was investigated with an initial acicular microstructure which was achieved by β-solution heat-treating the as-received Ti-6Al-4V material. The influence of hot working parameters such as strain, strain rate and temperature on the microstructure evolution of Ti-6Al-4V have been studied, to understand the different phase volume fractions of alpha and the effect of initial microstructure.

In this chapter, the findings on the microstructural examinations, carried out to study the morphological changes due to various processing parameters using image analysis software MATLAB MTEX- Tool and Image J, is reported.

5.1 Equiaxed (as-received) microstructure

The microstructure of the as-received Ti-6Al-4V was bimodal (Figure 4.2(a)) and composed of equiaxed primary alpha, secondary (platelet) α and small amount of intergranular β. The beta-transus temperature of Ti-6Al-4V was determined to be 995°C via a common technique involving heat treating a specimen at various temperatures and capturing the respective microstructure to find the change in the phase volume fraction. The beta approach curve was also measured via a series of heat treatments[168].

Processing history of Ti-6Al-4V alloy consists of a series of hot working and heat treatment steps, each of which has specific microstructural targets. Generally, ingot breakdown is usually conducted above the beta transus temperature to produce homogeneous wrought material, resulting in a transformed microstructure where the morphology is significantly influenced by the cooling rate. Further, dynamic globularization with subsequent annealing is employed below the beta transus temperature to produce an equiaxed (α +β) microstructure from the transformed beta microstructure

Figure 5.1 illustrates the microstructure characteristics of the as-received Ti-6Al-4V, heat treated at a temperature of 1020°C and followed by cooling in various medium. For this study, specimens measuring 4.5mm x 10mm were heat treated at 1020°C and soaked for 30 minutes and finally cooled either by fan, in air, in furnace or water quenched. The resultant microstructures showed significant changes in acicular α lath thickness. The morphology of secondary α can be easily noticed from its typical martensitic structure, consisting of misoriented colonies of needle-like α within prior β grains. Apart from the effect of temperature, the cooling rate seems to be one of the most important parameters affecting

microstructural development. Usually, slow and intermediate cooling rates lead to nucleation and growth of α-lamellae into the initial β grains through a diffusion controlled process, whereas higher cooling rates render a martensitic transformation[2]. A slow cooling rate leads to a diffusion controlled growth process of α-phase lamellae, and neighbouring α and β lamellae possess highly coincident interfaces. On the other hand, high cooling rates result in a martensitic transformation and differences in the crystallographic orientation of adjacent lamellae are considerably larger, resulting in interfaces with low coincidence.

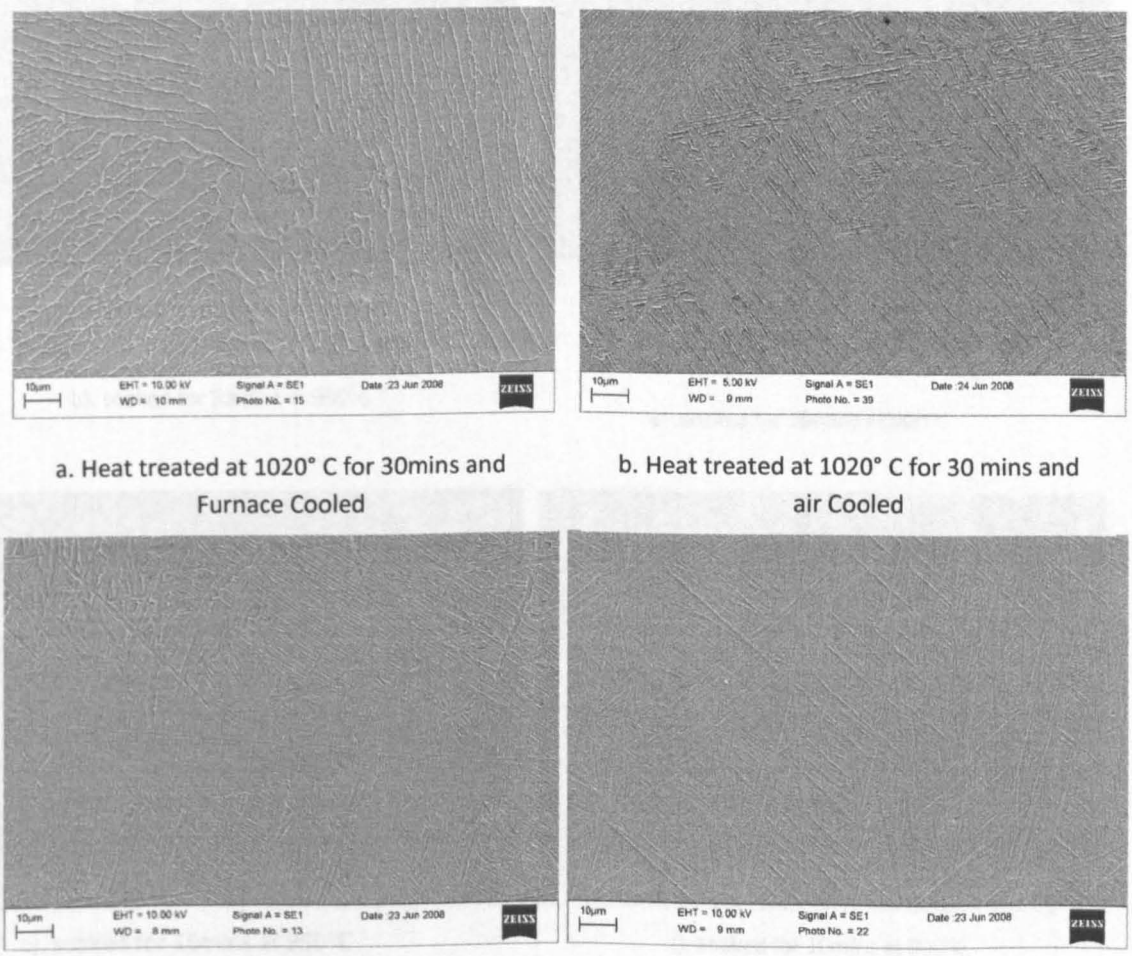

a. Heat treated at 1020° C for 30mins and Furnace Cooled

b. Heat treated at 1020° C for 30 mins and air Cooled

c. Heat treated at 1020° C for 30 mins and Fan Cooled

d. Heat treated at 1020° C for 30 mins and Water Cooled

Figure 5.1: SEM micrographs (Secondary imaging) of as-received Ti-6Al-4V heat treated at 1020°C and cooled in various medium: (a) Furnace cooled, (b). Air cooled, (c). Fan cooled, and (d). Water cooled.

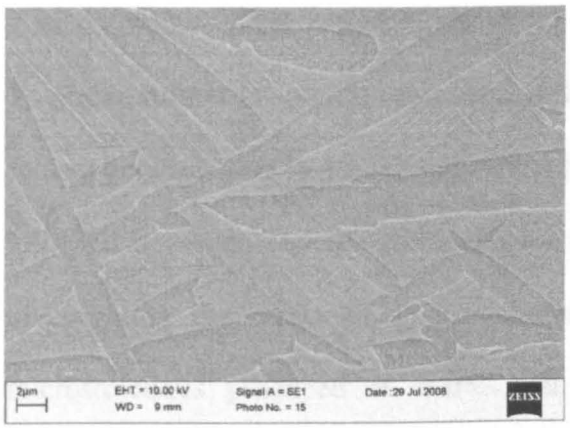

a). soaked for 2hrs at 950°C

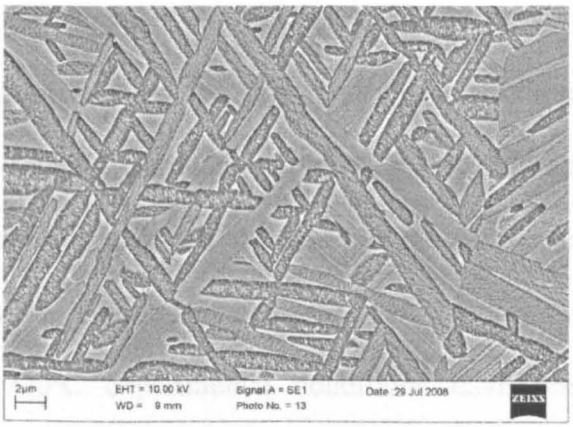

d). soaked for 2hrs at 900°C

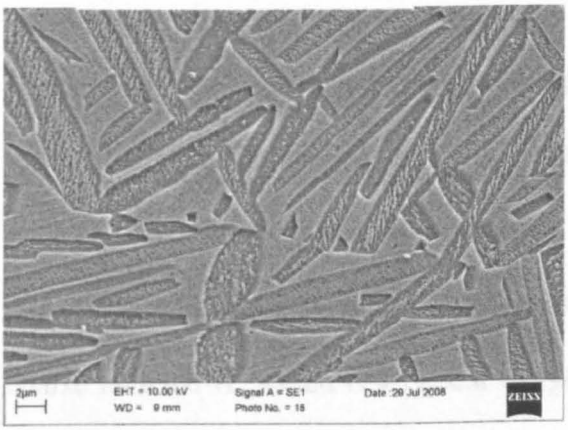

b). soaked for 30mins at 950°C

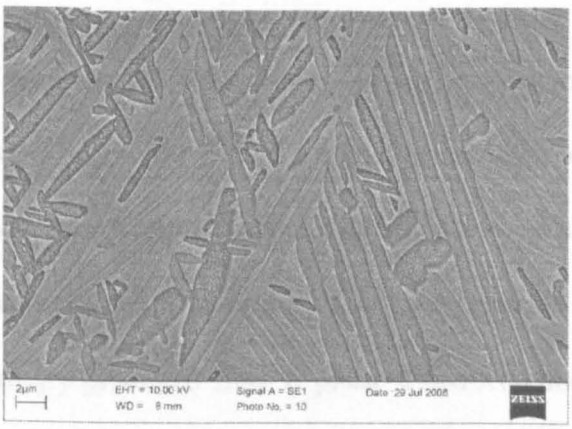

e). soaked for 30mins at 900°C

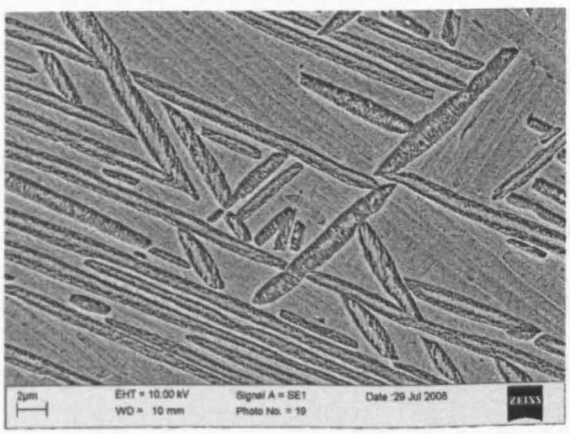

c). soaked for 10mins at 950°C

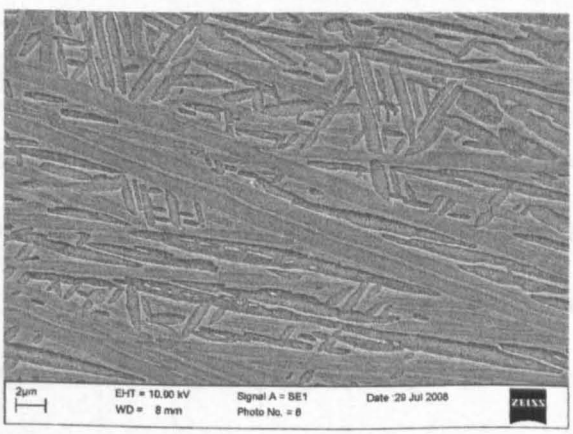

f). soaked for 10mins at 900°C

Figure 5.2: SEM micrographs (secondary imaging) of as-received Ti-6Al-4V alloy heat-treated below beta-transus (950°C & 900°C) temperature and then water quenched.

To obtain further insight into the effect of heat treatment, the Ti-6Al-4V specimens were soaked between 8hrs to 10mins below the β-transus temperatures (900°C and 950°C) and followed by water quenching in order to coarsen the α-lath structure for the purpose of investigating the effect of lath thickness on subsequent deformation. The various microstructures produced at 900°C and 950°C experimental conditions have been presented in Figure 5.2 (a-f).

It is noted that, increasing the annealing temperature will speed up the process of metastable phase decomposition. This results in increased size of α-lamellae colonies as well as increased thickness of α-lamellae and growth of equiaxial α-phase grains. The closer examination of the microstructures developed at 950°C (Figure 5.2 (a - c)) reveals a coarse lamellar α which is a typical morphology produced from β phase transformation upon sudden quenching, comparing to microstructures developed at lower temperatures (900°C) as shown in Figure 5.2 (d - f)).

Further, previous studies [184] showed the effect of soaking temperature on the alpha lath thickness – which could be an important consideration because this is known to have an effect on plastic flow behaviour at certain hot working temperatures. In order to characterise the variation in thickness of the alpha phase, measurements were made using the linear intercept method on SEM (Scanning electron microscope) images processed using Image J software. The time versus alpha laths thickness plot is illustrated in Figure5.3. The thicknesses of alpha laths were measured and tabled (Tables 5.1 and 5.2). It has been observed (from Table 5.2) that with varying cooling rate from slow to high, there was a decrease in alpha lath thickness with increase in cooling rate.

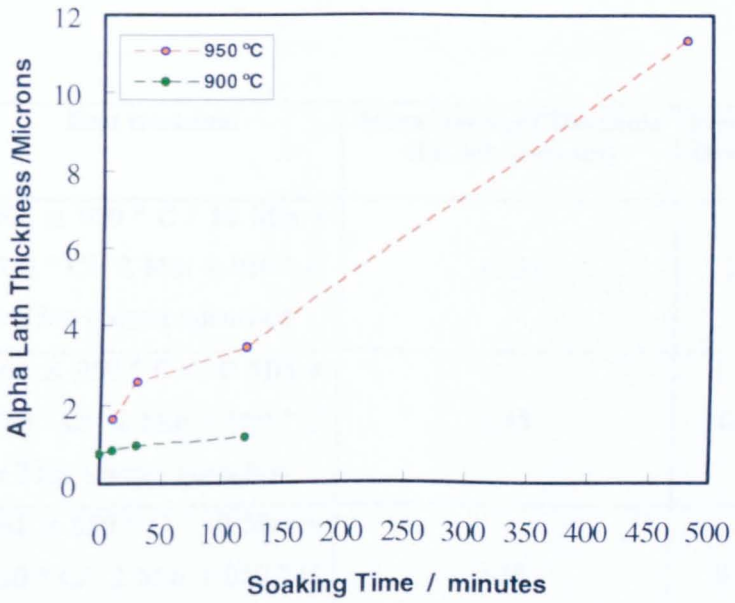

Figure 5.3: Measured alpha lath thickness vs. time plot for Ti-6Al-4V.

For example, the thickness of furnace cooled (i.e. slow cooled) alpha laths was observed to be more than thickness of air and fan cooled alpha laths. Below the β transus temperature, there was an increase in alpha lath thickness with increasing soaking time.

Table 5.1: Varying alpha lath thickness of Ti-6Al-4V with various cooling rates.

Heat treated Alloy	Mean (average) thickness of lath Microns	Standard Deviation
Ti64-Furnace cooled	1.88	0.35
Ti64 –Air Cooled	1.27	0.34
Ti64-Fan cooled	0.94	0.13

Table 5.2 The measured alpha lath thickness for water quenched Ti-6Al-4V samples.

Heat treatment	Mean (average) Thickness of α lath (microns)	Standard Deviation
Ti64 at 950 ° C / 10 Min + 1030 ° C/ 2 Min + 950 ° C for 8 hrs + water quenched	11.33	2.27
Ti64 at 950 ° C / 10 Min + 1030 ° C/ 2 Min + 950 ° C for 2 hrs + water quenched	3.43	0.71
Ti64 at 950 ° C / 10 Min + 1030 ° C/ 2 Min + 950 ° C for 30 Min + Water quenched	2.58	0.76
Ti64 at 950 ° C / 10 Min + 1030 ° C/ 2 Min + 950 ° C for 10 Min + Water quenched	1.60	0.60
Ti64 at 950 ° C / 10 Min + 1030 ° C/ 2 Min + 900 ° C for 2 hrs +Water quenched	1.17	0.37
Ti64 at 950 ° C / 10 Min + 1030 ° C/ 2 Min + 900 ° C for 30 Min+ water quenched	0.95	0.28
Ti64 at 950 ° C / 10 Min + 1030 ° C/ 2 Min + 900 ° C for 10 Min + water quenched	0.84	0.24
Ti64 at 950 ° C / 10 Min + 1030 ° C/ 2 Min+ 900 ° C for 0 Min + Water quenched	0.74	0.19

5.2 Microstructure evolution of Ti-6Al-4V during Isothermal forging

Cylindrical specimens of the as-received Ti-6Al-4V bar stock measuring a diameter of 10.0 mm and a height of 15.0 mm were heated to a sub-transus temperature of 950°C at a

rate of 1°C/s, soaked at this temperature for 10 minutes, then heated to a super-transus temperature of 1030 °C, soaked there for 2 minutes, and then followed by water quenching as schematically illustrated in Figure 5.4. This heat treatment was carried out to produce transformed beta grains, containing colonies of acicular (needle-like) α phase as shown in Figure 4.2 (b).

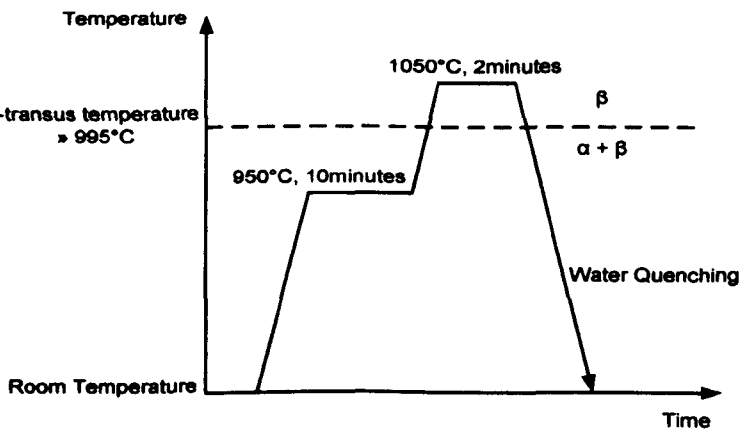

Figure 5.4: Schematic representation of the heat treatment used to produce the transformed acicular microstructure.

Figure 4.2 (b), acicular microstructure was further coarsened to varying degrees by the following procedures. Ti-6Al-4V specimens tested at 950°C was further soaked for ½ hr, 2hrs and 8hrs at 950°C to produce ' fine', 'medium' and 'coarser' alpha platelets with average thicknesses of 2.3μm, 2.9μm and 4.0μm respectively. The specimens tested at 880°C was heat treated in the same way except the final ½ hr of each soak was carried out at the test temperature of 880°C which produced slightly coarser laths with average thicknesses of 2.8μm, 3.7μm and 4.6 μm respectively.

5.2.1 Isothermal forging at 950°C

The microstructure evolution of Ti-6Al-4V during isothermal forging has been studied at a

deformation temperature of 950°C with the alloy showing the 'medium' alpha lath microstructure (Figure 5.5(a-e)).

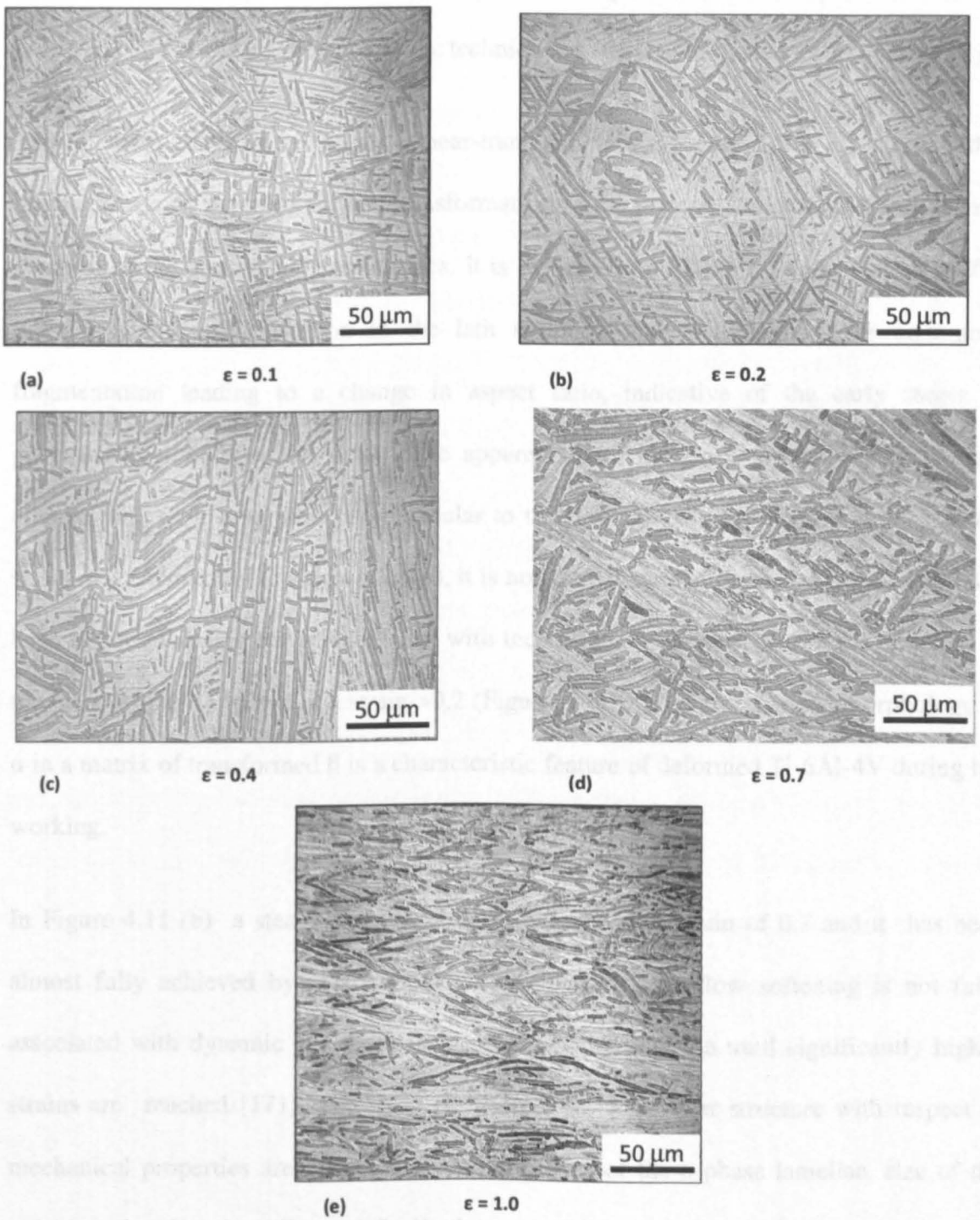

Figure 5.5: Microstructure evolution of medium alpha lath of Ti-6Al-4V at 950°C and at constant strain rate of 0.1/s (a). $\varepsilon = 0$, (b). $\varepsilon = 0.2$, (c). $\varepsilon = 0.4$, (d). $\varepsilon = 0.7$, and (e). $\varepsilon = 1.0$.

The tests were conducted at constant strain rate of $0.1s^{-1}$ until up to the final strains of 0.1, 0.2, 0.4, 0.7 and 1.0. The measured flow stress curves for the above experimental

conditions are shown in Figure 4.11(b). After isothermal compression testing to the predetermined strain level, the cylindrical specimens were water quenched to room temperature. These specimens were axially sectioned parallel to the compression axis and prepared using standard metallographic techniques as discussed in chapter 3 (section 3.1).

The microstructural examinations at near-transus (950°C) (Figure 5.5 (a-e)) suggests that the behaviour of deformation and transformation of the prior alpha lamellar phase is very complex at the processing temperatures. It is evident from Figure 5.5 (a-e) that, at 950°C, there is significant distortion in the lath structure and many laths have undergone fragmentation leading to a change in aspect ratio, indicative of the early stages of progressive globularization. It is more apparent that laths have a tendency to become aligned with their long axes perpendicular to the direction of compressive loading at the strain of 1. According to figure 5.7(a-e), it is noted that some of the lamellar α phases have been distorted during hot working and with increasing strain showed that the break-up of the prior α lamella started at a strain >0.2 (Figure 5.7(c)). The globularized morphology of α in a matrix of transformed β is a characteristic feature of deformed Ti-6Al-4V during hot working.

In Figure 4.11 (b) a steady-state flow stress is reached at strain of 0.7 and it has been almost fully achieved by a strain of 1, it is apparent that flow softening is not fully associated with dynamic globularization, which is not possible until significantly higher strains are reached [171]. The basic parameters for a lamellar structure with respect to mechanical properties are the β-grain size, thickness of the α-phase lamellae, size of the colonies of α-phase lamellae and finally the nature of the inter-lamellar interface (β-phase). These microstructural features have a direct influence on the mechanical properties of the alloy. For example, the fatigue strength of the alloy depends on the forging temperature, which controls the type of microstructure and the level of plastic deformation. On the other

hand, increasing the amount of the lamellar α-phase improves the fracture toughness of the alloy because the colonies of α-phase lamellae, with various orientations hinder crack growth [185].

In order to carry out a quantitative examination of changes in lath morphology, orientation image maps were constructed from EBSD patterns of the hcp alpha phase in the same transverse plan as the optical micrographs. These measurements were made using a step size of 1μm, small enough to enable identification of primary alpha laths with thicknesses above ~ 1μm, while also being large enough to enable coverage of a significant area, 600 μm x 600 μm, which encompassed several alpha colonies in a reasonable period of time.

All of the alpha maps were constructed by drawing boundaries between regions of alpha phase with orientation differences greater than 10°. The alpha lath morphology of initial pre-tested and deformed 'medium' thickness α – lath microstructure of Ti-6Al-4V at 0.1/s with various strains (0.0, 0.2, 0.7 and 1.0) have been presented in Figure 5.6. It is noted that, in order to avoid small grains, grains with perimeter less than 10μm are not shown here. In Figure 5.6 (a), the alpha phase texture evolution of pre-tested acicular microstructure shows random orientation of alpha laths in the basal pole figure for strains of 0.0, 0.2, and 0.7, predominately very strong in one direction with increasing strain (ε = 1) and at constant strain rate of 0.1/s. Therefore, the effect of deformation temperature and increasing strain can rotate and break the laths towards the direction perpendicular to the loading axis.

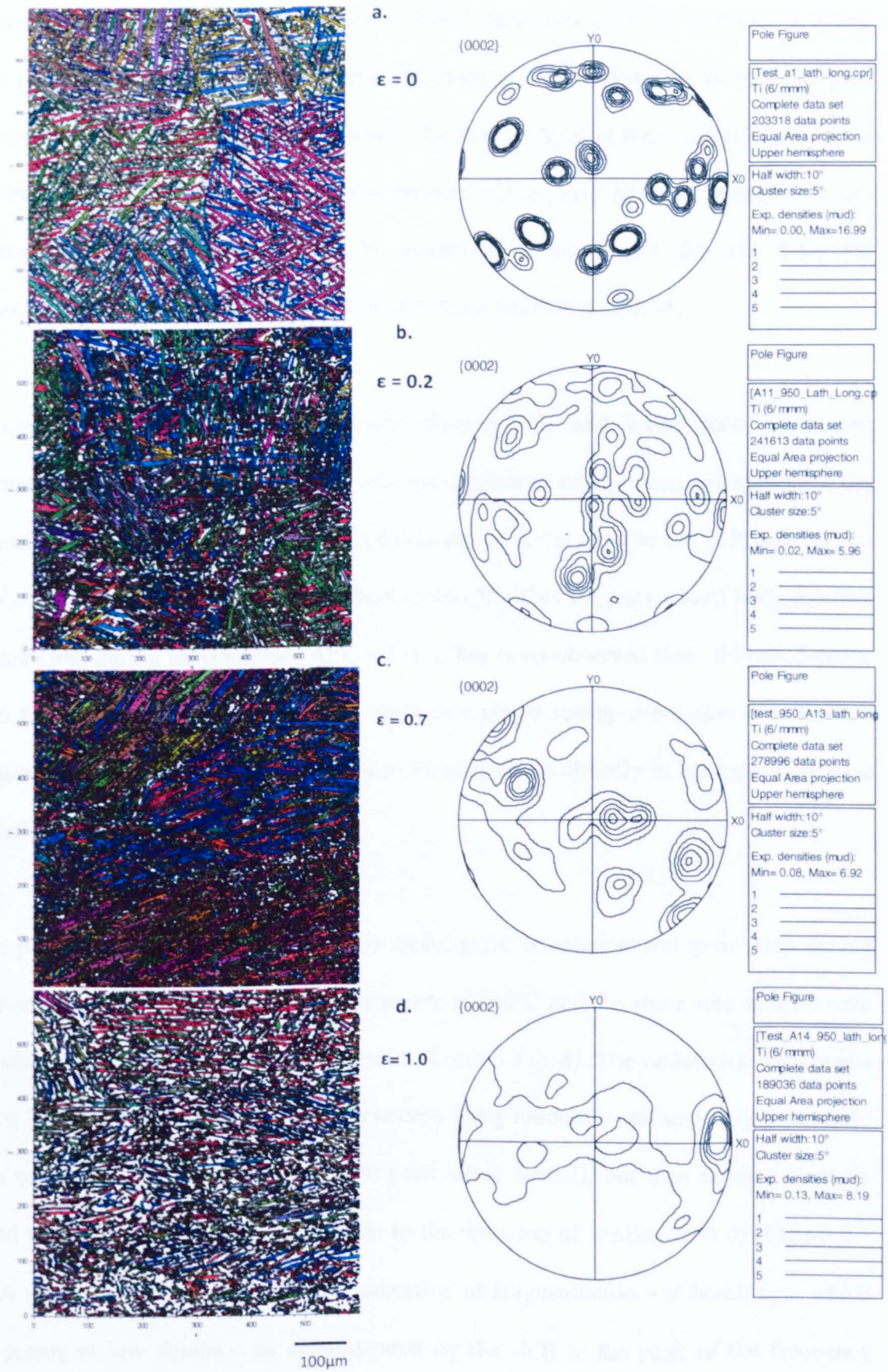

Figure 5.6: The EBSD grain mapping and orientation of alpha laths on medium alpha lath of Ti-6Al-4V at 950°C and 0.1/s with various strains (a). $\varepsilon = 0$, (b). $\varepsilon = 0.2$, (c).$\varepsilon = 0.7$, and, (d). $\varepsilon = 1.0$.

The orientation of alpha laths at strain of 1.0 and strain rate of 0.1/s, indicates a strong single pole orientation towards transverse direction and also shows in increase in pole intensity as compared to lower strain levels. Further looking at these EBSD maps, it is noted that, these maps clearly reflect the primary alpha grain structure apparent in the optical micrographs (Figure 4.3 (a) for undeformed and Figure 5.5 for deformed specimens) at 950°C for strains of 0.2, 0.7and 1.0 and strain rate of 0.1/s.

The constructed orientation image maps (Figure 5.6) and basal pole orientation distribution, confirms that most of the laths have followed nearly same orientation in the beta matrix. This might be due to the free rotation of alpha laths in the soft beta matrix because of the high volume fraction of beta at 950 °C. This suggests a hard body rotation of alpha laths during deformation. At $\varepsilon = 1.0$, it has been observed that (Figure 5.6(d)), due to high beta-phase volume-fraction, there is a single strong orientation developed – indicating that the alpha laths have become oriented predominantly in a single transverse orientation.

In the present work, the evolution of the alpha grain orientation and grain area during deformation of the 'medium' lath microstructure at 950°C and the strain rate of 0.1/s with local strains of 0.1, 0.2, and 1.0 are shown in Figure 5.7 (a-d). The orientation histograms (Figure 5.7(c)) clearly indicates that laths remain fairly randomly oriented during the early stages of deformation, until well past the peak stress (ε=0.2), but then became strongly aligned with their long axes perpendicular to the direction of loading (ε=1.0) (Figure 5.7 (d)). A decrease in alpha grain size is indicative of fragmentation and break ups, which even occurs at low strains – as demonstrated by the shift in the peak of the frequency distribution with increasing strain.

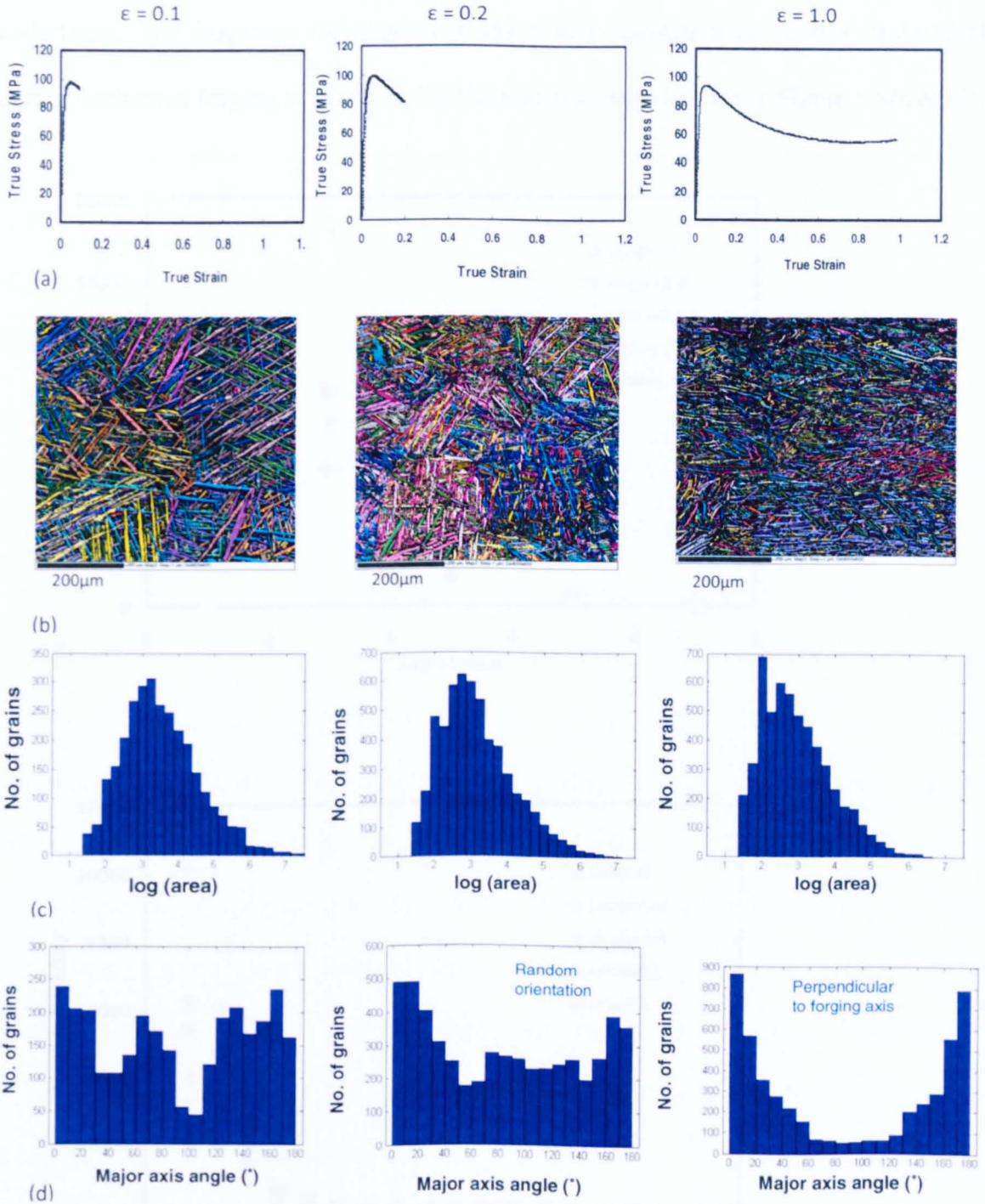

Figure 5.7: Alpha grain evolution of Ti-6Al-4V deformed at 950°C and strain rate of 0.1/s. (a). Flow curves, (b). Orientation maps, (c). Grain area histogram maps, (d). Laths orientation distribution.

The grain measurements are easily extracted by fitting an ellipse to each grain shape, which allows a statistical examination of changes in lath orientation and aspect ratio to be undertaken. The frequency distribution of the α-lath orientation at various strain levels during isothermal forging at 950°C and 0.1/s have been summarised in Figure 5.8(a & b)).

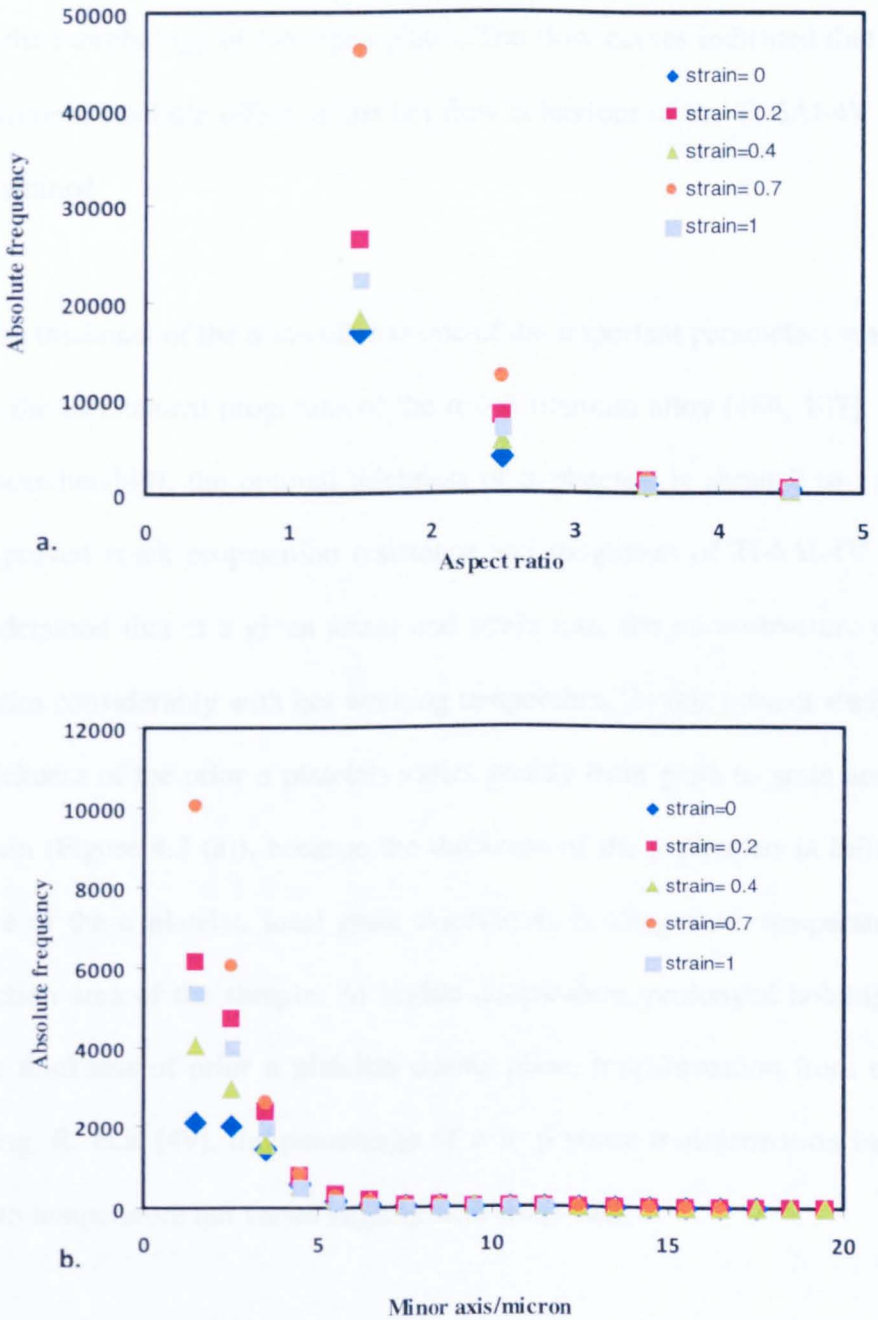

Figure 5.8: Frequency distribution of α laths aspect ratio during isothermal forging at 950°C and 0.1/s. (a) Absolute frequency vs. Aspect ratio (b) Absolute frequency vs Minor axis/micron

This shows that the average grain size remains stable with increasing strain, with only a slight tendency to increase with increasing strain. In the present study, the absence of a measurable amount of globularization at strains less than $\approx$ 1.0 suggests that the large amount of flow softening observed at strains less than this level is not related to a change in the morphology of the alpha phase. The flow curves indicated that the initial alpha-lath thickness has little effect on the hot flow behaviour of the Ti-6Al-4V under the conditions examined.

The thickness of the α-lamellae is one of the important parameters which has a great effect on the mechanical properties of the α + β titanium alloy [186, 187]. According to earlier researchers[49], the optimal thickness of α platelets is about 2 to 5μm, which led to an improved crack propagation resistance and toughness of Ti-6Al-4V alloy. Further, it is understood that at a given strain and strain rate, the microstructure of the titanium alloy varies considerably with hot working temperature. In this present study, it is noted that the thickness of the prior α platelets varies greatly from grain to grain and area to area in one grain (Figure 4.3 (a)), because the thickness of the α platelets is influenced by the initial size of the α platelet, local grain orientation, holding time, temperature, strain rate cross section area of the sample. At higher temperature, prolonged holding time can influence the thickness of prior α platelets during phase transformation from α to β. According to Ding, R, et.al.[49], the percentage of α to β phase transformation increases significantly with temperature but varies slightly with strain rate.

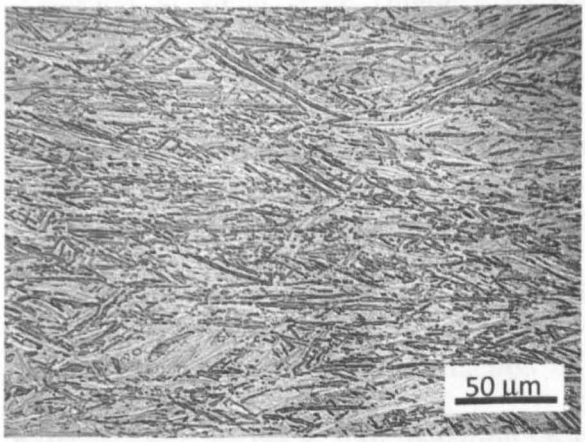

(a) 30mins at 950 ºC, ε = 1.

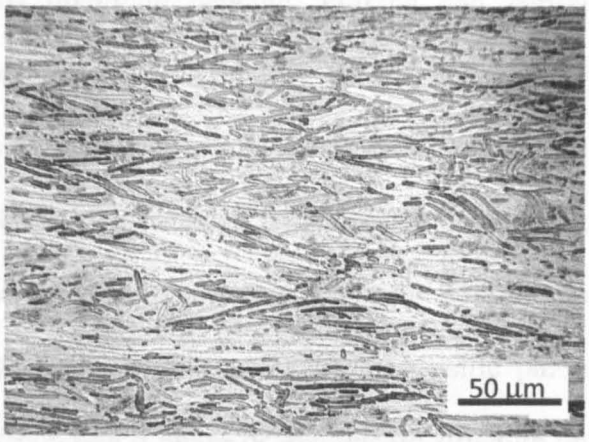

(b) 2hrs at 950 ºC, ε = 1.

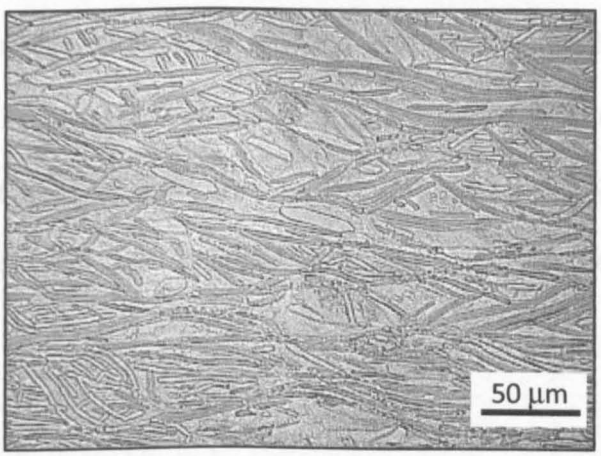

(c) 8hrs at 950 ºC, ε = 1.

Figure 5.9: Optical micrographs of the deformed microstructure of Ti-6Al-4V alloy processed by (a-c) water cooling at 950 ºC with constant strain (ε = 1.0) and strain rate of 0.1/s.

It is evident from Figure 4.3 (b) that, the microstructure of the undeformed Ti-6Al-4V samples heat-treated at 950 ºC in the (α + β) phase field for ½ hr, 2hrs, and 8hrs and water quenched consists of prior α lamella (thick) and the newly formed α lamella (thin) and there is coarsening of α lamella with increasing holding time. The hot-compressed Ti-6Al-4V at constant strain (ε =1) and strain rate (0.1/s) in the (α + β) phase field at 950 ºC for ½ hr, 2hrs, and 8hrs have been presented in Figure 5.10 (a-c). It has been observed that part of the prior α phase lamellae is transformed into high temperature β phase, and most of the retained prior α lamellae has become distorted because of variation in local stresses during

hot working. It can be seen that under deformed conditions the laths undergo significant distortion at some stage (Figure.5.10 (a-b)) involving bending, kinking and partial globularization. The second important phenomenon observed during hot forging is phase transformation, which is influenced by factors such as temperature, strain rate and the level of plastic deformation. The lower volume fraction of α at higher temperatures is the result of α to β transformation. In the (α+β) phase field, the volume percentage of the β phase can be estimated from the volume fraction of the secondary α phase or martensitic phase because some of the β will transform into secondary α phase or martensitic structure on cooling. The processing temperature influences the phase transformation greatly and the strain rate has minor influence on the ratio which is well documented in literature [49] for strain rate ranges from 0.05 to $1.0s^{-1}$. It can also be concluded that, most of the prior α lamellar phase inside the grain has been transformed into the β phase at higher temperatures and further into the secondary α phase during the post-deformation quenching.

Dynamic recrystallization (DRX) is another important phenomenon usually observed during hot working of the Ti-6Al-4V alloy. Usually, in most metallic materials, the driving force required for recrystallization arises from the stored energy in the form of dislocation density. The driving force for solid phase transformation is about 1.0 $kJmol^{-1}$ which usually comes from the differences in the free energies between different phases [188]. The percentage of DRX increases with increasing deformation temperature with strain rates of 0.5 and $1.0s^{-1}$ [49]. In theory, during hot compression testing for titanium alloys, the occurrence of phase transformation is more difficult than DRX because the required driving force for phase transformation is much higher than that of DRX. However, hot working in the (α + β) phase field, the phase transformation would occur concurrently with mechanical deformation and DRX does not occur in this temperature range.

Therefore, it is clear that, the DRX of the β phase and/or metadynamic recrystallization cannot take place in the (α + β) phase field under the experimental conditions given above.

5.2.2 Isothermal forging at 880°C

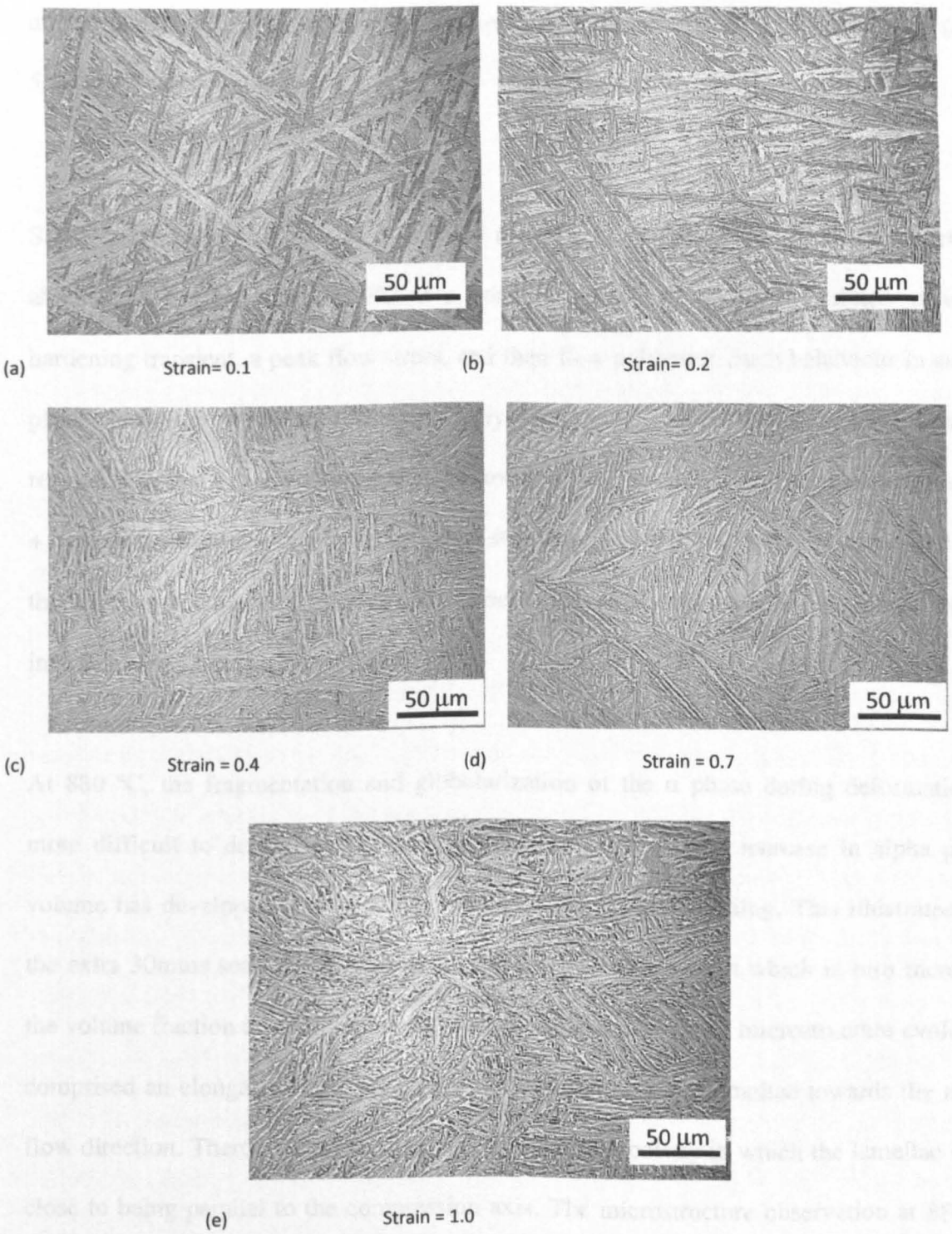

Figure 5.10: Optical micrographs of medium alpha lath of Ti-6Al-4V deformed with various strains at 880°C and 0.1/s

Similar to the microstructural evolution at 950°C discussed in the previous section, the flow curve behaviour and microstructure evolution of Ti-6Al-4V during isothermal forging at 880°C, at constant strain rate of $0.1s^{-1}$ and strain of 0.1, 0.2, 0.4, 0.7, and 1.0 for 'medium' alpha lath have been studied. The flow stress curves and deformed microstructures for the above experimental conditions are shown in Figures 4.11 (a) & 5.10 (a-e)) respectively.

Stress-strain curves (Figure 4.11 (a)) of the Ti-6Al-4V alloy with 'medium' thickness alpha laths compressed at 880°C at a nominal strain rate of 0.1/s exhibited an initial hardening transient, a peak flow stress, and then flow softening. Such behaviour in single-phase metallic materials is commonly associated with discontinuous dynamic recrystallization, i.e. the nucleation and growth of new grains [189]. But, for two phase (α + β) titanium alloys with a lamellar initial structure, flow softening can be associated with the rotation of lamellae toward "softer" orientations with slip transmission across the α/β interfaces [163] and [189].

At 880 °C, the fragmentation and globularization of the α phase during deformation is more difficult to detect, due to its large volume fraction. The increase in alpha phase volume has developed coarser alpha lamellar after water quenching. This illustrates that the extra 30mins soak at 880 °C can lead to $\beta \rightarrow \alpha$ transformation which in turn increases the volume fraction of α-phase. During compression at 880°C, the microstructure evolution comprised an elongation of the β grains and rotation of the α lamellae towards the metal flow direction. There are bent α lamellae observed in α colony in which the lamellae were close to being parallel to the compression axis. The microstructure observation at 880 °C clearly indicates that, with increasing strain the initial uniform lath structure has undergone significant distortion including bending and kinking – noticed in those laths which lie

almost parallel to the (vertical) direction of loading. This particular mode of mechanical lath deformation is well-documented [163, 190]. Those laths in the colonies which are initially aligned with metal flow direction i.e., perpendicular to the compression axis have undergone little morphological change during deformation. At $\varepsilon = 1.0$ almost all of the lamellae had become aligned with the metal flow direction (Figure 5.10 (e)), confirming that the degree of lamellar rotation increased with strain. The work by Semiatin et al.[191], on microstructure evolution of Ti-6Al-4V on deformation at 880 °C was found to be mainly associated with the common processes of α platelet pinch-off/fragmentation and subsequent globularization of the remnant lamellae by termination migration.

It is evident from Figure 5.10 (b & c) that, during deformation at 880°C, there is a break up of α platelet and Figure 5.10 (d) shows that globularization of the remnant lamellae does also occur. At $\varepsilon = 1.0$, a mixed microstructure consisting of remnants of lamellae along the metal flow direction and globular α particles was formed (Figure 5.10 (e)). Here, the lamellar structure is very stable during deformation at 880°C. Nevertheless, a small amount of globularization is achieved through the kinking of the alpha laths whose plane normal is nearly perpendicular to the loading direction and the remaining alpha laths tended to be reoriented in a position with the plane normal nearly parallel to the compression direction. Hence, a change in strain path leading to the rotation of the workpiece during deformation may enhance the rate of globularization during warm deformation. Orientation image maps which have been constructed from EBSD images in order to determine the change in lath morphology and orientation of grains using MATLAB M-Tex software. Initially, the EBSD measurements were carried out to determine the basal texture of the deformed Ti-6Al-4V at constant strain rate of 0.1/s with strains of 0.0, 0.2, 0.7, and 1.0, to study the orientation of alpha laths in the basal plane. The grain orientation maps for both undeformed and deformed Ti-6Al-4V sample areas were analysed.

It can be seen that a sufficient number of grains were measured in order to construct the pole figures. Here, the specimens were sectioned axially and EBSD measurements were carried out at one third of the deformed specimen height, indicative of the average deformation. EBSD analysis was carried out using a Zeiss field emission gun scanning electron microscope, and orientation maps were constructed from orientation data using MTEX texture analysis software [192].

The alpha phase texture evolution of the pre-tested acicular microstructure shows this random orientation in the basal pole figure, predominately very strong in one particular direction with weak other orientations, seen as faint dots. Figure 5.16 (a) shows the orientation of grains at strain = 0 where the basal plane confirms the random orientation of laths which is similar to the grain orientation map at $\varepsilon = 0$. At $\varepsilon = 0.2$, three strong orientations of laths were observed in the basal pole (Figure 5.11 (b)), one of them seems to be strong as compared to the other two faint ones. With increase in strain ($\varepsilon = 0.4$ & $\varepsilon = 0.7$), it is seen that the previous three strong orientations were joined together to form intermediate single orientation of laths (Figure 5.11 (c& d). In Figure 5.16 (d) it is noted that, increasing in imposed strain can rotate the α–laths and makes them align in the direction perpendicular to the hot-compression direction. The significant points in Figure 5.11 (d) show that the intensity is only 2x random (the other are nearly 10x random) and are have less intense orientation. This correlates with the higher amount of spheroidisation.

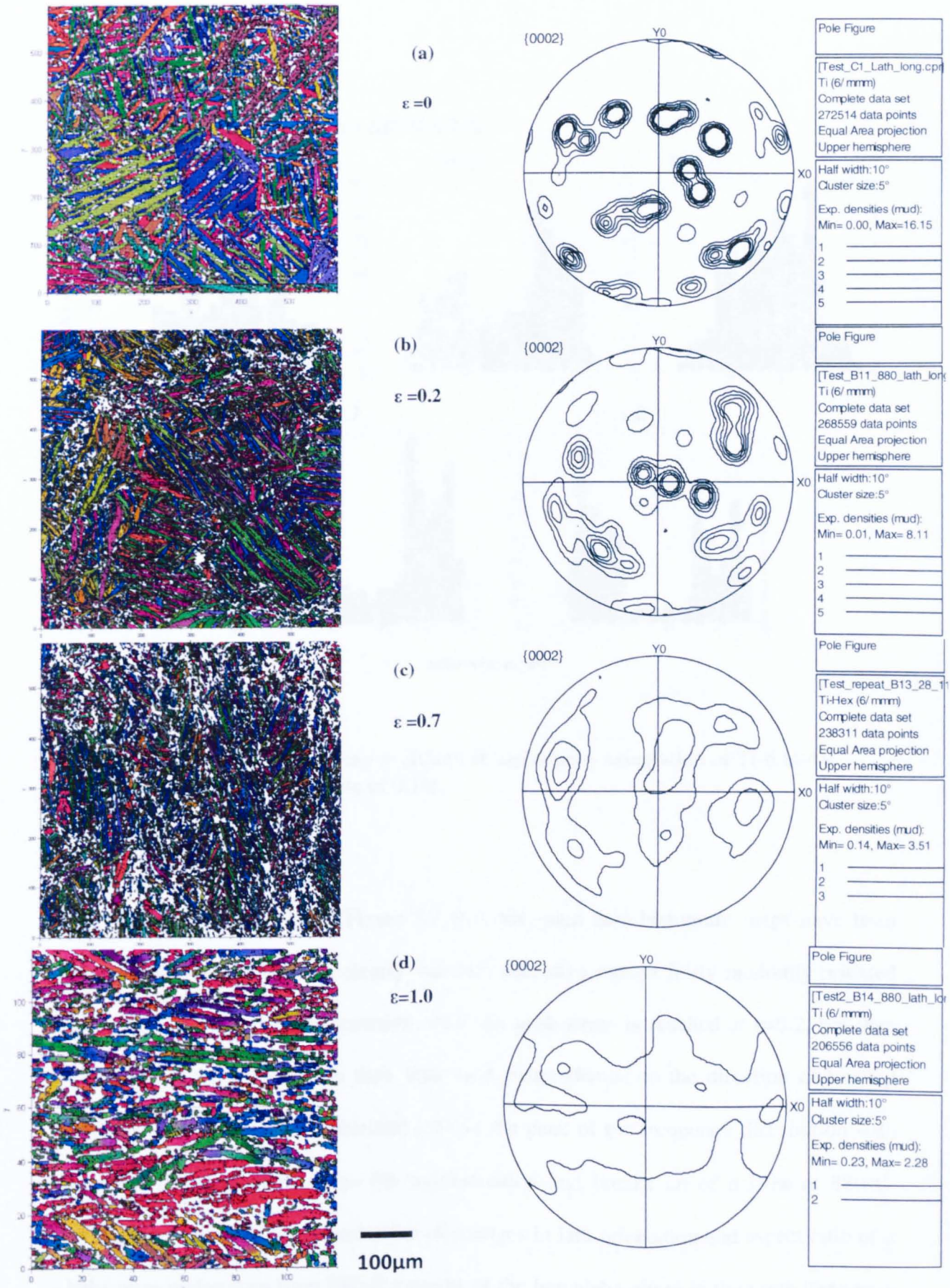

Figure 5.11: The EBSD grain mapping and orientation of alpha laths on medium alpha lath of Ti-6Al-4V at 880°C and 0.1/s with various strains (a). ε = 0, (b). ε = 0.2, ε = 0.7, and (d). ε = 1.0.

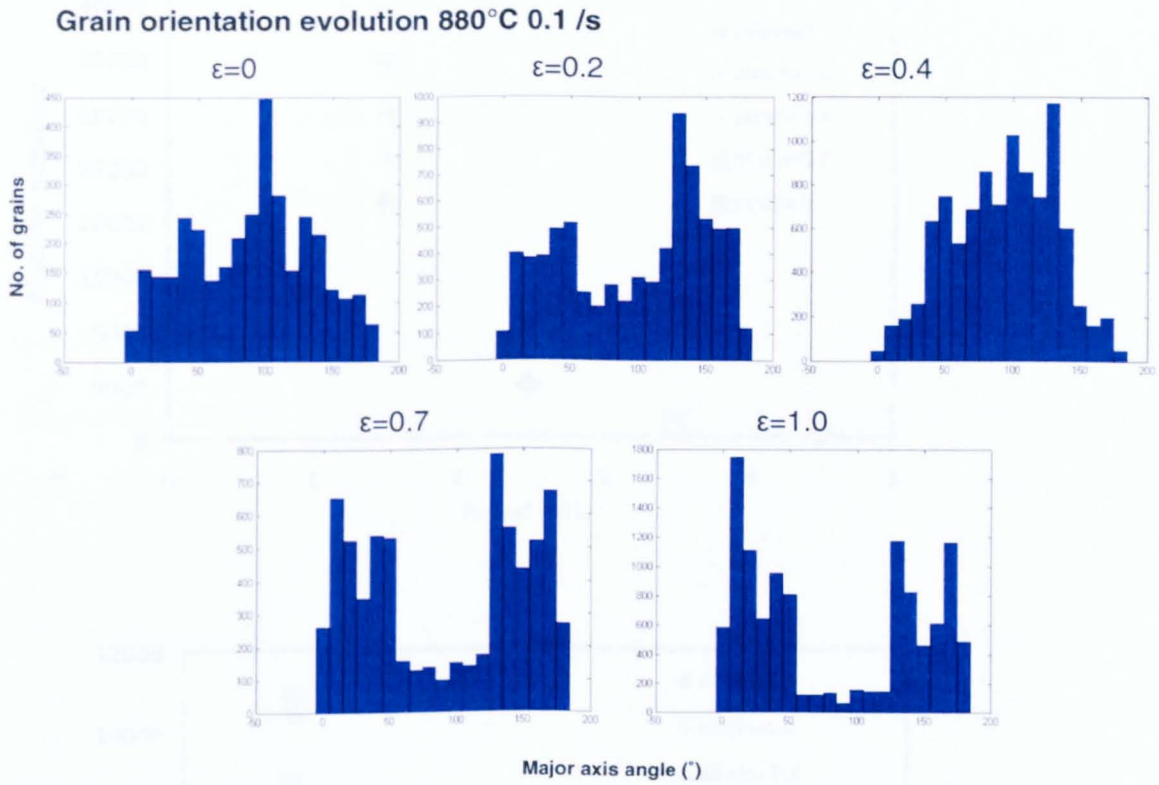

Figure 5.12: Histograms showing evolution of alpha grain orientation of Ti-6Al-4V deformed at 880°C and strain rate of 0.1/s.

Similar to the tests at 950°C (Figure 5.7 (c)), the grain area histogram maps have been presented in Figure 5.12. This clearly indicates that laths remain fairly randomly oriented during the early stages of deformation, until the peak stress is reached at ε=0.2, but then becomes strongly aligned with their long axes perpendicular to the direction of loading (ε=1.0) (Figure 5.6 (d)). The obtained shift in the peak of the frequency distribution with increasing strain is an evidence for fragmentation and breaks up of α-laths at 880°C. Furthermore, the statistical examination of changes in lath orientation and aspect ratio of α - laths were undertaken from EBSD patterns of the hcp alpha phase in the same transverse plane as the optical micrographs.

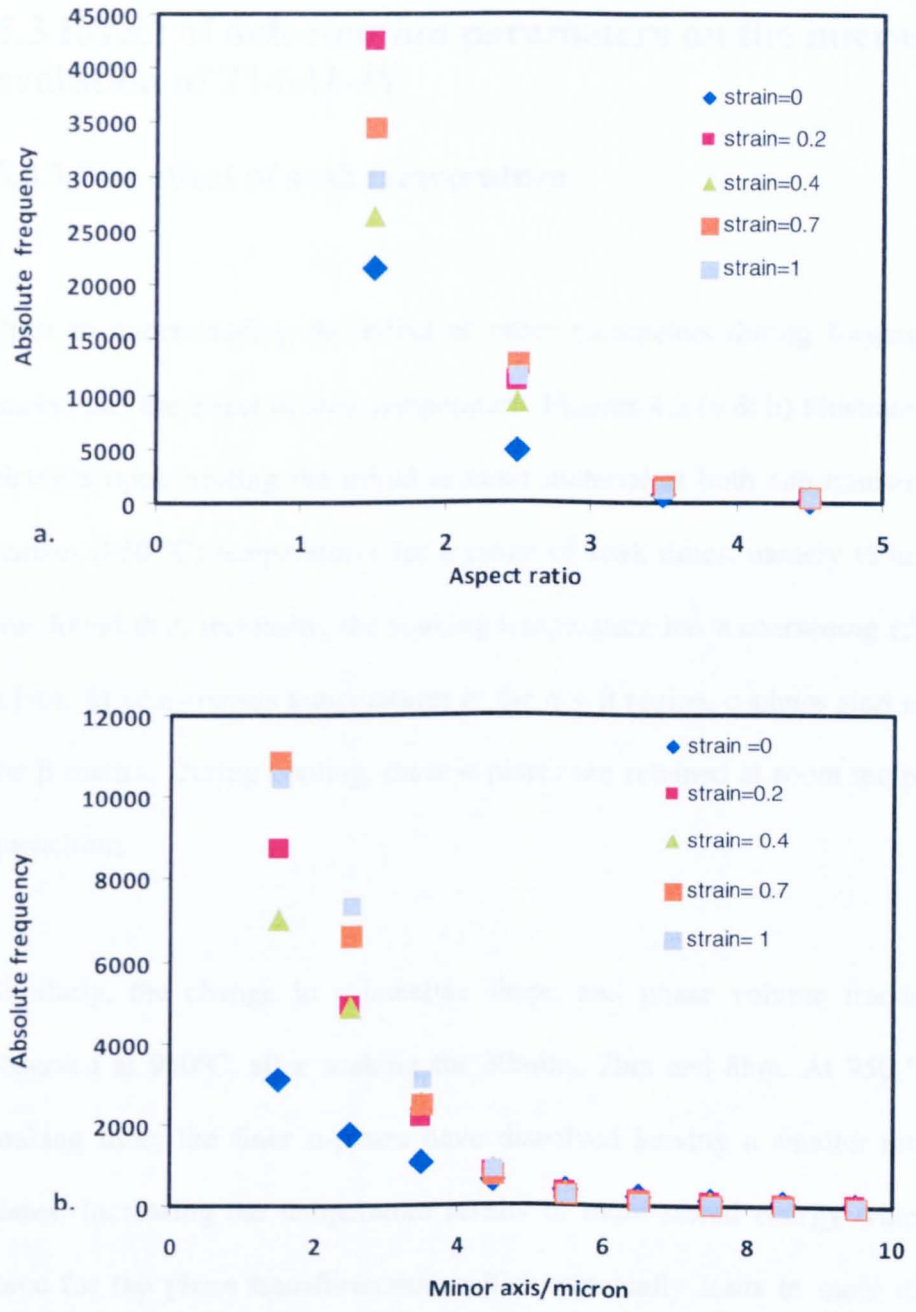

Figure 5.13: Frequency distribution of α laths aspect ratio during isothermal forging at 880°C and strain rate of 0.1/s. (a) Absolute frequency vs. Aspect ratio (b) Absolute frequency vs. Minor axis/micron.

The frequency distribution of the α-lath orientation at various strain levels during isothermal forging at 880°C and 0.1/s have been summarised in Figure 5.13 (a & b). This also confirms that the average grain size is nearly the same with increasing strain rate at 880°C, with only a slight tendency to increase with increasing strain.

5.3 Effect of deformation parameters on the microstructure evolution of Ti-6Al-4V

5.3.1 The effect of soak temperature

Prior to understanding the effect of other parameters during forging, it is pertinent to understand the effect of soak temperature. Figures 4.3 (a & b) illustrate the microstructural changes upon heating the initial acicular material at both sub-transus (880°C) and near-transus (950 °C) temperatures for a range of soak times, namely ½ hr, 2hrs and 8 hrs. It was found that, increasing the soaking temperature has a coarsening effect on the primary α lath. At near-transus temperatures in the α + β region, α-plates start to precipitate within the β matrix. During cooling, these α-plates are retained at room temperature upon water quenching.

Similarly, the change in α-lamellae shape and phase volume fraction of the α-plates observed at 950°C, after soaking for 30mins, 2hrs and 8hrs. At 950 °C, with increasing soaking time, the finer α-plates have dissolved leaving a smaller number of coarser α plates. Increasing the temperature results in more stored energy which act as a driving force for the phase transformation, which eventually leads to more dissolution of the α laths into the β phase. Hence, this results in a decrease in the α volume fraction at higher soaking temperatures. From Figure 4.3 (a & b), it is noted that both temperature and soaking time at temperature influence the phase volume fraction of α-plates within β-phase. Jackson et al., [184], observed that during subtransus heating of Ti-6246, the α-plates coarsen with increasing time and the volume fraction of α-plates reduces with increased time at temperature.

5.3.2 The effect of strain rate

The effect of strain rate on microstructure during hot-forging has been studied at both sub-transus and near-transus temperatures. Figure 5.14 and 5.15 illustrate the effect of strain rate at 850 °C and 950 °C, respectively. At 850 °C, the strain rate of 0.01/s provides more time for coarsening of the α lamellae and β sub grains (Figure 5.15 (a)). At relatively fast strain rate of 1.0/s (Figure 5.15 (b)) the break-ups of α plate in the β matrix initiate. At 950°C (Figure 5.15), a microstructural change similar to that described for 880 °C occurs.

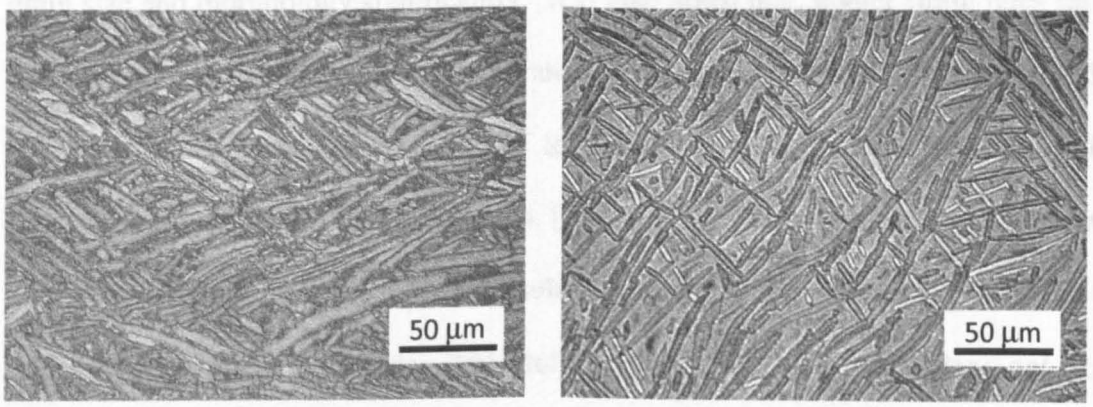

Figure 5.14: Optical micrographs illustrating the microstrural evolution of Ti-6Al-4V specimen deformed to a strain of ε = 1 at 880°C at the strain rate of (a) 0.01/s, (b) 1.0/s.

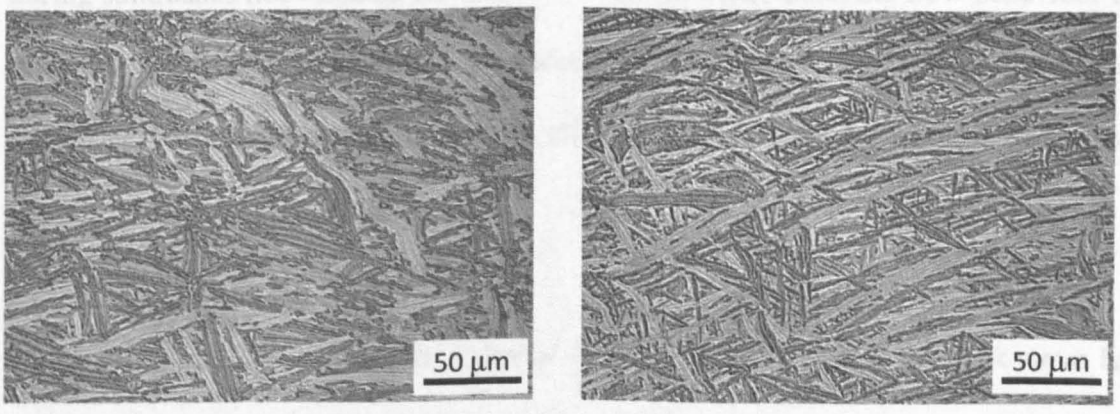

Figure 5.15: Optical micrographs illustrating the microstructural evolution of Ti-6Al-4V specimen deformed to a strain of ε = 1 at 950°C at the strain rate of (a) 0.01 /s, (b) 1.0 /s.

The primary α has similar directionality, with respect to the compression direction but slightly varying size and morphology as compared to the primary α observed at 880 °C. At the strain rate of 0.01/s and 1.0/s, the α-plates are almost dissolved into the β subgrains. This shows that deformation and globularization of the α during deformation increases the dissolution rate of the α in the β matrix. It can be seen from Figures 5.14 & 5.15 that the strain rate has no influence on the volume fraction of the primary α phase but affects its grain size and morphology significantly. It is also noted that, higher strain rates result in a finer microstructure. At higher strain rates, there is an increase in dislocation density, distortion energy and recrystallization locations so there is more possibility for the occurrence of dynamic recrystallization [193]. In the present study, the persistence of microstructural observations during the sub-transus hot compression with a lamellar colony starting microstructure confirms that globularization of the α-plates does not occur by dynamic recrystallization but may occur by localized deformation of the plates and penetration by the β phase. This was well documented by Semiatin et al.[194], while investigating the effect of starting transformed microstructure on globularization kinetics during subtransus hot working of Ti-6Al-4V. On the other hand, the flow behaviour of the material with 'medium' lath thickness deformed at 880°C, strain rates of 0.01/s, 0.1/s and 1.0/s and with constant strain ($\varepsilon = 1$) showed a noticeable dependence on strain rate (Figure 4.10 (a & b)).

At the lower strain rate of 0.01/s, a similar behaviour was observed; the peak stress for the microstructure with slightly coarser alpha exhibited the lowest peak stress. This flow behaviour might be due to the difference in the deformation mechanisms between the lower and higher strain rates respectively.

The effects of strain rate and microstructure evolution on the peak stress were similar at 950 °C as shown in Figure 4.10 (b). It is noted that the flow stress increases with strain rate at constant deformation temperature, as multiplication rate of dislocations is higher at higher strain rates which is well documented in the literature[195, 196]. There is evidence from previous researchers [197, 198], that a higher strain rate would probably result in a higher dislocation density in the deformation process of metals or alloys. There is also significant flow softening at higher strain rate during isothermal compression, which might be due to the adiabatic heating and the resulting α to β phase transformation.

For deformation at the slowest strain rate (0.01/s) at temperatures of 880 °C and 950 °C, the volume fraction of the laths was reduced slightly, as compared to that at higher strain rates. This was rationalised previously by [184] that, at the slowest strain rate, there is more time for diffusion-controlled processes to take place, which leads to greater dissolution of the α phase in the β matrix. This also suggests that a degree of $\alpha \rightarrow \beta$ phase transformation can occur concurrently during hot deformation in the two-phase α + β phase filed.

5.3.3 The effect of deformation temperature

Sha et al [198] studied the effect of deformation temperature on mechanical properties of TC18 alloy and found that ultimate strength and fracture toughness are sensitive to the deformation temperature. Deformation below the β transus is a thermally activated process and an adiabatic temperature rise has a great effect on the primary α volume fraction as well as secondary α phase. The deformation temperature has a significant effect on both the volume fraction and grain size of the primary α phase. In the (α + β) two-phase region, the volume fraction of the primary α phase decreases with increasing deformation temperature in the range from 850°C to 950°C due to the $\alpha \rightarrow \beta \rightarrow \alpha$ transformation.

It is evident from Figure 4.10 (a & b) that at a given strain rate, the flow stress decreases with increasing deformation temperature. This behaviour indicates that the amount of the soft β phase increases with increasing deformation temperature. It is also noted that, there is limited flow softening occurring at higher strain rates with increases in temperature, before the steady state condition is reached; however, the magnitude of this effect is small.

The post-deformed microstructures of 'Coarser', 'Medium' and 'Fine' thickness alpha-laths, deformed at 0.1/s to a true strain of 1, were also observed at both test temperatures 880 & 950°C, in order to determine the microstructure developed at various soaking times (8hrs, 2hrs and 30mins), under the same test conditions (Figure 5.23 (a-f)). The volume fraction of primary α phase as well as the grain size of primary α phase decreases sharply at a deformation temperature of 950°C compared with a sample deformed at the temperature of 850°C.

On the other hand, higher temperature enhances the diffusion process greatly and the merging of the adjacent α grains increases with increasing deformation temperature so that the primary α grain size does not significantly vary with increasing deformation temperature in the range from 850 to 950°C. It is obvious that the change in morphology of secondary α phase with deformation temperature is usually different at a given strain rate (as shown in Figures 5.14 & 5.15). This is mainly due to the formation of coarser lamellae of secondary α phase and the increased amount of the secondary α phase at higher deformation temperatures. At the lower deformation temperature of 880°C, there is significant disordered distribution of the secondary α phase that can be seen as little grains or short platelets.

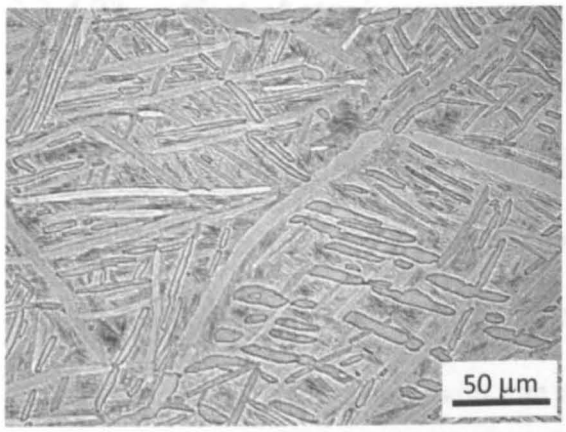

(a). Coarser lath, 950°C, 0.1/s

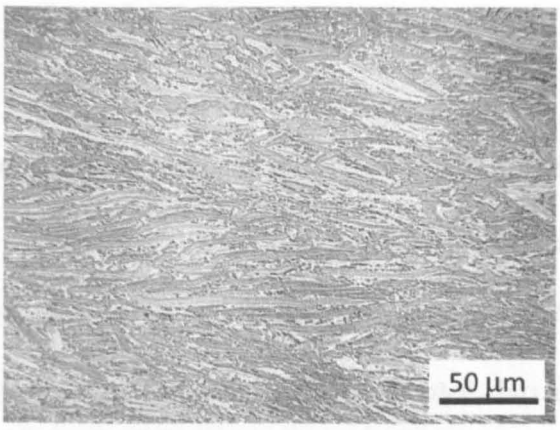

(d). Coarser lath, 880°C, 0.1/s

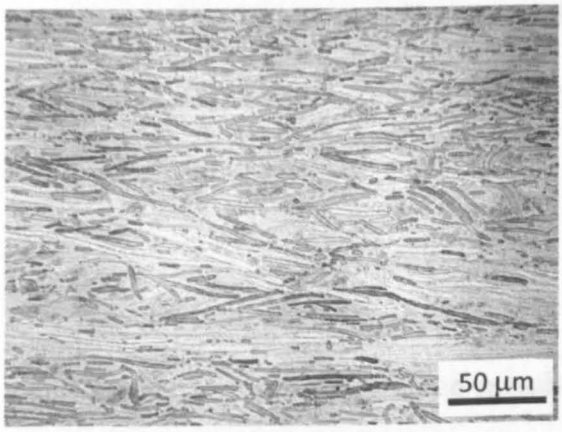

(b). Medium lath, 950°C, 0.1/s

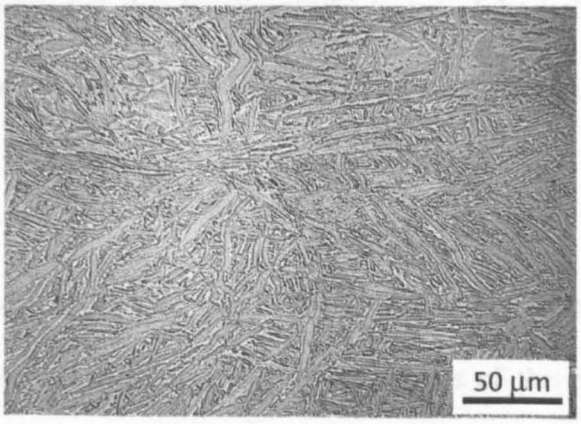

(e). Medium lath, 950°C, 0.1/s

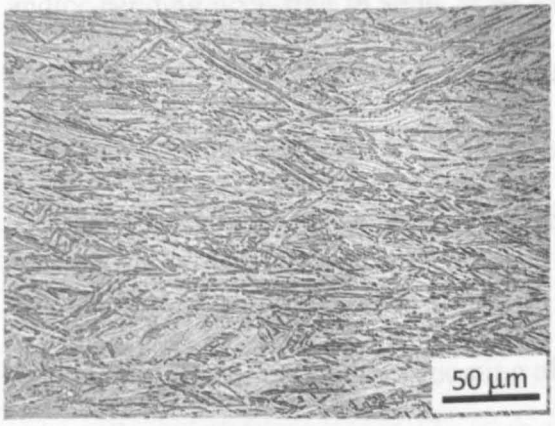

(c). Fine lath, 950°C, 0.1/s

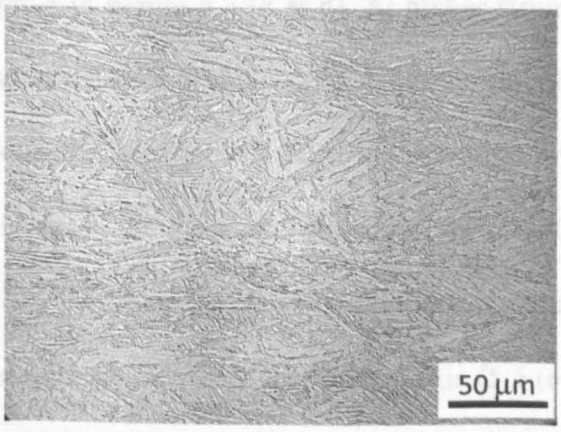

(f). Coarser lath, 880ºC, 0.1/s

Figure 5.16: Post-deformed microstructures of 'Coarser' 'Medium' and 'Fine' thickness alpha-lath, deformed at 0.1/s to a true strain of 1 for temperatures 880 and 950°C.

5.3.4 The effect of strain

The post-deformation microstructure evolution during isothermal forging at 950°C for the material with 'medium' thickness alpha-laths, deformed at 0.1/s was systematically studied with regard to its dependence on local strain (Figure 5.7 (a-e)). These micrographs clearly show the break-up of the α laths with true strain and the formation of a nearly globularized α structure. On the other hand, it is evident from Figure 5.15 (a-e) that the microstructure evolution during isothermal forging at 880°C for the 'medium' thickness alpha-lath, deformed at $0.1/s^{-1}$ with varying strain consists of significant distortion, including bending and kinking of the laths.

It is evident from Figures 5.5 (a-e) and 5.10 (a-e) that the imposed strain can make significant changes in the α-phase morphology. At lower strain, the structure of the α-phase consists of a combination of undeformed and partially distorted laths with kinking and/or bending occurring in some areas as shown in Figure 5.5 (c & d). At higher strains, the α-laths break up and transform the initial acicular morphology to a nearly globular equiaxed structure (Figure 5.5 (e)). This confirms that if α – lamellae structure was strongly aligned with their long axes perpendicular to the direction of loading, the α- laths became kinked (as observed at Figure 5.10 (e)) or otherwise, the α – lamellae structure rotated with strain, eventually becoming aligned perpendicular to the loading axis (5.5 (e)). Such alignment of α- laths is well documented by Semiatin et al., for Ti-6Al-4V deformed at relatively high temperature [163] and found that these alignments gradually eliminate the morphological differences between neighbouring α colonies and resulted in the formation of a relatively homogeneous microstructure.

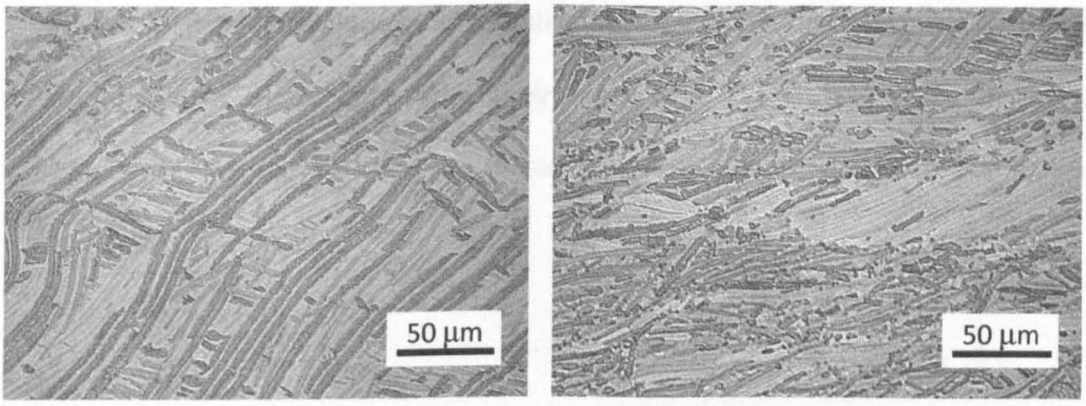

Figure 5.17: Optical micrographs illustrating the microstructural evolution of Ti-6Al-4V specimen deformed at 950°C at the strain rate 0.1/s. (a). ε = 0.7 (b). ε = 1.0

The above micrographs show the bending and break up of α-laths during deformation at 950°C and constant strain rate of 0.1/s. In Figure 5.24, the bending of the α-laths occurred at ε = 0.7, with increasing strain i.e. at ε = 1.0 there was a break up and initial globularization of α-laths occurring by transformation from α-lamellar structure to equi-axed globular α- particles.

5.4 Conclusion

- Hot compression behaviour of a commercial grade Ti-6Al-4V with an acicular starting microstructure has been characterized with the help of isothermal compression tests at both near-transus (950°C) and sub-transus temperatures (880°C) with various strain levels (0.1,0.2,0.4,0.7 and 1.0) and strain rate range (0.01-1.0s^{-1}).

- Significant flow softening, observed for all deformation conditions, was not solely associated with globularization of the lamellar structure. Instead, progressive realignment of alpha laths with their long axes perpendicular to the uniaxial compressive loading axis appears to coincide with the attainment of a steady-state flow stress.

- In the present study, the microstructural observations during the sub-transus hot compression with a lamellar colony starting microstructure confirms that globularization of the α-plates does not occur by dynamic recrystallization but may be due to localized deformation of the plates and penetration by the β phase.

- Microstructure evolution during deformation of Ti-6Al-4V is motivated mainly by the imposed strain and by kinking of the α lamellae. If the long axes of alpha laths are perpendicular to the loading direction, the α laths are kinked. Otherwise, the α laths rotate with strain, tending to became aligned perpendicular to the loading direction, and their thickness is reduced somewhat.

Chapter 6

Texture evolution of Ti-6Al-4V during hot compression testing

This chapter covers the crystallographic (bulk) texture evolution of heat-treated and hot forged Ti-6Al-4V at subtransus temperatures using GEM (General Materials Diffractometer), a time-of-flight (TOF) neutron diffractometer at the ISIS neutron spallation source at the Rutherford Appleton Laboratory, UK, making use of the multi-detector capabilities and a vacuum furnace. Diffraction spectra's were used to determine the orientation distribution functions (ODFs) from which the pole figures were calculated.

In addition to the neutron diffraction studies, supplementary texture measurements using an automated electron backscatter diffraction (EBSD) system in the scanning electron microscope (SEM) were carried out on identical cylindrical samples. The bulk crystallographic texture data obtained on GEM in a 'single exposure' and the EBSD texture dataset obtained over a smaller area (600 x 600 μm^2) are compared to clarify textural evolution before and after deformation in the bulk specimens.

6.1 Texture in hexagonal metals

Crystallographic texture is one of the essential parameters for microstructural characterization of polycrystalline materials used in materials science. It reflects the thermomechanical processing history of the material (e.g. plastic deformation, recrystallization, particle rotation and phase transition) and the existence of texture results in anisotropic physical properties. The texture of a polycrystalline material is the preferred orientation of crystal grains within the material and is described completely by its orientation-distribution function (ODF), which is a mapping of the probability of each possible grain orientation with respect to the macroscopic sample coordinates [122]. Each individual phase of a multi-phase material has its own texture [121], however, there is often a relationship between a pole figure and the orientation distribution function which is given by P_h (α, β) of an individual crystal direction (h) represented in stereographic projection. The quantitative texture information is roughly calculated by the product of the number of pole figures (hkl) times the number of sample orientations [199].

In general, the two-phase ($\alpha+\beta$) titanium alloys exhibit moderate-to-strong crystallographic textures that develop during large deformation in the ($\alpha+\beta$) phase field. A low temperature deformation tends to result in the basal/transverse (B/T) texture while a high temperature deformation near the beta transus ($\alpha+\beta\rightarrow\beta$) transformation temperature results in the transverse (T) texture [200]. The texture of primary α (α_p) and secondary α (α_s) evolve during deformation in the two-phase field and the decomposition of the hot-worked beta matrix during cooling, respectively. The primary α (α_p) grains arise from coarser α lamellae after deformation and/or dynamic recrystallization. The primary (α_p) grains are mainly oriented around a single crystal orientation.

The secondary α (α_s) colonies are inherited from the β→α phase transformation and exhibit a specific misorientation between them. The primary α (α_p) grains and secondary alpha (α_s) may develop different texture components during thermo-mechanical processing (TMP). The separation of both α_p deformation texture and the α_s transformation texture is complicated because the alpha phase in each instance consists of the same crystal structure and lattice parameters [201].

The texture evolution in hexagonal metals (Zirconium and Titanium) has always attracted significant interest due to the dependence of their excellent properties, such as high strength, corrosion resistance, creep resistance, thermal expansion and plasticity, on the crystallographic texture [200, 202]. For example, hexagonal metals such as Zircaloy are used for nuclear reactor fuel cladding while Titanium alloys are used in the aerospace and aircraft industries, [203]. In general, hexagonal metals are different from cubic metals due to the activation of twinning deformation modes at low temperatures in addition to conventional slip from dislocations. In HCP alpha-titanium, slip occurs most commonly on the basal {0001}, prismatic {10$\underline{1}$0}, and pyramidal {10$\underline{1}$1} slip planes (Figure 6.1).

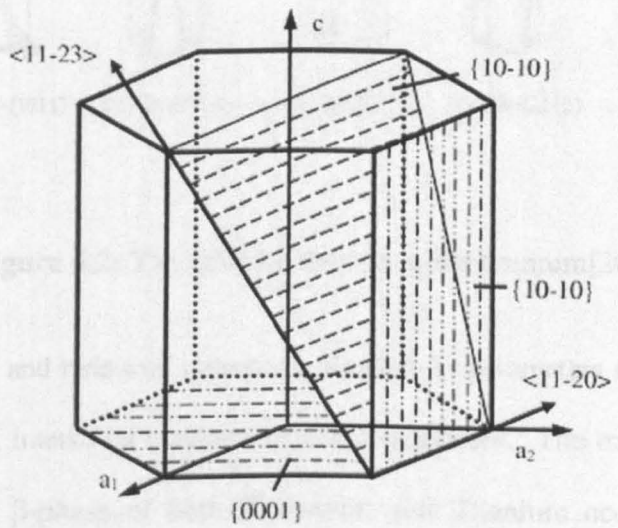

Figure 6.1: First order slip planes for hcp metals [204].

The primary slip systems in HCP metals are, the prismatic {10$\underline{1}$0} planes in the basal <12$\underline{1}$0> directions and the other possible slip systems are the basal (0001) and pyramidal (10$\underline{1}$1) planes with basal directions <12$\underline{1}$0>. Although they all occur in the basal direction, these systems will provide combinations of four independent slip systems. Materials with cubic crystalline structures have 5 or more glide systems but in HCP metals the most common basal and prismatic glide (as shown in Figure 6.2) have only two or three independent glide systems [205].

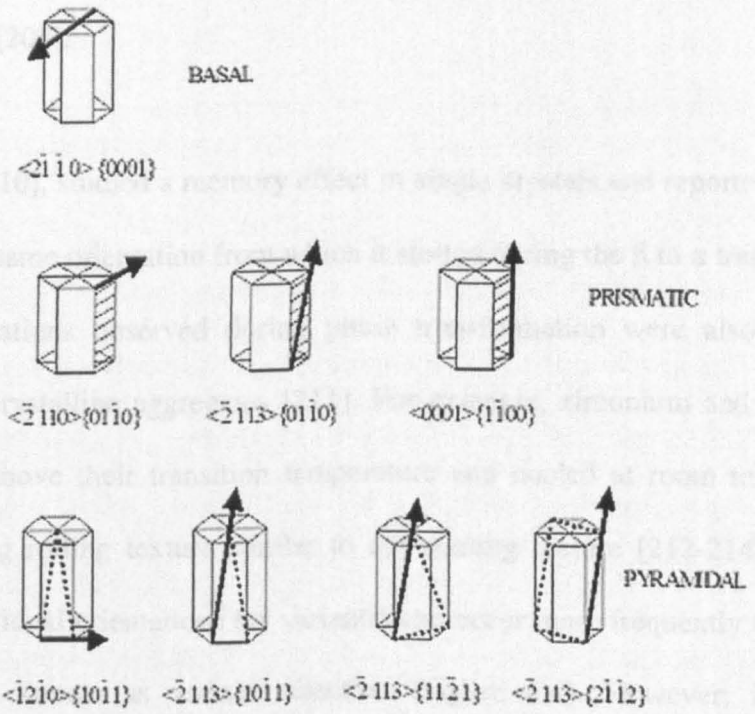

Figure 6.2: The glide systems in alpha titanium[206]

The activation of slip and twinning systems is affected by parameters such as c/a ratio, strain hardening, strain rate, interstitial constituents and temperature. The transformation between the α-phase and the β-phase of both Zirconium and Titanium occurs according to the orientation relation {0001} <1120> (hcp- α) → {110} <111> (bcc-β) observed by Burgers for single crystals [207].

According to this relation, during the α→β transition upon heating, six equivalent crystallographic β variants can occur from a single α orientation. Conversely, during the β→ α phase transition, there are 12 potential α-variants. The schematic representation of the crystallographic relationship and significant transformation strain is shown in Figure 6.3. For example, for the β→α transformation under unconstrained conditions, this amounts to ~ 10% contraction along a <100>$_\beta$ direction, and a ~ 2% contraction and ~ 10% expansion respectively along two perpendicular <110 >$_\beta$ directions [208]. When the material is transformed from the α-phase to β-phase and back to α-phase again, the original α-phase orientations are maintained either perfectly or to some extent; this is called texture memory effect [209].

Jourdan et al.[210], studied a memory effect in single crystals and reported that the crystal returned to the same orientation from which it started during the β to α transformation. The selective orientations observed during phase transformation were also investigated in deformed polycrystalline aggregates [211]. For example, zirconium and titanium, which are hot-rolled above their transition temperature and cooled at room temperature (RT); showed a strong rolling texture similar to the starting texture [212-214]. Under certain conditions individual orientations (or variants) can occur more frequently than others. This phenomenon is known as variant selection (Figure 6.4). However, in titanium and zirconium alloys there have been reports of variant selections during diffusional phase transformation [215]. For example, in titanium alloys, during hot rolling above the β transus and heavy cold rolling near β annealing have both led to transformation with variant selection [209, 211].

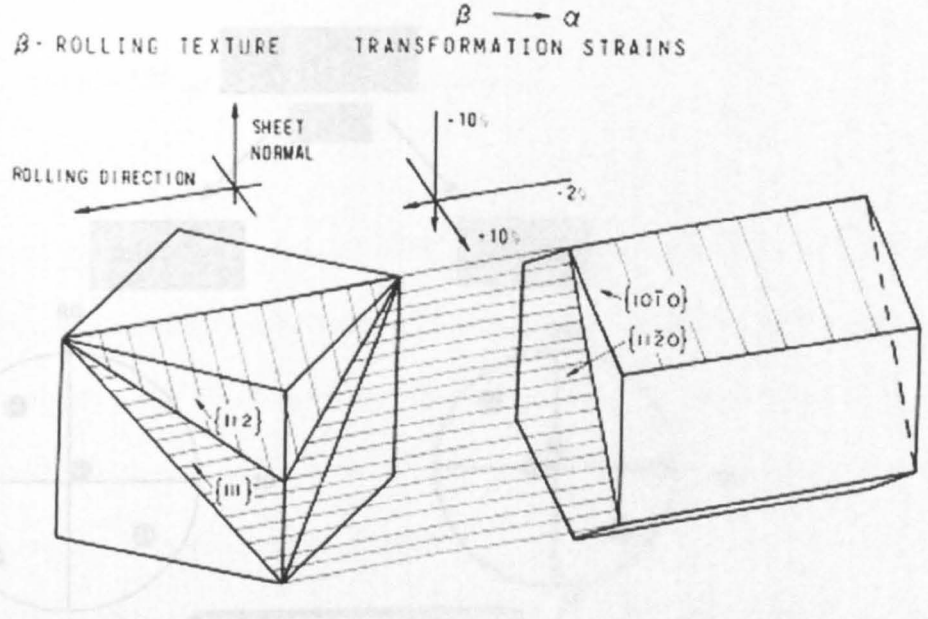

Figure 6.3: Schematic representations of the crystallographic relationship and significant transformation strain during β to α transformation [208].

In Zirconium alloys, variant selection has been observed during simple β annealing heat treatments [216]. The transformation strain occurs under the influence of external stress or strain. If it occurs under the influence of stress, some variants have a larger probability of formation and also generate a texture which can allow the shear strain to make a greater contribution to the macroscopic shape. However, each variant has an equal chance of existence. An applied stress can favour those variants that comply with the stress; that is, variant selection occurs. Bhattacharyya et al.[217] observed that in titanium there is a tendency for the prior β/β grain boundary to have α product on either side with close alignment of their (0001) poles. The transformation texture was attributed mainly to variant selection during the hcp→ bcc→hcp phase transformation. Thermomechanical processing of Ti-6Al-4V alloy generally induces a sharp α texture which is always the main phase at RT (room temperature). The texture of the α phase has a great influence on the mechanical properties i.e., fatigue strength of Ti-6Al-4V. So, the improvement of these properties for a given application requires good control of the induced texture.

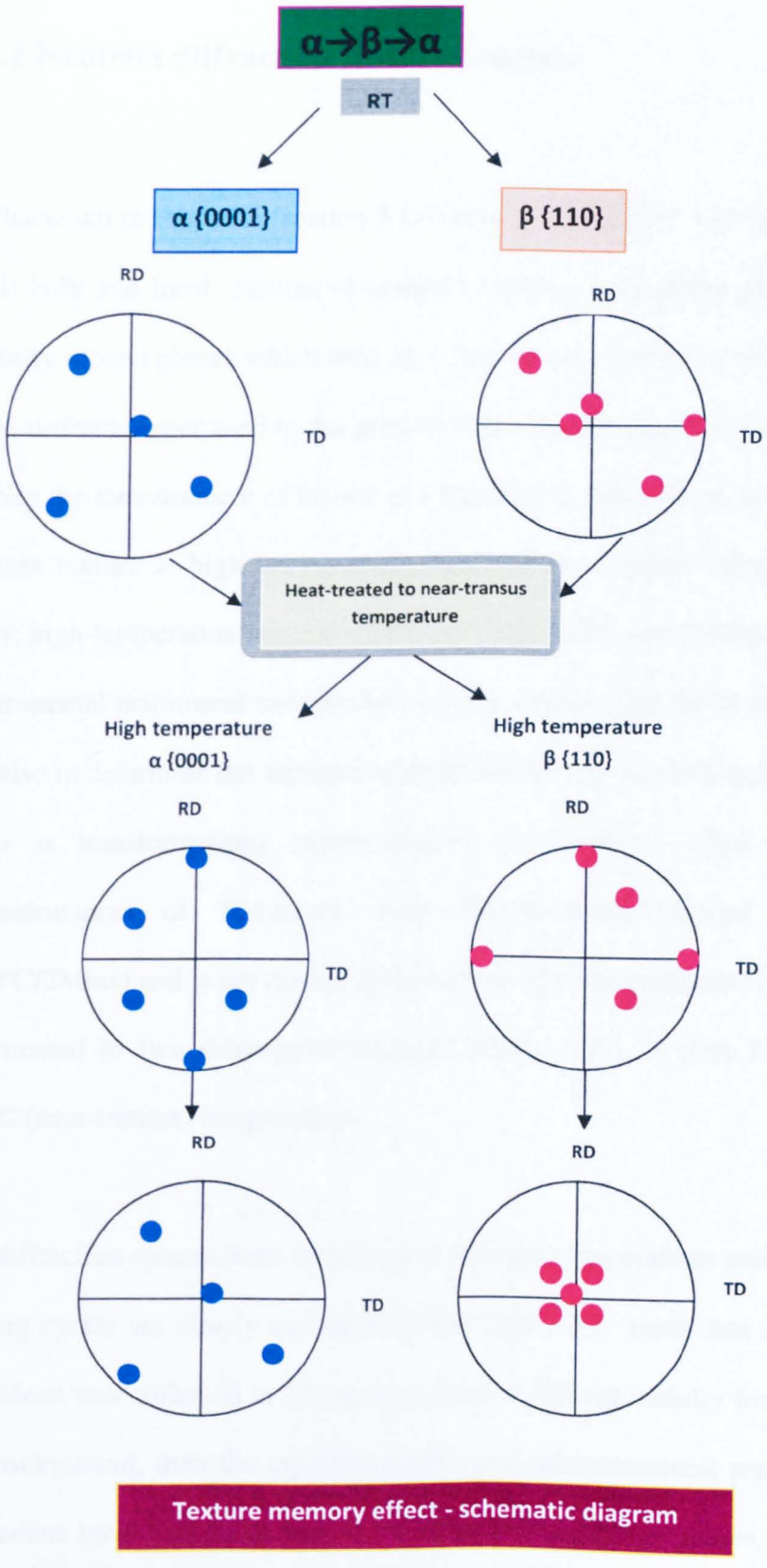

Figure 6.4: Schematic diagram for texture memory effect during the β to α transformation.

6.2 GEM – (Bulk) texture measurements

6.2.1 Neutron diffraction texture analysis

As discussed in chapter 3 (section 3.1.4) neutron diffraction was used for the determination of (i) bulk and local textures of compact samples, (ii) coarse grained materials and (iii) minority second phases which were less than 10 vol. % of the total constituents at RT. The GEM diffractometer used in the present work has the facility of a vacuum furnace which enables the measurement of texture as a function of temperature as well as determining the β-phase texture at high temperature, which is not possible using EBSD. In the present study, high-temperature neutron diffraction was undertaken to take advantages of the GEM experimental instrument and measure the bcc texture directly at high working temperature and also to determine the texture evolution during heating-cooling cycles in both $\alpha \rightarrow \beta$ and $\beta \rightarrow \alpha$ transformations experimentally in Ti6Al-4V alloy. As-received equiaxed microstructures of Ti-6Al-4V were beta-annealed (heated to 950°C/10Mins + 1030°C/2Mins) and water cooled. Furthermore, the beta-annealed Ti-6Al-4V samples were heat-treated to two subsequent heating-cooling cycles at both 850°C (sub-transus) and 980°C (near-transus) temperatures.

The diffraction spectra were measured at different temperatures and the respective heating-cooling cycles are clearly explained in the Figure 6.5. Each data set for all experimental conditions was collected in 20 minutes. Data is refined initially for instrument parameters and background, then the crystallographic and microstructural parameters and finally all parameters including the texture and volume fraction of the phases. For converting relative diffraction intensities to experimental pole figures, it is necessary to carry out data normalisation and corrections for detector normalisation.

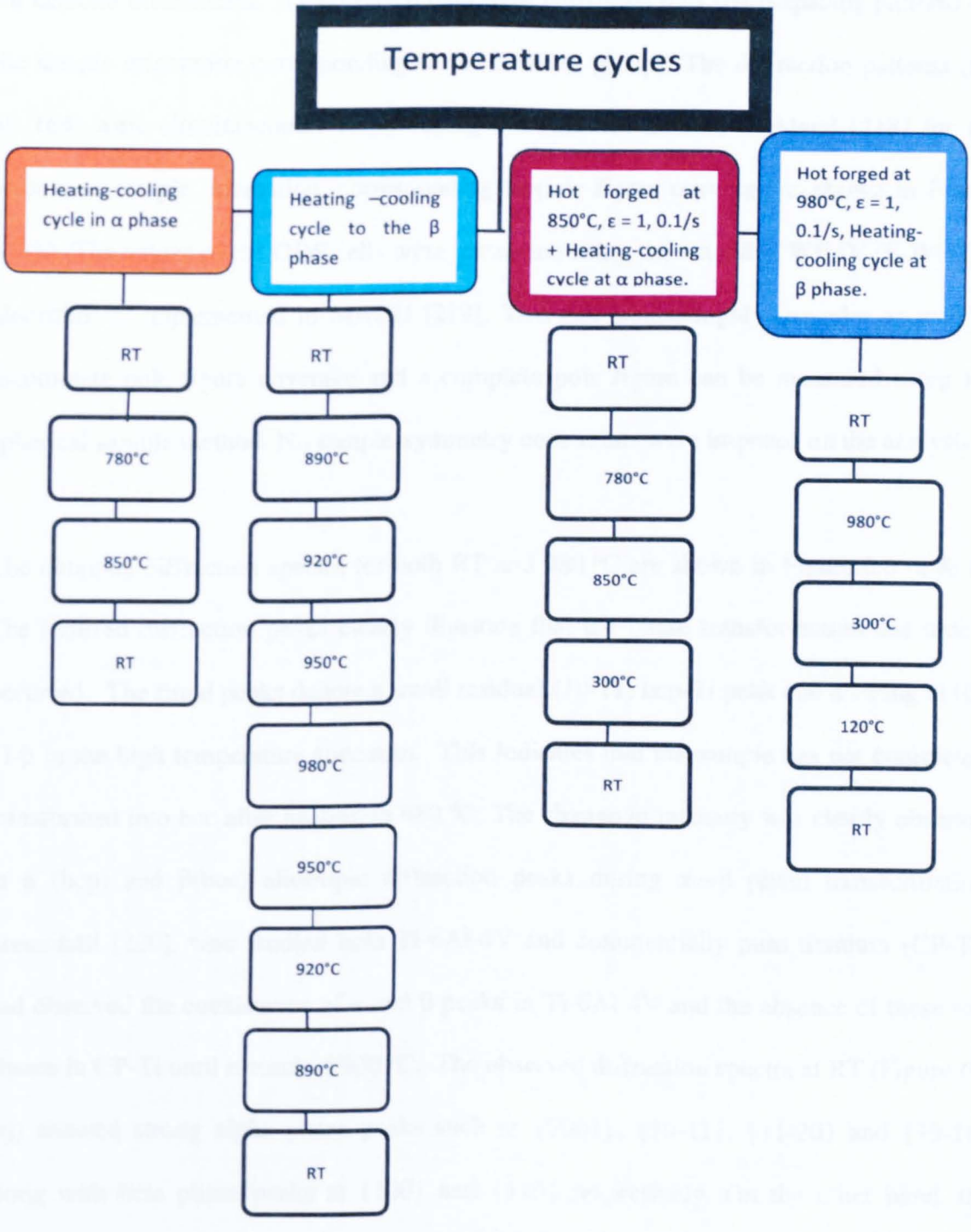

Figure 6.5: Heating and cooling cycles for bulk texture measurements.

The data obtained were normalized to an incident neutron flux distribution and corrected for detector efficiencies. The corrected data were converted into 164 d-spacing patterns for the sample orientation corresponding to the detector groups. The diffraction patterns (for all 164) were simultaneously fitted using the Rietveld method in Maud [218] for the respective sample orientation, corresponding to pole figure coverage as shown in Figure 6.7(b). The values of the ODF cells were extracted using the extended WIMV (E-WIMV) algorithm as implemented in MAUD [219]. This can handle highly irregular as well as incomplete pole figure coverage and a complete pole figure can be measured using the spherical sample method. No sample-symmetry constraints were imposed on the analysis.

The obtained diffraction spectra for both RT and 980 °C are shown in Figure 6.6 (a & b). The indexed diffraction peaks clearly illustrate that the phase transformation has indeed occurred. The fitted peaks denote a small residual (10-11) hcp-Ti peak and a strong (110)-Ti-β in the high temperature spectrum. This indicates that the sample has not completely transformed into bcc after heating to 980 °C. The change in intensity was clearly observed in α (hcp) and β(bcc) allotropic diffraction peaks during α→β phase transformation. Lonardelli [220], who studied both Ti-6Al-4V and commercially pure titanium (CP-Ti), had observed the coexistence of α and β peaks in Ti-6Al-4V and the absence of these two phases in CP-Ti until it reached 900 °C. The observed diffraction spectra at RT (Figure 6.6 (a)) showed strong alpha phase peaks such as {0001}, {10-11}, {11-20} and {10-10} along with beta phase peaks at {100} and {110} respectively. On the other hand, the diffraction spectra at 980 °C shows, strong appearance of {110},{100}, and {111} beta phase peak intensity (Figure 6.6 (b)) along with weak {10-11}, {10-10} and {11-20} alpha phase peaks. These diffraction peaks confirm that neutron scattering is capable of probing a bulk sample and is well suited for obtaining the texture from a minor β phase constituent in the Ti-6Al-4V alloy.

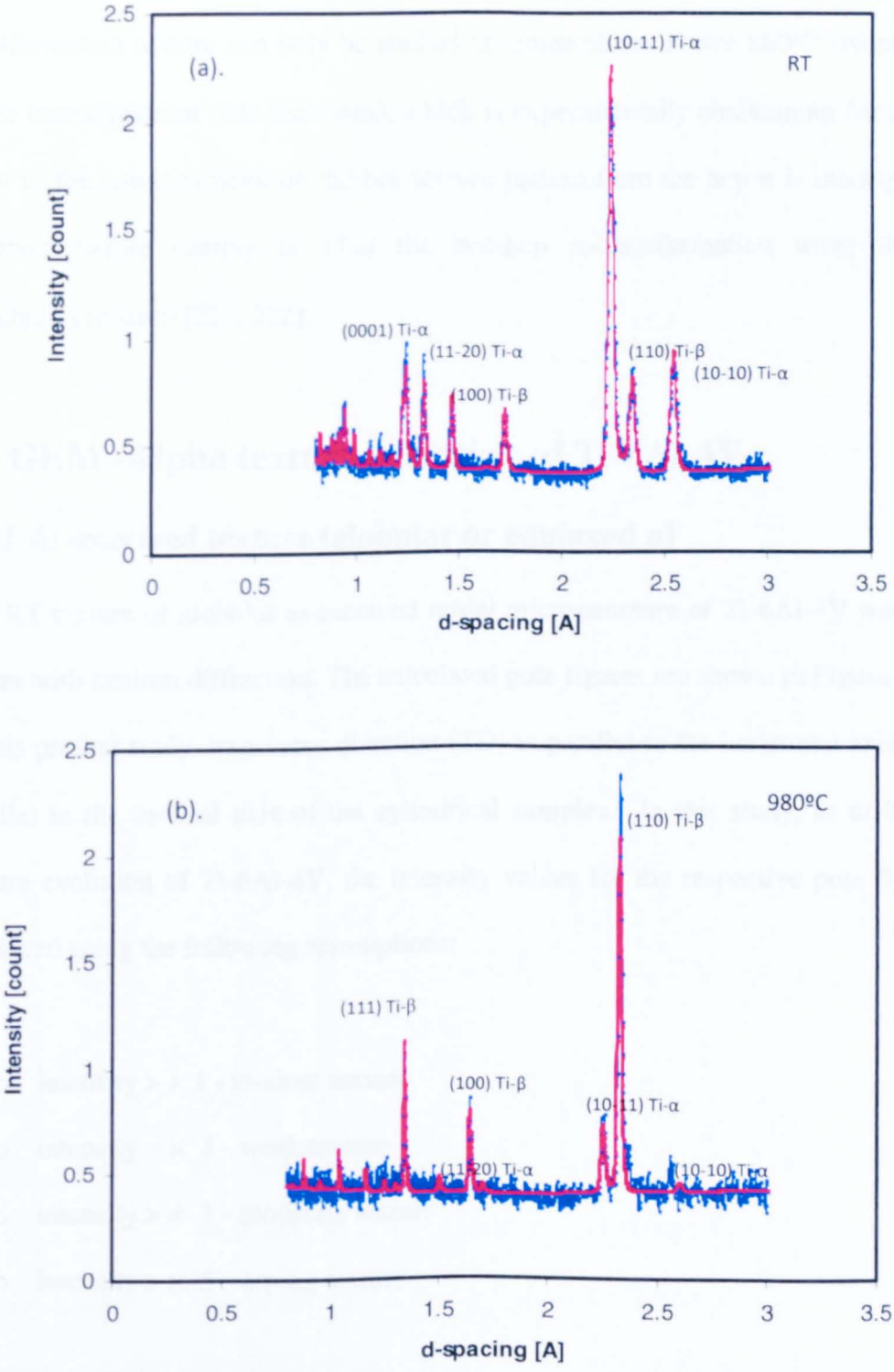

Figure 6.6: Typical time-of-flight diffraction patterns of Ti-6Al-4V collected at (a). RT, (b). At 980ºC (near-beta transus) with α and β coexisting.

Since the bcc phase in two-phase titanium alloy cannot be quenched to RT [214], the bcc transformation texture can only be studied at temperatures above 880°C (where the $\alpha \rightarrow \beta$ phase transformation rate increases), which is experimentally challenging for researchers. Most of the previous work on the bcc texture pattern from the hcp-α is incomplete, either observed before heating or after the bcc-hcp re-transformation using the Burgers orientation relation [221, 222].

6.3 GEM -Alpha texture evolution of Ti-6Al-4V

6.3.1 As-received texture (globular or equiaxed α)

The RT texture of globular as-received initial microstructure of Ti-6Al-4V was measured in situ with neutron diffraction. The calculated pole figures are shown in Figure 6.9(a & b). In this present study, transverse direction (TD) is parallel to the horizontal axis and RD is parallel to the vertical axis of the cylindrical samples. In this study, to understand the texture evolution of Ti-6Al-4V, the intensity values for the respective pole figures were measured using the following assumptions:

- intensity > × 1 - random texture
- intensity > × 2 - weak texture
- intensity > × 3 - moderate texture
- intensity > × 5 – strong texture

The α phase pole figures of the as-received material at RT shows a moderate hcp compression texture with a typical preferred orientation of the {0001} poles to the normal direction (ND). Luetjering [2] observed a similar texture in two (α+β) titanium alloys and considered it as a typical rolling texture of Ti-6Al-4V. This initial hexagonal texture shows a broad (0001) maximum in the normal direction.

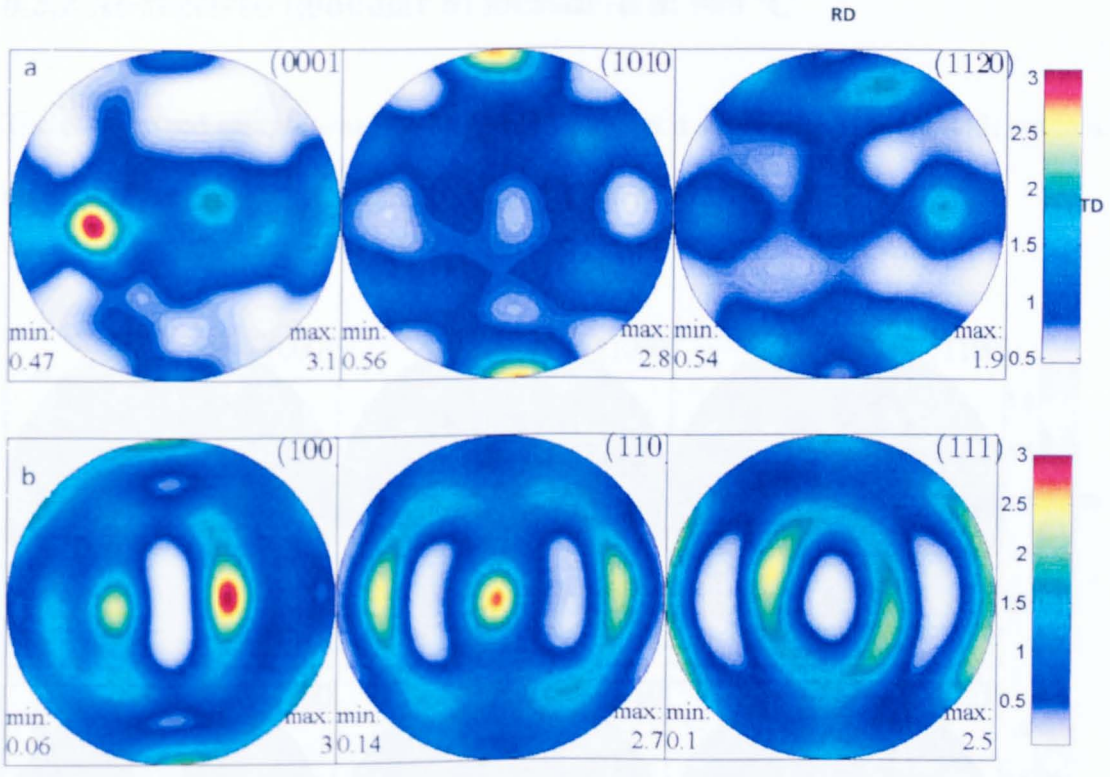

Figure 6.7: As-received (globular) texture of Ti-6Al-4V. (a) Alpha phase texture for the (0002), (10-10) and (11-20) pole figures (b) beta phase texture for the (100), (110) and (111) pole figures calculated at RT.

Kocks U.F et al. [200] also observed similar texture behaviour on rolled titanium. The (10-10) pole figure shows a maximum in the rolling direction. The (11-20) pole figure also has a maximum in the rolling direction but it is slightly broader than the (10-10) maximum but extended toward the transverse direction. This typical rolling texture was also found in the starting condition of cold-rolled Zircaloy-2 and Zircaloy-4 sheets [223, 224]. Similar RT texture has also been studied by other researchers for rolled Zircaloy [213] and Titanium using neutron diffraction. The obtained beta pole figures as shown in Figure 6.7(b) for as-received (globular) Ti-6Al-4V showed maximum around the normal direction (ND) and spread along the transverse direction (TD).

6.3.2 As-received (globular α) measured at 980 °C

The as-received sample was hot-forged at 980°C at a strain rate of 0.1/s with strain =1 and texture measurements were carried out at RT after water quenching.

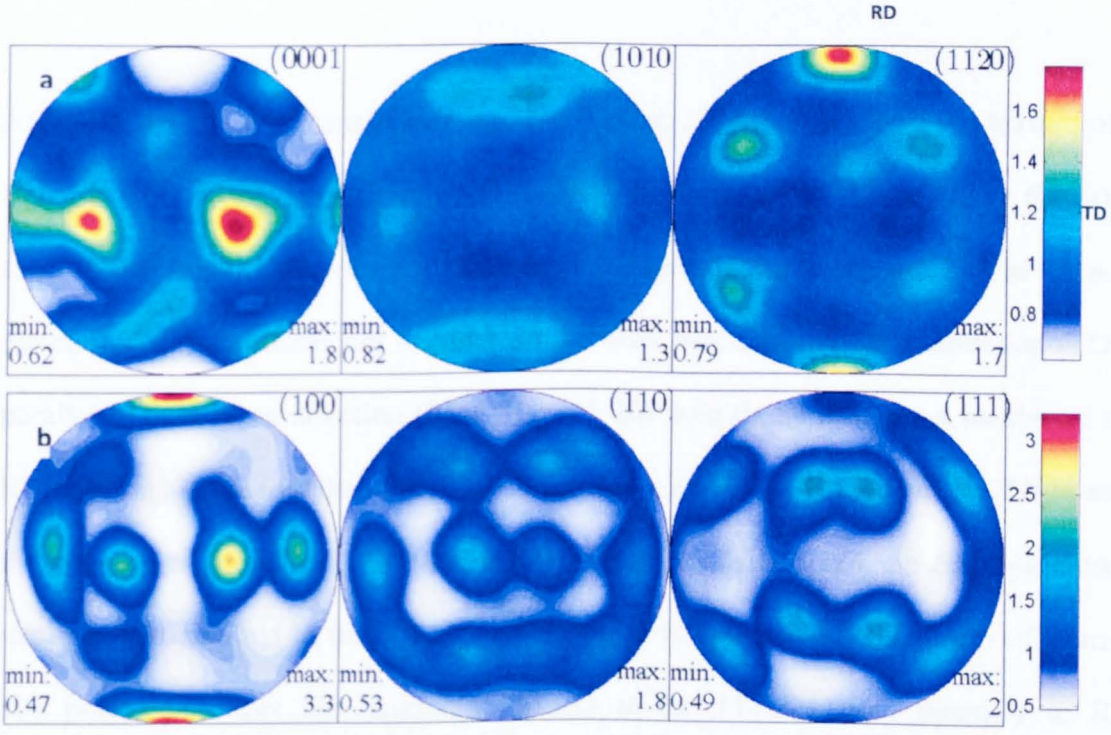

Figure 6.8: Hot forged texture of Ti-6Al-4V at 980°C, 0.1/s and ε =1 (a).The alpha phase texture for the (0002), (10-10), (11-20) and (b). The beta phase texture for the (100), (110), (111) pole figures calculated at RT

Hot-forged Ti-6Al-4V at near-transus temperature (Figure 6.8(a)), shows similar (0001) pole figure as in the as-received condition (Figure 6.7(a)) where the (0001) maximum splits more distinctly into two sub maxima. The (10-10) maximum for texture near transus temperature is broadly spread out in the transverse direction compared to the as-received (10-10) pole figure. There is a formation of new hcp texture noticed in (11-20) pole figure, which has a distinct (11-20) maximum spread out in the rolling direction. It occurs martensitically or by diffusion controlled nucleation with the growth process depending on

cooling rate and alloy composition. The obtained beta phase texture is completely different from the as-received beta-texture. This observation clearly indicates that Ti-6Al-4V hot-forged at 980°C at a strain rate of 0.1/s with strain =1 weakens both alpha and beta texture.

6.3.3 Beta-annealed (alpha-lamellar) measured at 980 °C

At 980 °C, α phase is transformed into the β phase. Figure 6.9 shows the texture of pre-tested and hot-forged beta annealed Ti-6Al-4V measured at 980 °C. In Figure 6.9 (a), pre-test (un-deformed) alpha phase {0001} texture shows multiple sub maxima in the normal direction (ND) and these sub maxima can be seen near the transverse direction (TD) and parallel to the rolling direction (RD). The (11-20) pole figure also has a maximum in the RD but is again broader than the (10-10) maximum and extended toward the TD as seen in the as-received globular Ti-6Al-4V at RT (Figure 6.9 (a)). In Figure 6.9 (b)), there is a strong single maxima in the ND along with other faint maxima. It is observed from {10-10} pole figure that the maximum in RD at the {11-20} pole intensity in RD is significantly lower than the pre-test RT and has a large spread towards RD. Figure 6.10 shows the beta-phase texture of pre-tested and hot-forged Ti-6Al-4V measured at 980 °C. The beta-phase texture observed in Figure 6.10 (a) has similar (100) and slightly different (110) and (111) pole figures, compared to the as-received (globular α) measured at 980 °C (Figure 6.9 (b)), which shows nearly the same intensity. The hot-forged beta-phase texture of Ti-6Al-4V observed at 980°C, 0.1/s, ε =1 (Figure 6.10 (b)) shows similar (100), (110) and (111) pole figures as compared with Figure 6.10 (b).

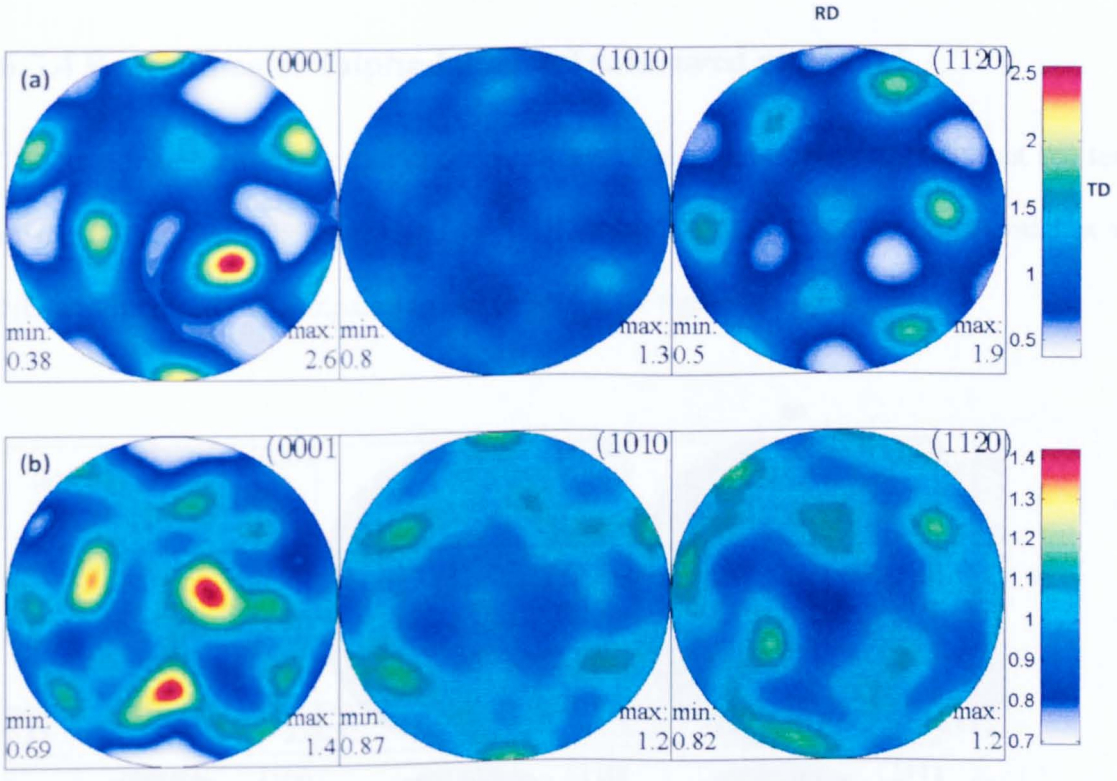

Figure 6.9: The beta-annealed Ti-6Al-4V measured for the (0002), (10-10) and (11-20) pole figures annealed at 980 °C (a). Pre-test (alpha-lamellar) texture annealed at 980°C, (b). Hot-forged texture observed at 980°C, 0.1/s, ε =1

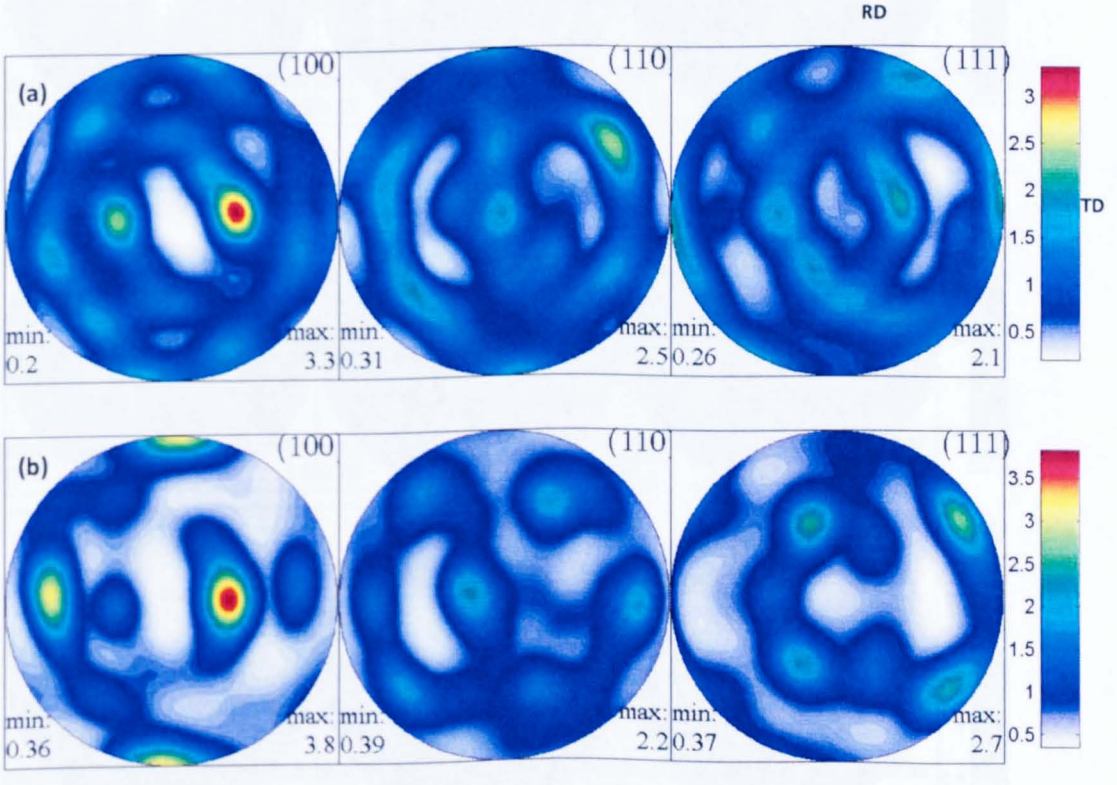

Figure 6.10: The beta-annealed Ti-6Al-4V measured for the (100), (110) and (111) pole figures annealed at 980 °C (a).Pre-test (alpha-lamellar) beta-phase texture (b). Hot-forged beta-phase texture observed at 980°C, 0.1/s, ε =1

6.3.4 Beta-annealed (alpha-lamellar) measured at 850 °C

The in situ neutron-diffraction experiments at RT showed (Figure 6.7 (a)) that the texture of the α phase was sharpened and the intensity of the {0001} preferred orientation along ND was increased as compared to the {0001} pole figure in Figure 6.8(a).

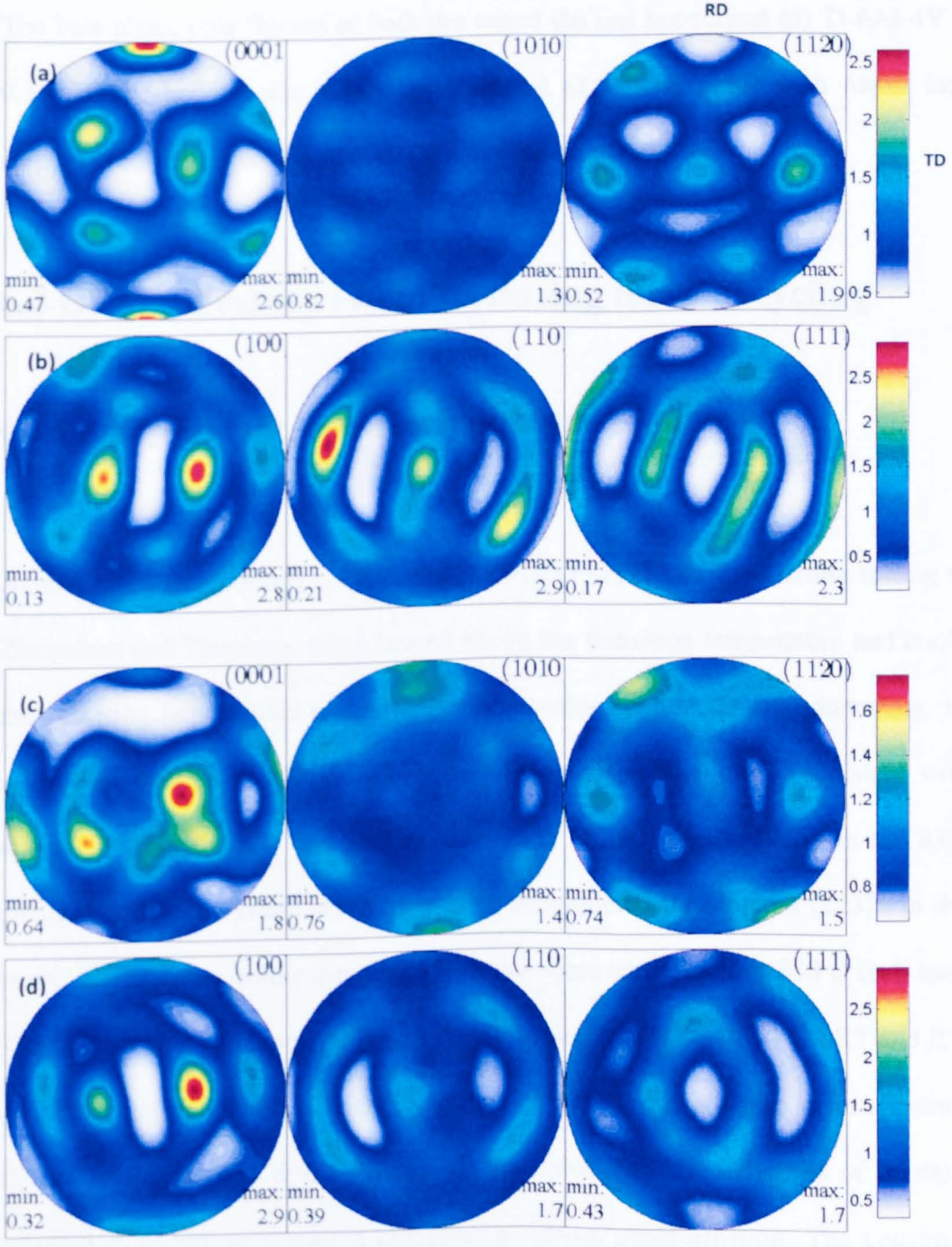

Figure 6.11: The beta-annealed Ti-6Al-4V measured for the (0002), (10-10) and (11-20) of alpha-phase and (100), (110) and (111) of beta-phase annealed at 850 °C (a). Alpha (a) and beta (b) textures of Pre-tested Ti-6Al-4V annealed at 850°C, (b). Alpha(c) and beta (d) texture of hot-forged Ti-6Al-4V observed at 850°C, 0.1/s, ε =1

In Figure 6.11(a), {10-10} and {11-20} pole figures are nearly similar texture as seen in Figure 6.9 (b). The hot-forged (Figure 6.7 (a)) alpha phase texture {0001} looks similar to the alpha phase texture annealed at 980°C (Figure 6.9 (b)). The {10-10} and {11-20} pole densities in RD are slightly larger than those after initiation of the ($\alpha \rightarrow \beta$) transformation. The beta-phase pole figures of both pre-tested (b) and hot-forged (d) Ti-6Al-4V at 850°C, 0.1/s, ε =1 show similar (100) but different (110) and (111) with lower intensity as compared to pre-tested (β) Ti-6Al-4V annealed at 850 °C.

6.4 GEM – Texture evolution during thermal cycling

6.4.1 Analysis of the $\alpha \rightarrow \beta$ texture changes

As discussed in section 6.1, Gey et al. [209, 211, 212] observed strong rolling texture of Zirconium and Titanium, when heated above the transition temperature and cooled again; the resulting hcp texture is similar to the starting texture. During annealing, there is a significant change in texture which usually develops a texture component with c axes about 30° from the ND and also exhibits axes (11-20) preferentially in the RD. Similar changes during recrystallization have been documented for titanium [223]. In the present study, the heating-cooling temperature cycles were carried out at 850°C (sub-transus) and 980°C (near-transus) temperatures in the sequence RT-780°C - 850°C - RT and RT - 890°C - 920°C - 950°C - 980°C - 950°C - 920°C - 890°C - RT. A series of re-constructed pole figures in Figure 6.15 & 6.16 illustrates the most significant changes of crystallographic orientation occurring during a complete $\alpha \rightarrow \beta \rightarrow \alpha$ transformation. The constructed pole figures show basal (0002), pyramidal (10-10) and prismatic (11-20) textures for the α-phase and the (100), (110) and (111) shows for the β-phase texture.

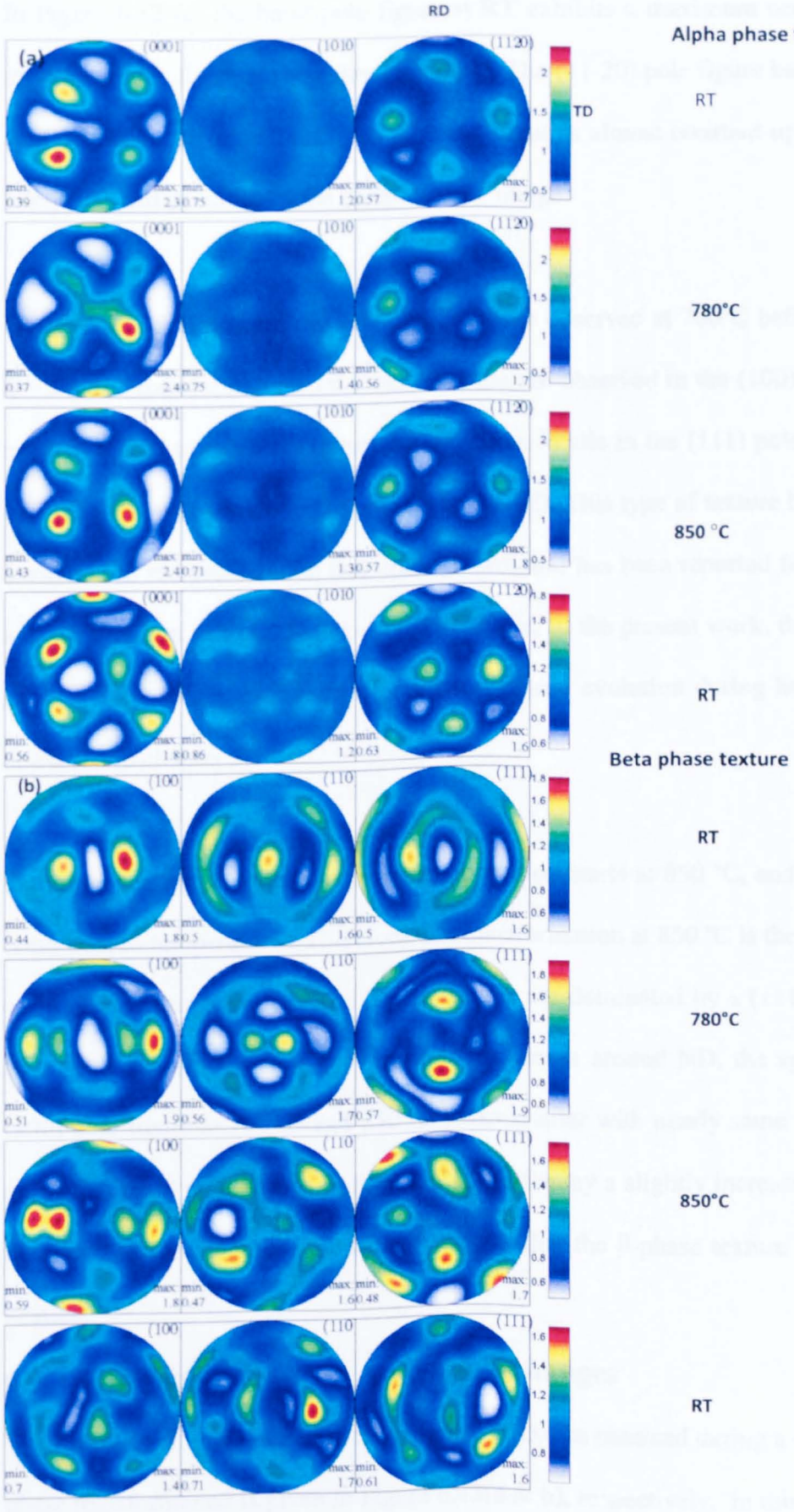

Figure 6.12: α and β pole figures obtained from in-situ neutron diffraction during a complete α→β phase transformation (a) alpha-phase texture during heating to 850 °C (b). Beta- phase texture during cooling from 850 °C.

In Figure 6.12 (a) the basal pole figure at RT exhibits a maximum near ND but slightly moved towards the transverse direction (TD). The (11-20) pole figure has multiple maxima split 30° from the rolling direction RD, and remains almost constant up to 850 °C but the intensities and positions of the poles start to change.

Figure 6.12 (b) illustrates the beta phase texture observed at 780°C before the start of the $\alpha \rightarrow \beta$ phase transformation. Two split maxima are observed in the (100) pole figure which is again biased towards the transverse direction. While in the (111) pole figure these have become a strong two maximum parallel to the RD. This type of texture behaviour has been attributed to recrystallization and grain growth and has been reported for Zirconium alloy and CP titanium [220, 225]. It is noted here that, in the present work, there is no evidence of recrystallization, grain growth or microstructure evolution during hot-compression (as discussed in chapter 5).

During annealing, the alpha to beta transformation starts at 850 °C, and finishes at 995 °C (beta-transus temperature). Therefore, the transformation at 850 °C is the initial stage of the $\alpha \rightarrow \beta$ phase transformation. The β pole figures are dominated by a (111) maximum in the RD, while the (110) pole figure exhibits maximum around ND, the split maxima of the (100) pole figure at 780 °C and 850 °C looks similar with nearly same intensity. It is also noted that the β pole figures in Figure 6.12(b) display a slightly increasing intensity of the dominant texture components, which suggests that the β-phase texture strengthens during heating.

6.4.2 Analysis of the $\alpha \rightarrow \beta \rightarrow \alpha$ texture changes

The evolution of α and the high temperature β texture obtained during a complete $\alpha \rightarrow \beta \rightarrow \alpha$ phase transformation is given in Figure 6.13(a & b), respectively. In this sample, α and β phases are always present at all conditions, but at different volume fractions.

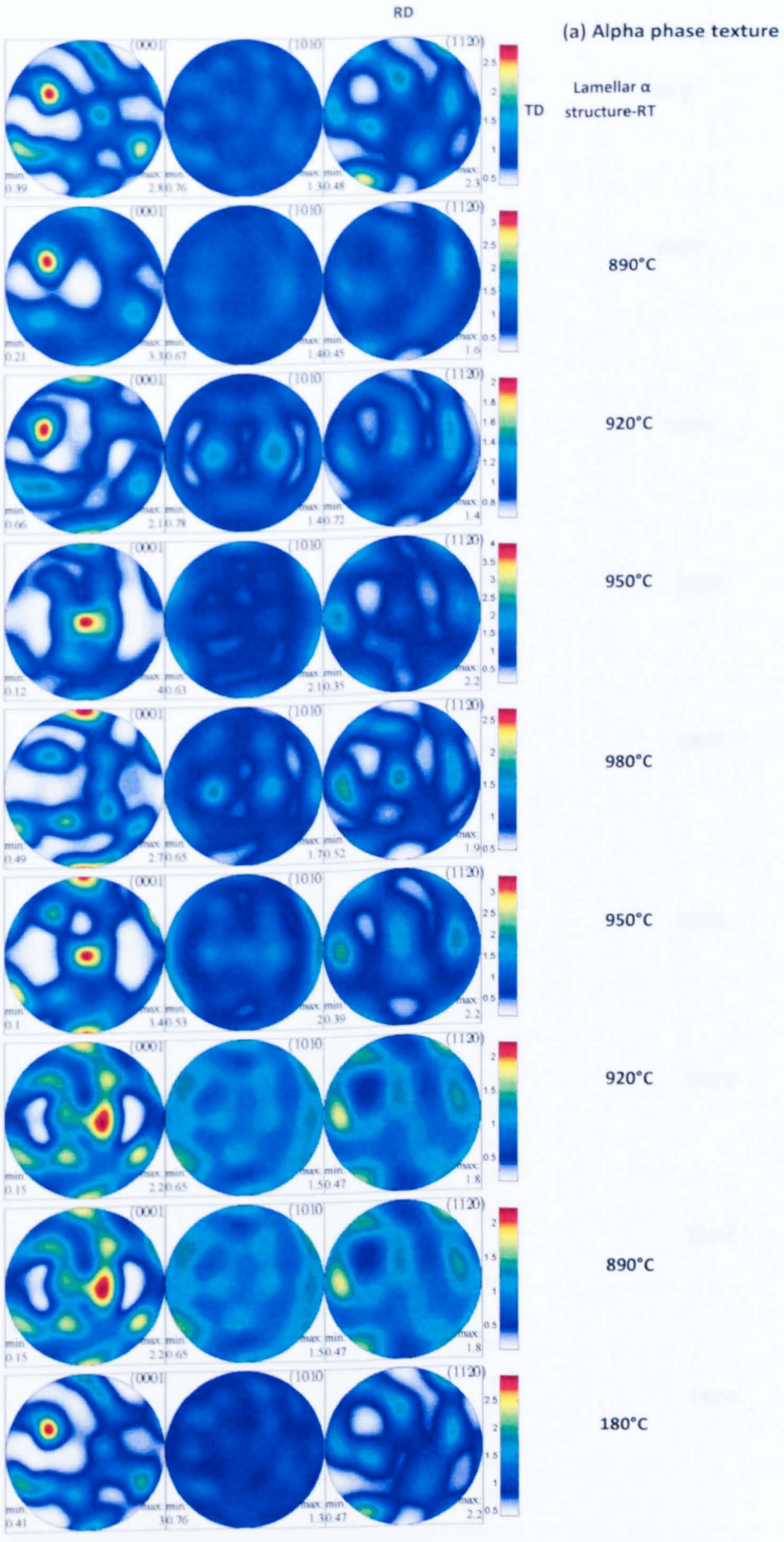
RD
TD
(a) Alpha phase texture
Lamellar α structure-RT
890°C
920°C
950°C
980°C
950°C
920°C
890°C
180°C

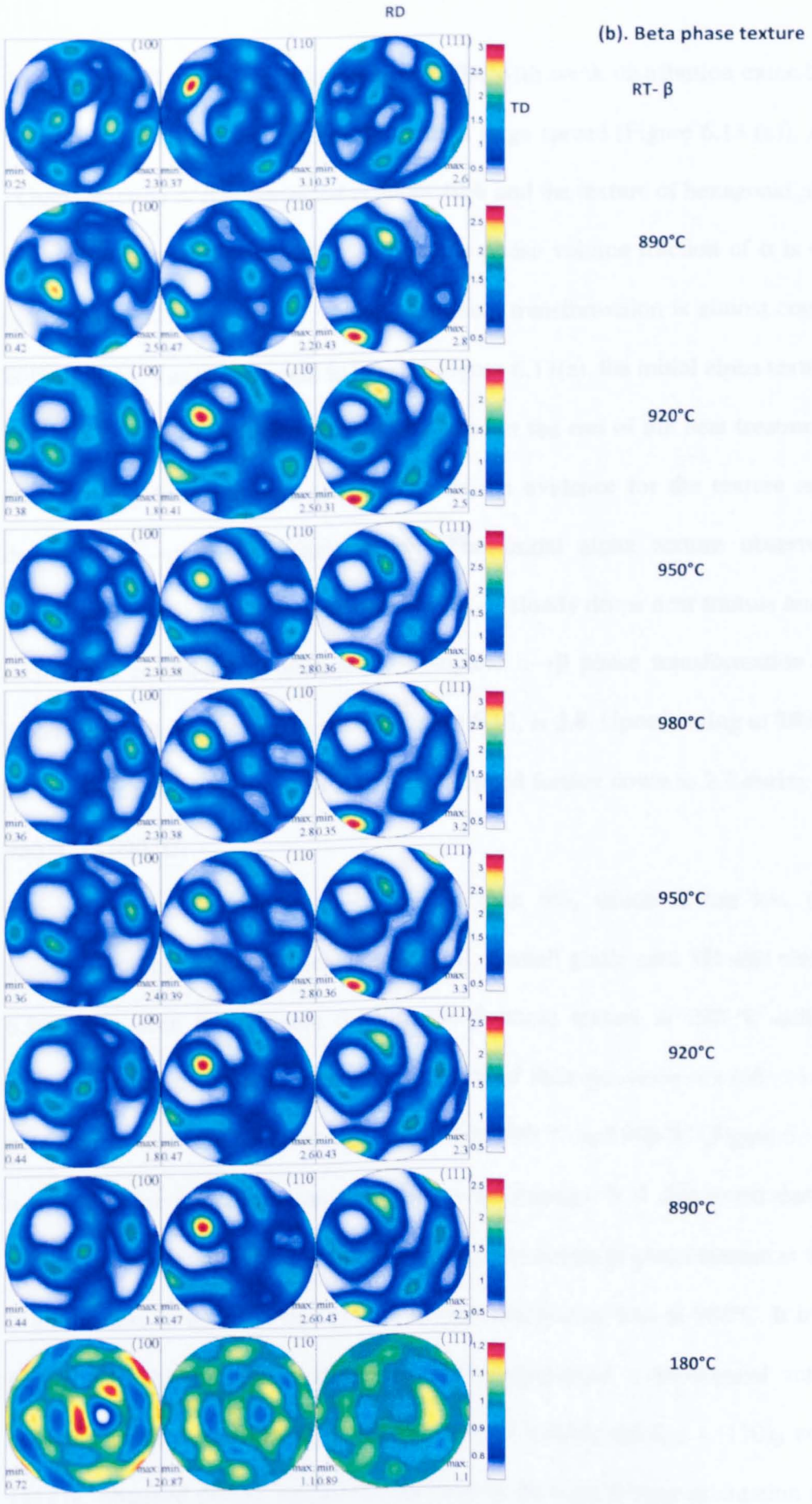

Figure 6.13: α and β pole figures obtained in-situ neutron diffraction during a complete α→β→α phase transformation (a) alpha-phase texture (b). Beta-phase texture

At RT, a small encircle can be seen near TD, with weak distribution extending over ND. The {10-10} pole concentrates in RD with a large spread (Figure 6.13 (a)). At 890 °C the volume fraction of β is estimated at about 40% and the texture of hexagonal phase is nearly identical to the texture at 920 °C, where the phase volume fraction of α is 48% and β is increased to 52%. At 980 °C, the alpha to beta transformation is almost complete; nearly 80% of alpha was transformed to beta. In Figure 6.13(a), the initial alpha texture developed at RT is similar to the alpha texture measured at the end of the heat treatment (i.e. at RT after cooling from the beta phase). This is the evidence for the texture memory effect during α→β→α phase transformation. The initial alpha texture observed at RT is significantly weakened by the heat-treatment. It slowly drops near transus temperature and then drops considerably through the complete α→β phase transformation. The starting alpha texture index, as can be seen in Figure 6.13, is 2.8. Upon heating to 980 °C, the alpha texture index dropped down to 2.7 and it dropped further down to 2.2 during cooling from 980 °C to 890 °C.

The amount of beta-phase at RT is less than 6%, which is too low for a reliable measurement to estimate its texture. But still, a small girdle near TD was observed (Figure 6.9(b)). As seen from Figure 6.12(b), the β–phase texture at 780 °C and 850°C show slightly similar pole figure maxima's in terms of their positions in (100), (110) and (111) pole figures. But the beta textures observed at 890 °C and 980 °C (Figure 6.13 (b)), during α→β→α phase transformation shows many similarities. It is also noted that the RT beta-texture is completely different from the high temperature β–phase texture at 980°C as there is an increase in intensity due to high volume fraction of beta at 980°C. It is evident from Figure 6.16 (b) that during the α→β→α transformation a preferential variant selection occurred in beta-phase texture and the parallel planes $(0002)_\alpha$ / $(110)_\beta$ and $\{11\text{-}20\}_\alpha$ / $\{111\}_\beta$ obtained during measurements confirm that the Burger orientation relationship is followed.

In previous studies, a strengthening of the β texture was observed in CP titanium [11] which was associated with competitive growth between β grains. The SEM and EBSD studies on rolled sheets of CP titanium [14] have shown that, in the early stages of the transformation, there is the possibility of nucleation of β-phase on the grain boundaries and within the grains as plates. Thus, the presence of grain boundary β tends to follow the Burgers relationship with one of the parent grains, whereas intergranular β orientation appears more random. The final stage of α→β→α phase transformation is a competitive growth of these two types of nuclei and dominated more by the formation of grain boundary β due to faster moving interfaces. In the present work, if it is assumed that the transformation is likely to occur in a similar manner in the Ti-6Al-4V, this can explain the strengthening of the β texture during the phase transformation on heating.

Once the sample was cooled down, α texture was again measured at RT (as shown in Figure 6.13). These α-phase pole figures show very weak β texture even after cooling down from near-transus temperatures. In Figure 6.13 (a), the {1120} pole in the RT α-phase is nearly parallel to the direction of the {111} poles of the strong β-phase texture observed at 980 °C at the ND. In addition to this, the strong {0001} poles of RT α-phase almost match with the {110} pole in the beta phase at 980 °C. This is an indication of the Burgers relationship obeyed for the retransformation from β to α when the specimen is cooled from near-transus temperature. In theory, this particular behaviour is usually expected if the growth of α forms by nucleation and growth from the β matrix.

6.4.3 Hot-forged Ti-6Al-4V: Analysis of the α→β→α texture changes

In this present work, a complete α→β→α phase transformation was carried out for the Ti-6Al-4V samples hot-forged at 850°C and 980°C with a strain rate of 0.1/s and ε = 1. After hot-compression at sub-transus and near-transus temperatures, the hot-forged Ti-6Al-4V samples were heated up to the target temperature and cooled again. Figure 6.14 illustrates the texture evolution of Ti-6Al-4V hot-forged at 850°C with a strain rate of 0.1/s and ε = 1. This shows nearly similar alpha phase texture during complete α→β→α phase transformation but the β-phase deformed texture shows completely different texture evolution. The textures of the Ti-6Al-4V sample hot-forged at 980°C, 0.1/s, and ε = 1 at the start and at the end of the heating cycle are different as shown in Figure 6.15.

Figure 6.4, the initial alpha texture developed at RT is similar to the alpha texture measured at the end of the heat treatment (i.e. at RT after cooling). This is evidence for the texture memory effect of hot-forged Ti-6Al-4V during heating-cooling cycle. The investigation of the β-phase texture of hot-forged Ti-6Al-4V specimens during thermal-cycling led to two different observations. Firstly, the β-phase texture at 850°C and 980°C (Figure 6.4& 6.15) clearly shows that there are no similarities and not much strengthening of the β-phase texture on heating the sample from 890°C to 980 °C. During the heating-cooling cycle, the β-phase textures of heat-treated Ti-6Al-4V specimens show similar β-phase texture at 890°C and 980 °C (as shown in Figure 6.13 (b)) and there is strengthening of the β-phase texture observed on heating the sample from 890°C to 980°C. Secondly, it is evident from Figure 6.4, the β-phase texture at 850°C does not exhibit the Burger relationship with the α-phase texture observed at 850°C.

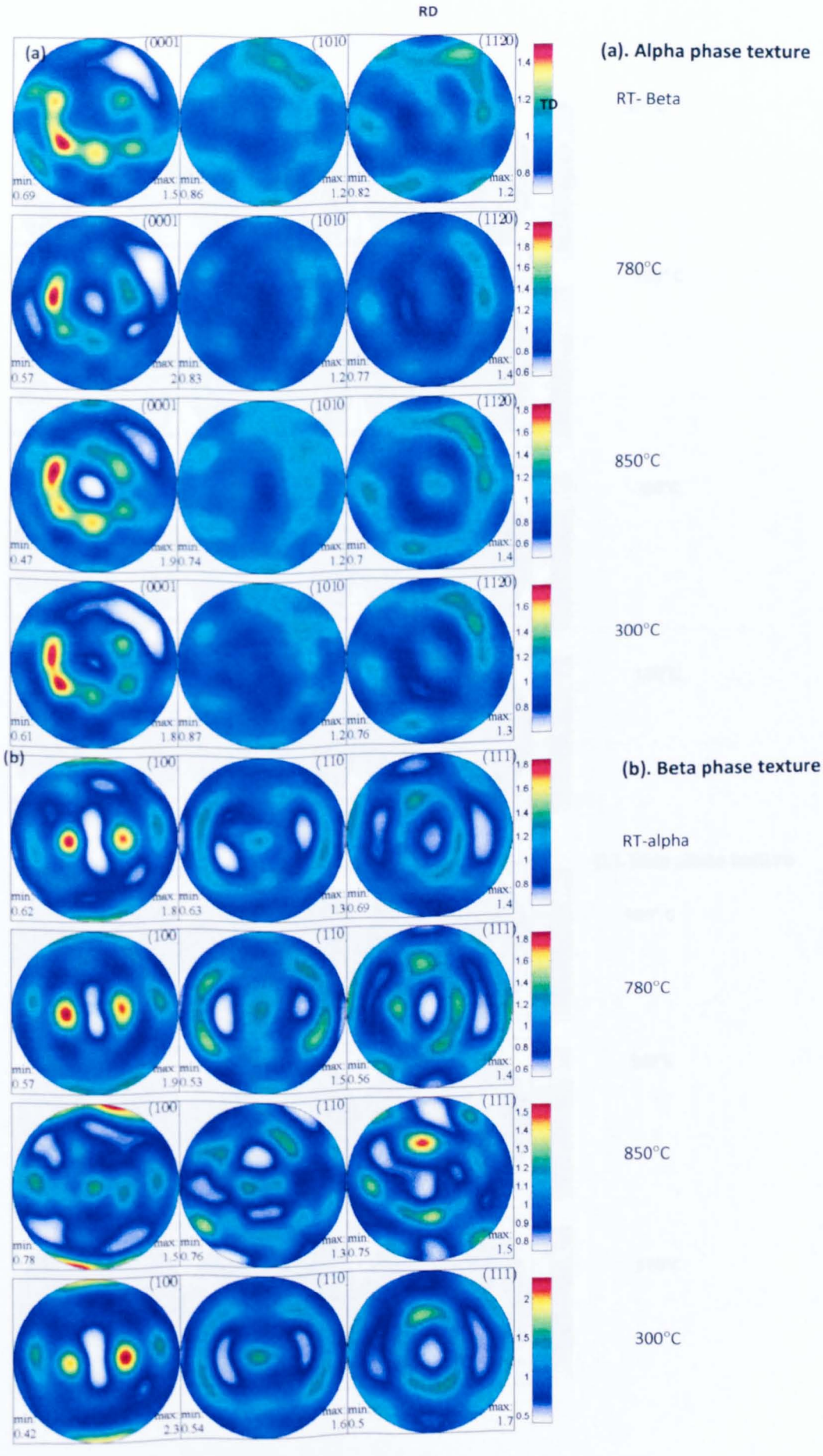

Figure 6.14: α and β pole figures obtained during thermal cycle of hot-forged Ti-6Al-4V at 850 °C, 0.1/s, and ε = 1.

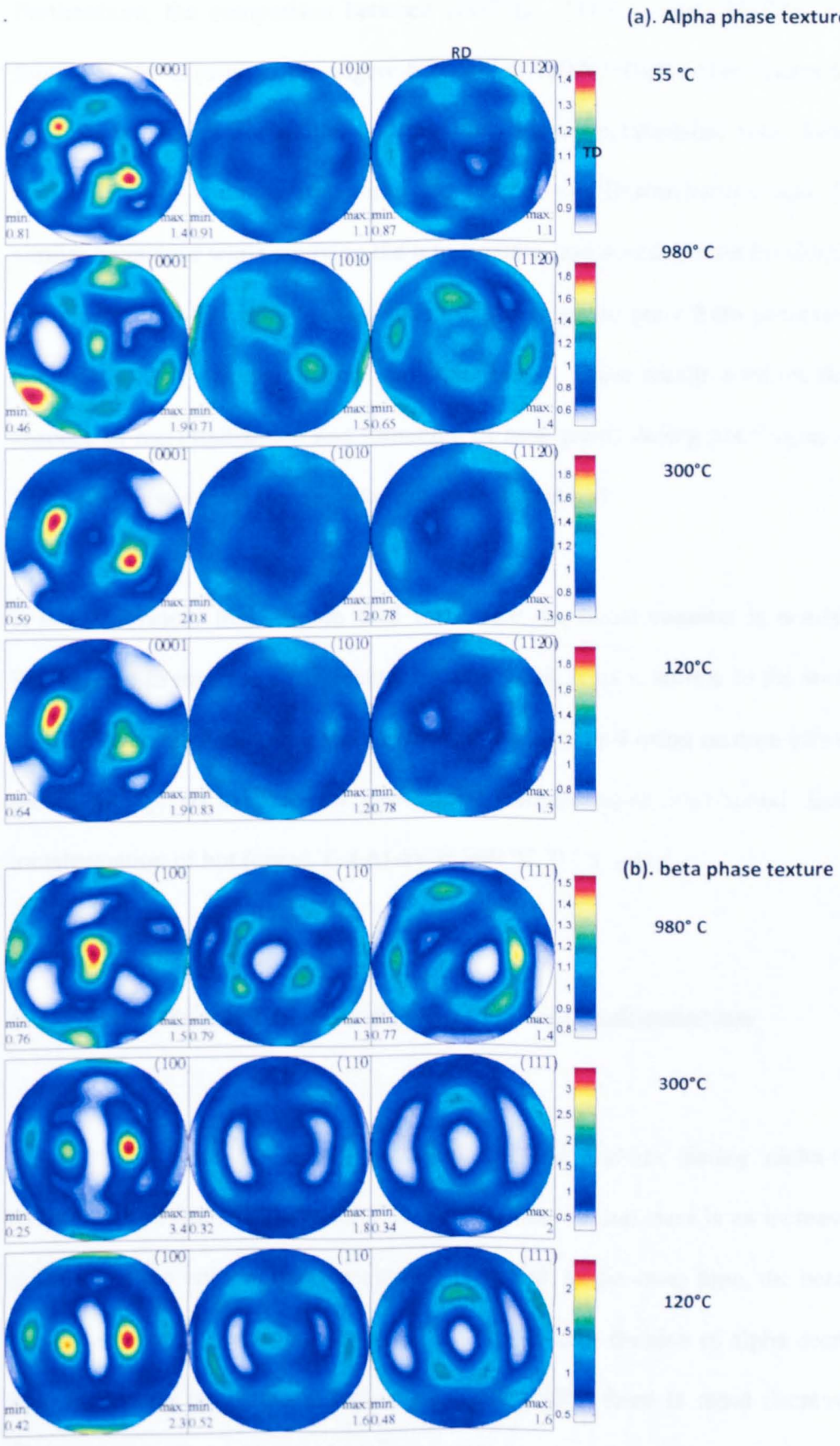

Figure 6.15: α and β pole figures obtained during thermal cycle of hot-forged Ti-6Al-4V at 980 °C, 0.1/s, and ε = 1.

Furthermore, the comparison between $\{0002\}_\alpha$ / $\{110\}_\beta$ and $\{1120\}_\alpha$ / $\{111\}_\beta$ pole figures at 850°C (α-phase) in Figure 6.14 and at 980 °C (β-phase) in Figure 6.15 show that the pole intensities are similar and thus the Burgers relationship was followed on hot-forged Ti-6Al-4V during transformation from α→β. Bhattacharyya et.al. [225]observed similar behaviour while studying the α to β phase transformation on hot-forged Ti-6Al-4V using neutron diffraction and concluded that beta phase grew from pre-existing β grains, not by the fresh nucleation from the alpha phase. These results confirm that there is an absence of recrystallization and formation of new grains during hot-forging of Ti-6Al-4V in the α +β phase field (below beta-transus temperature).

It is also evident from Figure 6.15 that, once the transformation is nearly complete at 980°C (near to transus), the β texture became weak. This is similar to the work of Wenk et al. [226] who studied bulk texture evolution in Zircaloy-4 using neutron diffraction. In the present study, no evidence of preferential transformation was found during the α→β transformation of hot forged Ti-6Al-4V at 980 °C, 0.1/s, and $\varepsilon = 1$.

6.4.4 Texture index of beta during phase transformation

Figure 6.16 shows the texture intensities of the β-phase during alpha-to-beta phase transformation from 780°C to 980 °C. It was observed that there is an increase in β texture index when the volume fraction exceeds 50% and, at the same time, the beta pole figures become stronger. It was also observed that, the volume fraction of alpha decreased slowly with increasing temperature. However, above 950°C there is rapid decrease in volume fraction of alpha with increasing temperature.

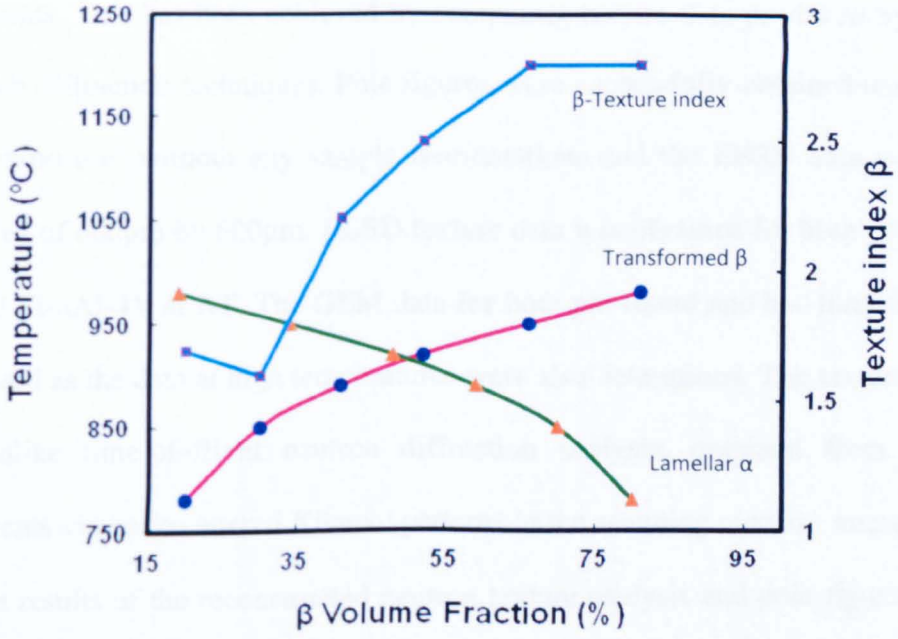

Figure 6.16: Evolution of texture indices of β phases during α→β phase transformation on heating.

6.5 Validation of GEM (bulk) Texture data using EBSD

In the present study, the texture measurements of Ti-6Al-4V alloy were carried out using neutron diffraction and EBSD. The angular coverage of the general materials diffractometer (GEM) at the ISIS pulsed neutron source located at the UK Rutherford Appleton Laboratory has the capability of obtaining quantitative bulk crystallographic texture data in a 'single exposure' within few minutes. This enables the possibility of in situ texture measurements that can be made to quantify texture change during phase transformation. In this study, electron backscatter diffraction (EBSD) texture measurements were carried out at RT to measure the texture changes in hot-forged Ti-6Al-4V tested at sub-transus temperatures. The main advantage of EBSD measurements includes a smaller beam size (5 nm to 10 μm), ability to collect compositional information from the same area probed for diffraction, and SEM imaging capabilities. However, analysis of very fine microstructures can be difficult using EBSD. The purpose of different

texture measurements is to verify the texture data produced from GEM by EBSD measurements. This has been achieved by comparing texture data produced by the EBSD and neutron diffraction techniques. Pole figures were successfully obtained using GEM in a 'single exposure' without any sample reorientations and the EBSD data was obtained over an area of 600μm by 600μm. EBSD texture data was obtained for both pre-tested and hot-forged Ti-6Al-4V at RT. The GEM data for both pre-tested and hot-forged Ti-6Al-4V at RT as well as the data at high temperatures were also determined. The texture data using EBSD, unlike time-of–flight neutron diffraction analysis, obtained from orientation measurements via backscattered Kikuchi patterns in the scanning electron microscope. The pole figure results of the reconstructed neutron texture analysis and pole figures of EBDS measurements are presented in Figures 6.17 (a & b). The alpha-phase texture developed during compression testing at 850°C with strain rate of 0.1/s and $\varepsilon = 1$ measured using GEM is shown in Figure 6.17 (a) and using EBSD is shown in Figure 6.17 (b).

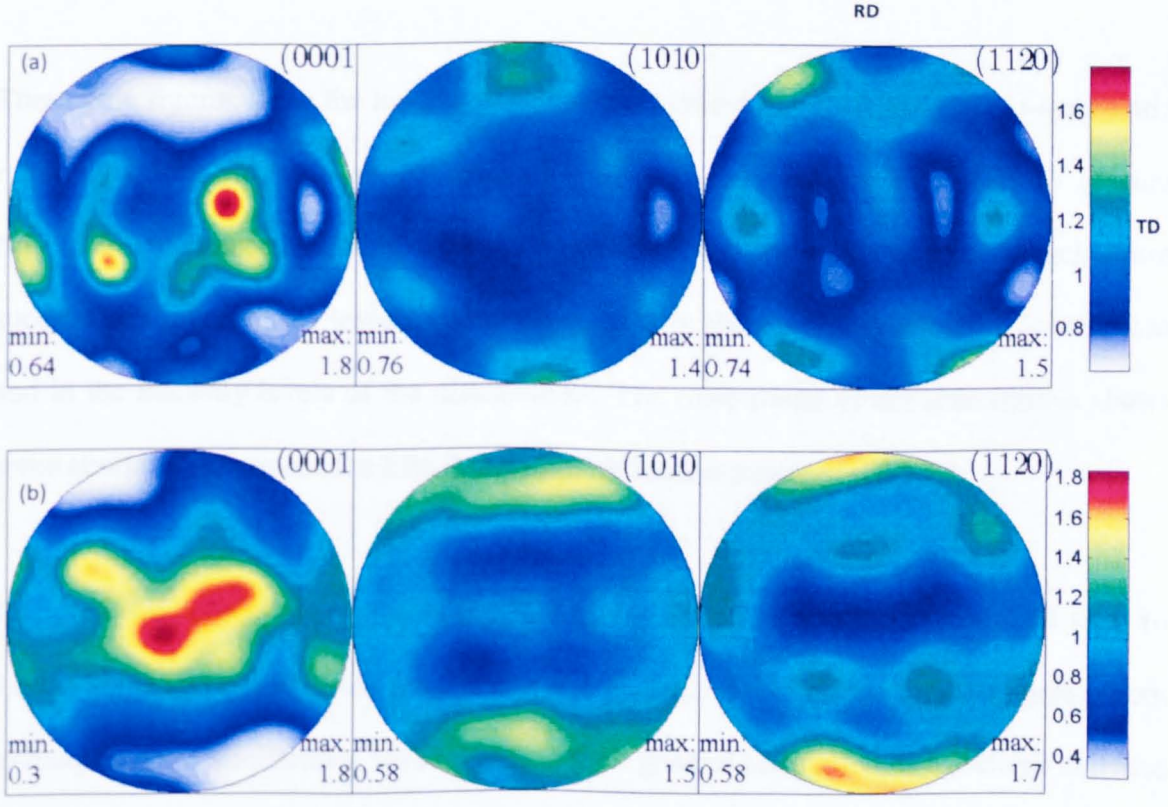

Figure 6.17: A comparison of texture measured using neutron texture analysis (GEM) and EBSD at 880°C. (a). GEM alpha-phase pole figures (bulk measurement), (b). EBSD alpha-phase pole figures (local measurement)

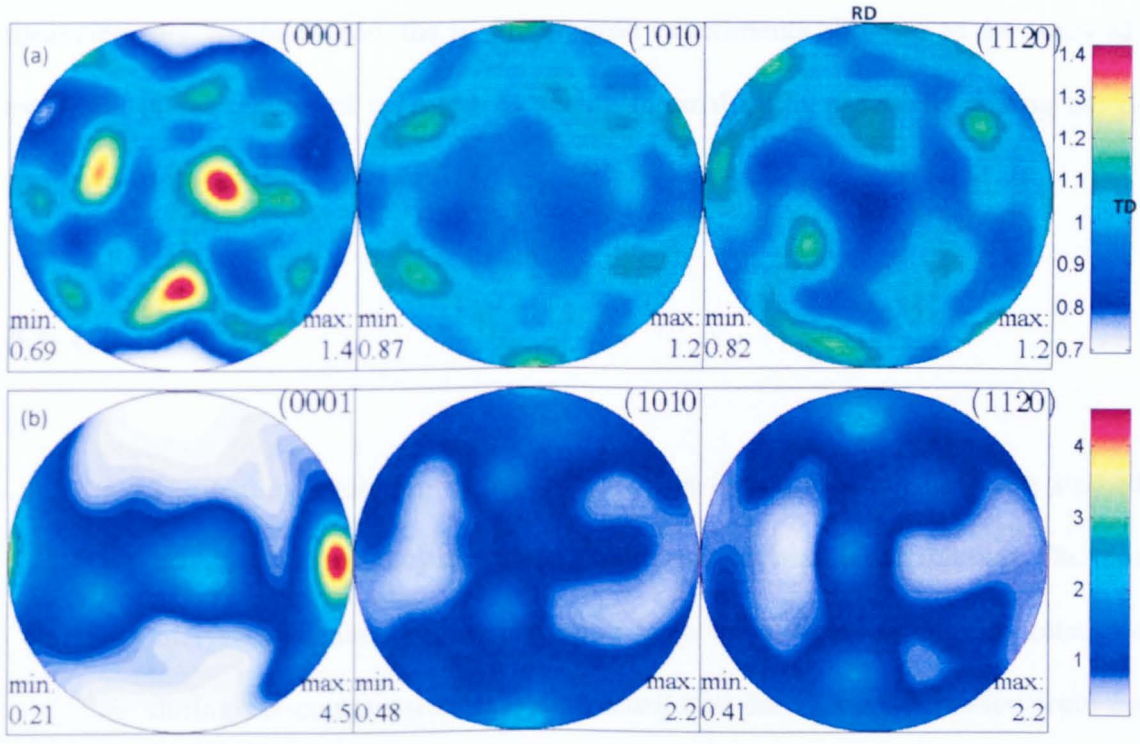

Figure 6.18: A comparison of texture measured using neutron texture analysis (GEM) and EBSD at 950°C (a). Alpha-phase pole figures of Ti-6Al-4V (b). EBSD – alpha-phase pole figures of Ti-6Al-4V

These pole figures show the loading axis is in the vertical direction and the axi-symmetric radial directions are arbitrary. By comparing the texture of hot-forged Ti-6Al-4V (Figure 6.17 (a & b)) observed at 880°C with strain rate of 0.1/s and $\varepsilon = 1$, from the two techniques successfully revealed the texture components, both in the general orientation distributions and in the intensity levels of the distributions. The comparison of the pole figures shows some similarities between the EBSD and neutron texture measurements.

The same was observed for hot-forged Ti-6Al-4V sample at 950 °C (Figure 6.18 (a & b) for the same strain and strain rates (i.e. $\varepsilon = 1$ and 0.1/s). In all the analysed areas, both techniques show similarities, with regards to their general orientation distributions and also the levels of intensity of distributions. This clearly demonstrates the capability of the neutron diffraction GEM for the accurate determination of bulk textures in a 'single

exposure' and also confirms its suitability for in situ high temperature β-phase texture measurements. In conclusion, the in situ neutron experiments allow us to the study of the evolution of the texture of both phases during thermal cycle, especially during the β→α phase transformation.

6.6 Conclusion

- The texture evolution of hcp and bcc hot-forged titanium has been studied in situ during thermal cycling, using time-of-flight neutron diffraction. The texture analysis indicates definite deviation from the Burgers orientation relationship during hot-compression. It is also noted that during transformation from α→β, the pole intensities are similar and thus the Burgers relationship was followed on hot-forged Ti-6Al-4V.

- The development and evolution of crystallographic texture during the α→β→α phase transformation was also determined. Annealing at a sub-transus temperature (850°C) shows similar α-phase and β-phase pole figures from RT up to 850°C but a slight increase in the intensity of the β-phase pole figures was observed. This showed that the β-phase texture strengthens during heating. During cooling, the beta to alpha transformation occurs very quickly and the initial alpha-texture obtained at RT is significantly weakened by the heat-treatment.

- At 980°C, the RT β-phase texture is completely different from the high temperature β-phase texture with increase in intensity because of high beta volume fraction (80%).

- The texture observed after hot-compression at 850°C with a strain rate of 0.1/s and ε=1 shows similar α-phase texture during the $\alpha \rightarrow \beta \rightarrow \alpha$ phase transformation but the evolved β-phase textures are dissimilar. Furthermore, no similarity was observed with the sample that was hot-compressed at 980 °C for the same strain and strain rate.

- The strengthening of the β-phase texture is observed on heating the sample from 890°C to 980°C and these two temperatures show a Burgers relationship ($(0002)_\alpha$ / $(110)_\beta$ and $\{11\text{-}20\}_\alpha$ / $\{111\}_\beta$) with the α-phase texture at RT. This clearly indicates the presence of a Burgers relationship from $\alpha \rightarrow \beta$ phase transformation, but no evidence of variant selection was observed during $\alpha \rightarrow \beta$ transformation.

- During the $\beta \rightarrow \alpha$ phase transformation on cooling, the Burgers relationship holds. This indicates a texture memory effect due to the growth of the primary alpha phase present at high temperature. It also appears that, there may be a variant selection during $\beta \rightarrow \alpha$ transformation on cooling.

- The comparison of pole figures from the reconstructed neutron texture analysis and those obtained using EBSD measurements shows some similarities.

Chapter 7

Conclusions and Future work

The following conclusion can be drawn from the investigation carried out during the present study on Ti-6Al-4V.

- The flow-stress of Ti-6Al-4V decreases with increasing temperature and increases as the strain rate increases.
- Significant flow softening was observed at subtransus temperatures which was associated with spheroidisation of the lamellar structure as well as progressive realignment of the alpha laths such that their long axes became perpendicular to the loading axis with the attainment of the steady-state flow stress.
- The variation of strain rate sensitivity, m estimated at the two subtransus temperatures was found to be in the range of 0.15-0.20 which suggests that dislocation glide and climb are the dominant deformation modes.
- The investigation of the hot deformation behaviour of Ti-6Al-4V at 880°C and 950°C has proved that there was little influence of initial alpha lath thickness on overall flow behaviour for the range studied.
- Post-deformation microstructures for the 'medium' thickness alpha-lath material, deformed at 0.1/s to a true strain of 1, at subtransus temperatures (880°C and 950°C), showed that the initial uniform lath structure had undergone significant distortion, including bending and kinking. Many laths had undergone fragmentation leading to a change in aspect ratio, indicative of the early stages of progressive spheroidisation. It was evident from the examination of basal texture at 950°C that

there is a tendency for the laths to become aligned with their long axes perpendicular to the direction of compressive loading. However, it was not observed at 880° C.

- The evolution of crystallographic texture during the $\alpha \rightarrow \beta \rightarrow \alpha$ phase transformation showed that the Burgers relationship was not followed for deformed Ti-6Al-4V and it was destroyed during thermal-cycling. There is some similarities in the pole intensities are observed during transformation from $\alpha \rightarrow \beta$
- The increase in the intensity of the β-pole figures confirmed that the β-phase texture strengthens during heating. In contrast, during $\beta \rightarrow \alpha$ transformation, the initial alpha-texture was significantly weakened by the heat-treatment and there was variant selection on cooling due to the growth of untransformed hcp domains.
- During the $\alpha \rightarrow \beta \rightarrow \alpha$ phase transformation, the Burgers relationship ($(0002)_\alpha$ / $(110)_\beta$ and $\{11\text{-}20\}_\alpha$ / $\{111\}_\beta$) was followed and confirmed that there is also a texture memory effect which is strongly influenced by the peak temperature.
- Correlation of experimental results such as flow softening, rotation of α lamellae, microstructure, and texture evolutions of Ti-6Al-4V has showed that the rotation of the lamellar microstructure during hot working. The observed strain for initiation of globularization suggests that the formation of a sharp or stable crystallographic texture may enhance the microscopic strain localization process which may initiate dynamic globularization.
- In compression, crystals with the c-axis nearly parallel to the deformation axis are a stable hard orientation, this would resist breakdown. In these hard orientations, basal and prism slip are not highly active.
- The microstructure observations of Ti-6Al-4V confirm that the differently oriented lamellae regions are broken at different rates may be due to an anisotropic crystal slip behaviour. It appears that, the reorientation by transformation may contribute

to the process of breaking down the larger grain lamellar microstructure.

- The findings have considerable contributions to the understanding of deformation mechanisms in two phase titanium alloys, which has importance in the generation of physically based models. These models will help to develop improved manufacturing routes and result in more durable components with enhanced properties.

Future work

During this work, many questions have arisen which need further investigation, Therefore it is recommended that the following further research be undertaken based on the conclusions and problems identified in the course of the present work.

- During the investigation, In-situ characterisation of texture evolution of the β phase texture above the β transus was not done due to lack of time. Therefore, to study the evolution of the β-phase texture at temperatures above the β-transus using neutron diffraction is necessary in order to complete the results presented in this work. It will also reveal many un-answered question about beta-phase texture of Ti-6Al-4V during the $\alpha \rightarrow \beta \rightarrow \alpha$ thermal-cycle.

- During this study, the EBSD texture measurements were studied for Ti-6Al-4V deformed at a strain rate of 0.1/s with varying strain (0.1, 0.2, 0.4, 0.7 and 1.0) but the (bulk) texture measurements was not done for the interrupted tests at both subtransus and near transus temperatures. Thus, the direct comparison of EBSD and neutron diffraction measurements was not done. In particular this measurement is important to understand the influence of increasing strain in

texture development. It would also be useful to incorporate the effect of crystallographic texture on flow softening behaviour of hot-forged Ti-6Al-4V with acicular α initial microstructure.

- In the present work, the texture memory effect and preferential variant selection have been observed during β→α phase transformation on cooling. In all cases, the size, morphology and texture of the parent grains are important parameters in the mechanical models. More studies are still required to determine the variant indexes inside each parent grain and then determine the parent grain orientation. The prior particle grain boundaries are often imagined as preferential paths for fracture. Therefore, in order to validate the method, SEM-EBSD experiments and reconstruction of the parent β-grains using post-processing of the EBSD data on the α-grains should be carried out to have complete understanding of the variant selection obtained in the present work.

References

1. Semiatin, S.L., Thomas, J., and Dadras, P., *Processing-microstructure relationships for Ti-6Al-2Sn-4Zr-2Mo-0.1Si.* Metallurgical and Materials Transactions A, 1983. 14(11): p. 2363-2374.
2. Lutjering, G., *Influence of processing on microstructures and mechanical properties of alpha+beta titanium alloys.* Mater. Sci. Eng, 1998. A243: p. 32-45.
3. Leyens, C., and Peters, M., Eds, *The metallurgy of titanium alloys*, in *Titanium and Titanium Alloys: Fundamentals and Applications*. 2003, Wiley-VCH GmbH & Co.KGaA: Germany. p. 4-5.
4. Semiatin, S.L., Stefansson, N., and Doherty, R.D., Metall. Mater. Trans., 2005. 36A: p. 1372-76.
5. Weiss, I., Froes, F., Eylon, D., and Welsch, G., *Modification of alpha morphology in Ti-6Al-4V by thermomechanical processing.* Metallurgical and Materials Transactions A, 1986. 17(11): p. 1935-1947.
6. Semiatin SL and Furrer DU., *Modeling of microstructure evolution during the thermomechanical processing of titanium alloys. In: Semiatin SL, Furrer DU, editors.*, in *ASM Handbook. Fundamentals of Modeling for Metals Processing.* 2009, Materials Park, OH: ASM International.
7. Stefansson, N., and Semiatin, S.L, *Mechanisms of globularization of Ti-6Al-4V during static heat treatment.* Metallurgical and Materials Transactions A, 2003. 34(3): p. 691-698.
8. Stefansson, N., Semiatin, S.L., and Eylon, D., Metall. Mater. Trans. A, 2002. 33A: p. 3527-34.
9. Mullins.W.W., J Appl Phys 28 (1957): p. 333.
10. Lennon, A.M., and Ramesh, K. T., *The influence of crystal structure on the dynamic behavior of materials at high temperatures.* International Journal of Plasticity, 2004. 20(2): p. 269-290.
11. Evans, R.W., and Scharning, P.J, *Axisymmetric Compression Test and Hot Working Properties of Alloys.* Materials Science and Technology, 2001. 17: p. 995-1004.
12. Bache, M.R., and Evans, W. J., *Impact of texture on mechanical properties in an advanced titanium alloy.* Materials Science and Engineering A, 2001. 319-321: p. 409-414.

13. Bache, M.R., Evans, W. J., Suddell, B., and Herrouin, F. R. M., *The effects of texture in titanium alloys for engineering components under fatigue.* International Journal of Fatigue, 2001. 23(Supplement 1): p. 153-159.

14. Whittaker, M.T., Evans, W. J., Lancaster, R., Harrison, W., and Webster, P. S., *The effect of microstructure and texture on mechanical properties of Ti6-4.* International Journal of Fatigue, 2009. 31(11-12): p. 2022-2030.

15. Zeng, Z., Zhang ,Y., and Jonsson ,S., *Microstructure and texture evolution of commercial pure titanium deformed at elevated temperatures.* Mater Sci Eng A, 2009,: p. 513-514: 83-90.

16. Krebs, R.E., *The History and Use of Our Earth's Chemical Elements: A reference guide, Greenwood Press.* Westport CT, 1998(ISBN 0-313-30123-9).

17. Lutjering, G., and Williams.J.C, *Fundamental aspects*, in *Titanium.* 2003, Springer-Verlag:Heidelberg, Germany. p. 13-50.

18. Caron, R., and Staley, J., *Effects of Composition, Processing, and Structure on Properties of Nonferrous Alloys* in *Materials Selection and Design* 1997, ASM International.

19. Smith, W., *Structure and Properties of Engineering Alloys.* 1993, 2nd ed., McGraw-Hill: New york.

20. Peter, M., Hemptenmacher, J., Kumpfert, J., and Leyens, C., *Structure and Properties of Titanium and Titanium Alloys*, in *Titanium and Titanium Alloys: Fundamentals and Applications*, C.Leyens, Editor. 2003, Wiley-VCH GmbH & Co.KGaA: Germany. p. 1-36.

21. Sibum, H., *Titanium and Titanium Alloys – From Raw Material to Semi-finished Products.* Titanium and Titanium Alloys. 2005: Wiley-VCH Verlag GmbH & Co. KGaA. 231-244.

22. Boyer, R.R., *An overview on the use of titanium in the aerospace industry.* Materials Science and Engineering: A, 1996. 213(1-2): p. 103-114.

23. Boyer, R., *Introduction and Overview of Titanium and Titanium Alloys : Alloy Systems.* 2002, In Metals Handbook Desk Edition. Electronic File: ASM International.

24. Holleman, A.F., and Wiberg, E., *"Inorganic Chemistry"* Academic Press: Salk; n Diego, 2001(ISBN 0-12-352651-5).

25. Cambridge, G.Z., Chen, D. J., and Farthing, T. W., *Direct Electrochemical Reduction of Titanium Dioxide to Titanium in Molten Calcium Chloride.* Nature, 2000. 407: p. 361-364.

26. Donachie, M.J., *"Chapter 4". TITANIUM* A Technical Guide.Metals Park, OH: ASM International, 1988(ISBN 0871703092).

27. Joshi, V.A., *Physical Metallurgy of Titanium Alloys*, in *Titanium Alloys: An Atlas of Structures and Fracture Features.* 2006, Taylor & Francis Group. p. 7-15.

28. http://www.explainthatstuff.com/alloys.html.

29. Altan, T., Oh, S., and Gegel, H., *Recent Developments in Metal Forming Technology and Application of CAD/CAM*, in *Metal Forming: Fundamentals and Applications.* 2000, American Society for Metals: Metals Park, OH. p. 313-327.

30. Kar, S., *"Modelling of mechanical properties of Alpha/Beta Titanium Alloys". Dessertation.* 2004, Ohio state university.

31. Donachie Jr., M.J., *Ingot Metallurgy and Mill Products*, in *Titanium - A Technical Guide.* 2000, ASM International: Metals Park, OH. p. 25-32.

32. M.J.Donachie jr., *Titanium -A Technical Guide.* ASM International, Metal Park, OH, 1988: p. 353–365.

33. Polmear, I.J., *Titanium Alloys*, in *Light Alloys: Metallurgy of the Light Metals*, R. Honeycombe, Editor. 1989, Edward Arnold: London, UK. p. 162-187.

34. Eylon, D., and Seagle, S.R., in:I.V.Gorynin., S.S.Ushkov(Eds.), *Titanium 99: Science and technology.* CRISM PROMETEY , St,Petersburg,, 2000: p. 37-41.

35. Semiatin, S. and G. Lahoti, *Deformation and unstable flow in hot forging of Ti-6Ai-2Sn-4Zr-2Mo-0.1Si.* Metallurgical and Materials Transactions A, 1981. 12(10): p. 1705-1717.

36. Jonas, J.J., Holt, R.A., and Coleman, C.E., *Plastic Stability in Tension and Compression.* Acta Metallurgica, 1976. 24: p. 911-918.

37. Eylon, D., and Pierce, C.M., *Effect of Microstructure on Notch Fatigue Properties of Ti-6Al-4V.* Metallurgical Transactions, 1976. 7A: p. 111-121.

38. Froes, F.H., and Highberger, W.T, *Synthesis of CORONA 5 (Ti-4.5Al-5Mo-1.5Cr).* Journal of Metals, 1980. 32: p. 57-64.

39. Freese, H.L., Volas, M. G., Wood, J. R., and Textor, M., , *Titanium and its Alloys in Biomedical Engineering*, in *Encyclopedia of Materials: Science and Technology.* 2001, Elsevier: Oxford. p. 9374-9380.

40. R.R.Boyer and H.W. Rosenberg, *Beta titanium on the SR-71: Historical note I, Beta Titanium Alloys in the 1980's.* TMS, Warrendale,PA, 1984: p. 1-8.

41. Boyer, R.R. *Application of Beta Titanium alloys in Airframes.* in *Beta Titanium Alloys in the 1990's.* 1993. Denver, CO (United States): TMS.

42. Bania, P.J., *Beta Titanium Alloys and Their Role in the Titanium Industry.* J.Met., 1994. 46: p. 16-19.

43. Weiss, I. and S.L. Semiatin, *Thermomechanical processing of beta titanium alloys--an overview.* Materials Science and Engineering A, 1998. 243(1-2): p. 46-65.

44. Duerig, T.W., Middleton, R.M., Terlinde, G.T, and Williams, J.C., *Stress Assisted Transformation in Ti-10V-2Fe-3AL,* in *Titanium'80:Science and Technology,* H.Kimura, Editor. 1980, TMS: Warrendale, PA. p. 1503-1512.

45. Terlinde, G., and Fischer, G., *Beta Titanium Alloys,* in *Titanium and Titanium Alloys: Fundamentals and Applications,* C.Leyens, Editor. 2003, Wiley-VCH GmbH & Co.KGaA: Germany. p. 37-57.

46. Flower, H.M., *Microstructural Development in Relation to Hot Working of Titanium Alloys.* Materials Science and Technology, 1990. 6: p. 1082-1092.

47. Duerig, T.W., and Williams, J.C. *Overview:Microstructure and Properties of Beta Titanium Alloys.* in *Beta Titanium Alloys of the 1980's.* 1984. Warrendale, PA, USA: TMS.

48. Kuhlman, G.W. *Critical appraisal of thermomechanical processing of structural Titanium alloys.* 1991.

49. Ding, R., Z.X. Guo, and A. Wilson, *Microstructural evolution of a Ti-6Al-4V alloy during thermomechanical processing.* Materials Science and Engineering A, 2002. 327(2): p. 233-245.

50. Shakhanova, G.V. and M.Y. Brun, *Structure of titanium alloys and methods used for its control.* Metal Science and Heat Treatment, 1982. 24(7): p. 467-471.

51. Donachie Jr., M.J., *Understanding The Metallurgy of Titanium,* in *Titanium - A Technical Guide.* 2000, ASM International: Metals Park, OH. p. 13-24.

52. Collings, E.W., *Titanium Alloys,* in *Materials Properties Handbook,* R. Boyer, Welsch,G. and Collings,E.W., Editor. 1994, ASM, Material Park: OH. p. 5-11.

53. Rath, B.B., *Kinetics of Nucleation and Growth Process.* Materials Science and Engineering B, 1995. B32: p. 101-106.

54. Terlinde, G., Witulski, T., and Fischer, G., *Forging of Titanium.* Titanium and Titanium Alloys. 2005: Wiley-VCH Verlag GmbH & Co. KGaA. 289-304.

55. Revised by Roger Gilbert, I.T. and T.A. C. Richard Shannon, *Heat Treating of Titanium and Titanium Alloys* in *ASM Handbook.* 1991, ASM International.

56. F.H.Froes and W.T. Highberger, *Metals Handbook, vol.4.* 1981. Volume.4., p. 763.

57. Wood, R.A. and R.J. Favor, *Titanium Alloys Handbook,*. DEC 1972: Battelle Memorial Institute, Columbus.

58. Benhaddad.S., Q.C., and Peneller. R., *Characterization of Microstructure and Texture of a Titanium Alloy CORONA 5.* B3t 413 Universit Paris-Sud, 91405 Orsay Cedex France, 1994.

59. Froes, F.H. and W.T. Highberger, *Synthesis of Corona 5 (Ti-4.5Al-5Mo-1.5Cr).* Titanium Technology: Present Status and Future Trends, 1985: p. 95-102.

60. Boyer, R., G. Welsh, and E.W. Collings, *Materilas Properties Hand book-Titanium Alloys.* 1994, ASM International, Materials Park, OH. p. 483-636.

61. Carleo, J., ed. *Metal -shaping Processes/ Vukota Boljanovic.* 2009, Industrial Press Inc.: New york. 428.

62. Yang, H.F., XiaoGuang Sun, ZhiChao Guo, LiangGang Zhan, and Mei, *Recent developments in plastic forming technology of titanium alloys.* SCIENCE CHINA Technological Sciences. 54(2): p. 490-501.

63. Kuhlman, G.W., *Forging of Titanium Alloys*, in *ASM Handbook: Forming and Forging.* 1988, ASM International. p. 267-287.

64. Semiatin, S., Seetharaman, V., and Weiss, I., *The thermomechanical processing of alpha/beta titanium alloys.* JOM Journal of the Minerals, Metals and Materials Society, 1997. 49(6): p. 33-39.

65. Terlinde, G., Witulski, T., and Fischer, G., *Forging of Titanium*, in *Titanium and Titanium Alloys: Fundamentals and Applications*, C. Leyens, Editor. 2003, Wiley-VCH GmbH & Co.KGaA: Germany. p. 289-304.

66. Williams, J.C., *High Performance Materials in Aerospace*, ed. H.M.Flower. 1995, London: Chapman Hall. 85-134.

67. Dieter, G.E., *Hot-Compression Testing*, in *Handbook of Workability and Process Design*, G.E. Dieter, Editor. 2003, ASM International: Materials Park, OH 44073-0002. p. 61-67.

68. Dieter, G.E., *Bulk Workability Testing*, in *Handbook of Workability and Process Design*, G.E. Dieter, Kuhn, H.A., Semiatin, S.L, Editor. 2003, ASM International: Materials Park, OH 44073-0002. p. 48-56.

69. Bonte, M.H.A., Vanden, Boogaard, A.H., and Huétink J. , *An optimization strategy for industrial metal forming processes: modelling, screening and solving of optimization problems in metal forming.* Struct Multidiscipl Optim (2008) 35(6): p. 571–586.

70. Weiss, I., Welsch, G.E., Froes, F.H., and Eylon, D., *Titanium '84: Science and Technology, G. Lutjering, U. Zwicker, andW. Bunk, eds.,*. DeutscheGesellschaft fur Metallkunde, E.V., Oberursel, Germany, 1985: p. 1503-10.

71. Reed-hill.R.E and Abbaschian.R and (editors), *Physical metallurgy principles. 3rd ed.*, in *PWS-KENT.* 1992.

72. Higgins.R.A, *Engineering metallurgy - Applied physical metallurgy.* 6th ed,Elsevier, 1993.

73. McGregor Tegart, W.J., *Elements of Mechanical Metallurgy.* 1966, MacMillan Company.

74. Sakai.T and Jonas.J.J, *Overview no. 35 Dynamic recrystallization: Mechanical and microstructural considerations,*. Acta Metallurgica, 1984. 32, (2): p. 189-209.

75. Kenneth, M.R., Thomas, H. Courtney., and John Wulff., *Introduction to Materials Science and Engineering- Structural and Property changes.* 1976, New York: John wiley & Sons. 372-409.

76. Bahman Mirzakhani, M.T.S., Shahin Khoddam, Seyed Hosein Seyedein, and a.M.R. Aboutalebi, *Investigation of Dynamic and Static Recrystallization Behavior During Thermomechanical Processing in a API-X70 Microalloyed Steel.* JMEPEG 2009. 18: p. 1029–1034.

77. Hugh J. McQueen and W.J.M. Tegart, *The Deformation of Metals at High Temperatures.* Scientific American, 1975. 232 [4] p. 116-125.

78. Malcor, J.G., Montheillet, F., and Champin, B., *Mechanical and Microstructural Behavior of Ti-6Al-4V in the Hot Working Range*, in *Titanium: science and technology*, G.Luetjering, Editor. 1985: Oberursel, Germany. p. 1495-1502.

79. Courtney.T.H. and Malzahn Kampe.J.C., Acta Metall., 1989,. 37: p. 1747-58.

80. Malzahn Kampe.J.C., Courtney.T.H., and Leng.Y, Acta Metall, 1989. 37: p.1735-45.

81. Courtney.T.H. and Comstock.R.J., *Jr :in Modeling of Coarsening and Grain Growth, C.S. Pande and S.P. Marsh, eds.,*. TMS, Warrendale, PA, 1993: p. 71-84.

82. Sharma.G., Ramanujan.R.V., and Tiwari.G.P., Acta Mater, 2000. 48: p. 875-89.

83. Nakagawa.Y.G. and Weatherly.G.C., Metall. Trans, 1972. 3: p. 3223-29.

84. Lin.J.Y., Courtney.T.H., and Ralls.K.M., Acta Metall, 1977. 25: p. 99-106.

85. Nakagawa. Y.G. , Weatherly. G.C., and E. Ho:, Trans. JIM, 1974. 15: p. 114-20.

86. Mullins.W.W:, Trans. AIME, 1960. 218: p. 354-61.

87. Tian.Y.L. and Kraft.R.W., Metall. Trans. A, 1987. 18A: p. 1403-14.

88. Graham.L.D. and Kraft.R.W.. Trans. AIME, 1966. vol. 236: p. 94-102.

89. Nichols.F.A. and Mullins.W.W., Trans. TMS-AIME, 1965. vol.233: p. 1840-48.

90. Racek.R. and Lesoult.G., J. Cryst. Growth, 1972. vol. 16: p. 223-26.

91. Margolin, H., and Cohen, P., *Evolution of The Equiaxed Morphology of Phases in Ti-6Al-4V*, in *Titanium'80: Science and Technology*. 1980, TMS: Warrendale, PA. p. 1555-1561.

92. Welsch.G., et al., *6th World Conf. on - Titanium, P. Lacombe, R. Tricot, and B. Beranger, eds.* SF2M, Les Ulis Cedex, France,, 1988: p. 1289-93.

93. Weiss.I., W.G.E., Froes.F.H., and Eylon.D.: , *Titanium '84: Science and Technology, G. Lutjering, U. Zwicker, andW. Bunk, eds.*,. DeutscheGesellschaft fur Metallkunde, e.V., Oberursel, Germany, 1985: p. 1503-10.

94. Welsch, G., Weiss,I., Eylon,D., and Froes,F.H., *6th World Conf. on - Titanium, P. Lacombe, R. Tricot, and B. Beranger, eds.* SF2M, Les Ulis Cedex, France,, 1988: p. 1289-93.

95. Peters.M, L.G., and Ziegler:G. , Z. Metallkd., 1983. vol. 74: p. 274-82.

96. Weiss, I., Froes, F.H., Eylon, D., and Welsch, G.E., *Modification of Alpha Morphology in Ti-6Al-4V by Thermomechanical Processing*. Metallurgical Transactions, 1986. 17A: p. 1935-1947.

97. S.L. Semiatin, V., Seetharaman, I.Weiss, *Advances in the Science and Technology of Titanium Alloy Processing, TMS, Warrendale,PA.* 1997: p. 3-73.

98. Margolin, H., Williams, J.C., Chesnutt,J.C. and Lutjering, G., , in *Titanium '80:Science and Technology*. 1980, TMS: Warrendale, PA. p. 169-216.

99. Randle V. and Engler O, e., *Introduction to Texture Analysis: Macrotexture, microtexture and Orientation Mapping*. Gordon and Breach Science Publishers, 2000.

100. Wang, Y.N., and Huang, J. C., *Texture analysis in hexagonal materials*. Materials Chemistry and Physics, 2003. 81(1): p. 11-26.

101. Larson.F. and Zarkades.A., *Properties of Textured Titanium Alloys* Report MCIC-74-20 (Columbus, OH: Metals and Ceramics Information Center, Battelle's Columbus Laboratoties,, 1974.

102. Luetjeting.G. and Gysler.A., in Ref. 7: p. 2065-2083.
103. Peters.M. and Luetjering.G., in Ref. 13, : p. 925-935.
104. Wang Y.N. and H. J.C., *Texture analysis in hexagonal materials.* Materials Chemistry and Physics 2003. 81: p. 11–26.
105. Williams, J.C., and Starke, E.A., *The Role of Thermomechanical Processing in Tailoring the Properties of Aluminium and Titanium Alloys*, in *Deformation Processing and Structure*. 1982, ASM: Ohio. p. 279-354.
106. Sommer., *Titanium and Titanium Alloys: Scientific and Technological Aspects, ed. J.C. Williams and A.F. Belov.* New York: Plenum Press, 1982: p. 1863-1874.
107. Glavicic, M.G. and Semiatin.S.L., Acta Meterialia, 2006. 54: p. 5337.
108. Luetjering.G., *Mechanical Properties of a Titanium Blading Alloy*, in *Technische Universitat Hamburg*. 1983.
109. Takeuchi.Y. and Mae.Y. , Metallkunde, (1974). 65 (11): p. 676–680.
110. Divinski.S.V., Dnieprenko.V.N., and Ivasishin.O.M., *An analysis of the elastic property anisotropy for the Ti–6Al–4V two-phased rolled alloy, in: P.A. Blenkinsop et al. (Eds.), Titanium 1995 Scince and Technology,*, in *Proc. 8th World Conf. on Titanium*. 1995: Birmingnam.
111. Moustanfid.H., Gey.N., and Humbert.M., Metall. Mater. Trans. A, (1997). 28 p. 51–59.
112. Donachie.M.J., *Titanium a technical guide.* Materials Park,ASM International (OH), 2000: p. 22.
113. Lutjering, G., and Williams, J.C., *Alpha + Beta Alloys*, in *Titanium*. 2003, Springer-Verlag: Heidelberg, Germany. p. 177-232.
114. Partridge.P.G., Met Rev 1967. 12: p. 169.
115. Dunst .D and Mecking.H.Z, Metallkd 1996. 87: p. 498.
116. Bailey, J.A., Barson, J., Blau, P., Budinski, K., and Bulsara, V., Kuhn, H., Editor., *Mechanical testing and evaluation.* ASM International, 2000.
117. Shen.G and Furrer.D, *Manufacturing of aerospace forgings.* Journal of Materials Processing Technology 98, (2), 2000: p. 189-195.
118. http://rsbweb.nih.gov/ij/.
119. http://rsb.info.nih.gov/ij/. [cited.
120. http://ddsdx.uthscsa.edu/dig/itdesc.html. [cited.
121. Brokmeier.H.G, *Neutron diffraction texture analysis.* Physica B: Condensed Matter, 1997. 234-236: p. 977-979.

122. Bunge H.J., *Texture Analysis in Materials Science.* Butterworth, London, 1982.

123. Hielscher, R., and Schaeben, H., J. Appl. Cryst, 2008. 41: p. 1024–1037.

124. Schaeben, H., Hielscher, R., Fundenberger, J.J., Potts, D., and Prestin, J., J. Appl. Cryst, 2007. 40: p. 570–579.

125. Hielschera.R. and Schaebena.H., *A novel pole figure inversion method: specification of the MTEX algorithm.* Applied Crystallography,International Union of Crystallography, 2008.

126. http://ebsd.com/ebsd-explained/.

127. Adams B.L., Ultramicroscopy 1997. 67: p. 11.

128. http://www.ifw-dresden.de/institutes/ikm/organisation/dep-31/methods/electron-back-scatter-diffraction-ebsd.

129. Pilchak A.L., Williams R.E.A., and Williams J.C., *Crystallography of Fatigue Crack Initiation and Growth in Fully Lamellar Ti-6Al-4V.* Metallurgical and Materials Transactions A, 2009. 41-1: p. 106-124.

130. Glavicic, M.G., Kobryn, P. A., Bieler, T. R., and Semiatin, S. L., *An automated method to determine the orientation of the high-temperature beta phase from measured EBSD data for the low-temperature alpha-phase in Ti-6Al-4V.* Materials Science and Engineering A, 2003. 351(1-2): p. 258-264.

131. Bunge H.J., Z. Metallk., 1985b. 76: p. 92.

132. Dahms M. and Bunge H. J., J.Appl.Cryst.,, 1989. 22: p. 439.

133. Kallend J.S., Schwartz R.B., and Rollett A.D., *Textures and Microstructures.* 1991b. 13: p. 189.

134. Rietveld H.M., J.Appl.Cryst.,, 1969. 2: p. 65.

135. Wenk H. R., *Time-of-flight-Diffraction at Pulsed Neutron Sources (Ed. J.D.Jorgensen and A.J. Schultz),* . Trans. Am.Cryst.Ass., , 1994. 29: p. 95.

136. Bookmeier H.G., *Textures and Microtstructures* 1989. 10: p. 325.

137. Engler O. and Juul Jensen D., Scripta Materialia. Mat., , 1994. 30: p. 25.

138. Lutterotti, L., Matthies, S., Wenk, H.-R., Schultz, A.J., and Richardson, J.W., J. Appl. Phys.,, 1997. 81: p. 594-600.

139. Larson.A.C. and Von Dreele R.B., *GSAS, General Structure Analysis System* Los Alamos National Laboratory Report LAUR86-748, 1986).

140. http://wwwisis2.isis.rl.ac.uk/disordered/gem/gem_home.htm.

141. Day, P., Enderby, J.E., Williams, W.G., Chapon, L.C., Hannon, A.C., Radaelli, P.G., and Soper, A.K., *Neutron News 15.* (2004) p. 19.

142. Wilson, A., *Private Communication*. 2006: TIMET UK, Birmingham.

143. Roebuck, B., Lord, J.D., Brooks, M., Loveday, M.S., Sellars, C.M., and Evans, R.W., *Measurement Good Practice Guide: Measuring Flow Stress in Hot Axisymmetric Compression Tests*. 2002, The National Physics Laboratory: Teddington, United Kingdom.

144. *Operation Manual of Control Unit Model No:CU1856B*. April 2005, Instron SFL.

145. *Operating Instructions of 1100 C Radiant Furnace RHS1856A*. April 2005, Instron SFL.

146. http://www.mts.com/en/products/producttype/test-components/software/mpt/index.htm.

147. Sofuoglu, H. and H. Gedikli, *Determination of friction coefficient encountered in large deformation processes*. Tribology International, 2002. 35(1): p. 27-34.

148. Male, A.T., *Variation in Friction Coefficients of Metals during Compressive Deformation*. Journal Institute of Metals, 1966. 94: p. 121.

149. Douglas, J.R., and Altan, T., *Flow Stress Determination for Metals at Forging Rates and Temperatures*. Journal of Engineering for Industry-Transactions of ASME, 1975: p. 66.

150. Kunogi, M., J.Sci.Res.Inst., Tokyo, 1956. 50: p. 215.

151. Male, A.T. and M.G. Cockcroft, *A Method for the Determination of the Coefficient of Friction of Metals under Conditions of Bulk Plastic Deformation*. Journal of the Institute of Metals, 1964-1965. Vol.93: p. 38-46.

152. Sofuoğlu, H., Gedikli, H., and Rasty, J., *Determination of Friction Coefficient by Employing the Ring Compression Test*. Transactions of ASME, Journal of Engineering Materials and Technology, 2001. Vol. 123: p. 338-348.

153. www.struers.com.

154. Lonardelli, I., Gey, N., Wenk, H. R., Humbert, M., Vogel, S.C., and Lutterotti, L., *In situ observation of texture evolution during [alpha] --> [beta] and [beta] --> [alpha] phase transformations in titanium alloys investigated by neutron diffraction*. Acta Materialia, 2007. 55(17): p. 5718-5727.

155. Von Dreele, R.B., J. Appl. Cryst., , 1997. 30,: p. 517-525.

156. Matthies, S., Wenk, H.-R., and Vinel, G., J. Appl. Cryst., , 1988. 21: p. 285-304.

157. Sven C. Vogel, et al., *Texture Measurements Using the New Neutron Diffractometer HIPPO and their Analysis Using the Rietveld Method*. International Centre for Diffraction Data 2004, Advances in X-ray Analysis, , 2004. 47.

158. Wahlen, A., U. Feurer, and J. Reissner, *Computer controlled measurement and analytical modelling of flow stresses during hot deformation of the cooper alloy CuZn42Mn2.* Journal of Materials Processing Technology, 1997. 63(1-3): p. 233-237.

159. Dan, W.J., Zhang, W. G., Li, S.H., and Lin, Z.Q., *A model for strain-induced martensitic transformation of TRIP steel with strain rate.* Computational Materials Science, 2007. 40(1): p. 101-107.

160. Salem, A.A., Kalidindi, S.R., and Semiatin, S.L., Acta Mater, 2005. 53: p. pp.3495-502.

161. Jeoung Han Kim., N.S.R., Jong Taek Yeom., Jae Keun Hong., Chong Soo Lee., and Nho-Kwang Park., *Microstructure Prediction of Two-Phase Titanium Alloy during Hot Forging Using Artificial Neural Networks and FE simulation.* Met. Mater. Int., 2009. 15: p. 427-437.

162. Semiatin, S.L., Montheillet, F., Shen, G., and Jonas, J.J, *Self-Consistent Modelling of the Flow Behavior of Wrought Alpha/Beta Titanium Alloys under Isothermal and Nonisothermal Hot-Working Conditions.* Metallurgical and Materials Transactions A, 2002. 33A: p. 2719-2727.

163. Semiatin S.L. , Seetharaman V., and Weiss.I, *Flow Behaviour and Globularization Kinetics during Hot Working of Ti-6Al-4V with a Colony Alpha Microstructure.* . Materials Science Engineering A, 1999. A263: p. 257-271.

164. Seshacharyulu, T., Medeiros, S. C., Morgan, J. T., Malas, J. C., Frazier, W. G., and Prasad, Y. V. R. K., *Hot deformation mechanisms in ELI Grade Ti-6Al-4V.* Scripta Materialia, 1999. 41(3): p. 283-288.

165. Prasad, Y.V.R.K., Seshacharyulu, T., Medeiros, S.C., and Frazier, W.G. , *Microstructural Modeling and Process control during Hot working of Commercial Ti-6Al-4V: Response of Lamellar and Equiaxed Strating Microstructures.* Materials and Manufacturing processes, 2000. 15:4: p. 581-604.

166. Richardson, G.J., Hawkins,D.N., and Sellars,C.M, (editors). *Worked examples in metal-working.* The institute of metals., 1985.

167. Brooks J.W. and Dickenson M., *Real-time data capture and analysis with application to process modelling.* Proceedings of the Institute of Mechanical Engineers, C546 (014/98). 1998: p. 219–227.

168. Mulyadi.M, *PhD Thesis: Hot compression behaviour of two-phse Ti-6Al-4V: Experiments and state-variable modelling*, in *Materials Engineering*, . 2007, The Open University: Milton Keynes, United Kingdom.

169. Brooks.J.W, *Private communication: Mathcad routine.* 2008.

170. Dieter, G.E., *Mechanical Metallurgy.* 2nd ed. International Student Edition. 1989, Newyork, NY: McGraw-Hill. 563.

171. Shell, E.B., and Semiatin, S.L., *Effect of Initial Microstructure and Plastic Flow and Dynamic Globularisation during Hot Working of Ti-6Al-4V.* Metallurgical and Materials Transactions, 1999. 30A: p. 3219-3229.

172. Seshacharyulu, T., Medeiros, S.C., Frazier, W.G., and Prasad, Y.V.R.K., *Microstructural Mechanisms during Hot Working of Commercial Grade Ti-6Al-4V with Lamellar Starting Structure.* Materials Science and Engineering, 2002. A325: p. 112-125.

173. Wilson, A.F., Venkatesh, V., Pather, R., Brooks, J.W., and Fox, S.P., Ti-2003: Science and Technology, ed. by G. Luetjering and J. Albrech, (Wiley-VCH Verlag GmbH, 2004) pp. 321-329.

174. Li, A.B., Huang, L.J., Meng,Q.Y., Geng, L., and Cui, X.P., Mater. Des. 30 (2009) 1625-1631.

175. Seshacharyulu, T., *Hot deformation and microstructural damage mechanisms in extra-low interstitial (ELI) grade Ti-6Al-4V.* Materials Science and Engineering A, 2000. 279(1-2): p. 289-299.

176. Wanjara, P., Jahazi, M., Monajati, H., and Yue, S., Materials Science Engineering A, 2006. 416: p. 300–311.

177. Ding, R., and Guo, Z. X., *Microstructural evolution of a Ti-6Al-4V alloy during [beta]-phase processing: experimental and simulative investigations.* Materials Science and Engineering A, 2004. 365(1-2): p. 172-179.

178. Jain.M., C., N.L., Richards, N.L., and Good, N.C., Materials Science and Engineering, 1991. A138: p. 205-211.

179. Asay, R., and Kerely, G.I., Int. J. Impact Eng., 1987. 5: p. 69--99.

180. Jackson, M., Jones, N. G., Dye, D., and Dashwood, R. J., *Effect of initial microstructure on plastic flow behaviour during isothermal forging of Ti-10V-2Fe-3Al.* Materials Science and Engineering: A, 2009. 501(1-2): p. 248-254.

181. Semiatin, S.L., Seetharaman,V., and Ghosh, A.K., *Plastic flow, microstructure evolution, and defect formation during primary hot working of titanium and titanium aluminide alloys with lamelar colony microstructures.* The Philosophical Transactions of The Royal Society of London A, 1999. 357: p. 1487-1512.

182. Seetharaman, V., and Semiatin, S.L, *Influence of Temperature Transients on The Hot Workability of a Two-Phase Gamma Titanium Aluminide Alloy.* Metallurgical and Materials Transactions, 1996. 27A: p. 1987-2004.

183. Weiju Jia., W.Z., Yigang Zhou.,Jianrong Liu.,and Qingjiang Wang., *High-temperature deformation behaviour of Ti60 titanium alloy.* Materials Science and Engineering A, 2011. 528: p. 4068-4074.

184. Jackson, M., Dashwood, R. J.,Christodoulou, L., and Flower, H. M., *Isothermal subtransus forging of Ti-6Al-2Sn-4Zr-6Mo.* Journal of Light Metals, 2002. 2(3): p. 185-195.

185. Kubiak, K. and J. Sieniawski, *Development of the microstructure and fatigue strength of two phase titanium alloys in the processes of forging and heat treatment.* Journal of Materials Processing Technology, 1998. 78: p. 117-121.

186. Greenfield. M.A. and Margolin. H., Metallurgical and Materials Transactions 3, 1971: p. 2649.

187. Greenfield. M.A. and Margolin. H., Metallurgical and Materials Transactions 2, 1971: p. 841.

188. Humpbreys, F.J. and Hatherly M., *Recrystallization and related annealing phenomena,* . 1995, Pergamon Press: New york. p. 8,373.

189. Miller, R.M., Bieler,T.R., and Semiatin,S.L., *Flow softening during hot working of Ti-6Al-4V with a lamellar colony Microstructure.* Scripta Materialia, 1999. 40,No. 12: p. 1387–1393.

190. Bieler, T.R. and S.L. Semiatin, *The origins of heterogeneous deformation during primary hot working of Ti-6Al-4V.* International Journal of Plasticity, 2002. 18(9): p. 1165-1189.

191. Zherebtsov, S., Murzinova, M.,Salishchev, G., and Semiatin, S. L., *Spheroidization of the lamellar microstructure in Ti-6Al-4V alloy during warm deformation and annealing.* Acta Materialia, 2011. 59(10): p. 4138-4150.

192. R. Hielscher and H. Schaeben, J. Appl. Cryst, 2008. 41: p. 1024-1037.

193. Seetharaman V. and Semiatin S.L., *Effect of the Lamellar Grain Size on Plastic Flow Behaviour and Microstructure Evolution during Hot Working of a Gamma Titanium Aluminide Alloy.* Metallurgical and Materials Transactions, 2002. 33A: p. 3817-3830.

194. Air-Gur P. and Semiatin S.L., *Evolution of microstructure, macrotexture and microstructure during hot-rolling of Ti-6Al-4V.* Materials Science and Engineering A, 1998. 257: p. 118-127.

195. Hasegawa, T., Takahashi, T., and Okazaki, K., *Deformation parameters governing tensile elongation for a mechanically milled Al-1.1%Mg-1.2%Cu alloy tested in tension at constant true strain rates.* Acta Materialia, 2000. 48(8): p. 1789-1796.

196. Luo, J., Li, Miaoquan., Li, Xiaoli., and Shi, Yanpei., *Constitutive model for high temperature deformation of titanium alloys using internal state variables.* Mechanics of Materials, 2010. 42(2): p. 157-165.

197. Lin, J., and Dean, T. A., *Modelling of microstructure evolution in hot forming using unified constitutive equations.* Journal of Materials Processing Technology, 2005. 167(2-3): p. 354-362.

198. Sha Aixue., L., Xing Wu., Wang Qing ru., and PAO Ru- Qiang. , *Influence of hot deformation temperature on microstructure and mechanical properties of TC18 alloy.* The chinese journal of nonferrous metals, China, 2005(Vol.15 No.8): p. 1167-06.

199. Wenk H R and Van Houtte P., *Texture and anisotrophy.* Reports on Progress in Physics, 2004. 67: p. 1367-1428.

200. Kocks, U.F., Tome, C. N. & Wenk, H.-R., *Texture and Anisotropy. Preferred Orientations in Polycrystals and Their Effect on Materials Properties.* . Cambridge University Press, 1998.

201. Salem, A.A., Glavicic, M.G., and Semiatin, S.L., *The Effect of Preheat Temperature and Inter-Pass Reheating on Microstructure and Texture Evolution during Hot Rolling of Ti-6Al-4V.* Metals Branch, Metals, Ceramics, and NDE Division, 2008: p. 4344.

202. Holt RA., Journal of Nuclear Materials, 2008. 372 (2-3): p. 182-214.

203. Wang Y.N. and Huang J.C., *Texture analysis in hexagonal materials.* Materials Chemistry and Physics 2003. 81: p. 11–26.

204. Gong, J. and A.J. Wilkinson, *Anisotropy in the plastic flow properties of single-crystal ß± titanium determined from micro-cantilever beams.* Acta Materialia, 2009. 57(19): p. 5693-5705.

205. Groves G.W. and Kelly A. , in *Philosophic Magazine.* (1963). p. 877.

206. Honeycombe, R.W.K., *'The Plastic Deformation of Metals"*. Edward Arnold Publ. Ltd., London, 1984: p. 112.

207. Burgers, W.G., Physica, (1934). 1: p. 561

208. Holt RA. and Aldridge SA., J Nucl Mate, 1985. 135: p. 246–59.

209. Zhu Zs., G.J., Liu RY, Chen NP,and Yan MG., Mater. Sci. Eng A, 2000: p. 280:199.

210. Jourdan, C., Gastaldi, J., Marzo, P., and Grange, G., *In situ statistical study of the nucleation, the variant selection and the orientation memory effect during the alpha = beta titanium martensitic transformation.* Journal of Materials Science, 1991. 26(16): p. 4355-4360.

211. Gey, N. and M. Humbert, *Characterization of the variant selection occurring during the alpha+beta phase transformations of a cold rolled titanium sheet.* Acta Materialia, 2002. 50(2): p. 277-287.

212. Gey, N., M. Humbert, and H. Moustahfid, *Study of the alpha - beta phase transformation of a Ti-6Al-4V sheet by means of texture change.* Scripta Materialia, 2000. 42(6): p. 525-530.

213. Ciurchea, D., Pop, A. V., Gheorghiu, C., FurtunÇŽ, I., TodicÇŽ, M., Dinu, A., and Roth, M., *Texture, morphology and deformation mechanisms in Î²-transformed Zircaloy-4.* Journal of Nuclear Materials, 1996. 231(1-2): p. 83-91.

214. Wenk, H.R., Lonardelli, I., and Williams, D., *Texture changes in the hcp → bcc → hcp transformation of zirconium studied in situ by neutron diffraction.* Acta Materialia, 2004. 52(7): p. 1899-1907.

215. Stanford, N. and P.S. Bate, *Crystallographic variant selection in Ti-6Al-4V.* Acta Materialia, 2004. 52(17): p. 5215-5224.

216. Gey, N. and M. Humbert, Acta Materialia, 2003. 51: p. 4783.

217. Bhattacharyya, D., Viswanathan, G. B., Denkenberger R., Furrer D., and Fraser, Hamish L., Acta Materialia, 2003. 51: p. 4679.

218. Lutterotti L., M.S., and Wenk H-R., , *12th International Conference Texture of Materials(ICOTOM-12).* (Montreal, 9-13 August 1999)ed J.A Szpuna (Montreal: NRC Research press), 1999: p. 1599-604.

219. VON DREELE R. B., *Quantitative texture analysis by Rietveld refinement.* J. Appl. Cryst. (1997).,, 1997. 30: p. 517-525.

220. Lonardelli L, Gey N., Wenk HR., Humbert M., Vogel S., and Lutterotti L., Acta Materialia, 2007. 55: p. 5718.

221. Gey, N., Gautier E., Humbert, M., Cerqueira A., Bechade JL., and Archambault P.J. , Nucl Mater., 2002. 302:175.

222. Inakazu, N. and Inoue H.J., Jap Inst Met, 1988. 52:18.

223. Wagner, F., Bozzolo, N., Van Landuyt, O., and Grosdidier, T., *Evolution of recrystallisation texture and microstructure in low alloyed titanium sheets.* Acta Materialia, 2002. 50(5): p. 1245-1259.

224. Dahlback, M., Limback, M., Hallstadius, L., Barberis, P., Bunel, G., and Simonot, C., J ASTM Int, 2005. 2: p. 1.

225. Bhattacharyya, D., Viswanathan, G. B.,Vogel, S. C., Williams, D. J., Venkatesh, V., and Fraser, H. L., *A study of the mechanism of $\alpha \rightarrow \beta$ to phase transformation by tracking texture evolution with temperature in Ti-6Al-4V using neutron diffraction.* Scripta Materialia, 2006. 54(2): p. 231-236.

226. Wenk HR., Lonardelli I., and Williams D., Acta Materialia, 2004. 52: p. 1899.